University of Strathclyde

Department of Pure and Applied Chemistry

Development of Novel Intelligent Inks and Pigments

by

Pauline Grosshans

A thesis presented in fulfilment of the requirements for the degree of
Doctor of Philosophy

2012

This thesis is the result of the author's original research. It has been composed by the author and has not been previously submitted for examination which has led to the award of a degree.

Signed: Date:

Abstract

This thesis details the development and characterisation of several novel optical indicators covering a range of different analytes including UV dose, relative humidity, hydrogen peroxide vapour, ammonia and volatile amines.

Two UV dosimeters and the use of these novel dosimeters to measure solar UV exposure dose are discussed. The first dosimeter is based on a redox dye which is reduced by means of a UVB activated semiconductor photocatalyst. The second dosimeter is based on a redox dye capable of undergoing a UV induced reduction. The spectral characteristics of a typical UV dosimeter film and the mechanism through which the colour change occurs are detailed. Such indicators have potential for measuring solar radiation exposure and providing an early warning of erythema for most Caucasian skin (i.e. skin type II).

A new relative-humidity sensitive ink based on methylene blue and urea is described which can utilise the deliquescent nature of urea. The notable features of this type of relative-humidity indicator are not only that it can be used exclusively for monitoring high (>85%) relative humidities, but it is quick to respond, highly reversible and has a good long-term stability.

Intelligent pigments comprised of dye-coated inorganic substrates which have been incorporated into extrudable thermoplastics are described. These so-called intelligent plastics are characterised with respect to their response to gaseous ammonia and volatile amines and their suitability as a fish freshness indicator evaluated.

A hydrogen peroxide vapour indicator that is highly coloured in the absence of hydrogen peroxide vapour but is rapidly bleached in the presence of hydrogen peroxide vapour is discussed. The proposed mechanism and the kinetics of the photobleaching are described. This particular indicator may be used to screen the headspace above liquids for hydrogen peroxide, which can be used for making *in situ* explosives, such as triacetone triperoxide.

Acknowledgements

I would first and foremost like to thank God for giving me the wisdom, strength and perseverance to see this thesis through to completion. It has been a long road with many ups and downs, thankfully the former significantly outweighing the later. Without His faithful encouragement I fear this would have remained a work in progress indefinitely.

My next round of gratitude is directed at my supervisor Prof Andrew Mills. I am grateful for your approachable manner and continual advice and guidance throughout my PhD. Without your enthusiastic and highly creative mind dreaming up new projects I fear this thesis would be a much duller read.

I cannot go any further without expressing an appreciation for the Mills group. A constant source of laughter and cheer, you are among the most wonderful set of personalities I have ever worked with. You made the long winter days in the lab pass in the blink of an eye and I have cultivated friendships with some of you that will last a lifetime.

The legendary Dr Michael McFarlane, I will forever be indebted to you for passing on your wealth of knowledge and experience on UV dosimetry, and for always having a solution to my problems. Your friendship and technical support were both crucial to getting me where I am today.

Dr Graham A. Skinner, my wedding usher, faithful friend and expert proof-reader, I extend a special thanks for your constant support and encouragement.

A wider thanks to all the technicians and support staff in the Chemistry Department who have helped me in many ways throughout my PhD.

Thanks are due also to the University of Strathclyde for funding this research.

Now for the mushy stuff. My parents, Charlie and Pamela, my twin pillars without whom I could not stand. I am proud to be your daughter and will be forever grateful

to you for all that you have done for me in my 27 years. Your unconditional love and constant guidance are an inspiration to me. I only aspire to have the same impact on my own children one day. And to my extended family, my sisters, grandparents, in-laws and ever-faithful church family, for all your prayer that upheld me when the going got tough – I thank you.

Lastly to the two most precious people in my life - my wonderful husband Evan and my beautiful daughter Abigail Rose. Evan, I am honored to call myself your wife and am so blessed to have such a sweet and loving husband whose unfailing belief in me has pushed me to this point. Abigail, you are a constant source of joy in my life and you are by far my proudest accomplishment and so it only seems fitting that I dedicate this thesis (my second proudest accomplishment (so far)) to you and your father. I love you both.

I can do all things through Christ who strengthens me

NKJV - Phillipians 4:13

Contents

Table of Figures

Table of Tables

Chapter 1

Introduction

1. Introduction

1.1 Optical sensors

1.1.1 What are optical sensors?

Optical chemical sensors have been defined as "miniaturized analytical devices that can deliver real-time analysis and on-line information on the presence of specific compounds or ions in complex samples".[1] Over the last 30 years there has been a growing interest in such sensors following the invention of optical fibres and transducers. Optical chemical sensors in the form of analyte-specific indicating films have become increasingly researched because of their ability to be coupled with fibre-optic systems. The analytes of interest include pH, carbon dioxide, UV radiation, oxygen, ammonia, water vapour and volatile amines.[1] There is also an increased interest in using optical sensor films as simple colorimetric indicators, which have several advantages including being simple and easy to use by untrained operators such as the general public.

1.1.2 Typical properties of optical sensors

Traditionally most analyte-specific sensors are electronic or contain sensitive electrical parts e.g. pH, oxygen and ammonia electrodes, hygrometers, UV meters etc. Such systems are effective and work well for their respective analytes. They do however possess some disadvantages which make them less than ideal for certain applications. Most notable are the size and price of many electronic sensors. Generally bulky and expensive they are often prone to electrical interference and their operating environment is restricted by the limitations of the instrument. This has prompted an increase in research into optical sensors which have several advantages over their electronic counterparts including:

- Optical sensors are simple systems which are cheap and easy to construct..

- Optical sensors do not suffer from electrical interference nor do they require an external power source.
- Coupling to fibre optics allows remote in-line sensing.
- Generally, analysis is non-destructive.
- Can provide real-time analysis.

As with most technologies, optical sensors are imperfect systems and possess some drawbacks. The lifetime and efficacy of the sensor will depend on the stability of the indicating material e.g. dye degradation over time. Some systems are sensitive to temperature and humidity fluctuations or have a low dynamic range, and those involving fibre optics, while free from electromagnetic interference, are subject to light interferences. Despite these potential problems optical sensors are still an attractive alternative to their bulky and/or expensive electronic equivalents.

1.1.3 Novel optical sensors

This thesis details the development of several different novel indicator systems for UV dose, humidity, ammonia and volatile amines. The background literature to these three different fields is outlined in the following pages.

1.2 UV doismetry

1.2.1 What is ultraviolet radiation?

Ultraviolet radiation (UV) is the section of the electromagnetic spectrum which lies between x-rays and visible light. The greatest natural source of UV radiation is the sun, although many artificial sources also exist, including black-lights, halogen lights, fluorescent and incandescent lamps, welding arcs and certain types of lasers. UVA, *i.e.* electromagnetic radiation spanning the wavelength range 315-400 nm, is

the most common, naturally-encountered form of UVR, as only a small portion of solar UVA is absorbed by atmospheric ozone while the reverse is true for solar UVB *i.e.* 280-315 nm, a large portion of which is blocked by the ozone layer. On a typical summer's day approximately 6% of terrestrial light is UVB and this contributes 80% towards the harmful effects associated with the sun, while the remaining 94% UVA contributes to the remaining 20%.[2] The higher energy UVC light ($\lambda < 280$ nm) is not observed in nature at significant levels as it is absorbed by the earth's atmosphere.

1.2.2 Health implications

1.2.2.1 Beneficial effects

Ultraviolet radiation can play a role in maintaining the human body. The main recognised benefit of UVR is its role in the synthesis of vitamin D3 and UVB specifically has been described by W. B. Grant as 'the most important source of the vitamin [D] for most people on Earth'.[3] Exposure to sunlight causes the 7-dehydrocholesterol present in human skin to transform *via* an electrocyclic ring opening, the product of which, when formed, undergoes a temperature-dependent sigmatropic rearrangement to give vitamin D3. Vitamin D3 is necessary for several essential functions within the human body e.g. aiding the absorption of the dietary calcium in the gut required to sustain healthy bones.[3-5] Studies suggest that vitamin D deficiency, arising from a lack of sunlight exposure, is linked to conditions such as rickets and osteoporosis.[3-5]

Individuals suffering from skin conditions such as psoriasis can also benefit from UV phototherapy.[6, 7] Among the most effective treatments are those which involve UVB phototherapy sessions in conjunction with topical treatments including corticosteroids, retinoids and tazarotene.[5] Ingestion of 8-methoxy psoralen (8-MOP) coupled with UVA irradiation (PUVA) has become a well-established treatment for psoriasis.[6, 7] Y. Matsumura *et al.*, however, stresses that despite these treatments being 'highly effective' they are also 'associated with acute and chronic side effects

on human skin, which cannot be separated from the beneficial effects of UV radiation'.[7]

1.2.2.2 Acute harmful effects

Over-exposure to UVR is known to be harmful to human health, with human skin being the main organ affected.[7-12] The severity of the UV-induced damage depends on several factors, including the source of UV, its wavelength and intensity, the duration of exposure and an individual's sensitivity towards UVR.

Short term exposure can cause acute effects such as erythema *i.e.* the reddening of the skin or sunburn, and enhanced melanogenesis, the process that causes an individual to develop a suntan. While the latter still remains a largely socially-desired side effect, the former is often painful and unsightly. UVR can even damage DNA under the skin resulting in local immune suppression.[8] The adverse effects of sunlight also extend to the human eye.[8] Acute UV induced ocular conditions include photokeratitis and photoconjunctivitis, which are best described as the reversible sunburn of the cornea and conjunctiva respectively.[8] Neither condition normally results in long-term damage, however, in some severe cases of photokeratitis snow blindness can occur, resulting in the loss of vision for 2-3 days.

1.2.2.3 Chronic harmful effects

Perhaps an issue of greater concern is that of the risks associated with chronic exposure. R. M. MacKie, from the University of Glasgow public health department, has written a review outlining the long-term risks to the skin from UVR, most notably the development of skin cancers.[10] It is well established that UVR can damage human DNA and while DNA has the capability to mend itself, errors can arise during the repair and replication steps. The result of cumulative DNA damage is the occurrence of skin cancer.[4-8]

Skin cancers are classified as either malignant melanoma (MM) or non-melanoma skin cancer (NMSC). NMSC is described as either basal cell carcinoma (BCC) or squamaous cell carcinoma (SCC). According to Cancer Research UK, over 91,100 cases of NMSC were diagnosed in 2009 in the UK; however, since it is readily treatable and frequently cured, it is often omitted from national statistics.[13] In contrast, MM is not easily treated and statistics show in the UK in 2010 approximately 12,800 cases were diagnosed (48.4% men 51.6% women), and out of the 2,750 recorded skin cancer deaths, 2,200 (~80%) were attributed to MM.[13]

In the last 3 decades MM has become the fastest-growing cancer within the top 10 cancers associated with both males and females. In 1979 the occurrence rate per 100,000 persons was 2.9 for men and 4.8 for women; by 2010 these have risen to 17.2 (i.e. ~6 times increase) for men and 17.3 (i.e.~ 3.5 times increase) for women. MacKie points out that the increase in skin cancer occurrences coincides with a change in cultural attitude towards skin colour, where individuals in the western world 'regard some degree of a tan as cosmetically desirable' while those elsewhere in the world seek out 'destructive and expensive bleaching techniques, to lighten their skin'.[10] The former of these is compounded by the introduction of budget airlines in the UK, providing inexpensive travel to warmer, sunnier climates during the summer months. Other effects of chronic UVR exposure include photoaging[9] which manifests as dry and often rough skin marked by pigmentation irregularities such as freckles, moles and liver spots. Skin also loses its elasticity and wrinkles begin to develop.

Chronic ocular conditions associated with long-term UVR exposure include one of the most common causes of vision impairment worldwide, cataracts.[14] This is a clouding of the lens, which blocks the passage of light entering the eye and consequently obscures vision. Cataracts are commonly encountered among the elderly and require surgery to correct. Tissue growth on the conjunctiva known as pterygium[8] has also been linked to long-term UVR exposure. Typically encountered in individuals who experience a high degree of occupational sunlight exposure, this can affect vision if it spreads to the cornea.

As previously stated, ultraviolet radiation can alter the DNA of human skin cells. This in turn can affect the activity of the biological triggers of the body's natural defence system causing immunosuppression.[8, 9] This suppression of the immune response increases the individual's susceptibility to infectious diseases and reduces his or her body's defence capabilities against cancerous tumors.[8, 9]

1.2.3 Measurements of ultraviolet radiation

1.2.3.1 Ultraviolet index

With an increase in the number of individuals suffering from UVR-related conditions, it is necessary for the general public to be made aware of just how damaging the sun's rays are on any given day. Incident UV levels are often reported in terms of the Global Solar UV Index (UVI) [15] which characterises ultraviolet radiation levels on the earth with a value that provides an overall indication of the UV intensity of the incident sunlight and thus its ability to cause erythema. It can take on values ranging from zero upward, with higher values signifying a greater potential to cause harm in a given time period. Thus, on a typical UK summer's day the UVI is typically 5 (Glasgow) or 6 (London) (*i.e.* 125-150 mW m^{-2}) at around mid-day.[16] Cultural changes within society that have caused a suntan to be a desirable trait have resulted in the concomitant rise in the incidence rate of skin cancer among the Caucasian population. Thus, it is now more important than ever to make the public aware of the dangers of UVR. UVI values are a useful method for such a task and are grouped into exposure categories, each of which is defined by a colour as shown in Table 1.1.[15]

Exposure category	UVI Range
Low	<2
Moderate	3 to 5
High	6 to 7
Very high	8 to 10
Extreme	11+

Table 1. 1 Ultraviolet Index Exposure Categories[15]

It is now common practice in many countries, during the summer months to incorporate Global Solar UVI measurements into the daily weather forecast. Values are issued with a public health warning and a recommended sun protection scheme as outlined in Table 1.2.

UVI	Protection
1 – 2	No protection required
3 – 7	Seek shade at midday, use sunscreen, wearing a shirt and hat recommended
8 – 11	Avoid midday sun, shirt, hat and sunscreen a must, seek shade

Table 1. 2 Recommended levels of protection of differing levels of UVI

The Global Solar UVI intensities are formulated with reference to the International Commission on Illumination (CIE) reference action spectrum for UV-induced erythema on human skin. The values are unitless quantities calculated from equation (1.1)

$$I_{UV} = k_{er} \cdot \int_{250nm}^{400nm} E_{\lambda} \cdot S_{er}(\lambda) d\lambda \qquad (1.1)$$

Where E_λ = solar spectral irradiance in W m^{-2} nm^{-1}, $d\lambda$ = wavelength interval in the summation, $S_{er}(\lambda)$ = erythemal reference action spectrum, k_{er} = constant of 40 m^2 W^{-1}. From this equation UVI 1 = 25 mW m^{-2}, UVI 2 = 50 mW m^{-2} etc.

The calculation requires the determination of the total spectral irradiance at all wavelengths and weighting it against the effectiveness of the radiation to cause erythema. The initial stage involves measuring the intensity of light at all wavelengths in the range 290 to 400 nm. This value is then modified using McKinlay and Diffey's erythemal action spectrum ($S_{er}(\lambda)$) shown in Figure 1.1.

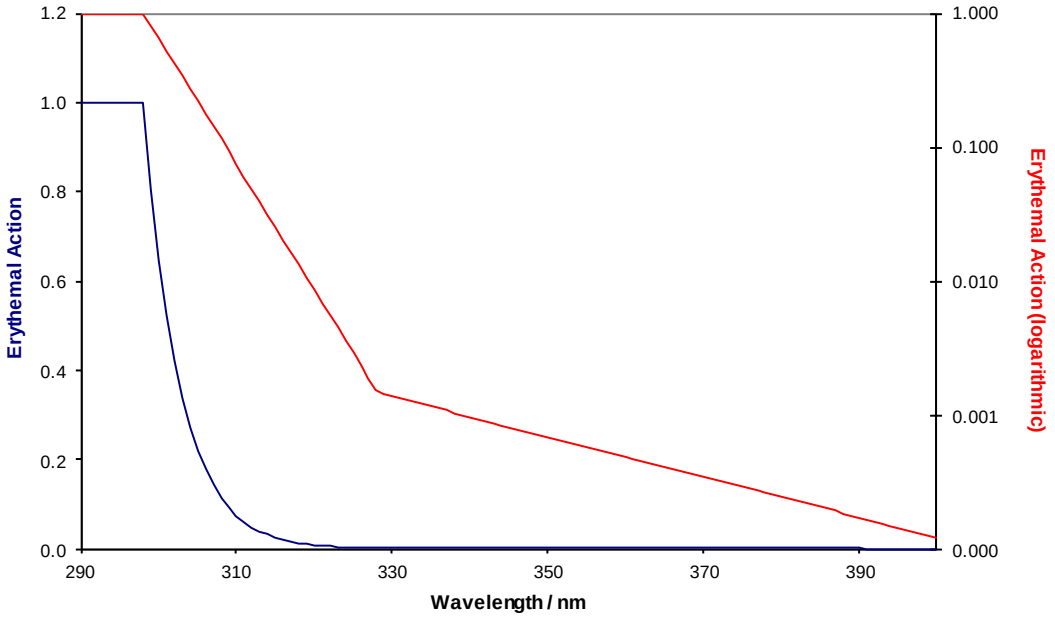

Figure 1. 1 The erythemal action spectrum shown on a standard and logarithmic scale.[17]

The above spectrum is described by equations (1.2) to (1.4).

$$\lambda_{290\text{-}298} = 1 \qquad (1.\ 2)$$

$$\lambda_{299\text{-}328} = 10^{\,0.094x\,(298-\lambda)} \qquad (1.\ 3)$$

$$\lambda_{329\text{-}400} = 10^{\,0.015x\,(139-\lambda)} \qquad (1.\ 4)$$

The action spectrum is used to assess the biological effect of UV on human skin. Applying this factor to the measured spectral irradiances to the solar spectrum shown in Figure 1.2 provides the modified erythemal spectrum shown in Figure 1.3.

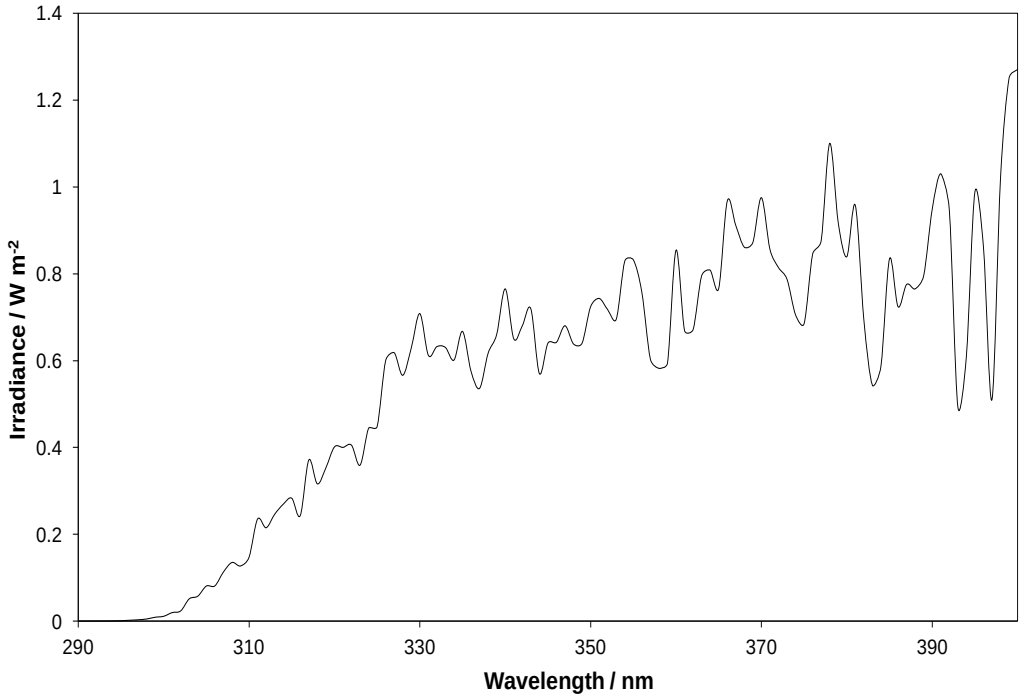

Figure 1.2 A solar spectrum recorded on a clear summer's day in Melbourne (53° S) at 12 noon, on 17th January 1990.[18]

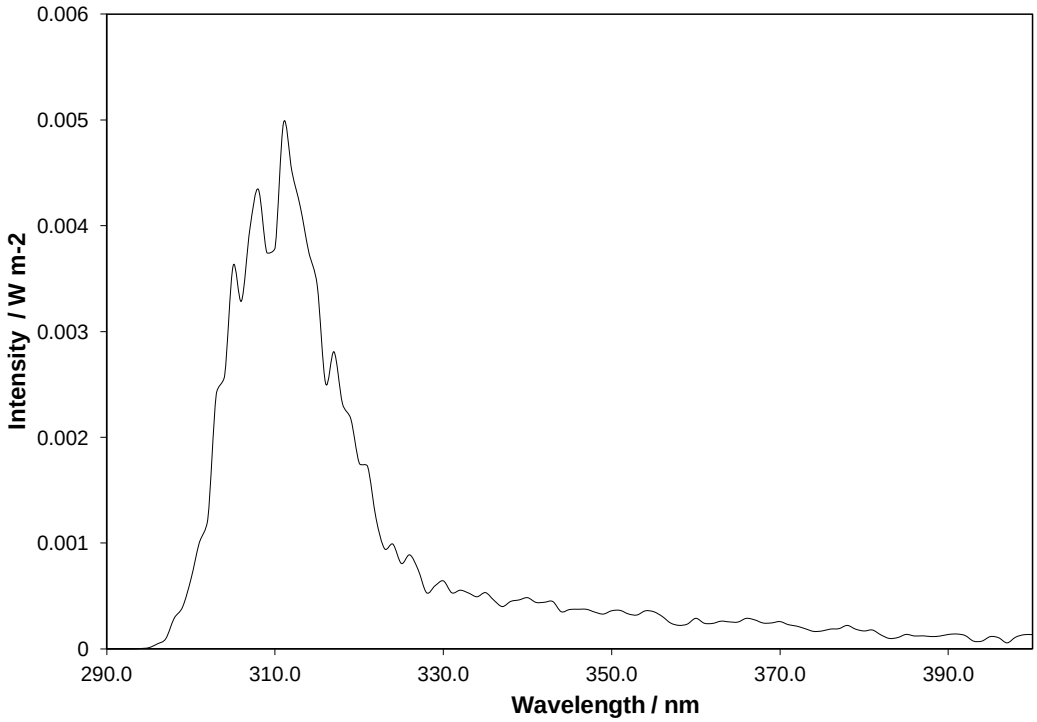

Figure 1.3 Solar spectrum on earth after the application of erythemal weighting factors.[18]

This new plot highlights the wavelengths of light that have the most damaging effect on human health. Figure 1.3 shows that it is the higher energy, shorter wavelength UVB radiation present in solar light which poses the greatest risk to human health. Finally, the value of the modified total intensity is multiplied by the k_{er} constant to give the UVI number.

1.2.3.2 Minimum erythemal dose

The cumulative amount of solar UV radiation absorbed by the skin is known as the erythemal dose. In quantifying an individual's personal exposure to UVR, the term '*minimum erythemal dose'* (MED) is useful, where the MED is defined as the minimum amount of radiation likely to cause erythema. The MED for an individual is largely dependent on their skin type of which there are six (I – VI).[19] For example, for individuals with skin phototype II, which is typical for many Caucasians, the

MED is equal to 250 J m^{-2} *i.e.* 69.4 mW m^{-2} per hour. Since a UV Index value of 1 ≡ 25 mW m^{-2} it follows that even under mild UV solar conditions such as a UVI value of 3 (*i.e.* 75 mW m^{-2}), as may be observed on a clear day in April or September in the UK,[16] most Caucasians will sunburn within 1 hour if not properly protected. The skin types and their MED values are listed in Table 1.3 and 1.4 below.

	Skin type classification	**Burns in the sun**	**Tans after having been in the sun**
I.	Melano-compromised	Always	Seldom
II.		Usually	Sometimes
III.	Melano-competent	Sometimes	Usually
IV.		Seldom	Always
V.	Melano-Protected	Naturally brown skin	
VI.		Naturally black skin	

Table 1. 3 Classification of Skin Types[17]

	Skin type classification	MED (J m^{-2} h^{-1})	MED (mW m^{-2})
I.	Melano Compromised	200	55.6
II.		250	69.4
III.	Melano Competent	300	83.3
IV.		450	125.0
V.	Melano Protected	600	166.7
VI.		1000	277.8

Table 1. 4 MED values for the Fitzpatrick skin types. The values shown are the minimum for each skin type.[17]

1.2.3.3 Exposure times

The time an individual can spend in the sun before erythema is likely to occur, can be calculated from the MED values. For example, we know that UVI 1 ≡ 25 mW m^{-2} and for skin type II MED = 69.4 mW m^{-2}. Thus, at any UVI value, for skin type II, the time taken to burn, *ttb*, will be as follows:

$$ttb = \frac{69.4}{25 \cdot UVI} = \frac{2.78}{UVI} \tag{1.5}$$

So, using equation 1.5, at UVI 5, an individual with skin type II could expose themselves to a minimum of 0.556 hours or 33.4 minutes of sunlight before their skin will begin to be affected by erythema. The same method of calculation can be applied to all skin types, allowing the development of Table 1.5 showing minimum erythemal exposure times, at different UVI levels, for all skin types in minutes.

	Skin Types					
UVI	**I**	**II**	**III**	**IV**	**V**	**VI**
1	133	167	200	300	400	667
2	67	83	100	150	200	333
3	44	56	67	100	133	222
4	33	42	50	75	100	167
5	27	33	40	60	80	133
6	22	28	33	50	67	111
7	19	24	29	43	57	95
8	17	21	25	38	50	83
9	15	19	22	33	44	74
10	13	17	20	30	40	67

Table 1. 5 A table showing the exposure times, in minutes, likely to lead to erythema at various different UVI values, for different skin types.

The data from Table 1.5 is illustrated in Figure 1.4, as a plot of the exposure time required to reach 1 MED as a function of UVI, for each of the different skin types.

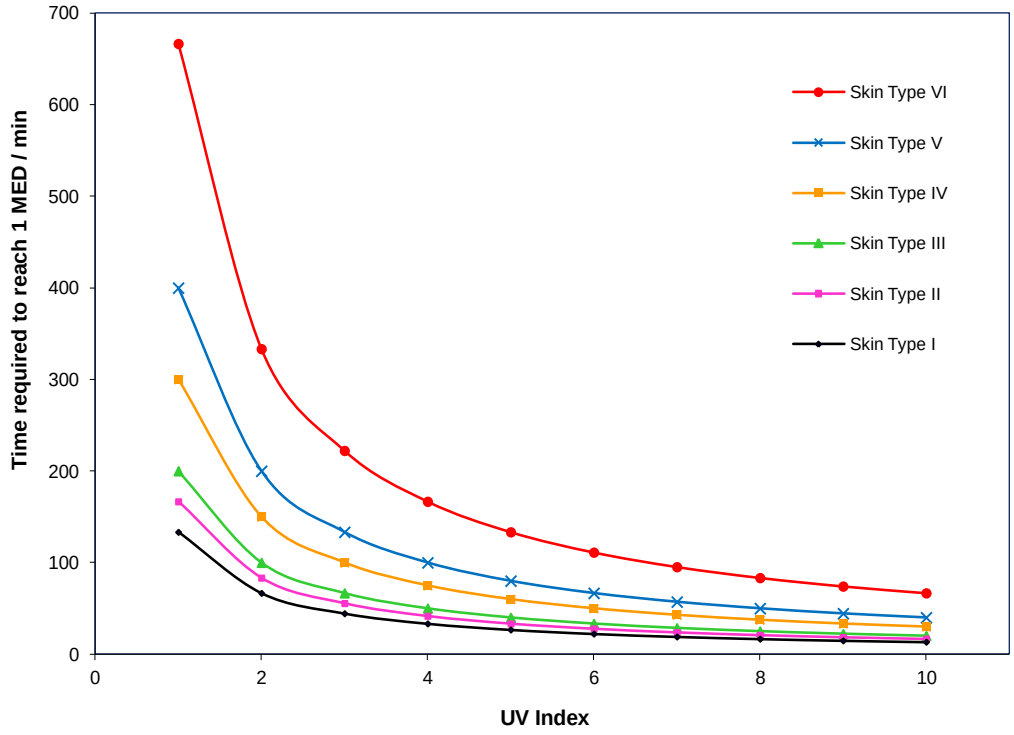

Figure 1. 4 A plot showing the exposure time required to reach 1 MED as a function of UVI. Curves are shown for skin types I, II, III, IV, V, and VI.

The measurement of effective UV dosage experienced by an individual is essential if they are to avoid exceeding their MED, i.e. to avoid sunburn. With the rise in the number of people suffering from UVR-related health problems there is a growing need for a real-time, inexpensive, disposable, personal solar UV dosimeter to provide the user with a current measure of the cumulative dose of UV they have been exposed to during the day.

1.2.4 UV detection

There is an array of different technologies available to monitor UV intensities and/or the absorbed dose of radiation. Typically, UV indicators operate on the basis of a reversible reaction and can give a measure of UV intensity at a given time. Dosimeters on the other hand measure the cumulative exposure and provide

information about the absorbed dose. Both UV indicators and dosimeters can utilise opto-electric, spectrophotometric and colorimetric technologies. The main focus of this discussion is colorimetric systems.

1.2.4.1 Electronic dosimeters

A series of modestly priced electronic devices designed for UV monitoring have been developed. These include a miniaturised portable battery-operated radiometer developed by Gat,[20] Wuest,[21] Heydenreich[22] *et al.*, the commercially available SunSafe ™ personal UV meter by Optix Tech Inc. and the NSecssity UV meter[23] designed to measure UV intensity and daily UV exposure dose.

(a) (b)

Figure 1. 5 A picture of (a) a SunSafe™ and (b) an NSecssity personal UV meter.

The SunSafe meter, pictured in Figure 1.5(a) above, is a hand-held device that contains a sensor designed to imitate the skin's sensitivity to burning by the sun's UV rays, according to McKinlay and Diffey's Erythemal Spectrum. It operates by passing solar light through a series of optical filters to isolate the UV component which is then passed to a silicon photodiode. It runs continually and is designed to both provide the user with real-time solar UVI measurements and determine the total

erythemal dose absorbed in MEDs. By programming the UV meter with the user's skin type and sunscreen SPF information it is possible to calculate a 'safe exposure time'.[23] The NSecessity UV meter is also a photocell device. Rather than constantly monitoring the UVI levels, the device will measure the UVI only when the button is pressed and held.[23] Using this measurement, and information inputted by the user (skintype and sunscreen SPF), the device will sound an audible alarm when a reapplication of sunscreen is required, but does not give a cumulative measure of the absorbed dose.[23] The NScessity UV meter would work well on a clear, sunny day where the UVI levels do not vary greatly with time in the middle of the day, however with more variable conditions resulting in fluctuating UVI levels the calculated 'safe exposure times' based only on one reading would no longer hold true. As electronic devices, they are subject to some drawbacks. They can be quite expensive to purchase, particularly the SafeSun meter, which retails at around £100 (the NScessity UVI meter costs £15.50), and are more prone to environmental damage e.g. sand, sea or swimming pool. They are also considered inconvenient to wear on your person or carry around and are often put in beach bags or pockets where they are no longer able to provide the continuous monitoring required to accurately determine the erythemal dose.

1.2.4.2 Biological dosimeters

In contrast to the moderately bulky and often inconvenient personal electronic UV dosimeters, biological dosimeters are generally discrete sensors with no battery or power source required and thus are ideal for personal UV monitoring. Described as a device which 'indicates the effect of irradiance on a specific biological system over a designated period of time' by A. R. Webb in her review, biological systems have clear advantages over electronic devices.[24] Their small size and lack of power requirements provide a greater degree of flexibility, and they boast an action response spectrum which mimics that of human skin. A review of the literature reveals that there are a number of systems, based on different biological reagents, some of which are listed in Table 1.6 below.

Author	**Year**	**Type of Dosimeter**	**Ref**
N. Munakata	1981	*B. subtilis* spores, colony counting	25
T. V. Wang	1991	*B. subtilis* spores, survivor fraction	26
M. Puskeppeleit *et al.*	1992	*B. subtilis* spores, colony counting	27
L.E.Quintern *et al.*	1992 1997	*B. subtilis* spores, post-irradiation staining, photometry	28, 29
Y. Ishigaki *et al*.	1999	DNA, post-irradiation immunostaining, photometery	30
M. Moehrle *et al.*	2000	*B. subtilis* spores, post-irradiation staining, photometery	31
I. Terenetskaya	2003	vitamin D, *in vitro*	32
J. Sandby-Møller *et al*.	2004	skin autofluorescence, *in vivo*	33
P. Rettberg *et al.*	2004	*B. subtilis* spores, DLR-biofilm, optical density	34

Table 1. 6 Biological UV dosimeters

Ideally the dosimeter should yield a linear response to increasing radiation and should be independent of environmental factors such as temperature and humidity.[24] A selection of the dosimeters listed in the table are discussed in more detail below.

(a) Bacillus subtilus spores

Since erythema is a consequence of DNA damage, it follows that the best UV dosimeters are ones which utilize biological material, such as spores, bacterial cells or bacteriophages.[28] Work on spores, most noticeably *Bacillus subtilus*, has been particularly successful in generating an effective biofilm for use as a UV-dosimeter. With an appropriate filter, the spectral responsivity of this system is very close to the responsivity curve attributed to human skin.[28] The latter feature renders the UV-dosimeter an effective indicator of erythema regardless of UV source and UV emission profile. The only downside to such biological dosimetry is the need to

develop the films by treating with a dye to enable spectrophotometric determination of the absorbed dose, which in the case of the biofilm developed by L. E. Quintern *et al.* can take typically up to a day.[28] This renders the film unable to provide real-time analysis. The same biofilm yields a response which is independent of typical environmental conditions ($-20^{o}C<T<70^{o}C$, $40\%<RH<80\%$) and is compliant with the reciprocity law.

(b) DNA

Another optical UV dosimeter for monitoring solar UV similar to the one discussed above utilises a DNA-based system coupled with a colour changing reaction as described by Y. Ishigaki *et al*.[30] The dosimeter consists of DNA molecules coated on a thin nylon membrane, sealed in a polyethylene filter with silica gel and operates by measuring the degree of UV induced DNA damage, which is determined using an immunochemical reaction.[30] After exposure to UV light, the nylon membrane is treated with a series of solutions to firstly block any non-specific antibody binding before being exposed to a solution containing antibodies, which bind specifically to sites on the membrane and generate a coloured species. The intensity of the colour change exhibited by the immunochemical reaction is linearly related to the UV dose received.[30] As the films require immersion in a series of solutions after UV exposure for the colour to develop, they do not provide real-time analysis.

(c) Polysulfone

Although not technically a biological dosimeter, polysulphone closely mimics the erythemal action spectrum which has made it a popular choice for a series of human studies.[35] For the purpose of this discussion polysulphone shall be considered as a pseudo-biological system. In reality it is a simple polymer which, upon exposure to UV, increases its absorbance in the UV region (330 nm) due to a photodegradation reaction. By measuring this increase, it is possible to determine the cumulative dose of absorbed radiation. Polysulfone, whose structure is shown in Figure 1.6, absorbs

UV light, which results in the cleavage of chain bonds leading to photodegradation of the polymer.

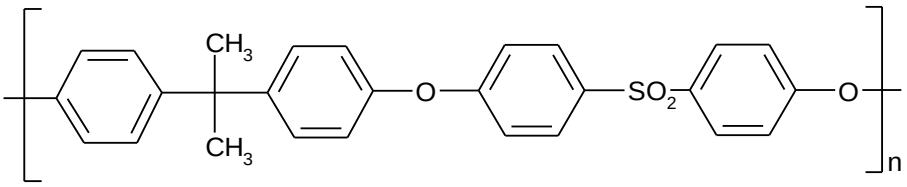

Figure 1.6 Structural unit of polysulfone

Photocleavage of the C-S bond is thought to occur first followed by removal of the methyl side groups.[36] The nature of the bond scission is such that photo-oxidation of the polymer fragments can occur. These processes cause a change in polysulfone's absorbance characteristics. As the polymer photodegrades, the absorbance at 330 nm increases.[35] By measuring this increase, it is possible to determine the cumulative dose of absorbed radiation. Polysulfone films can be calibrated using sunlight or artificial sources of UVR.

The polymer, which is normally incorporated in a badge, is particularly successful because the polymer has an initial spectral profile which resembles the spectral responsivity of human skin with respect to erythema, although not as closely as the *B. subtilus* UV dosimeter. The main practical drawback to this dosimeter is the need for a UV/visible absorbance spectrophotometer to measure the change in film absorbance, since it is outside the visible region and thus not assessable by eye (*i.e.* no distinct colour change occurs).

1.2.4.3 Other literature and patented dosimeters

In contrast to the above effective but non-real time UV dosimeters, a number of colour-based, real-time dosimeters have been reported in scientific and patent literature, some of which are listed in Table 1.7 and 1.8 respectively. The advantage

of such devices is that they provide a real-time measure of the UV dosage an individual might receive *via* a clearly perceivable colour change. However, their main disadvantage is that they often utilize UV-absorbing dyes that usually provide a poor match with the spectral sensitivity of human skin. As a result, such UV dosimeters are only appropriate when calibrated for use with a light source which has a fairly constant spectral profile. Thus, they are usually designed to work best on a clear day from mid-morning to mid-afternoon using the sun as the source of UV. That is as sunburn warning indicators, since the shape of the solar spectrum changes, with the relative level of UVA increasing with respect to UVB, particularly in the early and late hours of the day when sunburn is 'practically impossible.'[37]

Author	**Year**	**Type of Dosimeter**	**Ref**
I. Horkay *et al*.	1995	Colorimetric, silver mercury oxalate	38
A.A. Abdel-Fattah *et al*.	1997	Acidochomic, photo acid – chloral hydrate, pH dye - bromophenol blue	39
R. Rahn *et al*.	1998	Colorimetric, triiodide formation	40
J. Ramirez-Nino *et al*.	1999	Optical sensor coupled with electronic system, photodecomposition/photo-polymerisation	41
A.A. Abdel-Fattah *et al*.	2000	Acidochomic, photo acid – chloral hydrate, pH dye - thymol blue	42
S. Ebraheem *et al*.	2000	Colorimetric - redox indicator, triphenyl tetrazolium chloride	43
K. Takato *et al.*	2004	Acidochromic, photo acid- n-tosyloxy-phthalimide and propanol, acid induced ring opening of fluoran dye (3-methoxy-6-diethylamino-spiro[isobenzofuran-1(3H),9-[9H]xanthene]-3-one)	44
Andrew Mills *et al*.	2005	Colorimetric, semiconductor photocatalysis, redox dye, methylene blue	45
Andrew Mills *et al*.	2006	Colorimetric redox dye, benzyl viologen	46

Table 1. 7 Literature UV dosimeters

Inventor	**Year**	**Type of Dosimeter**	**Ref**
W. E. McKee	1965	Photochromic, 2-(2`,4`-dinitrobenzyl) pyridine	47
K. H. Sylvester *et al.*	1969	Colorimetric, redox indicator 2,3,5-triphenyl-2H-tetrazolium chloride.	48
A. Zweig	1975	Phototropic, oxazolidine and xanthenone based derivatives	49
P. Dickenson *et al.*	1987	Acidochromic, photo acid- iodinium and sulphonium ions, pH dye- bromocresol green, leuco mal-achite green, dispersal rubine, indophenol blue, N,N-bis(2-hydroxyethyl)-4-amino-azobenzene.	50
K. B. Mullis	1991 1995	Acidochrmoic, photo acid- nitro substituted aro-matic aldehyde, leuco base dye - brilliant green, aniline blue, methyl violet, crystal violet, ethyl violet, oralochite green oxalate, methyl green, erythrosin B, cresol red, quinaldine red, *p*-methyl red, metanil yellow, thymol blue, *m*-cresol purple, orange IV, phenylazoaniline, benzopurpurin 4B, bromophenol blue, congo red, methyl orange, resazurin, ethyl orange, bromo-cresol green, ethyl red, methyl red, alizarin red chlorophenol red, bromocresol purple	51, 52
P. M. Goman *et al.*	1994	Acidochromic, photo acid- *o*-nitro benzaldehyde derivatives, pH dye- thymol blue, bromophenol blue, phenol red, ethyl orange, *m*-cresol purple, lissamine green, New fuchsin, *p*-methyl red	53

Inventor	**Year**	**Type of Dosimeter**	**Ref**
K. Goudjil	1996	Photochromic, photosensitive compounds, Spirooxazines, oxazalidinospirooxazine	54
O. Faran *et al.*	2000	Photochromic, photosensitive compounds, aromatic o-nitro, azasuccinic anhydride and spiropyraan derivatives, bis imidazoles.	55
S. E. Forrest *et al.*	2002	Photochromic, photosensitive coupounds, spirooxazines, spiropyrans, fulgides, fulgimides, bisimidazoles, commercial Photosol photochromic pigments.	56
S. A Jackson *et al.*	2003	Acidochromic, organic halogens- 1,2-dibromo-tetrachloroethane, hexachloro-ethane, 1,2,4,5-tetrabromobenzene and iodoadamantane, pH dye- congo red, methyl red, methyl orange, analine blue, methyl yellow, bromocresol green, phenol red, ethyl orange, bromocresol purple.	57
G. N. Patel	2004	Acidochromic, organic halogens, chlorinated polymers, iodinium and sulfonium salts, pH dyes.	58

Table 1. 8 Patent UV dosimeters

It is clear from both the patents and papers listed above that colorimetric UV dosimeters may be categorised based on their method of operation. Some of the key groups are discussed below.

(a) Acidochromic dyes

One of the more popular UV dosimeter constructions involves the use of both a photo acid and an indicator which is sensitive to a change in pH. Such a dosimeter is

often referred to as acidochromic. In general, a species capable of undergoing a photo-induced H^+ release is combined with a pH indicator within a transparent matrix. One example of a so-called acidochromic dosimeter is reported by Abdel-Fattah *et al.*[42] Here thymol blue can act as a colorimetric UV dosimeter by effectively monitoring the UV-induced decomposition of chloral hydrate. Like most acid/base indicators, thymol blue is known to exist in equilibrium between different structural forms. The position of the equilibrium is dependent on the concentration of hydrogen ions in the surrounding environment. In the range pH 2.8 – pH 8 the thymol blue is yellow in colour while at pH levels lower than 1.2 it is red, see Figure 1.7.

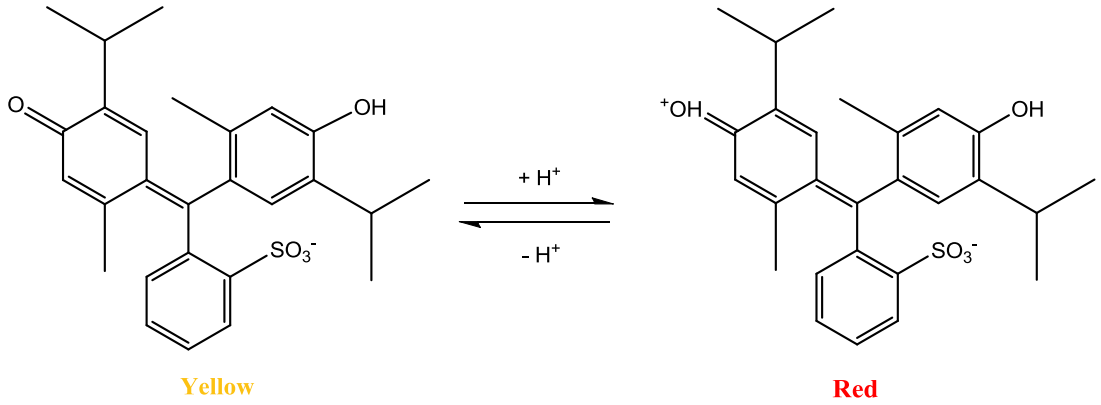

Figure 1.7 pH transition of thymol blue

In order for thymol blue to undergo a colour change, the pH within the polyvinyl butyral encapsulation polymer must be lowered. This is achieved *via* the acid releasing agent chloral hydrate which releases H^+Cl^- on exposure to UV radiation.[42] As the $[H^+]$ increases, the pH of the polymer system decreases and thus the equilibrium tends towards the more acidic form. The overall result is a film which changes colour (yellow to pink/red) when exposed to UV radiation. Abdel-Fattah has shown that the dosimeter response to UVA, UVB and UVC and the sensitivity depends on the concentration of chloral hydrate. [42] Furthermore if their dosimeter were to be 'suitably filtered' there is scope for developing a 'UV badge' for a variety of different applications. Similar UV indicators have been developed, by the same workers, with a bromophenyl blue indicator and chloral hydrate in PVB films.[39]

Other variants of acidochromic UV dosimeters utilise different combinations of pH dyes, many of which are triarylmethane dyes, particularly sulphonephthaleins and the preferred choice of acid release agent is typically a organic halide,[57,58] a *o*-nitrobenhaldehyde derivative[51-53,58] or an iodinium or sulphonium photo acid.[50, 58]

(b) Redox dyes

Mills *et al.* [45, 46] recently proposed two colorimetric dosimeters based on redox dyes. The first is a UVA dosimeter comprising a hydroxy ethyl cellulose film containing the dye methylene blue, the sacrificial electron donor triethanolamine and titania particles for use as a UV indicator and dosimeter.[43] It works on the principle of semiconductor photocatalysis, where the TiO_2 act as a photocatalyst. Thus, when the TiO_2 is exposed to UV light, electron/hole pairs are produced which then oxidise the triethanolamine, thereby providing electrons to fuel the reduction of methylene blue to its leuco form.[43] This reduction reaction is illustrated in Figure 1.8. The chemical structure of the readily oxidised triethanolamine is shown Figure 1.9.

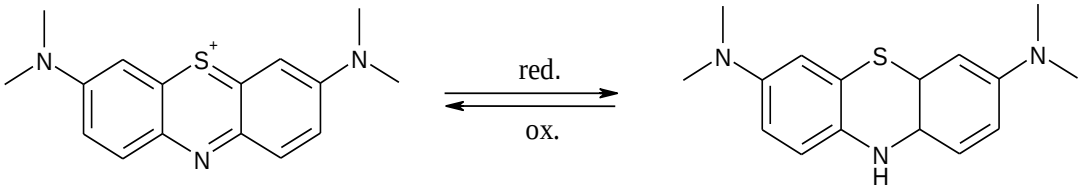

methylene blue - blue leucomethylene blue - colourless

Figure 1.8 The chemical structures of the reduced and oxidized form of methylene blue.

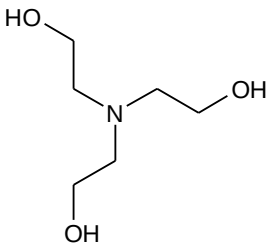

Figure 1.9 The chemical structure of the readily oxidised triethanolamine.

The film is blue prior to exposure to UV and loses its colour under the influence of UV light. Such films recover their initial colour once the source of UV has been removed, as the reaction is reversible in the presence of oxygen. Covering the indicator with an oxygen-impermeable barrier inhibits this reverse reaction and enables the film to act as a UV dosimeter. [43]

The second of Mills' dosimeters is based on benzyl viologen (BV^{2+}) encapsulated within an oxygen-impermeable polymer.[46] Upon exposure to UVR the colourless BV^{2+} becomes a photoexcited state BV^{2+*}, which in turn will photo-oxidise the encapsulating polymer, reducing itself to the highly coloured, purple benzyl viologen radical cation $BV^{+\cdot}$ as outlined in equations (1.5) and (1.6) below

$$BV^{2+} + h\upsilon \longrightarrow BV^{2+*} \quad (1.5)$$

$$BV^{2+*} + red \longrightarrow BV^{\cdot+} + ox^{+} \quad (1.6)$$

where *red* is the polymer species being reduced and *ox* is the oxidised form of *red*. The preferred polymer for this dosimeter is PVA, because of its ability to act as an oxygen barrier, preventing the oxidation of the cation radical reverting it back to the colourless starting BV^{2+}.[46] This dosimeter was evaluated with solar-simulated light at a range of different UV indices and found to have a linear relationship between the degree of colouration and irradiance level. Further work with solar light found that the dosimeter can be used as an indicator to warn the user when they are approaching

1 MED.[46] The main drawbacks are the water-soluble nature of the dosimeter coupled with the toxicity of viologens.

(c) Photochromic dye

Other colorimetric UV-detection systems more prevalent in the patent literature include indicators and dosimeters based on the colour changes of spirooxazines, benzopyrylospirans and spiropyrans. These molecules fall in the category of photochromic dyes, which undergo a structural rearrangement following exposure to solar UVR. The photoisomers produced have absorption spectra that are markedly different from the starting materials. Typically, the reactant absorbs in the UV region and as such is colourless, while the rearranged product absorbs in the visible region and is therefore highly coloured. The photochromic rearrangements of a spirooxazine and a spiropyran can be seen below in Figure 1.10 and Figure 1.11.

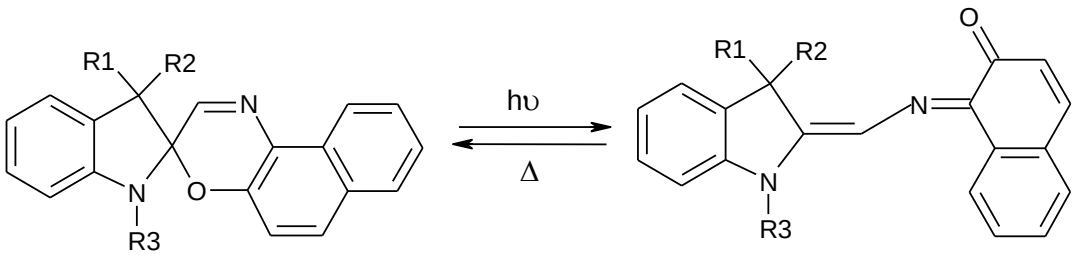

Closed form - Colourless Open form - Coloured

Figure 1.10 Photochromic Rearrangement of Spirooxazine Molecules

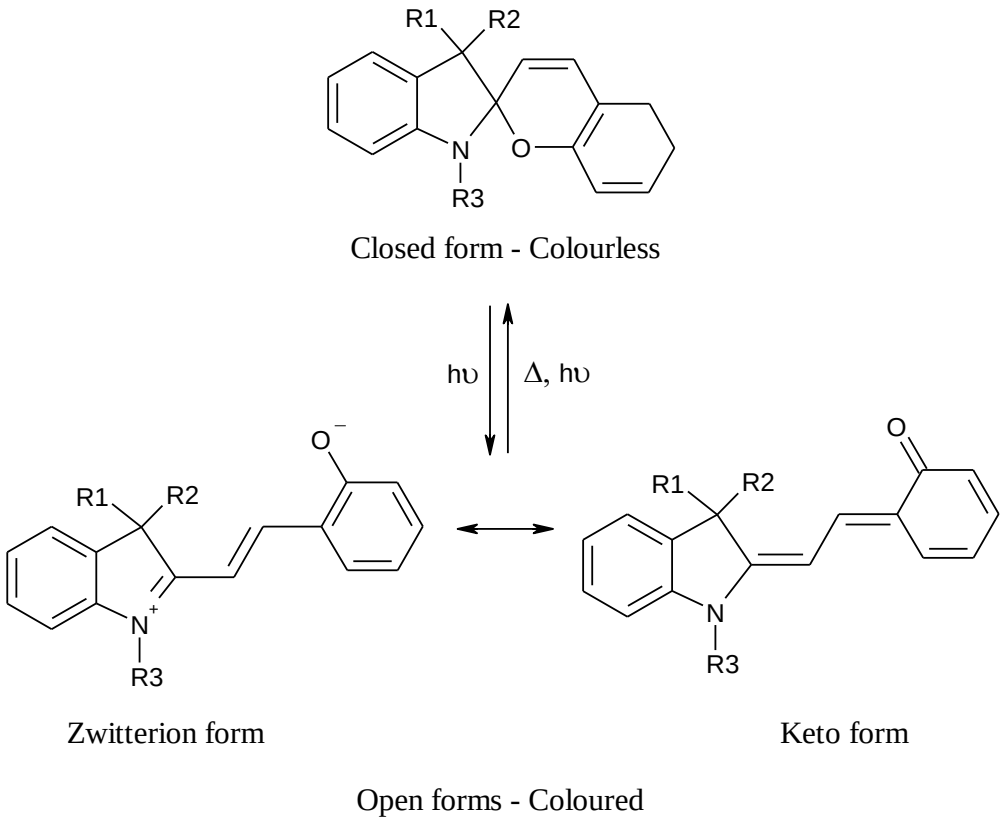

Figure 1.11 Photochromic Rearrangement of a Spiropyran

UV-induced rearrangements of photochromic compounds are on the whole reversible by thermal mechanisms, although thermally stable products can be reversed *via* photochemical means. These types of compounds have been incorporated into a clear plastic for use as a reusable dosimeter [54, 55] and as transparent films[58] for use as an UV indicator.

(d) Other colorimetric dosimeters

A novel dosimeter developed by R. Rahn *et al.*[40] makes use of the 'UVB-sensitive chromophore' iodouracil (IU) which, when in solution, forms triiodide when irradiated with UVB as outlined below.

$$IU + h\nu \longrightarrow U^{\bullet} + I^{\bullet} \qquad (1.\ 7)$$

$$2I^{\bullet} + I^{-} \longrightarrow I_3^{-} \quad (1.\ 8)$$

The occurrence of triiodide in the presence of thyodene results in the formation of the starch-iodide complex which is dark blue in colour.[40] This process can be monitored spectrophotometrically, with the degree of colouration proportional to the level of exposure. While the dosimeter responds well to UVB the main drawback of this system is that it is solution-based. As yet no steps have been taken to develop an analogous solid phase system. If this were possible, the resulting product would have a potential application as a personal dosimeter.

I. Horkay *et al.*[38] have developed a chemical UVB radiation dosimeter *vis.* SUNTEST based on the colour change of a silver-mercury(I)-oxalate suspension. The suspension, which undergoes a visible colour change from white to dark brown on exposure to UVR, is embedded within a gelatine encapsulating media which is supported on a paper strip.[38] This is attributed to the chemical reactions shown below.

$$2Hg_2(C_2O_4)^{2-} \rightarrow 3Hg + (C_2O_4)^{2-} + 2CO_2 + Hg^{2+} \quad (1.\ 9)$$

$$Hg + Ag^{+} \longrightarrow Hg^{+} + Ag \quad (1.\ 10)$$

Equation (1.9) is the photochemical reaction and (1.10) is the colouring effect. Unlike previously described dosimeters SUNTEST is predicative and can be used to estimate a maximum 'safe' sunbathing time. It is Horkay's suggestion that the user exposes the sensor for 5 minutes, after which the colour of the dosimeter is compared with a reference card.[38] Depending on the user's skin type and the degree of colouration, after 5 minutes the user will be advised of the recommended sunbathing time. This is based on the assumption that the UVI does not vary considerably during the advised sunbathing time, which may not necessarily be the case.

1.2.4.4 Commercial dosimeters

SunHealth Solutions LCC has produced a dosimeter called a SunSignal UV Sensor.[57, 59] These respond specifically to UVB radiation, and are comprised of a radiation-sensitive material including an organic halogen such as hexachloroethane, which is capable of producing at least one acidic product such as HCl, upon UV exposure, and a pH indicator such as methyl orange capable of producing a colour change in response to the UV generation of the acidic product. [57, 59] The dosimeter is originally yellow in colour and progresses though various shades of orange before finally turning red and indicating it is time to get out of the sun.

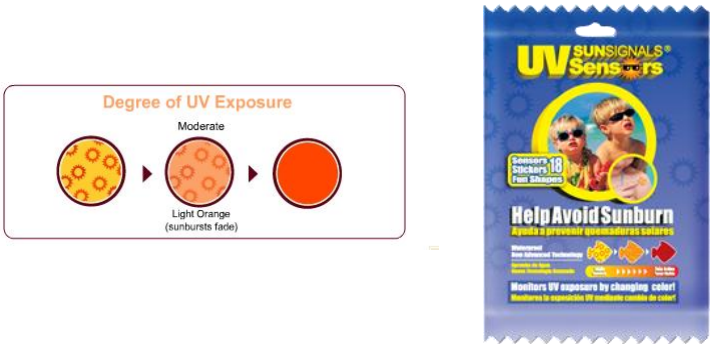

Figure 1.12 SunSignal UV sensors[60]

Another commercial product which undergoes a visible colour change is the solar wrist band developed by Solar Safe®[55] designed for people with skin type II. It comprises a polymer matrix in which a structurally photochromic material is dispersed. The wristbands are personal dosimeters which change colour upon exposure to UVR and are designed to indicate when to apply sunscreen and when it is time to get out of the sun. The wristband changes from light brown to purple upon initial exposure to UV as a result of a photochromic reaction and, over time, this species degrades and the wristband turns dark brown, indicating the need to reapply sunscreen. Prolonged UV radiation of the wristband returns it to its original light brown colour and signals sunburn is imminent.[55] The wristbands are calibrated for use with SPF 15 sun cream, hence the user is advised to apply sun cream to the

wristband when applying to their skin. It is unclear what effect if any using a higher or lower level SPF sun cream would have or whether it would still provide a warning of imminent erythema. Interestingly, others have reported on the limited applicability of photochromics as inexpensive UV indicators due to the often marked temperature sensitivity of the colour change.[61]

Figure 1.13 The proposed colour changing scheme of the Solar Safe wristband. The stages are, from top to bottom, pre-exposure to UV, initial exposure to UV, time to re-apply sun screen, and time to get out of the sun.

It is clear that simple colorimetric sensors for monitoring UV exposure are effective form of personal dosimetery. Despite the success of many of the systems discussed above, with the exception of Mills[46] and his viologen-based dosimeter, most literature dosimeter responses have not been specifically characterised with respect to erythemal dose for different skin phototypes. It is the desire of this author to introduce two novel colorimetric dosimeters containing redox dyes capable of being reduced directly or indirectly by solar UV radiation and characterise them as "sunburn warning indicators" for individuals with sensitive skin, typically skin phototype II.

1.3 Humidity indicators

1.3.1 What is humidity?

Humidity is the term used to describe the amount of water vapour in air. The most common term used is relative humidity, which is defined as the amount of water vapour in a sample of air (partial pressure of water vapour in gas) compared to the maximum amount of water the air can hold at any specific temperature (saturation vapour pressure), as in equation 1.11:

$$H = {p(H_2O)}\Big/{p^*(H_2O)^*} \times 100\% \qquad (1.\ 11)$$

where *RH* = relative humidity, $p(H_2O)$ = partial pressure of H_2O (Pa) and $p^*(H_2O)$ = saturation vapour pressure of water (Pa). It can take on values of 0 to 100%, with the relative humidity in the head space above pure water equal to 100% humidity.

Humidity can further be defined as absolute humidity, which is the quantity of water in a given volume of air, as in equation 1.12:

$$AH = \frac{Mw}{Va} \qquad (1.\ 12)$$

where *AH* = absolute humidity (g m^{-3}), *Mw* = mass of water vapour (g) and *Va* = volume of air (m^3). This value varies with changes in air pressure and temperature and consequently is not often referred to.

Humidity can also be defined as specific humidity, which is the ratio of water vapour to air in a certain volume, as in

equation 1.13:

$$SH = Mw / (Ma + Mw) \quad (1.\ 13)$$

where SH = specific humidity, Mw = mass of water vapour (kg) and Ma = mass of air (kg). The humidity values referred to throughout this review are all relative humidity (% RH) levels.

1.3.2 Why measure humidity?

In order to extend the lifetime of many foods and manufactured products, it is important to consider their storage requirements such as temperature and humidity. In the food packaging industry active moisture management is crucial to ensure the food is of the highest quality and has a good shelf life. For example, excess moisture in meat packaging can accelerate food bacterial growth, leading to spoilage. This can be combated *via* the incorporation of drip-adsorbent pads/sheets within the packaging in order to reduce the humidity and impede such bacterial growth and thus extend the serviceable lifetime of the product.[62] At low relative humidities, on the other hand, some dry grain products can undergo rapid free radical oxidation and become rancid.[62] Other foods which are detrimentally affected by gaining or losing moisture include brown sugar, raisins, cereals, jerky and fruit-filled cookies.[62] Most fruits and vegetables are composed largely of water, consequently their optimum storage conditions are typically >95% RH, T = 1-2^{o}C.[63] Thus most foodstuffs require a degree of moisture management and humidity measurement to obtain optimum storage conditions.[62]

Humidity control is important for the preservation of books, paintings and historical artefacts exhibited in art galleries and museums.[64] Materials which can absorb moisture such as wood, bone, ivory, parchment and leather can swell under high RH conditions and shrink as moisture escapes under low RH conditions, which can cause such materials to warp and crack.[64] High RH conditions also favour bacterial and mould growth, particularly on organic-based materials, and can accelerate corrosion in iron-based metal exhibits.[64] Another

area in which relative humidity monitoring is key is in the transportation and operation of sensitive electrical appliances/components which are adversely affected by high relative humidity and therefore require accurate monitoring to ensure efficient functionality. Under high RH conditions printed wiring can corrode and transistors have been known to fail.[65] Condensation within electronic components can occur at high RH which can cause localised corrosion, delamination of printed circuits, electrical shorts and can significantly degrade the performance level of the equipment.[65]

Further applications in which humidity control is important include the storage of musical instruments, e.g. wooden instruments can absorb moisture and undergo swelling and shrinkage which can cause joints to split and affect the quality of the sound. Some metals and automotive parts can tarnish or corrode under high humidity conditions so humidity control is crucial for the storage of car parts, tools and firearms. Moisture management is also vital for military operations which involve transporting humidity-sensitive components in potentially humid conditions.

1.3.2.1 Water activity

When dealing with moisture management issues it is useful to define the term water activity, a_w. This quantifiable term is the ratio based on Raoult's law expressing the relationship between the vapour pressure of a product (p_s) and the vapour pressure of pure water (P_w):

$$a_w = \frac{p_s}{P_w} \tag{1. 14}$$

a_w can have values ranging from 0.00 for an absolutely dry substance, to 1.00 for pure water and gives an estimate of the water content of the product. From this value, the equilibrium relative humidity (ERH) can be calculated:

$$ERH = a_w \times 100 \quad (1.\ 15)$$

which describes relative humidity in the headspace of products in sealed containers.[66] This value is particularly useful when dealing with natural and manufactured food products. Each food product will have a unique a_w value at which the texture and taste will be optimal. The a_w of processed foods such as cookies can be changed by the addition of sugars and sweeteners. Agrarian foods such as grains, fruit and vegetables experience different a_w values at different stages of growth. During ripening most fruit will experience a reduction in a_w as it progresses towards being fit for human consumption. This change in water activity is generally attributed to polysaccharides such a starch breaking down to mono- and di-saccharides e.g. glucose and fructose.[66] After being harvested, in order to preserve themselves, many fruits eat up these sugars.[66] The result of this is a loss of moisture which is reflected by wilting/wrinkling and a loss of crispness. This process can be retarded by increasing the RH of the storage environment; however, high RH conditions bring with them their own problems. In particular, condensation forming as a result of temperature variations can promote microbial growth and dehydrate the produce.

1.3.3 Humidity sensors/indicators

1.3.3.1 Natural humidity indicators

Many things in nature are affected by RH and as such can often be used to give an estimation of the moisture levels in the air. Pine cones are an example of this: under humid conditions the pine cone fins remain closed while in drier environments the pine cone opens up as illustrated in Figure 1.14 below.

Figure 1.14 Natural humidity indcators - pine cones

Despite this interesting feature, pine cones do not make good hygrometers, as their response is vague and not readily quantifiable. Other natural devices use catgut or human/animal hair which shrinks and swells in response to changes in RH. This is the principle behind the novelty 'weather houses' (pictured in Figure 1.15), where typically a male and female figurine on a turntable stand in their respective doorways. On rainy days when RH is high the hair twisted around the turn table absorbs water and slackens and the turntable rotates such that the man moves out of his doorway. Under dry conditions, the reverse occurs as the hair tightens, bringing the man indoors and sending the woman out. While these are a fun addition to your household they do not give an accurate quantifiable measure of RH.

(a) (b)

Figure 1.15 Natural humidity indicators (a) weather house and (b) clock hygrometer.

The developent of synthetic hair has led to the invention of simple humidity dials which operate on the same principle. These so-called clock hygrometers operate on a non-linear scale and require regular calibration to give accurate RH meaurements.

1.3.3.2 Electronic sensors

There are a wide range of commercial products currently available for monitoring humidity. These are more often than not electronic hygrometers based on capacitive or resistive systems which measure the change in conductivity of a polymer or ceramic film at different relative humidity levels.[67] Capacitive humidity sensors are widely used in industrial, commercial and weather telemetry applications and typically consist of a substrate (glass, ceramic or silicone) between two conductive electrodes, which has been coated with a thin layer of metal oxide or polymer.[68] Changes in the relative humidity of the surrounding environment cause an almost directly proportional change in the dielectric

constant of the capacitor.[68] A commercial example of this is the hand-held HI 9564 thermo-hygrometer by Hanna instruments, which is a thin-film polymer capacitance humidity sensor, pictured below in Figure 1.16 (a).

Resistive humidity sensors on the other hand operate by measuring the change in electrical impedance of a hygroscopic medium such as a conductive polymer or salt.[68] Such sensors usually contain a noble metal electrode deposited on a substrate coated with the hygroscopic medium. At high relative humidities the hygroscopic medium absorbs water, causing dissociation of ionic functional groups which increases the conductivity.[68] A hand-held device which utilises a resistive polymer sensor is the Cotrol Company's Traceable® Hydrometer, pictured below in Figure 1.16 (b). Both of these systems have limitations in their operating conditions and can be expensive and bulky to use.[69, 70]

(a) (b)

Figure 1.16 Electronic humidity sensors (a) capacitive and (b) resistive hydrometers.

While electronic humidity detection techniques have their uses, they do have certain drawbacks. As they are reliant on electrical signals they are subject to interference, they involve complex data collection processes and require bulky display units.

1.3.3.3 Colorimetric indicators

For some time now there has been a move towards the development of simple optical sensors which undergo a colour change at a specified RH level. A survey of scientific and patent literature reveals a great variety of such indicator systems, some of which are listed in the tables below.

Author	**Year**	**Type of humidity indicator**	**Ref**
R. A. McGill *et al.*	1992	Solvatochromic, Reichartd's dye	71
S. Otsuki *et al.*	1995	Ionic dyes, aggregation, methylene blue, rodamine 6G	72
R. Matsushima *et al.*	2002	Ionic dyes, aggregation, 7-diethylamino-4`dimethylaminoflavylium perchlorate, methylene blue, thionine	73
P. R. Somani *et al.*	2001	Protonation/deprotonation, charge transfer complex, crystal violet	74
R. Matsushima *et al.*	2003	Ionic dyes, aggregation, 7-diethylamino-4`dimethylaminoflavylium perchlorate, thionine	75
R. Shinozaki *et al.*	2004	Ionic dyes, aggregation, rhodamine 6G	76
M. A. Zanjanchi *et al.*	2005	Protonation/deprotonation, methylene blue, zeolites	77
M. Kleeman *et al.*	2005	Solvatochromic, Reichartd's dye	78
A. Tsigara *et al.*	2006	Anhydrous salts, cobalt (II) chloride	79

Author	**Year**	**Type of humidity indicator**	**Ref**
J. Kunzelman *et al.*	2007	Self-assembly of chromogenic dyes, oligo(p-phenylene vinylene)	80
S. Sohrabnezhad *et al.*	2007	Protonation/deprotonation, new methylene blue, zeolites	81
J. Shi *et al.*	2008	Photonic crystals, band gap shift, rose bengal	82
E. Tian *et al.*	2008	Photonic crystals, band gap shift, Polyacrylamide	83

Table 1. 9 Literature colorimetric humidity indicators

Inventor	**Year**	**Type of humidity indicator**	**Ref**
M. G. Snelling	1937 1941	Deliquescent /hygroscopic material, water soluble dye, pH dye, chemical reactions, irreversible, phosphorous pentachloride, zinc chloride, calcium chloride, calcium nitrate, ammonium nitrate, ammonium chloride, urea, urea nitrate, dextrose, sodium nitrate, copper nitrate, potassium nitrate, phenolphthalein, acid and alkaline reagents.	84, 85
P. B. Davis	1949 1950 1952	Anhydrous salt, cobalt phosphate, cobalt sulphate, cobalt bromide, copper bromide, zinc chloride, cobalt (II) chloride	86-93
S. D. Price	1964	Anhydrous salt, cobalt (II) iodide	94
D. L. Fuller	1977 1979	Anhydrous salt, cobalt thiocyanate, fluorescent markers	95, 96

Inventor	**Year**	**Type of humidity indicator**	**Ref**
W. O. Krause	1970	Dual anhydrous salt, cobalt acetate, cobalt bromide, acetate salts, bromide salts	97, 98
R. K. Stewart *et al.* (Humidial/Sud-chemie)	1988	Dye coated deliquescent/hygroscopic materials, irreversible, alkali salts, brilliant orange	99
J. F. McBride	1990	Anhydrous salts, cobalt (II) halides, copper and nickels, chloride and sulphate.	100
J. S. Haswell	1996	Anhydrous salt, cobalt chloride	101
E. Wroth *et al.*	1999	Anhydrous salt, cobalt chloride	102
M. Martin *et al.* (Humidial/Sud-chemie)	1999	Anhydrous salt, cobalt chloride	103
M. Gattiglia *et al.*	2002 2003	Anhydrous salt, synergistic and/or hygroscopic salts, copper (II) halides, alkali and alkaline earth metal salts, organic dyes	104, 105
S. O. Dick *et al.* (Sud-Chemie)	2004 2005	Anhydrous salt, cobalt chloride, Deliquescent /hygroscopic material, coloured blotting sheet, irreversible, Zinc halides nitrates and sulfates, Lithium halides, alkali/alkaline earth salts,	106-108
M. Hamada	2007	Anhydrous salt, modified cobalt chloride, polyethylene glycol	109
Y. Yamakawa	2008	Anhydrous salt, cobalt chloride	110

Table 1.10 Patent colorimetric humidity indicators

It is clear from the tables above that humidity indicators can be readily categorised into several distinct groups, each of which shall be discussed in greater detail below.

(a) Anhydrous inorganic salts

There have been a vast number of proposed colorimetric humidity indicators, the majority of which are based on the use of an inorganic salt,[86-98, 100-105, 107, 109-111] in particular cobalt(II) chloride, $CoCl_2$, which at a defined RH level (typically RH 40%) converts from its anhydrous form to its hydrated form. This process is marked by a colour change, in the case of $CoCl_2$ blue (anhydrous) to pink (hydrated). It is possible to tailor the sensitivity of this type of indicator to suit the desired application by one of three methods:

- Changing the concentration of the inorganic salt[109]
- Adding a deliquescent/hygroscopic synergic salt[93, 104, 105]
- For systems with a silica support, altering the drying and activation temperatures of the dyed silica[86]

Changing the [$CoCl_2$] for example, can be achieved by increasing or decreasing the amount of salt that is used to dope the encapsulating media. Alternatively, by adding compounds such as polyethylene glycol to the indicator support, it is possible to reduce the relative concentration of $CoCl_2$.[109] Regardless of the method, increasing [$CoCl_2$] enables the colour change to occur at a lower level of RH, while decreasing the [$CoCl_2$] increases the RH level required to drive colour change.[109]

The addition of deliquescent chlorides including $ZnCl_2$, $MgCl_2$, NaCl, KCl and LiCl can be used to alter the RH level at which the $CoCl_2$ (or equivalent anhydrous salt e.g. $CuCl_2$) changes colour.[93, 104, 105] This is due to the synergic effect of mixing the $CoCl_2$ with hygroscopic salts which deliquesce at different

RH levels (e.g. $MgCl_2$ at RH >33%). Not only do the additions of such synergic hygroscopic salts at different levels result in a range of RH sensitivities, they also increase the chromatic contrast of the colour change, making it a more visually striking indicator.[93, 104, 105]

For inorganic salt indicators which have a silica/silica-gel support, it is also possible to modify the RH response level by altering the conditions under which the indicator is fabricated. Typically this involves changing the drying and activation temperature of the dye-coated silica, which enables indicators to undergo the step colour change at a range of different RH conditions.[86]

Such humidity indicators have been proposed for a variety of applications including refrigerated systems,[97,98] clothes dryers,[100] shoe storage,[102] desiccant absorbent capacity indicators[104,105,109] and the storage of electronic devices,[110] and are usually reversible by heating the hydrated salt to regenerate the anhydrous starting material. A typical commercial form based on $CoCl_2$ is the Humitector® Humidity Indicator Card from Süd-Chemie Inc., US (FKA United Desiccants/ Humidial).[99,103,106-108,112] These are small paper cards, some of which are pictured in Figure 1.17 below, designed to indicate the level of RH (0 to 95% RH) by colorimetric means. Süd-Chemie Inc. produces both reversible and irreversible indicators for a range of applications including conservation of historical artefacts in museums, metals, semiconductors, electronics and military components.[112] The main drawback of these indicators is the toxicity of $CoCl_2$ to humans *via* ingestion rendering them unsuitable for use as humidity indicators for food packaging.

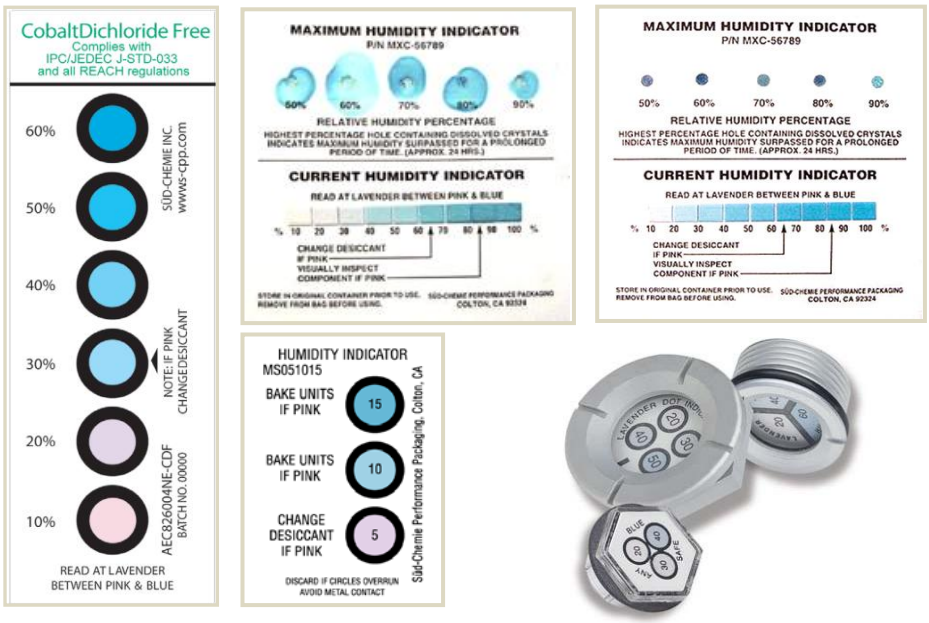

Figure 1.17 Süd-Chemie humidity indicator cards

(b) Solvatochromic dyes

The highly solvatochromic dye Reichardt's dye (RD), when incorporated in the polymer polyvinyl acetate (PVAc), undergoes a reversible, linear shift in absorption maximum as a function of relative humidity, and thus has a potential application as a humidity sensor.[71] R. A. McGill *et al.* demonstrated that under dry conditions (0% RH) the RD/PVA film is green (λ_{max} = 714 nm) but at high relative humidity (100% RH) it absorbs water, its maximum absorbance peak undergoes linear hypsochromic shift in wavelength (λ_{max} = 600 nm) and is blue in colour.[71] A typical RD/PVA film takes around 3 minutes to wholly change colour in the presence of 100% RH air, and is fully reversible with films recovering in 4 minutes at 0% RH under dry nitrogen.[71] A similar effect has been observed for RD in polyvinyl pyrrolidone (PVP) and to a lesser extent in polyvinyl chloride (PVC) and polymethyl methacrylate (PMMA).[71]

(c) Dyes and deliquescent agents

A number of irreversible systems have been reported which utilise a deliquescent material.[84,85,106,108] Such systems function as a result of the deliquescent material absorbing water from the atmosphere to dissolve itself completely and become a liquid. In one system the liquefied agent runs on to a water soluble dye (e.g. Acid Green, Methylene Blue, Methyl Violet), dissolving the dye and carrying it by capillary action through a porous medium to the indicator viewing area, generating an irreversible colour change.[84,85] Alternatively, the colourless deliquescent material can be housed within the holes of a supporting medium mounted on a coloured absorbent material.[106,108] Thus, the holes of the support material appear white, until deliquescent materials in the holes liquefies and is absorbed by the coloured absorbent sheet, consequently the colour of the absorbent sheet shows through the holes in the carrier support.[106,108] By using salts which deliquesce at different RH levels, e.g. $CaCl_2$ at >45% RH, $Ca(NO_3)_2$ at >65% RH, $NaNO_3$ at >75% RH and KNO_3 at >95% RH, these irreversible RH indicators can be tailored to respond to specific RH levels. An indicator of this kind is useful for determining the maximum humidity/humidity history rather than the current humidity levels. Such an indicator would be useful for monitoring humidity conditions when transporting sensitive electronic components, as it will indicate whether they have been exposed to damagingly high levels of RH, even for a short period of time and even if the RH level drops to a safe level when the components are checked at a later time.

(d) Photonic crystals

In more recent years there has been a growing interest in photonic crystals for use as humidity indicators. Photonic crystals are the optical equivalent of semiconductors. They are periodic structures, and just as semiconductors have energy bandgaps which dictate the movement of charge carriers, photonic crystals are dielectric structures with bandgaps, which forbid the propagation of certain frequency ranges of light. These bandgaps arise from areas of low refractive

indices. E. Tian *et al.* reported a photonic crystal hydrogel, which undergoes a reversible step colour change across the whole visible spectrum.[83] The device works by combining the humidity-sensitive polyarcylamide with the PC P(St-MMA-AA) which provides luminious colour ranging from violet at 20% RH through to red at 100%.[83]

(e) Ionic dyes

Ionic dyes such as thiazine salts have been used as colorimetric RH humidity indicators. S. Sohrabnezhad *et al.*[77, 81] report that both methylene blue (MB) [77] and new methylene blue (NMB), [81] the chemical structures for which are shown in Figure 1.18, when incorporated within zeolite act as humidity sensors, changing colour from blue-violet when dehydrated to blue when hydrated. The colour change is attributed to the protonation of MB during the dehydration of the zeolite by protons generated by the dissociation of water during the drying process.[77] The fully hydrated MB/zeolite spectrum consists of two main bands at 650 and 600 nm.[77] The 650 nm band is associated with the monomer and the 600 nm band with the dimer aggregate.[77] Also present at very low intensity is a peak at 754 nm which arises as a result of a small amount of the MB undergoing protonation i.e. from MB^+ to HMB^{2+}.[77] Following dehydration the peaks at 600 nm and 650 nm are substantially diminished and the peak at 754 nm is greatly increased.[77] Both dyes give a linear response over 10 to 90 % RH.[77, 81]

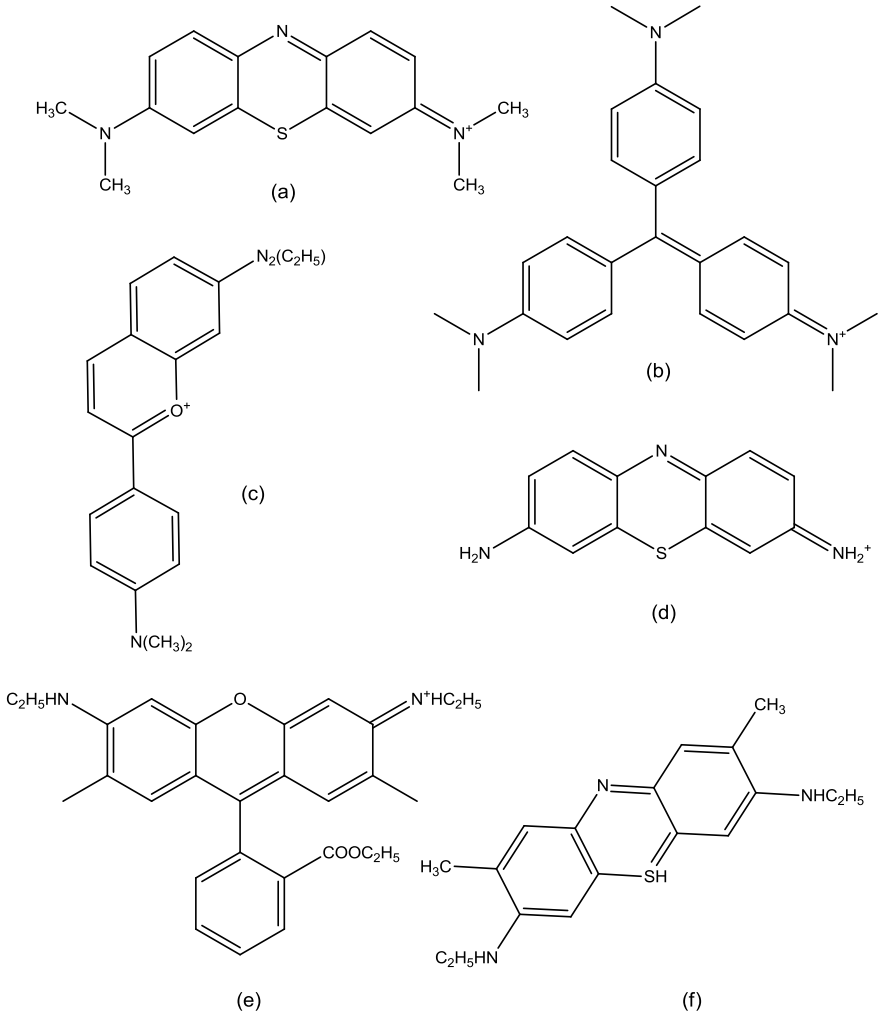

Figure 1.18 The chemical structures of (a) Methylene Blue (MB), (b) Crystal Violet (CV), (c) 7-dethylamino'-methylamionflavylium (FV), (d) Thionine (TH), (e) Rhodamine 6G (R6G) and (f) New Methylene Blue (NMB).

A similar effect is observed by Somani *et al.* by crystal violet (CV) and MB incorporated within polyvinyl alcohol (PVA) and phosphoric acid (H_3PO_4).[74, 113] PVA/H_3PO_4 is a well known solid polymer electrolyte and a good proton conductor. It is also acidic, allowing the dye to exist in its protonated form, which for CV is yellow in colour at low RH. At high RH levels the film absorbs water, and the increase in water content causes the film to become less acidic, thus deprotonation of the CV occurs, which is marked by a colour change from

yellow to purple. Similar humido-chromic effects have also been shown by other dyes such as MB.[74, 113]

As alluded to above, certain ionic dyes at high enough concentrations are known to undergo aggregation to form dimers and some in some cases higher aggregates. As a result of this concentration-dependant phenomena such dyes have been used as humidity indicators. Among those commonly encountered are Rhodamine 6G (R6G) and MB, whose structures are shown in Figure 1.18. Both R6G and MB have been incorporated within poly(n-vinylpyrrolidone) (PVP) films by S. Otsuki *et al.*[72] to create simple reversible RH indicators based on the effect of moisture on the formation of dye aggregates. Under dry conditions the thin films of MB/PVP the MB exists predominantly in its monomeric form as illustrated by the broad UV/visible absorption at 668 nm and a smaller dimer shoulder peak at 620 nm .A similar effect is seen for the analogous R6G/PVP films. Otsuki rationalises this behaviour by proposing that changes in the RH humidity of the film affect the polarity of the polymer micro-environment increasing the films ability to support the formation of dye aggregates at increasing RH levels.[72] Otsuki also suggests the formation of water clusters at higher RH may result in the dyes (both of which are very soluble in water) concentrating in the water cluster regions may be a contributing factor.[72]

More recently, Matsushima *et al*. have proposed using thiazine (TH) and flavylium perchlorate (FC) salts (dye structures for which are shown in Figure 1.18) in agar and carrageenan gels as simple colorimetric humidity and temperature sensors.[73, 75, 114] These salts exhibit reversible colour changes from purple (dry) to red (humid) as a result of a change in RH. This has been attributed to the absorption of water vapour by the gel in humid conditions which encourages the dye to form dimers and so leads to a shift in λ_{max} absorbance ($\approx$ 20-30 nm) to a lower wavelength. The explanation offered by Matsushima for the dye's tendency to form dimers under high RH conditions is that water has the

potential to stabilise the aggregates of charged dyes as a result of its high dielectric constant and hydrogen bonding capabilities. Consequently, the TH and FC dimers are more stable than the monomer equivalents in the presence of water vapour.[73] Matsushima also reports similar behaviour for a MB-doped film.[73]

It is the desire of this author to expand on this work by investigating the behaviour of methylene blue in a polymer with and without urea (a deliquescent material) as an additive and its potential application as a humidity-indicating device.

1.4 Ammonia and volatile amine sensor for fish freshness

1.4.1 Food safety

In recent years a number of cumulative factors have combined to reinforce the need for improved food safety measures. The last 30 years have seen several food crises including bovine spongiform encephalopathy (BSE), foot and mouth disease and more recently bird flu. As a result there is a need to rebuild consumer confidence and provide reassurance of food safety.[115] In 2002 the European parliament published regulation (EC) no 178/2002, which discussed the importance of food 'traceability' stating that 'food operators shall be able to identify any person from whom they have been supplied with a food'. This idea of the 'harvest to home' history of food is designed to ensure that all food products are compliant with food safety standards by generating a 'chain of responsibility'.[115]

One industry which has remained unaffected by the above-mentioned food crises is the fishing industry. Fish is a good source of protein providing many nutritional and health benefits. Rich in vitamins (A, B_3, B_6, B_{12}, E and D), minerals (Ca, Fe, Se and Zn) and omega-3 polyunsaturated fatty acids (PUFA), fish has many associated health benefits some of which are outlined by K. S. Sidhu in his review article.[116] The benefits include lower risks of coronary heart disease due to the omega-3 PUFA, which can lower cholesterol and blood pressure and reduce the risk of strokes, cardiac arrhythmia, rheumatoid arthritis, Alzheimer's, depression and certain types of cancer.[116] Furthermore, the NHS recommendation of two portions of fish or shellfish a week has made fish a popular choice among consumers. Seafood, both shellfish and fish, are however highly perishable commodities, and thus it is important to ensure that the consumer is receiving fresh produce.

1.4.2 Evaluation of fish freshness

1.4.2.1 Sensory

At present all fish and shellfish are evaluated at fish auctions by trained specialists *via* sensory methods. Each fish is examined and scored on a series of properties, given an overall grade (E, A, B or C) and an estimated shelf life. The table below outlines some of the features considered when evaluating the freshness of a typical white fish e.g. Cod.

Feature	**Characteristics (fresh (grade E) ⟶ spoiled (grade C))**
Skin	Bright, shiny, iridescent, waxy, dull, gritty
Outer slime	Transparent, milky, grey, yellow, brown
Eyes	Convex, plane, concave, sunken
Gills	Dark red, red/pink, brown/grey, brown
Gills (odour)	Fresh, seaweedy, odourless, musty, amine

Table 1.11 Multilingual guide to EC freshness grades for fishery products, FSD research station MoAgr, fisheries and food, Aberdeen, 1992.[117]

After classifying the fish is given an estimated shelf life as a guide to the consumer. This works well for the initial evaluation but requires a trained individual to carry out the evaluation and the predicted shelf life assumes that the fish is being stored under appropriate conditions e.g. on ice or refrigerated etc.

1.4.2.2 Physical properties

Alternative methods for determining the quality of seafood include measuring the physical properties of the food sample, in particular the electrical conductivity and texture. The former can be achieved using a differential electrode system like the Torrymeter from Distell, pictured below in Figure 1.19, as after death the membranes within the muscle tissue begin to degrade as the fish spoils.

Figure 1.19 A Distell Torrymeter for fish freshness determination

This in turn affects the impedance of the fish. This technique correlates well with the sensory methods, however usually requires the skin to be attached and thus is only suitable for whole fish samples and not filleted fish. J. Y. Lee and his group at the National University of Singapore have proposed an alternative method for determining the freshness of fish samples based on the their dielectric properties.[118] Lee *et al.* have investigated the correlations between degree of fish spoilage and dielectric properties using Electrochemical Impedance Spectroscopy (EIS) and have successfully demonstrated that their method can be used to classify fish sample into one of 4 categories *viz.* 'fresh, semi-fresh, semi-deteriorated and deteriorated.'[118] This method, while simple and easy to execute, suffers from the same drawback as the Distell torrymeter as it has only been tested for whole fish samples with the skin still attached.

Changes in texture can be monitored by taking force deformation readings over a period of time to generate force deformation curves. These curves can in turn be

used to determine the firmness of the fish, a property which is directly related to the freshness of the fish.

1.4.2.3 Biochemical

The quality of a fish sample can also be determined *via* biochemical methods. Most notable is measuring the extent of adenosine triphosphate (ATP) deterioration. Post mortem ATP is rapidly enzymatically converted to inosinemonophosphate (IMP) (typically complete within 1 day of catch), which over time breaks down to form inosine and hypoxanthine (typically complete within 20 days of catch). ATP levels are characterised by the K values where:

$$K = \frac{[inosine] + [hypoxanthine]}{[inosine] + [hypoxanthine] + [other\ ATP\ metabolites]} \qquad (1.\ 16)$$

K values correlate well with the sensory methods and are generally very reliable. They are however somewhat problematic in that they are dependent on a wide range of variables including species, time since catch, storage and handling conditions and temperature.

1.4.2.4 TBV-N

After fish are caught and killed, micro-organisms present on the skin and scales known as specific spoilage organisms (SSO) gradually increase.[115] The SSO produce ammonia and volatile amines including trimethylamine (TMA) and dimethlyamine (DMA) from the amino acids present in the fish as the fish begins to spoil. These microbial degradation products are collectively known at total volatile basic nitrogen (TVB-N). As part of the EU Directive 95/149/EC these volatile amines are legally defined as indicators of seafood spoilage and maximum limits of TVB-N are defined for different categories of fish.

A review of scientific and patent literature reveals an array of different techniques used to monitor TVB-N for industrial fish freshness testing some of which are listed in Tables 1.12 and 1.13 below. Also included, in Table 1.14 are analogous sensors used to detect ammonia and volatile amines for industrial applications but which could be/have been adapted for use as food quality indicators.

Author	**Year**	**Sensor Type**	**Ref**
A. Paquit *et al.*	2008	Freshness Indicators, for Food Packaging, colorimetric, pH indicators, cresol red, phenol red, neutral red, cellulose, PET, TBV-N, Cod	115
A. Pacquit *et al.*	2007	Smart packing colorimetric sensor, pH indicator bromocresol green, polymer, PET, TVB-N, Cod & Whiting	119
A. Pacquit *et al.*	2006	Chemical barcode, colorimetric, pH indicator, bromocresol green, cellulose, polytetrafluoroethylene, reflectance colorimeter, real-time, ammonia 1-15 ppm, TBV-N, Cod & Roundhouse Grenadier	120
A. Pacquit	2004	Chemical barcode, colorimetric, pH indicator, bromocresol green, polymer, 1-15 ppm ammonia, TVB-N, Cod, real-time	121
L. Byrne *et al.*	2002	pH indicator, cresol red, cellulose/PET films, TVB-N, Cod & Orange roughy	122
L. Pivarnik	2001	Ammonia Ion Selective Electrode for fish freshness trimethylamine and TBV-N, Monkfish, Whiting, Summer Flounder, Mackerel, Tilefish, Blue fish	123

Author	**Year**	**Sensor Type**	**Ref**
M. Loughran *et al.*	2000	Acidochromic, monoazophenylnitrophenol calix[4]arene, fliter paper discs, fibre optic, TVB-N, Whiting and Cod	124
A. Lobnik *et al.*	1998	Fluorescence, aminofluorescein, ormosil –based sol-gel , tetramethoxysliane, dimethyldimethyoxsiloxane, diphenyldimethoxysilane, dissolved ammonia, 0 – 20 ppm	125

Table 1.12 Fish freshness indicator papers.

Inventor	**Year**	**Sensor Type**	**Ref**
J. R. Williams	2006	Food Quality Indicator (FQI), colorimetric, (pH azo, xanthene, triarylmethane dyes), food packaging, fresh and frozen	126
J. R Williams	2005	Indicator for detecting food spoilage, colorimetric Natural compounds (Betalaines, flavinoids)	127
D. Wallach	2002	Colorimetric/Fluorometric, volatile amines, carbon dioxide, Food spoilage	128
D. W. Miller	1999	Food quality indicator, colorimetric (azo dyes and pH indicators),Volatile bases, pork, meat, fish freshness, fresh and frozen	129

Table 1.13 Fish freshness indicator patents.

Author	**Year**	**Type of Sensor**	**Ref**
C. J. Lui *et al.*	2007	Optical amine sensor, colorimetric Coordination of amine to Zinc complex	130

Author	**Year**	**Type of Sensor**	**Ref**
K. I. Ober	2006	pH indicator, Bromocresol Green, dyed silica microspheres Tertybutyl amine, DEA, TEA, Pyridine and analine, 0-2 ppm	131
C. J. Lui *et al.*	2005	Chromogenic calixarene, nitrophenylazo-calix-[4]arenes, spun films, amine vapours 0-800 ppm	132
K. T. Lau	2004	Berthelot's reaction, dissolved ammonia, 0 – 10 ppm	133
W. Qin *et al*	2003	Monomer/ dimer equilibrium, indium(III)octaethylporphyrin hydroxide, ligation of amines, polyvinylchloride film, TEA, 0-200 ppm	134
G. E. Khalil	2001	Fluorescence, aminofluroscene, ormosil sol-gel, dissolved ammonia 1-10 $\mu g\ ml^{-1}$	135
T. Yagi	1997	Fibre optic sensor, colorimetric (pH indicator) Gaseous Ammonia	136
T. Grady	1997	Optical evanescence wave sensor, calixarene Colorimetric, Fibre optics	137
C. Perininger *et al.*	1996	Fluorescence, rhodamines, ethylcellulose, polyvinylchloride, polyvinyl acetate, dissolved ammonia, 0 - 10 $\mu g\ ml^{-1}$	138
A. Mills	1995	Plastic colorimetric indicator films pH Gaseous ammonia sensors	139
N. Nakano	1994	Colorimetric, pH indicator Monitoring tape, Rose Bengal, Phloxine B, Eosin Y, 0-1 ppm Ammonia	140
R. A. Potyrailo	1994	pH indicator, Bromocresol purple, poly(methylphenylsiloxane), portable photodiode sensor, ammonia 50-200 mg m^3	141

Author	Year	Type of Sensor	Ref
Q. Zhou *et al.*	1989	pH indicator, bromocresol purple, porous plastic fibre optic gas sensor, methyl methacrylate and triethylene glycol dimethylacrylate, ammonia, 0-100 ppm	142
M. R. Shahriari	1988	pH indicator, bromocresol purple, porous alkali borosilicate glass fibre optic gas sensor, ammonia 0-3 ppm	143
P. Caglar	1987	pH Indicator, bromothymol blue, polymer fibre optic probe, amberlite XAD-7, ammonia headspace, 1.5 - 6.0 $x10^{-3}$ M	144

Table 1.14 Ammonia and volatile amine sensor papers

These TBV-N and volatile amine sensors can be broadly split into several different categories which are discussed in more detail below.

(a) Calixarenes

Ammonia and amines have the ability to partake in guest-host interactions, this feature can be exploited when designing optical sensors. Calix[n]arenes are cyclic oligmers which are often described as 'vase-like' in appearance. They are 3D cone-shaped organic structures as illustrated in Figure 1.20 below and have internal cavities capable of hosting ions or small molecules including amines.

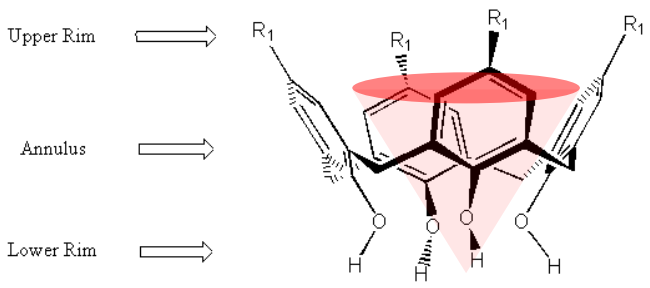

Figure 1.20 Diagramatic representation of a calixarene structure.

By varying the number of repeating units, [n], and the substitutes on the upper and lower rim, the volume of the cavity can be tailored to accommodate the target analyte. C. Wang and his group used this feature to design a piezoelectric quartz crystal (PQC) sensor array for the detection of volatile amines.[145] Based on para-*t*-butylcalix[n]arens (n=4, 6, 8) and mercaptoacetic acid bilayers immobilised on a PQC. When volatile amines undergo guest – host interactions with the calix[n]-arenes the resonance frequency of the PQC is reduced. It is possible to use a series of these modified PQC to create an array for use with binary mixtures. Wang claims that the sensors are easy to reproduce and are highly selective for organic amines, however they lack the desired feature of a visible colour change.[145]

By using selected R groups containing chromaphores it is possible to create chromogenic calixarenes which can be used as colorimetric indicators. Examples of chromogenic calixarenes for ammonia and amines include those developed by T. Grady *et al.,*[137] M. Loughran *et al.*[124] and C. J. Lui *et al*.[132] The first of these is comprised of a PVC film containing nitrophenylazophenol calix[4]arene which is coupled to a fibre optic probe to allow remote detection. The film undergoes a colour change shift from yellow to red in the presence of ammonia.[137] Grady has attributed this observation to deprotonation of the chromogenic nitropheny-lazophenol by the ammonia as it enters the calixarene cavity.[137] The resulting phenolate anion is stabilised by the newly generated conjugated π orbital system, causing a red shift in the λ_{max}. Grady has also demonstrated the sensitivity of the sensor to ammonia can be readily varied by introducing a lithium counterion (Li^+).[137] This work was furthered developed by Loughran who using the closely related monoazophenolnitrophenol calix[4]arene impregnated in filter paper created an analogous sensor for evaluating fish freshness.[124] Loughran's sensor responds to TVB-N and may be used to generate a 'response spectrum' for fish to estimate the shelf life. Liu has developed a similar sensor for amines, in particular hexylamine, based on thin-spun films of nitrophenolazo-calix[4]arenes.[146]

(b) pH indicators

By far the most popular approach when designing a colorimetric ammonia/amine/ fish freshness sensor is to employ a pH sensitive dye which will change colour in the presence of a basic gas(es). Sensors are constructed using dyes in their neutral or acidic form which on exposure to ammonia or volatile amines are deprotonated and converted to their basic form. Work carried out previously within the group involved the preparation and characterisation of three thin plastic film sensors for gaseous ammonia.[139] The dyes used belong to the class of molecules known as triarylmethanes, more specifically sulfonephthaliens, the general structure of which is shown in Figure 1.21 along with other common pH indicator frameworks.

Each dye was encapsulated within a plasticized ethylcellulose polymer matrix, and used to generate ammonia sensor films which yielded a reproducible and reversible response to ammonia vapour. The sensitivity of each film varied according to the pKa value of the indicator, with bromophenol blue (pKa = 4.1) the most sensitive, followed by bromocresol green (pKa = 4.9) and chlorophenol red (pKa = 6.25) the least sensitive. The sensitivity is further affected by the operating temperature, decreasing at higher temperature. Despite this drawback, the films remain unchanged and active after prolonged periods of storage and have great potential for use as ammonia sensors.

A review of the literature reveals a series of similar sensors as outlined previously in Table 1.14, which vary in the dye of choice e.g. other sulfonephthaleins such as bromocresol purple or bromothymol blue, or fluorscein based dyes including Rose Bengal, Phloxine B, Eosin Y, and in the encapsulating media. Such indicators are typically based on intelligent inks and indicating solutions.[140, 142-144] These are usually dyes dissolved in polymer solutions[141] or solvents.[142, 144-146] The resulting inks and solutions can be cast as thin films[141] or integrated within a support matrix such as a porous tape[140] or optical fibres.[144-146] All operate under the same principle and act as simple visual indicators for ammonia and volatile amines.

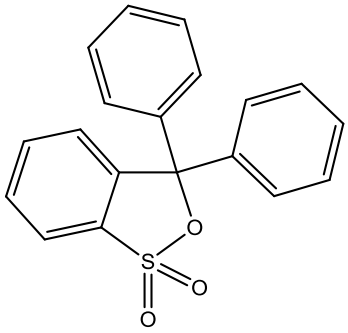

(a)

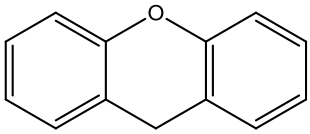

(b)

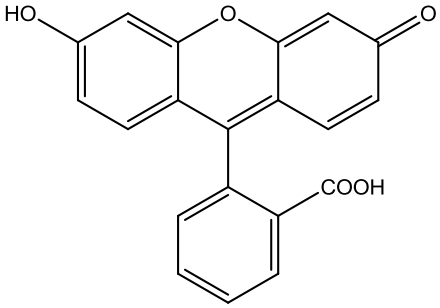

(c)

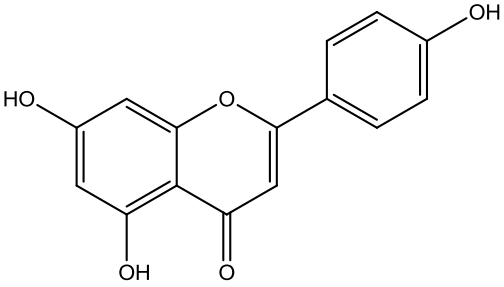

(d)

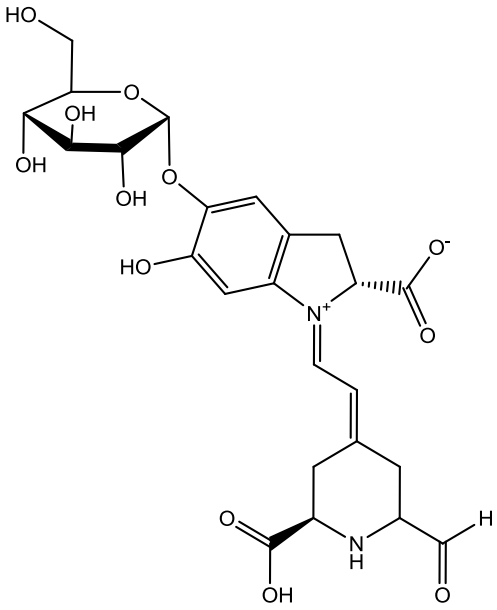

(e)

Figure 1.21 Chemical structures of (a) sulfonephthalein, (b) xanthene, (c) fluorescein, (d) flavone and (e) betanin.

Similar sensors have been designed specifically for detecting the ammonia and volatile amines associated with fish spoilage i.e. TBV-N.[119-122, 124, 127-129] Among those leading the research is D. Diamond, the principle investigator of the Adaptive Sensors Group (ASG) and his colleague and A. Pacquit of Dublin City University.[119-122,124] Their fish freshness sensors are cellulose-based films containing pH responsive indicators, cast on either polyethylene terephthalate (PET) or filter paper.[119-122, 124] These dyes are typically sulfonephthaliens and are yellow in colour in their acidic form. On exposure to TVB-N generated as a result of fish spoilage the sensors typically turn red or blue in their basic form depending on the dye.[119-122, 124] One such sensor, described as a 'chemical barcode for real-time monitoring of fish freshness,' uses the pH indicator bromocresol green, whose chemical structure is shown in Figure 1.22, in a polymer film coupled with a LED based reflectance colorimeter.[119, 120]

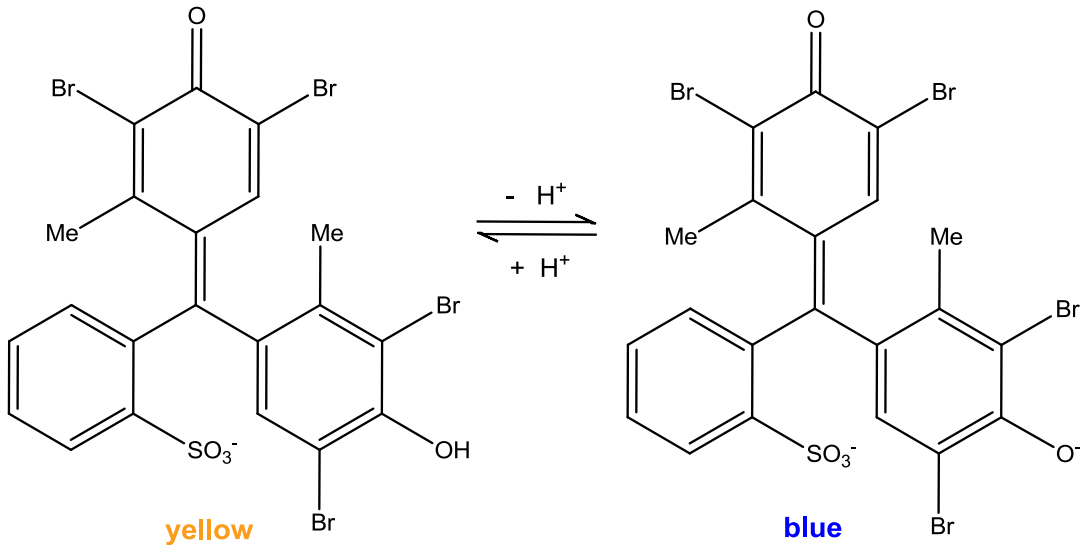

Figure 1.22 The proton dissociation/association of bromocresol green.

This simple device has been tested with real fish samples (Cod fillets) and has shown a colorimetric response that 'correlates with bacterial growth patterns' in fresh fish samples, thus provides a real-time measure of the degree of spoilage. [120, 121] Pacquit notes that the sensor which responds to ammonia and volatile amines has not yet been tested at refrigerated temperatures i.e. <5 ^{o}C and that to be used effectively as a best-before-end indicator the sensor must be able to yield a reliable response when subjected to 'temperature abuse'.

Another class of pH dyes that has been incorporated into ammonia/TVB-N sensors is xanthene based-dyes, the basic structure of which is shown in Figure 1.20.[129, 140] One example of this is the ammonia-sensitive monitoring tape developed by N. Nakano *et al*.[140] The tape which is dipped in a Rose Bengal (RB) processing solution yields a reproducible response that is proportional to the level of ammonia.[140]

The third main group of pH dyes used as ammonia/TVB-N sensors belong to the betalain and flavinoid dye classes. These highly coloured species are responsible for the red and purple colours of flower petals and coloured vegetables e.g. red cabbage and are also sensitive to pH. Under acidic conditions these dyes are typically red/pink in appearance, at a neutral pH they are purple and at higher pH levels they are green/yellow. Such dyes are ideal for use as food quality indicators for determining fish freshness because they are non-toxic and can be used in close proximity with food without fear of any hazardous side effects. Williams and Myers have patented such TBV-N indicating inks that can be printed on or supported by a range of different matrixes including hydrophobic paper, polymers and gelatine.[127] As with all previously mentioned pH-based systems in the presence of volatile amines, in this case arising from food spoilage, the indicators undergo a striking colour change. In this particular patent the use of a non pH responsive yellow layer has also been used to further enhance this colour change.

(c) Fluorescence

Several fluorescence-based sensors have been developed for the detection of dissolved ammonia and amines. Such sensors utilise fluorescent dyes such as aminofluorescein, AF, whose structure is shown Figure 1.23.

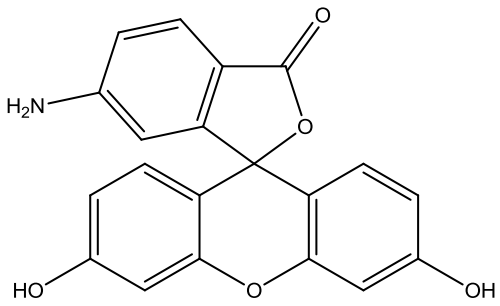

Figure 1.23 The chemical structure of aminofluorescein.

Under normal circumstances AF molecules undergo an intramolecular fluorescence self-quenching process which reduces the molecules' ability to fluoresce.[147] When exposed to aqueous ammonia, hydrogen bonding interactions between the ammonia and the NH_2 group on the AF reduces the molecules' quenching ability. The net result is an increase in the fluorescence intensity of the dye which is proportional to the concentration of ammonia.[125, 147, 148] Ammonia sensors based on AF have been constructed by immobilising the AF dye within ormosil i.e. organically modified silicate films.[125, 147, 148] The ormosils are based on tetramethoxysilane, TMOS, and organically modified sol-gel precursors including dimethyldimethoxysilane, DiMe-DiMOS, diphenyldimethosysilane, DiPh-DiMOS, methyltrimethoxysilane, Me-TriMOS and phenyltrimethoxysilane, Ph-TroMOS.[125, 147, 148] The sensitivity of the ormosil films to ammonia can be varied by altering the ratio of TMOS and the sol-gel precursors, which in turn affects the pore size and microenvironment polarity. At present these ammonia sensors have only been evaluated with solutions of ammonia and although they are very promising for this application it is not clear whether such sensors could be adapted to detect gaseous ammonia or TVB-N.

A novel ammonia fluorosensor-based polymer film containing rhodamine dyes has been designed by C. Preininger *et al.*[138] This simple optical sensor used for measuring low levels of dissolved ammonia works on the premise that lactonization of the dyes occurs in the presence of ammonia. This is illustrated diagrammatically for Rhodamine B in Figure 1.24 below.

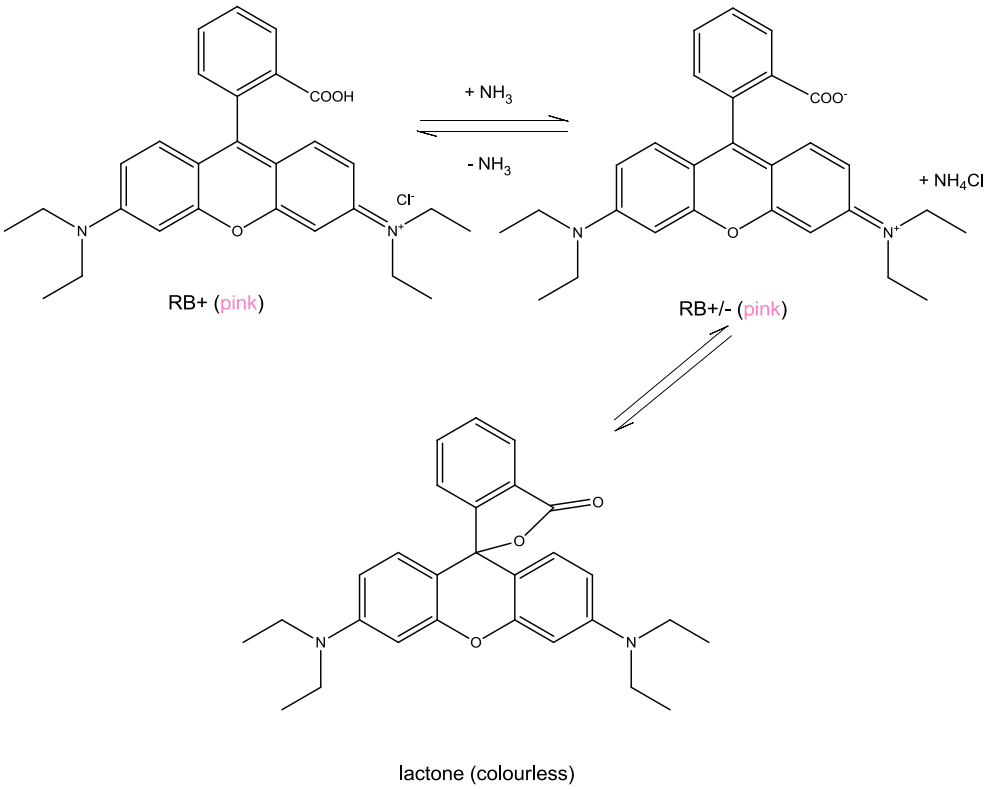

Figure 1.24 Chemical structures of cationic rhodamine B (RB^{+}), the rhodamine B zwitterion ($RB^{+/-}$) and the lactone form of rhodamine B.

In an aqueous buffer solution, the rhodamine B within the fluorsensor is transformed into the fluorescent zwitterion (RB+/-). The introduction of ammonia causes the carboxyl anion to undergo a nucleophillic attack on the central carbon atom forming the non fluorescing lactone.[138] Thus the observed decrease in fluorescent intensity can be used to quantitatively determine the concentration of dissolved ammonia. Response times and ammonia sensitivity can be varied by altering the polymer encapsulating material. Unlike the previous fluorosensors which are readily

reversible, the lactonization is irreversible and thus is not suitable for online monitoring.

(d) Other optical sensors

Researchers at the University of Michigan have developed a novel optical sensor for amine vapours.[134] The sensor is a thin polymer film containing indium(III) octaethylporphyrin hydroxide monomer units that are conditioned so that they form hydroxide ion bridged dimers as depicted in Figure 1.25.[134] In order for such dimers to form the sensors must first be doped with lipophilic counteranions. The resultant monomer-dimer equilibrium shifts in favour of the monomer species in the presence of volatile amines including, among others, ethylamine, diethylamine, methylamine and ammonia.[134] This process yields a measureable shift in the wavelength of maximum absorbance i.e. λ_{max} from 390 nm to 408 nm that can be monitored spectrophotometrically.[134]

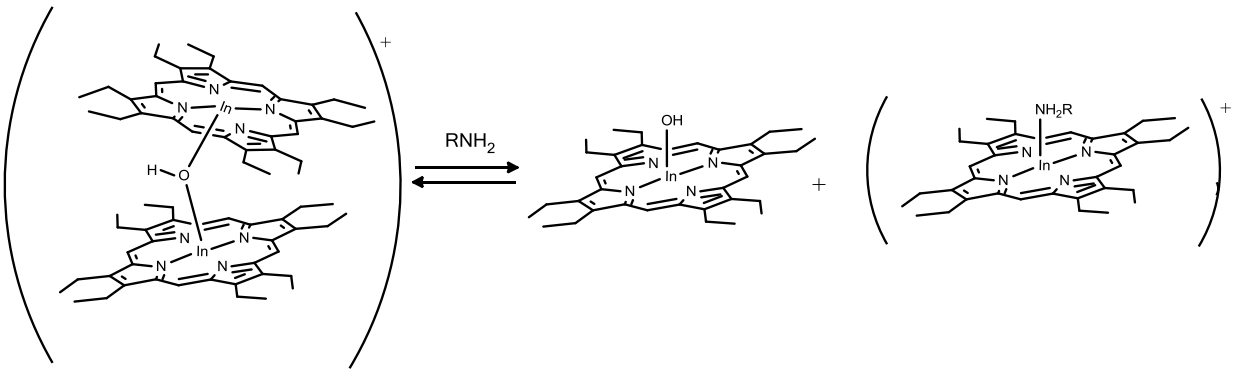

Figure 1.25 Dimer/monomer equilibrium of indium(III) poryphyrin in the presence of amine.

A similar amine optical sensor which relies on amines coordinating to a metal centre has been proposed by C. J. Liu *et al.*[130] This sensor is based on thin films of zinc(II)1,4,8,11,15,18,22,25-octabutoxy-phthalocyanine, whose structure is shown in Figure 1.26, spun from chloroform solutions.[130] The films as prepared exhibit a strong monomer absorbance at 750 nm and a smaller dimer shoulder at 690 nm. In the presence of volatile amines including methylamine, ethylamine, *n*-butylamine and n-hexylamine there is a notable increase in intensity at both of these

absorbances. This has been attributed to the ability of amine molecules to coordinate directly to the Zn metal centre which enhances the measured absorbance of the film.[130] Lui's sensors are fully reversible when purged with nitrogen and do not show any significant deterioration in performance after repeated amine-nitrogen purging cycling.[130] Sensitivity and rate of response vary with the amine under test. For example, primary amines show an increase in both sensitivity and response time with increasing alkyl chain length. This is rationalised by considering that longer chain alkyl groups have more electron density available to donate to the electron deficient N atom. This serves to strengthen the interaction between the amine and the Zn metal centre and increases the absorbance at both 690 nm and 750 nm.[130]

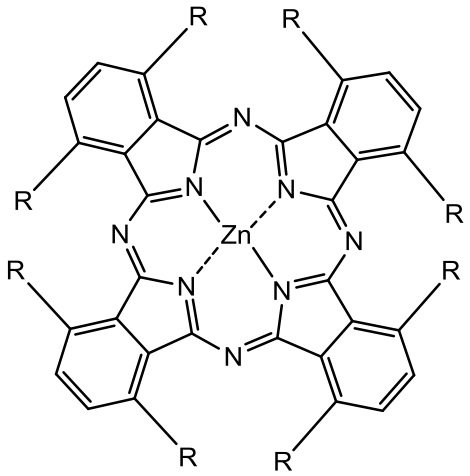

Figure 1.26 The chemical structure of zinc(II)1,4,8,11,15,18,22,25-octabutoxy-phthalocyanine.[130]

For secondary and tertiary amines sterics come into play when considering sensitivity, since more sterically hindered amines are less able to gain access to the Zn metal centre and as such have much slower response times than their comparable primary amines.[130]

Infra-red dyes based on 5-9(4`-dialkylaminophenylimino)quinolin-8-one copper(II)per chlorate complexes have also been employed as amine optical sensors.[149] C Malins *et al.* have developed 2 novel dyes which can be encapsulated within polyvinylchloride solution which can then be used to dip-coat optical fibres.[149] The dye-coated fibres have strong absorption maxima in the range 740 - 770 nm in the absence of ammonia, which is diminished on exposure to 10-100 ppm ammonia. Malins suggests the reason for this significant reduction in absorbance is as a result of a ligand exchange taking place at the Cu metal centre as illustrated in Figure 1.27.[149] This exchange is fully reversible and the response is not diminished by repeated cycling of ammonia and nitrogen. The system does however have one major drawback in that it is very sensitive to changes in relative humidity (RH).

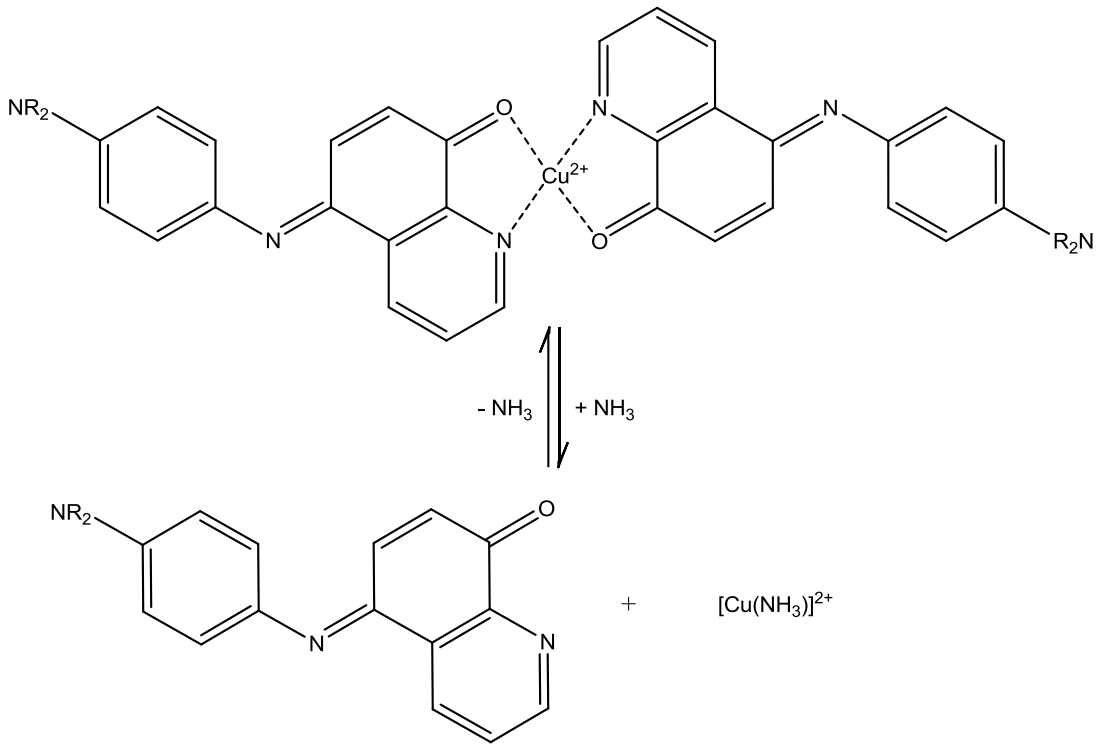

Figure 1.27 Malins' proposed ligand exchange mechanism of infrared dyes with ammonia.[149]

Under 100% RH the fibres display absorbance changes twice the magnitude of those under dry conditions on exposure to ammonia and thus would require extensive humidity calibration to be used under variable RH conditions.

The desire of the author is to investigate the possibility of expanding work carried out previously within the group on a solvent-based ammonia indicator based on pH-sensitive dyes by developing a novel ammonia/volatile amine pigment.[138] It is hoped that by investigating alternative substrates i.e. silica such pigments can be incorporated into flexible thermoplastics and used as smart packaging for monitoring fish spoilage.

1.5 Aims and Objectives

- To develop novel UV dosimeters for use as sunburn warning indicators targeted at individuals with sensitive skin. More specifically to investigate the possibility of using redox dyes with and without photocatalytic semiconductors and to characterise their erythemal responses to solar UV.

- To investigate previously reported reversible colorimetric humidity indicators based on monomer/dimer interactions in ionic dyes with a view to extending this work to develop a novel indicator specifically for high RH levels.

- To adopt the basic principles of pH dye based ammonia/volatile amine sensitive inks reported previously and extrapolate this to develop novel intelligent pigments. Such pigments would then ideally be incorporated within a flexible, extrudable thermoplastic leading to the development of the next generation of intelligent food packaging.

1.6 References

1. O. S. Wolfbeis and B. M. Weidgans, in *Optical Chemical Sensors*, eds. F. Baladini, A. N. Chester, J. Homola and S. Martellucci, Springer, Dordrecth, The Netherlands, 2006, pp. 17-44.
2. B. L. Diffey and A. F. McKinlay, *Phys. Med. Biol*, 1983, **28**, 351-358.
3. W. B. Grant, *Photochem. Photobiol. Sci*, 2003, **2**, 1307-1310.
4. R. P. Gallagher and T. K. Lee, *Prog. Biophys. Mol. Bio*, 2006, **92**,119-131.
5. P. Lips, *Prog. Biophys. Mol. Bio*, 2006, **92**, 4-8.
6. M. Lebwohl and S. Ali, *J. Am. Acad. Dermatol*., 2001, **45**, 487-499.
7. Y. Matsumura and H. N. Anathaswamy, *Toxicol. Appl. Pharmacol*., 2004, **195**, 298-308.
8. WHO, *Heat and Environmental Effects of Ultraviolet Radiation: a scientific summary of envrionmental health criteria*.
9. F. Urbach, *J. Photochem. Photobiol. B: Biol*., 1997, **40**, 3-7.
10. R. M. Mackie, *Prog. Biophys. Mol. Bio*, 2006, **92**, 92-96.
11. G. I. Harrison, *Methods*, 2000, **28**, 14-19.
12. D. W. Edstrome, A. Porwit and A. Ros, *Photodermatol. Photoimmunol. Photomed*., 2001, **17**, 66-70.
13. Cancer Research UK, *CancerStats Key Facts – skin cancer*, July 2012.
14. D. Allen and A. Vasavada, *Br. Med. J*, 2006, **333**, 128-132.
15. WHO, WMO, U. E. Programme and I. C. o. N.-I. R. Protection, *Global Solar UV Index – A Practical Guide.*
16. http://www.metoffice.gov.uk/weather/europe/europe_uv.html, Accessed 13/07/2012.
17. A. F. McKinlay and B. L. Diffey, *International Commision on Illumination Journal*, 1987, **66**, 17-22.
18. B. L. Diffey, *Methods*, 2002, **28**, 4-13.
19. T. B. Fitzpatrick, *Arch. Dermatol*., 1989, **124**, 869-871.
20. N. Gat, *US Pat. 5008548*, 1991.
21. M. P. Wuest, *US Pat. 6426503*, 2002.

22. J. Heydenreich and H. C. Wulf, *Photochem. Photobiol*., 2005, **81**, 1138-1144..
23. http://www.nscessity.co.uk/Sun-Essentials/Sun-Essentials.html, Accessed 19/01/2012.
24. W. Ann R, *J. Photochem. Photobiol. B: Biology*, 1995, **31**, 9-13.
25. M. Nabuo, *Mutation Research/Fundamental and Molecular Mechanisms of Mutagenesis*, 1981, **82**, 263-268.
26. T. Z. Wang, *Biochem. Biophys. Res. Commun*., 1991, **31**, 48-53.
27. M. Puskeppeleit, L. E. Quintern, S. E. Naggar, J. Schott, U. Eschweiler, G. Horneck and H. Bucker, *App. Envrion. Mircobiol*., 1992, **58**, 2355-2359.
28. L. E. Quintern, G. Horneck, U. Eschweiler and H. Bucker, *Photochem.Photobiol*., 1992, **55**, 389-395.
29. L. E. Quintern, Y. Furusawa, K. Fukutsu and H. Holtschmidt, *J. Photochem. Photobiol. B: Biol*., 1997, **37**, 158-166.
30. Y. Ishigaki, A. Takayama, S. Yamahita and O. Nikaido, *J. Photochem. Photobiol. B: Biol*., 1999, **50**, 184-188.
31. M. Moehrle, M. Korn and C. Garbe, *Int. Arch. Occup. Envrion. Health*, 2000, **78**, 575-580.
32. I. Terenetskaya, *Agr. Forest Meterol*., 2003, **120**, 45-50.
33. J. Sandby-Moller, E. Thieden, P. A. Philipsen, J. Heydenreich and H. C. Wulf, *Photodermatol. Photoimmunol. Photomed*., 2004, **20**, 33-40.
34. P. Rettberg and C. S. Cockell, *Photochem. Photobiol. Sci*., 2004, **3**, 781-787..
35. B. L. Diffey, *Radiation Measurements in Photobiolgy*, Academic Press Ltd., 1989.
36. A. Rivaton and J. L. Gardette, *Polym. Degrad. Stabil*., 1999, **66**, 385-403.
37. N. Kollias, A. H. Baqer and H. Ou-Yang, Photodermatology, Photoimmunology & Photomedicine, 2003, **19**, 89-92.
38. I. Horkay, N. Wikokal, J. Patko, G. Bazsa, M. Beck, A. Ferenczi, Z. Nagy, M. Racz and T. Szalay, *J. Photochem. Photobiol. B: Biol*., 1995, **31**, 79-82.
39. A. A. Abdel-Fattah, M. El-Kelany, F. Abdel-Rehim and A. A. El Miligy, *J. Photochem. Photobiol. A: Chem*., 1997, **110**, 291-297.

40. R. Rhan and M. A. Lee, *Photochem. Photobiol.* , 1998, **66**, 173-178.
41. J. Ramirez-Nino, D. Mendoza and V. M. Castano, *Radiat. Meas*., 1999, **30**, 181-187.
42. A. A. Abdel-Fattah, E. A. Hegazy and H. E. Dl-Din, *J. Photochem. Photobiol. A:Chem*, 2000, **137**, 37-43.
43. S. Ebraheem, A. A. Abdel-Fattah, F. I. Said and Z. I. Ali, *Radiat. Phys Chem*., 2000, **57**, 195-202.
44. K. Takato, Y. Kaburagi, Y. Kurimura, S. Tokita, T. Noguchi and M. Kaneko, *J. Photochem. Photobiol. A: Chem*., 2004, **163**, 271-276.
45. A. Mills, S. Lee and M. Sheridan, *Analyst*, 2005, **130**, 1046-1051.
46. A. Mills, M. McFarlane and S. Schneider, *Anal.Bioana.l Chem*., 2006, **386**, 299-305.
47. W. E. McKee, *US Pat. 3194963*, 1965.
48. K. H. Sylvester, W. E. Franz and R. M. McGlathery, *US Pat. 3449572*, 1969.
49. A. Zweig, *US Pat. 3903423*, 1975.
50. P. Dickinson and M. Ellwood, *US Pat. 4659649*, 1987.
51. K. B. Mullis, *US Pat. 5028792*, 1991.
52. K. B. Mullis, *US Pat. 5436115*, 1995.
53. P. M. Goman and S. Sirdesai, *US Pat. 5296275*, 1994.
54. K. Goudjil, *US Pat. 5581090*, 1996.
55. O. Faran and E. Nata, *US Pat. 6132681*, 2000.
56. S. E. Forest, M. S. Krummen and J. A. Yelton, *WO 02/03949*, 2002.
57. S. A. Jackson, J. R. Mercer, E. Atrazheva, K. Hudda and S. Wang, *US Pat. 6504161*, 2003.
58. G. N. Patel, *WO 2004/017095* A2, 2004.
59. S. A. Jackson, J. R. Mercer, E. Atrazheva, K. Hudda and S. Wang, *CA 2282084*, 2005.
60. http://sunsignals.com/, Accessed 13/07/2012.
61. M. Weber, K. Schulmeister and H. Brusl, *Photochem. Photobiol. Sci*, 2006, **5**, 707-713.

62. R. Esse and A. Saari, in *Smart Packaging Technologies*, eds. J. Kerry and P. Butler, John Wiley & Sons, West-Sussex, 2008, pp. 130-149.
63. J. E. Robinson, K. M. Browne and W. G. Burton, *Ann. Appl. Biol*., 1975, **81**, 399-408.
64. G. Pavlogeorgatos, *Build. Envrion*., 2003, **38**, 1457-1462.
65. R. H. Feinzig and D. Sullivan, National Conference on Building Commissioning, 2007.
66. R. Esse and A. Saari, *in Smart Packaging Technologies for Fast Moving Comsumer Goods*, eds. J. Kerry and P. Butler, John Wiley & Sons Ltd, Chichester, West Surrey, UK, 2008, pp. 129.
67. N. Yamazoe, *Sens. Acuat*. , 1986, **10**, 379-398.
68. Z. Chen and C. Lui, *Sensor Lett*., 2005, **3**, 274-295.
69. http://www.hannainst.com/usa/prods2.cfm?id=012001, Accessed 13/07/2012.
70. http://www.michell.co.uk/products/classification/browse/portables, Accessed 01/02/2009.
71. R. A. McGill, M. S. Paley and J. M. Harris, *Macromolecules*, 1992, **25**, 3015-3019.
72. S. Otsuki and K. Adachi, *Polym. J*., 1995, **27**, 655-658.
73. R. Matsushima, A. Ogiue and Y. Kohno, *Chem. Lett*., 2002, 436-437.
74. P. R. Somani, A. K. Viswanath, R. C. Aiyer and S. Radhakrishnan, *Sens. Acuat. B Chem*., 2001, **80**, 142-148.
75. R. Matsushima, N. Nishimura, K. Goto and Y. Kohno, Bull. *Chem. Soc. Jpn*., 2003, **76**, 1279-1283.
76. R. Shinozaki and T. Nakato, *Langmuir*, 2004, **20**, 7583-7588.
77. M. A. Zanjanchi and S. Sohrabnezhad, *Sens. Acuat. B*, 2005, **105**, 502-507.
78. M. Kleeman, A. Suisalu and K. Kikas, Optical materials and Applications, Bellingham, WA, 2005.
79. A. Tsigara, G. Mountrichas, K. Gatsouli, A. Nichelatti, S. Pispas, N. Madamopoulos, N. A. Vainos, H. L. Du and R. Roubani-Kalantzopoulou, *Sens. Acuat. B Chem*., 2007, **120**, 481-486.

80. J. Kunzelman, B. R. Crenshaw and C. Weder, *J. Mater. Chem*., 2007, **17**, 2989-2991.
81. S. Sohrabnezhad, A. Pourahmad and M. A. Sadjadi, *Mater. Lett*., 2007, **61**, 2311-2314.
82. J. Shi, V. K. S. Hsiao, T. R. Walker and T. J. Huang, *Sens. Acuat. B* Chemical, 2008, **129**, 391-396.
83. E. Tian, J. Wang, Y. Zheng, Y. Song, L. Jiang and D. Zhu, *J. Mater. Chem*., 2008, **18**, 1116-1122.
84. M. G. Snelling, *US Pat. 2214354*, 1937.
85. M. G. Snelling, *US Pat. 2249867*, 1941.
86. P. B. Davis, *US Pat. 2460065* to *2460070*, 1949.
87. P. B. Davis, *US Pat. 2460066*, 1949.
88. P. B. Davis, *US Pat. 2460067*, 1949.
89. P. B. Davis, *US Pat. 2460068*, 1949.
90. P. B. Davis, *US Pat. 2460069*, 1949.
91. P. B. Davis, *US Pat. 2460070*, 1949.
92. P. B. Davis, *US Pat. 2580737*, 1949.
93. P. B. Davis and J. N. Pryor, *US Pat. 2526938*, 1950.
94. S. D. Price, *US Pat. 3121615,* 1964.
95. D. L. Fuller, *US Pat. 4034609*, 1977.
96. D. L. Fuller, *US Pat. 4150570*, 1979.
97. W. O. Krause, *US Pat. 3533277*, 1970.
98. W. O. Krause, *US Pat. 3499616*, 1970.
99. R. K. Stewart and J. R. Bilnn, *US Pat. 4793180*, 1988.
100. J. F. McBride, *US Pat. 4909179*, 1990.
101. J. S. Haswell, *US Pat. 5520041*, 1996.
102. E. Wroth and K. Sheraw, *US Pat. 5950323*, 1999.
103. M. Martin and M. Beltran, *US Pat. 5875892*, 1999.
104. M. Gattiglia, *US Pat. 6655315 B1*, 2003.
105. M. Gattiglia and E. Gandolfo, *WO 02/44712 A1*, 2002.
106. S. O. Dick, *US Pat. 6698378 B1*, 2004.
107. S. O. Dick, *US Pat. 6827218 B1*, 2004.

108. S. O. Dick, *US Pat. 6877457 B1*, 2005.
109. M. Hamada, *US Pat. Appl. 2007/0157702 A1*, 2007.
110. Y. Yamakawa, *US Pat. 7316198 B2*, 2008.
111. F. O. Anderegg, *US Pat. 2687041*, 1954.
112. http://www.sud-chemie.com/scmcms/web/page_en_6254.htm, Accessed 01/02/2012.
113. P. R. Somani, A. K. Viswanath, R. C. Aiyer and S. Radhakrishnan, *Org. Electron.*, 2001, **2**, 83-88.
114. R. Matsushima, A. Ogiue and S. Fujimoto, *Chem. Lett*., 2000, 590-591.
115. A. Pacquit, K. Crowley and D. Diamond, *Smart Packaging Technologies for Fast Moving Consumer Goods*, eds. J. Kerry and P. Butler, John Wiley & Sons, Ltd, West Sussex, 2008, pp. 77-98.
116. S. Kirpal S, *Regul. Toxicol. and Pharmacol*., 2003, **38**, 336-344.
117. P. Howgate, A. Johnston and K. J. Whittle, eds. T. R. Station, F. S. Directorate and F. a. F. Ministry of Agriculture, FAR, Aberdeen, 1992.
118. J. Niu and J. Y. Lee, *J. Food. Sci*, 2000, **65**, 780-785.
119. A. Pacquit, J. Frisby, D. Diamonmd, K. T. Lau, A. Farrell, B. Quilty and D. Diamond, *Food Chem.*, 2007, **102**, 466-470.
120. A. Pacquit, K. T. Lau, H. McLaughlin, J. Frisby, B. Quilty and D. Diamond, *Talanta*, 2006, **69**, 515-520.
121. A. Pacquit, K. T. Lau and D. Diamond, *IEEE Sensors*, Vienna, Austria, 2004.
122. L. Byrne, K. T. Lau and D. Diamond, *Analyst*, 2002, **127**, 1338-1341.
123. L. Pivarnik, P. Ellis, X. Wang and T. Reily, *J. Food. Sci*, 2001, **66**, 945-952.
124. M. Loughran and D. Diamond, *Food Chem*., 2000, **69**, 97-103.
125. A. Lobnik and O. S. Wolfbeis, *Sens. Acuat. B*, 1998, **51**, 203-207.
126. J. Williams and K. Myers, *WO 2006/032025 A1*, 2006.
127. J. Williams and K. Myers, *WO 2005/071399 A1*, 2005.
128. D. F. H. Wallach, *WO 02/061399 A1*, 2002.
129. D. W. Miller, WO 99/061399, 1999.
130. C.-H. J. Liu and W.-C. Lu, *J. Chin. Inst. Chem. Engin*., 2007, **38**, 483-488.

131. K. I. Oberg, R. Hodyss and J. L. Beauchamp, *Sens. Acuat. B*, 2006, **115**, 79-85.

132. C. J. Lui, J. T. Lin, S. H. Wang, J. C. Jiang and L. G. Lin, *Sens. Acuat. B*, 2005, **108**, 521-527.

133. K. T. Lau, S. Edwards and D. Diamond, *Sens. Acuat. B*, 2004, **98**, 12-17.

134. W. Qin, P. Parzuchowski, W. Zhang and M. E. Meyerhoff, *Anal. Chem*., 2003, **75**, 332-340.

135. G. E. Khalil, D. L. Putnam and T. W. Hubbard, *WO 01/035057 A2*, 2000.

136. T. Yagi, N. Kuboki, Y. Suzuki, N. Uchino, K. Nakamura and K. Yoshida, *Opt. Rev.*, 1997, **4**, 596-600.

137. T. Grady, T. Butler, B. D. MacCraith, D. Diamond and M. A. McKervey, *Analyst*, 1997, **122**, 803-806.

138. C. Perininger, G. J. Mohr, I. Klimant and O. S. Wolfbeis, *Anal. Chim. Acta*, 1996, **334**, 113-123.

139. A. Mills, L. Wild and Q. Chang, *Mikrochim. Acta*., 1995, **121**, 225-236.

140. N. Nakano, Y. Kobayashi and K. Nagashima, *Analyst*, 1994, **119**, 2009-2012.

141. R. A. Potyrailo, S. P. Golubkov, P. S. Borsuk and P. M. Talanchuk, *Analyst*, 1994, **119**, 443-448.

142. Q. Zhou, D. Kritz, L. Bonnell and G. H. Sigel, *App. Opt*., 1989, **28**, 2022-2025.

143. M. R. Shahriari, Q. Zhou and G. H. Sigel, *Opt. Lett*., 1988, **13**, 407-409.

144. P. Caglar and R. Narayanaswamy, *Analyst*, 1987, **112**, 1285-1288.

145. C. Wang, X.-W. He and L.-X. Chen, *Talanta*, 2002, 1181-1188.

146. C. J. Liu, J. T. Lin, S. H. Wang, C. J. Jiang and L. G. Lin, *Sens. Acuat. B*, 2005, **108**, 521-527.

147. X. Chen, L. Lin, P. Li, Y. Dai and X. Wang, *Anal. Chim. Acta*, 2004, **506**, 9-15.

148. X. Chen, Y.-j. Dai, Z. Li, Z.-X. Zhang and X.-R. Wang, Fresenius *J. Anal. Chem*., 2001, **370**, 1048-1051.

149. C. Malins, M. Landl, P. Simon and B. D. MacCraith, *Sens. Acuat. B*, 1998, **51**, 359-367.

Chapter 2

Experimental

2 Experimental

2.1 Spectroscopic methods

2.1.1 *Theory of UV/Visible spectrophotometry*

Ultraviolet (UV) and visible light are both regions of the electromagnetic spectrum which fall between far-UV and infrared, spanning the wavelength range 200-750 nm. Electronic transitions can occur when a photon of UV/visible light transfers its energy to a molecule, causing an electron to be promoted from its ground state to a higher energy 'excited' state; this process is called absorption. The electron involved in the transition originates in either a bonding or non-bonding orbital, typically the highest occupied molecular orbital (HOMO). Upon absorption of the photon the electron is promoted to an anti-bonding orbital, usually the lowest unoccupied molecular orbital (LUMO). There are a series of different electronic transitions available in organic compounds, some of which are outlined in
Figure 2. 1.

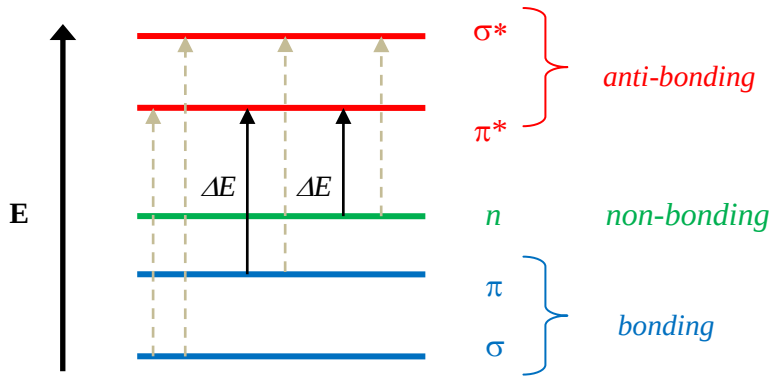

Figure 2. 1 Possible electronic transitions between molecular orbitals.

Of the 6 possibilities shown only 2, the $n \rightarrow \pi^*$ and the $\pi \rightarrow \pi^*$, are possible under UV/visible conditions. That is to say the ΔE associated with such transitions corresponds to the energies associated with photons of 200 – 750 nm.

Molecules which absorb significantly in the visible region are highly coloured. The colour of the substance, however, does not correspond to the colour of the absorbed light; rather it is the unabsorbed portion of the spectrum i.e. the complementary colour that is seen.

The absorption is generally associated with a particular functional group. Such moieties are called chromophores and tend to be heteroatoms with non-bonding lone pairs of electrons and π electron moieties. Almost all unconjugated chromaphores, however, absorb outside the UV/visible region. For conjugated systems the wavelength at which absorption takes place tends to increase with the length of the conjugation chain. This shift towards a longer λ_{max} value is called a bathochromic shift and can be rationalised by considering Figure 2. 2.

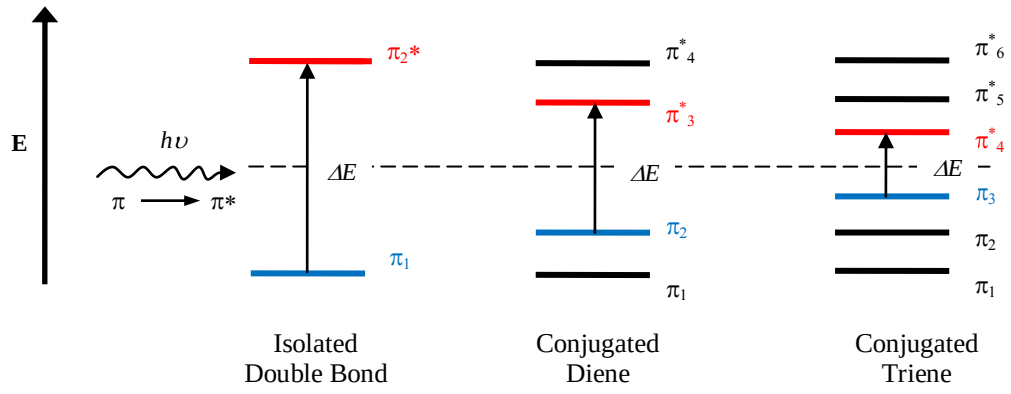

Figure 2. 2 HOMO to LUMO electronic transitions for an isolated double bond, a conjugated diene and conjugated triene.

For an isolated double bond, molecular orbital theory states that the p-orbitals on both of the carbon atoms combine to give two new molecular orbitals, π_1 and π_2^*. Similarly, for a conjugated diene there are 4 sets of p-orbitals which combine to give

four new orbitals π_1, π_2, π_3* and π_4*. These molecular orbitals, along with the analogous orbitals for a conjugated triene, are illustrated in Figure 2. 2. In each case the HOMO is in blue and the LUMO in red. As the level of conjugation increases the HOMO and LUMO orbitals move closer together, consequently reducing the energy required to promote an electron. As the energy of a photon is inversely proportional to the wavelength, when ΔE decreases the wavelength increases.

UV/visible spectrophotometry can be effectively used for quantitative analysis of solutions. Light of known intensity and of a suitable wavelength, i.e. the wavelength at which the analyte is most absorbing, λ_{max}, is shone through a small volume of solution. By measuring the transmitted light that passes through the solution the portion of light which is absorbed can be determined using a relationship known as the Beer-Lambert law. Figure 2.3 (a) illustrates this process.

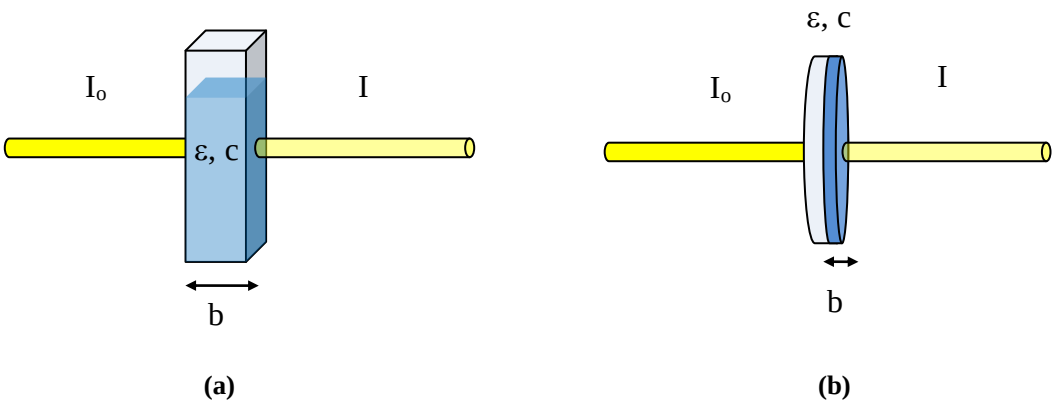

Figure 2.3 The Beer-Lambert law applied to (a) a liquid sample in a cuvette and (b) a thin film sample cast on a support.

The absorbance A is taken as the log of the ratio (I_o/I), where I_o is the incident light and I is the transmitted light;

$$A = \log_{10} \frac{I_o}{I} \qquad (2.\ 1)$$

The absorbance is related to the concentration, c (mol l^{-1}) of the analyte by Beer's law which states:

$$A = \varepsilon bc \qquad (2.\ 2)$$

where ε = molar absorptivity (l mol^{-1} cm^{-1}) and b = pathlength of analyte sample (cm). For much of the work detailed in this thesis the test samples are in the form of thin polymer films containing absorbing species rather than solutions. The films are typically supported on a glass or quartz substrate and can be analysed in the same manner as solutions as illustrated in Figure 2.3 (b).

2.1.2 UV/visible spectrophotometer

The instrument used in this analysis is a UV/visible spectrophotometer. There are two different configurations used as illustrated in Figure 2.4 below, (a) single beam and (b) dual beam.

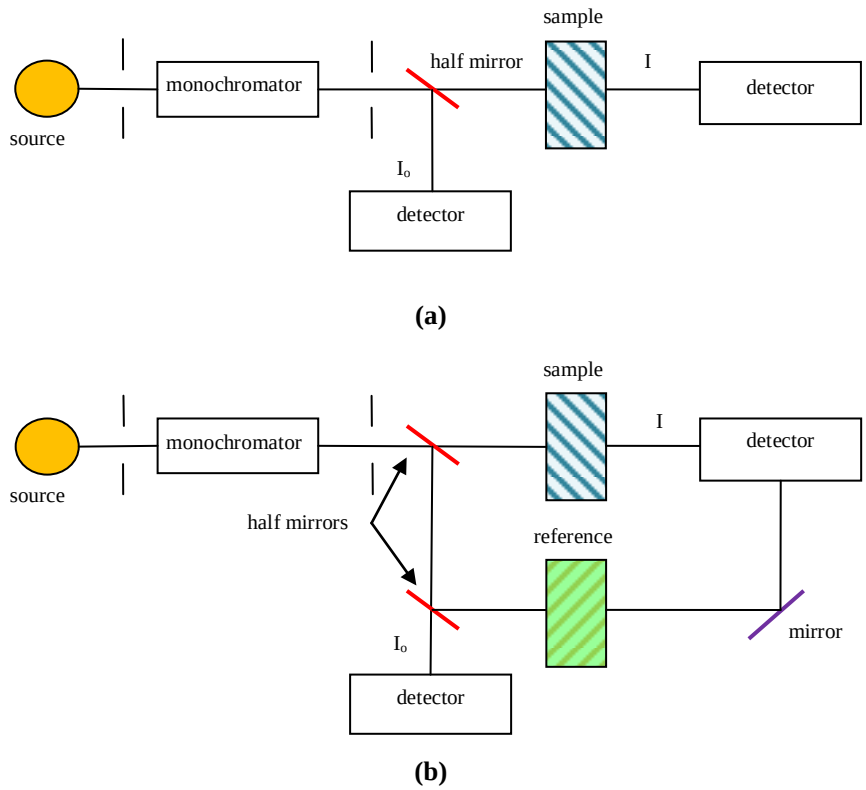

Figure 2.4 The basic components for a spectrophotometer operating in (a) single beam conditions and (b) dual beam conditions.

Analysis is performed by directing a light source through a monochromator and then through the sample, where some of the light will be absorbed by the analyte of interest. The remainder of the light passes into a detector and the response is

recorded. Traditionally the light source for UV/visible spectrophotometry is a deuterium lamp for the UV region coupled with a tungsten lamp for the visible region, although some modern spectrophotometers utilise xenon flash lamps. The monochromator is a device such as a prism or diffraction grating, capable of splitting polychromatic light into small wavelength ranges of narrow bandwidth. The light that is not absorbed by the sample i.e. transmitted light triggers a response in the detector, typically a photomultiplier tube or a photodiode array detector, and is recorded. This data can then be used to generate the absorption spectrum for the absorbing species.

All samples were analysed with UV/visible spectrophotometry using a Lambda 35 (Perkin Elmer, UK), Cary Model 50, or a Helios Beta UV/visible Spectrophotometer. The former two instruments operate in dual beam mode while the latter is a single beam spectrophotometer.

During analysis sample films were housed in a gas cell like that shown in Figure 2.5. The gas cell was then placed in-line with the beam of the spectrometer and the UV/visible spectrum or absorbance at λ_{max} of the samples was recorded at appropriate time intervals.

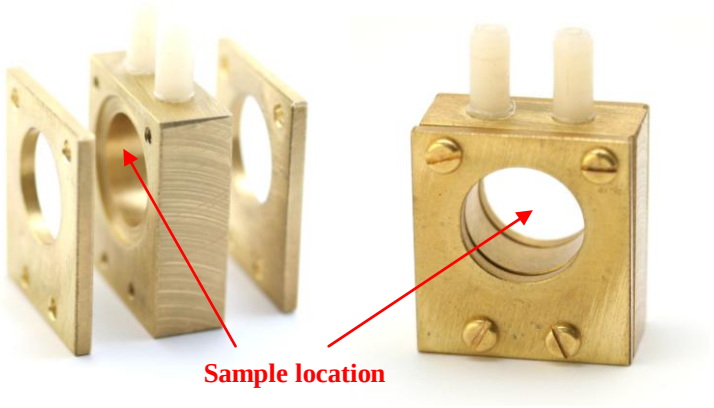

Figure 2.5 Photographs of the gas cell in which test films were mounted for recording spectra

2.2 UV light sources

UV irradiation of dosimeter samples was carried out using UVA and UVB light. In both cases two 8 W fluorescent bulbs were used. The irradiance (i.e. radiant power per unit area) for each lamp was measured using a Multi-Sense 100 UV light meter. The emission spectra of the UVA and UVB lamps are shown in Figure 2.6.

Solar radiation consists mainly of visible light, ultraviolet and infrared radiation. The set-up used to simulate solar radiation in this work was comprised of a 180 W xenon arc lamp (Speirs Robertson) with UG5 and WG20 filters inline as described in a previous method by Diffey.[1] The former allowed transmission at UV wavelengths and absorbed in the visible region, while the latter absorbed in the short wavelength UVC region. Figure 2.7 shows the absorption spectra of the filters used. When these filters are in place the solar simulator lamp has the emission spectrum shown in Figure 2.8, which compares well with the solar spectrum recorded on a clear summer's day in Melbourne (53^{o} S) at 12 noon on 17^{th} January 1990, shown for comparison.

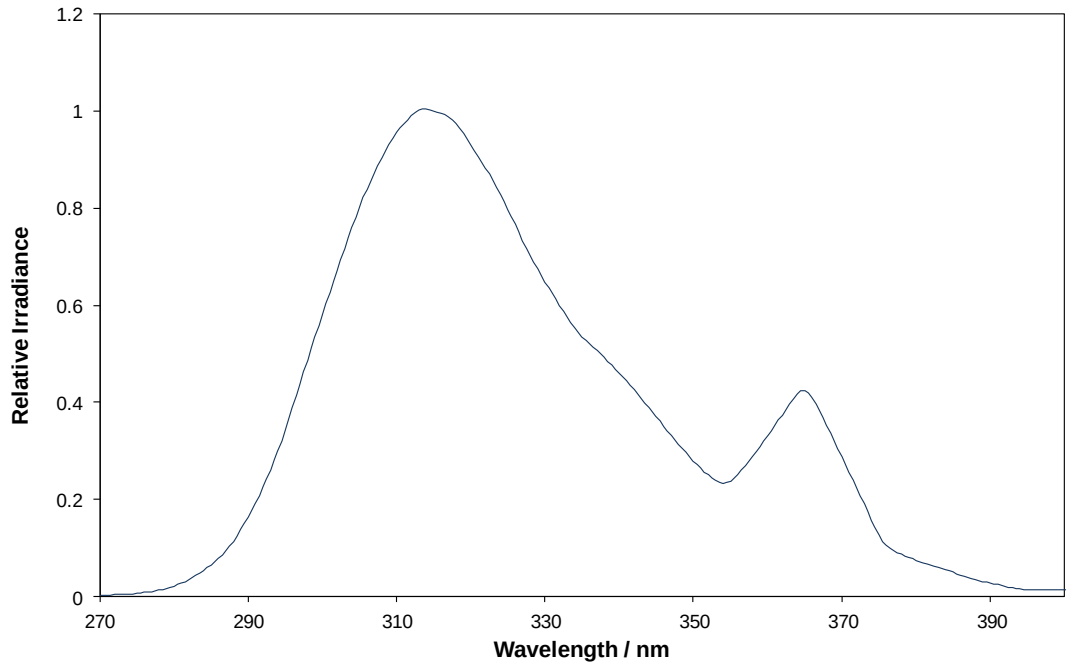

(a)

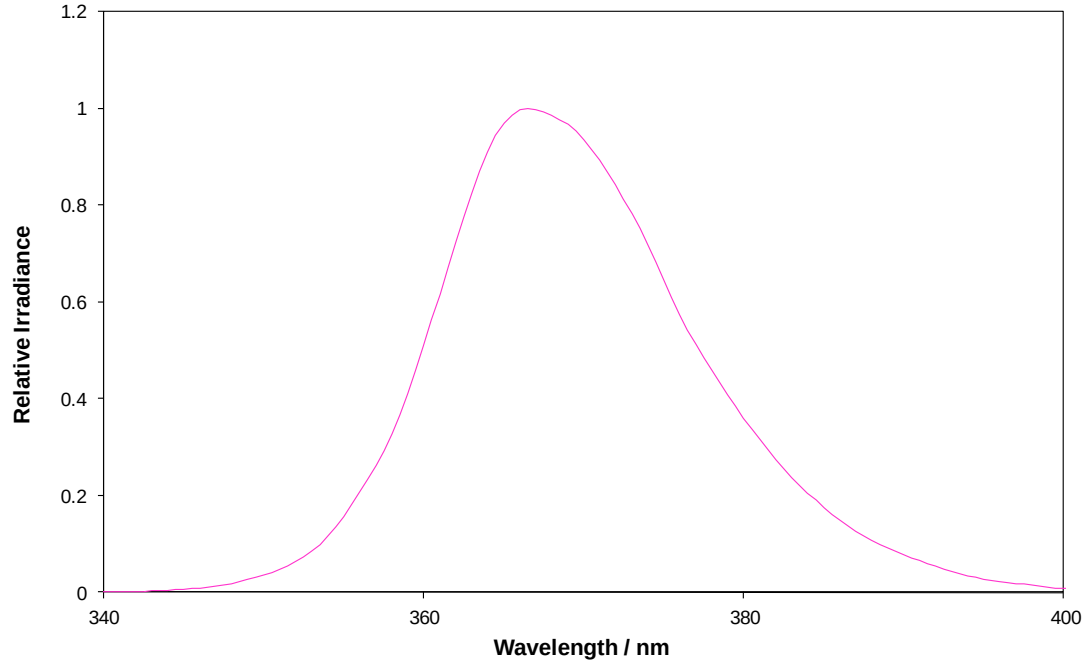

(b)

Figure 2.6 Emission spectra of (a) UVB (λmax_{315}) and (b) UVA (λmax_{365}) lamps.

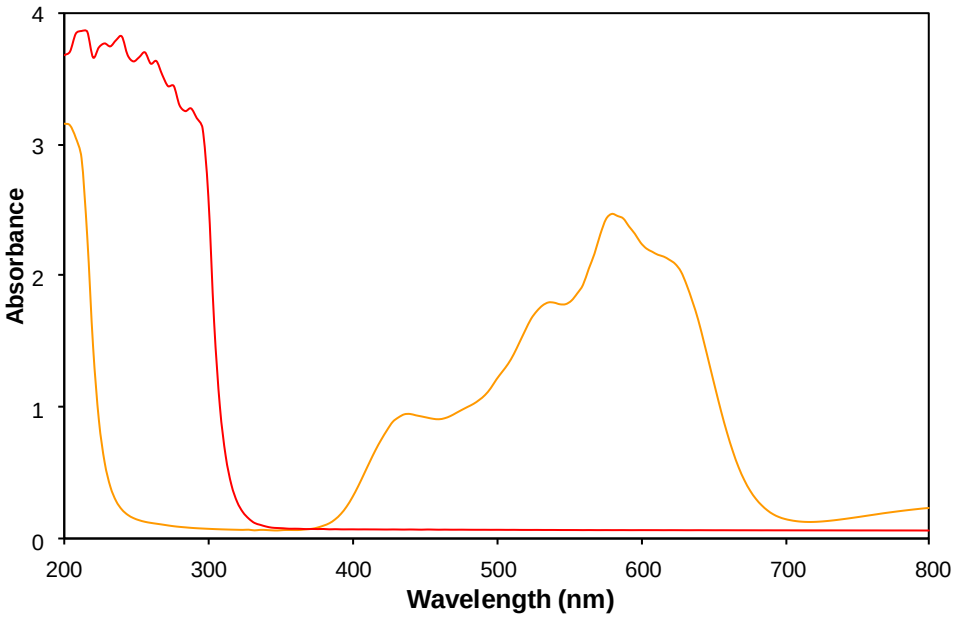

Figure 2.7 The UV Vis absorption spectra of UG5 and WG20 filters used in the solar simulator.

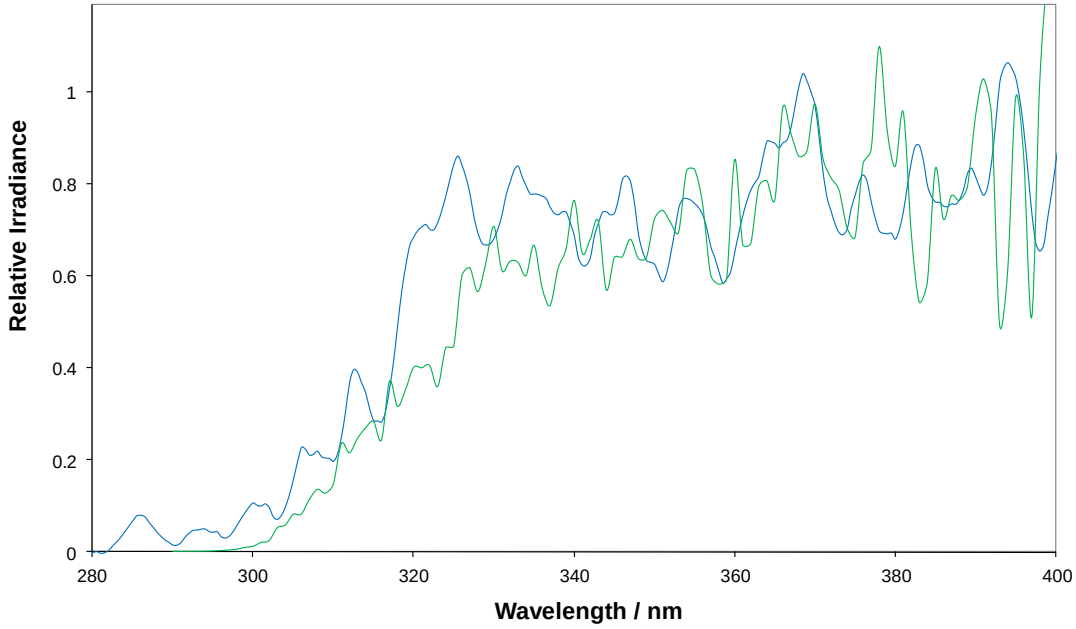

Figure 2.8 The solar simulator emission spectrum i.e. emission spectrum of xenon lamp with filters compared to a solar spectrum recorded on a clear summer's day in Melbourne (53^{o} S) at 12 noon, on 17th January 1990.

2.3 UV measurement

2.3.1 UV radiometer

The UV irradiance levels from the UVA and UVB lamps were monitored using a digital UVX Radiometer, UVP as seen in Figure 2.9. The radiometer was used with one of two interchangeable sensors for measuring the λ_{max} of emission for each lamp i.e. 365 nm (UVA) and 315 nm (UVB) UV wavelengths.

Figure 2.9 A UVX Radiometer

2.3.2 UVI meter

The UVI levels of the Solar Simulator system were monitored using a handheld electronic SafeSun^{TM} UV Meter as seen in Figure 2.10. The UV meter not only provided a measure of the UVI of the light emitted by the solar simulator but it also monitored the absorbed doses and indicated when one MED for skin type II had been reached.

Figure 2.10 A SafeSun™ UV Meter

2.4 General sample preparations

2.4.1 Ink preparation

The intelligent inks used to produce many of the sample films were typically prepared by dissolving a few milligrams of the dye of choice in 2-4 g of the polymer solution of choice. Any other key ingredients, e.g. semiconductor, sacrificial electron donor or deliquescent agent were also added and solutions stirred well and/or placed in an ultrasonic bath to ensure dissolution and dispersion of components.

2.4.2 Ink-based film preparation

Films of typical inks were cast onto either 25 mm diameter quartz or borosilicate glass discs using a Spin Coater Model 4000-1. Thus, a few drops of casting ink were deposited on to the surface of the disc and then spun at a set spin speed for a set time. Typically the product was then dried for 2 min in an oven at 70 °C and allowed to cool to room temperature before use. The specific details of each preparation can be found in the appropriate results and discussion chapters.

2.4.3 Intelligent pigment preparations

A number of different hydrophobic ammonia/volatile amine (A/VA) indicator pigments were prepared using different pH dyes. The following general procedure was used; 0.2-0.5 g dye added to a beaker containing 2 g of hydrophobic silica (Degussa/Evonik Aerosil R812, specific surface area = 260 ± 30 m^2g^{-1}, average particle size = 7 nm) and approx. 80 ml methanol. The mixture was well stirred and sonicated in an ultrasonic bath for 15 min to ensure dissolution of the dye and good coating of the silica. The resulting mixture was transferred to a round-bottomed flask. The methanol was then removed with the aid of a rotary evaporator at 30°C under reduced pressure. The dye coated silica product was removed and ground into a fine powder that will be referred to as the 'pigment'. The names and structures of each of the dyes used are given in the relevant results and discussion chapter.

2.4.4 Polyethylene film preparations

All 7 hydrophobic pigments were used to produce plastic polymer films. Typically 0.4 g of the hydrophobic pigment was added to 2 g of powdered polyethylene (Alfa Aesar, LDPE, 100 μm) and ground together using a mortar and pestle until the colour was homogeneous. A small amount of the hydrophobic pigment/polymer mixture was heat pressed using a Specac Atlas™ Series Heated Platens as pictured in Figure 2.11

The temperature gauge is set to a temperature close to the melting point of the polymer e.g. 115 ^oC for Polyethylene. A small amount (*ca.* 0.3-0.4 g) of the typical polymer mixture is sandwiched between two discs of aluminium foil and loaded in to the sample holder with the thickness guide ring in place. The sample holder is placed in between the heated platens which are hand tightened to secure the sample, taking care not to over-tighten. The sample is then left for a few minutes to allow the polymer to melt. The sample is ready to press when the top section of the sample holder will move easily as the handle is pushed. The sample is then pressed by

retightening the heated platens and applying a hydraulic load of 5 kg for 5 minutes. The sample holder is removed and placed in the water cooling system to cool to room temperature. The result is a thin, (0.1 mm thick), flexible coloured plastic film.

(a)

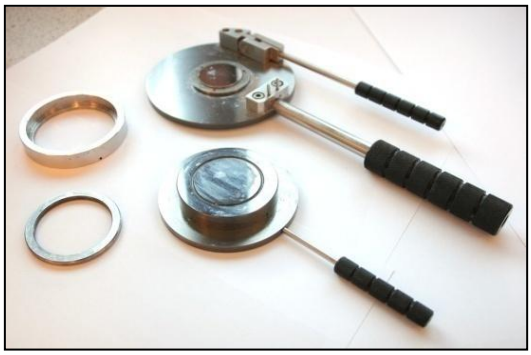

(c)

(d)

(b)

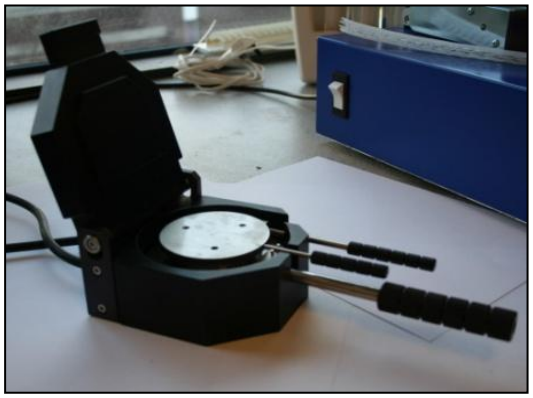

(e)

Figure 2.11 Photographs of the Specac Atlas^{TM} Series Heated Platens thin film system: (a) whole unit, (b) temperature control unit, (c) sample holder and size guide, (d) sample holder between heated platens and (e) the cooling system.

2.5 Film thickness

2.5.1 Scanning electron microscopy

As part of the process of characterising each of the sample films, their film thickness had to be determined. This was achieved using a Cambridge Instruments Stereoscan 90 scanning electron microscope (SEM).

2.5.1.1 Sample preparation

Samples of each of the ink-based films were prepared as follows. Each casting ink was used to cast a film on a borosilicate glass coverslip using a spin-coater as per their preparation. After drying the films, the coverslips were then carefully broken into smaller pieces with care taken not to damage the film. A small fragment of the coverslip coated with the film was then mounted onto conducting carbon adhesive pads attached to aluminium stubs and sputter coated with gold to ~ 20 nm thickness as illustrated in Figure 2.12 below.

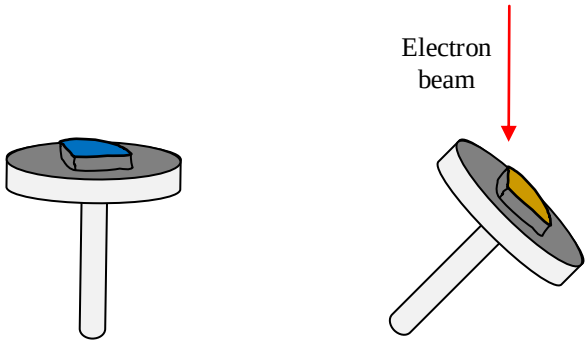

Figure 2.12 SEM sample

The samples were then tilted to 45^{o} in the SEM to obtain an edge-on view in order to determine the film thickness. Where possible multiple measurements were noted and the mean determined, an example of which can be found in Figure 2. 13 which shows an image generated for a typical LG/PVA H_2O_2 indicator film (see Chapter 7 for details). This was the primary method for determining film thickness.

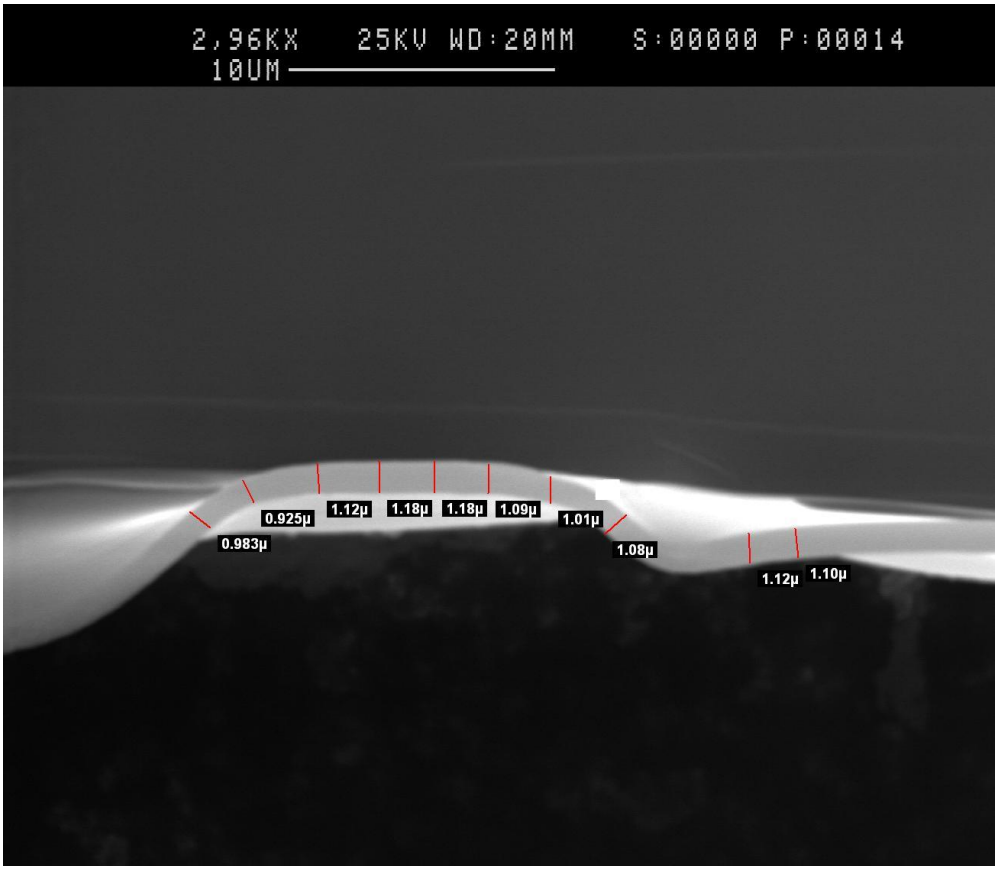

Figure 2. 13 A SEM image of a typical LG/PVA film edge on at x2,960 magnification. Mean film thickness = 1.1 μm.

N.B. Operation of SEM was carried out by the in-house SEM technician, James Morrow.

2.5.2 Profilometery

Certain film thicknesses were also determined by thin film profilometry to verify their SEM measurements. Profilometry involves moving a diamond stylus over a predetermined distance. The vertical displacement of the stylus changes with variations on the film's surface, thus enabling the determination of thin film thicknesses. A Dektak Profilometer was used for all such measurements.

2.5.2.1 Sample preparation

In order to carry out a thin film measurement, a borosilicate glass disc was half covered with sellotape. The disc was then coated with a thin film of polymer solution using a spin coater. After drying the sellotape was carefully removed, taking care not to stretch the polymer film. The final product is a half polymer-coated glass disc. When positioned in the profilometer the stylus maps the glass disc before lifting up at the polymer-glass boundary, thus giving a measure of film thickness. An example is shown below for a 10% PVA solution, spun at 1200 rpm and dried in the oven. From Figure 2.14 it is evident that the film thickness is 2.3 μm. Note this compares well with the SEM-measured value for an identical film which equals 2.5 μm (see Chapter 4 for data).

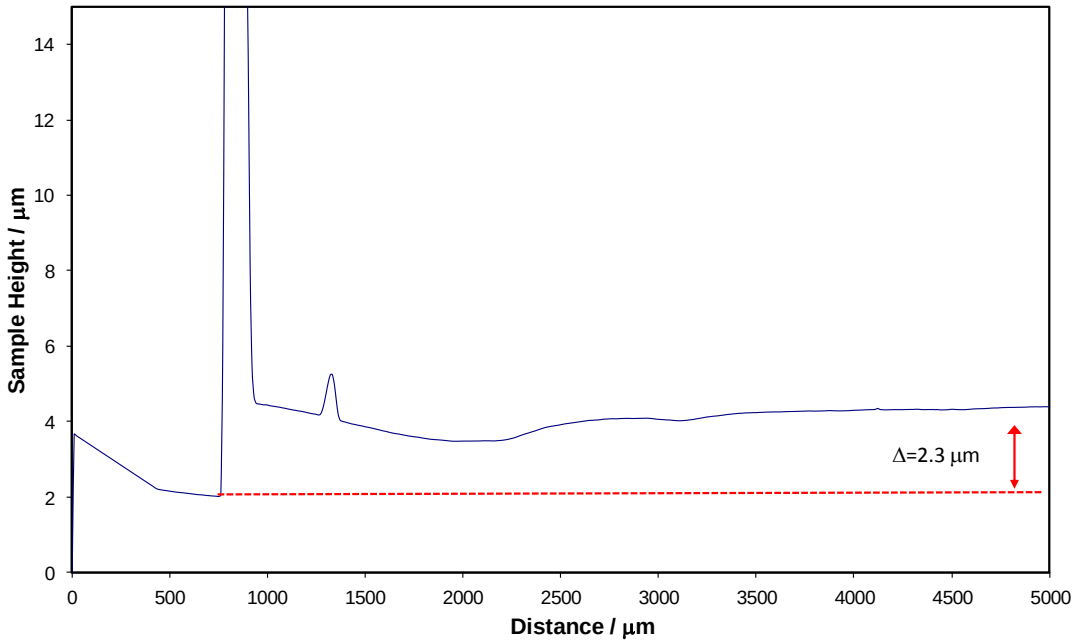

Figure 2. 14 Profilometry thin film thickness determination of a 10% PVA polymer film spun at 1200 rpm. Measured film thickness of 2.3 μm.

Not all films were suitable for measurement by this technique, particularly thin HEC films. Such films made with a softer polymer were partially removed (i.e. scratched

off the glass substrate) during the measurement, thus it was not possible to accurately define the glass-polymer boundary or determine the film thickness.

2.5.3 Micrometry

For thicker samples such as heat-pressed polymer films a Mitutoyo micrometer was used to measure the film thicknesses.

2.6 Gas blending

Different concentrations of ammonia gas were generated using Cole-Parmer rotameters. Typically a 1000 ppm ammonia gas stream was mixed with a nitrogen gas stream in varying ratios.

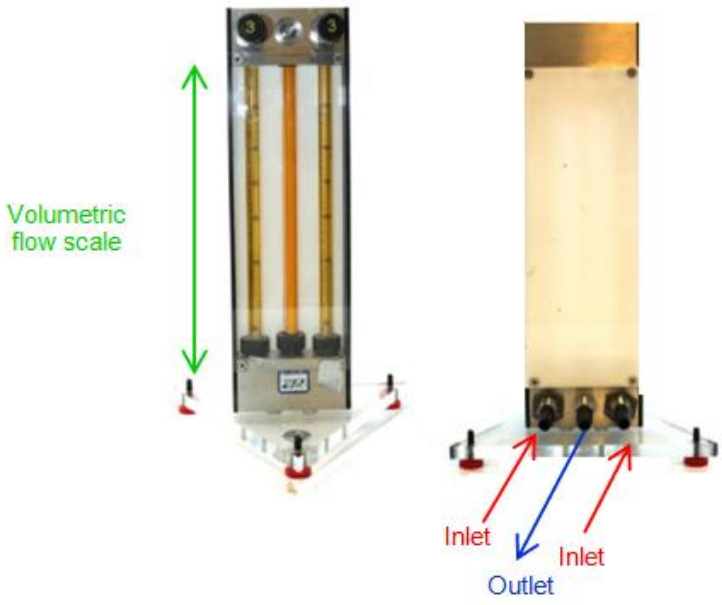

Figure 2. 15 Cole-Parmer rotameter.

In several experiments sample films were exposed to various humidity levels. This was achieved by mounting the sample film at the front of the cell holder facing

inwards while a blank quartz disc was mounted at the other side to create a small enclosure around the sample film allowing the atmosphere immediately surrounding the film to be varied. The humid air or gas was passed through the inlet and outlet valves labelled in Figure 2.16.

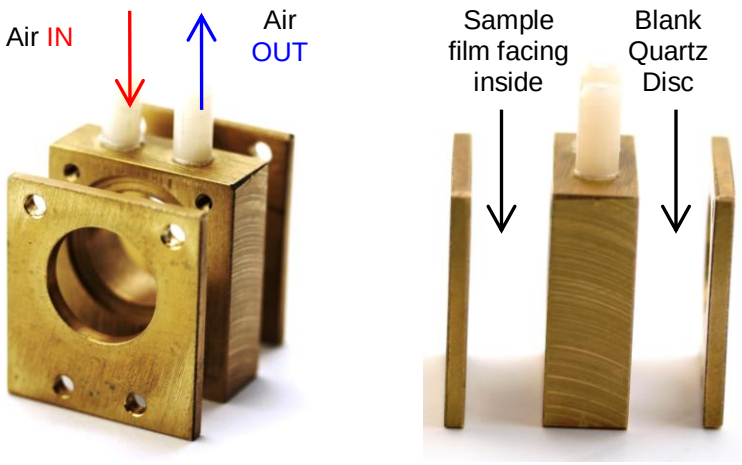

Figure 2. 16 Gas sample cells.

Humid air was generated using the experimental set-up illustrated in Figure 2. 17. Air is passed through two Dreschel bottles in series, each with a sintered glass inlet to ensure good dispersion of the carrier gas bubbles, containing 150 ml of water. This generates a 100% RH gas stream (blue line) which is mixed with a dry air stream (red line) to create a range of different RH levels as measured by a hand held Hanna HI hydrometer.

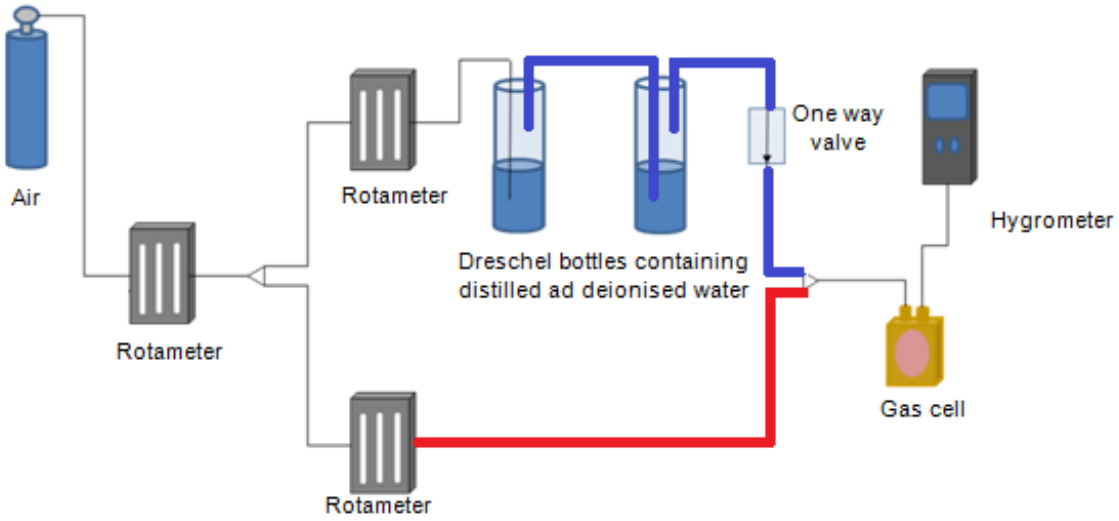

Figure 2. 17 Experimental set up for varying relative humidity conditions.

2.7 References

1. B. L. Diffey, *Materials*, 2002, **28**, 4-13.

Chapter 3

UV dosimeter based on DCIP and SnO_2

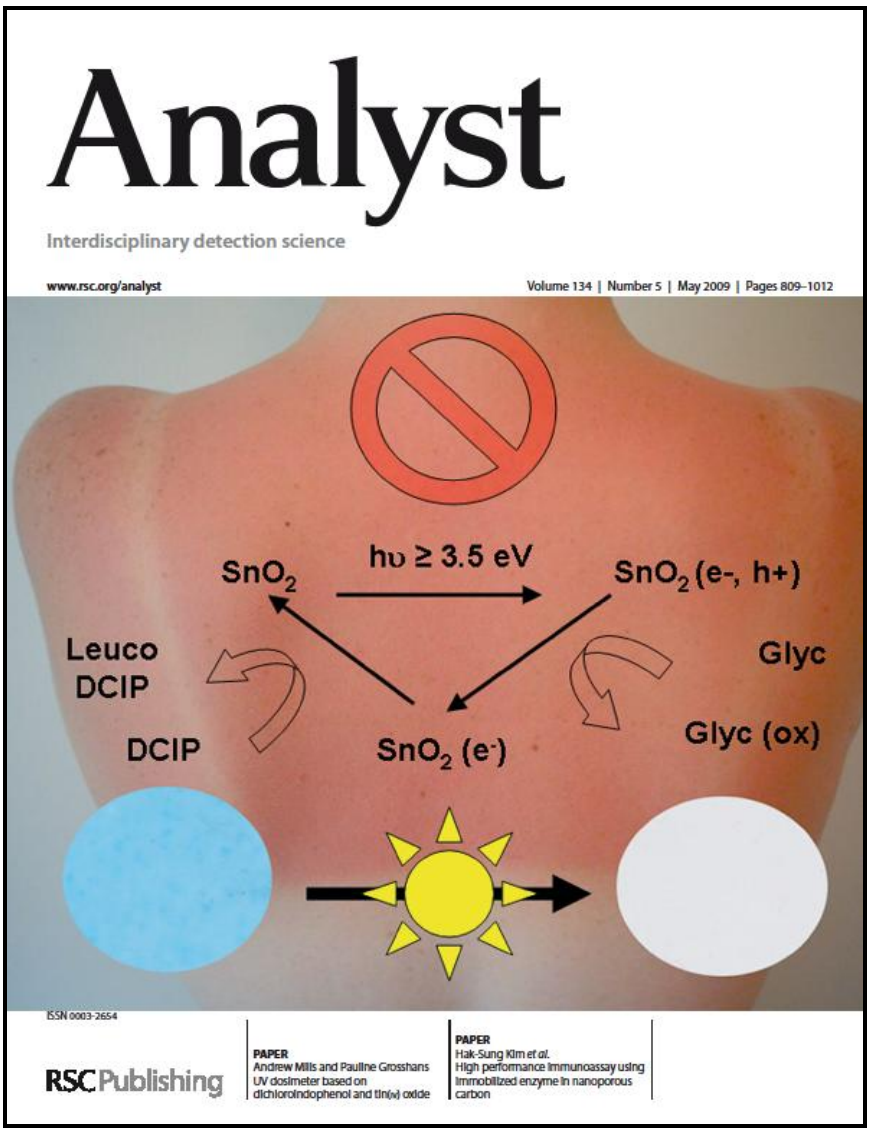

3 UV dosimeter based on DCIP and SnO_2

3.1 Introduction

In a recent paper the Mills group reported a colorimetric UV indicator and dosimeter that utilises semiconductor photocatalysis.[1] Photocatalysis is a term used to describe the "acceleration of a photoreaction by presence of a catalyst" where the phrase "photoreaction" is synonymous with the terms "photo induced" or "photo activated" reaction.[2]

The UVA indicator[1] comprised a hydroxy ethyl cellulose (HEC) film containing: the redox dye, methylene blue (MB), the sacrificial electron donor triethanolamine (TEOA) and titania nano particles (TiO_2). The TiO_2 nanoparticles absorb the UV light and photo-oxidise the TEOA. The trapped photogenerated electrons are then able to reduce the redox dye from its highly coloured (blue) oxidised form, i.e. MB, to its colourless form, leuco methylene blue, LMB. Oxygen present in air reacts rapidly with the LMB, re-oxidising it to MB. As a result the degree of bleaching exhibited by a naked MB film is directly dependent upon the level of UVR, due to a dynamic equilibrium between the photoreduction process (MB→LMB) and the dark re-oxidation process (LMB + O_2→MB). When covered with an O_2 impermeable barrier, such as glass or regenerated cellulose, the latter step is not possible and the covered MB film is able to act as a UV dosimeter.

In the above UV indicator/dosimeter the titania particles absorb light of wavelengths $\leq$ 380 nm thus are very responsive to both UVA and UVB light. However, as noted earlier, it is mostly the UVB component of solar UV that is responsible for solar-induced biological damage, such as sunburn. Clearly what is required is a semiconductor photocatalyst that has a larger band gap than titania (3.2 eV) and so is more effective in absorbing UVB light, than UVA. In addition, a more attractive alternative to MB as a redox indicator would be a dye that is not only readily reduced by the photogenerated electrons generated on the semiconductor photocatalyst particles but, unlike MB, has a reduced form that is not readily re-oxidised by

ambient O_2. Such a feature would avoid the need for an O_2 barrier and make fabrication of this UVB-sensitive dosimeter relatively simple. In this chapter the characteristics of such an improved UV dosimeter, using tin(IV)oxide, SnO_2, as the large band-gap, UVB-absorbing semiconductor (3.5 eV) and 2,6-dichloroindophenol (DCIP) as the O_2-insensitive redox indicating dye will be described.

3.2 Experimental

3.2.1 Materials

The tin(IV)oxide (SnO_2) used in the DCIP dosimeter films was <100 nm nanopowder purchased from Sigma Aldrich Chemicals, with particle sizes typically ranging from 10-70 nm as determined using SEM and TEM, see Figure 3.1.

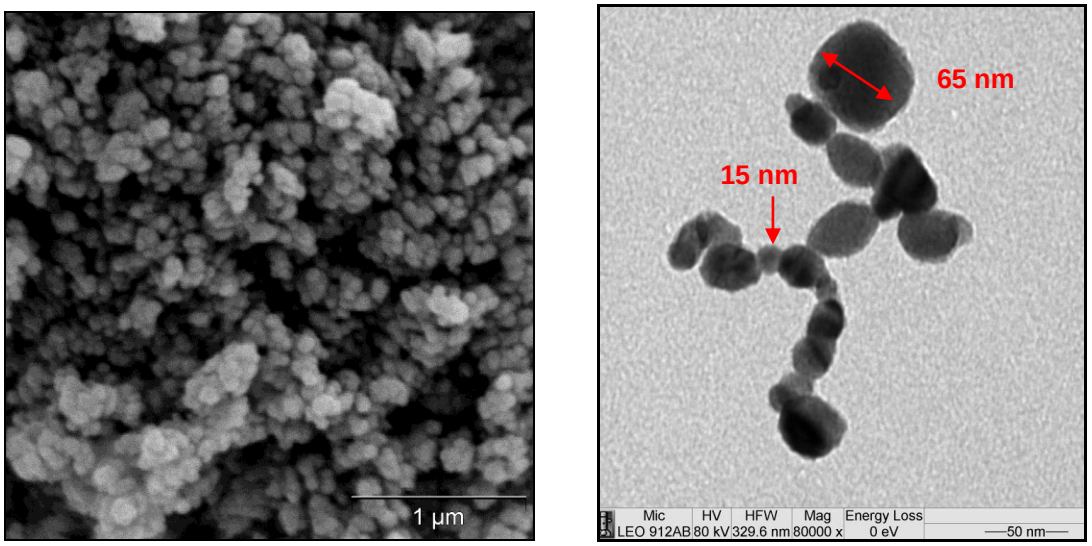

Figure 3.1 (a) SEM image of SnO_2 nanopowder at x30,000 magnification and (b) TEM image of SnO_2 nanopowder at x80,000 magnification.

Note: These SEM and TEM images were recorded by Dr Laurence Tetley at the University of Glasgow./

3.2.2 UV ink and dosimeter preparation

A typical UV dosimeter casting ink was prepared by dissolving 5 g of HEC in 95 ml water at room temperature, followed by stirring for 24 hours. 5 mg of DCIP, 100 mg SnO_2 and 100 mg glycerol were then added to 2 g of the HEC polymer solution. The solution was well stirred to ensure dissolution of the dye and the dispersion of the SnO_2. The blue-coloured casting solution contained 5 phr of DCIP *i.e.* 5 parts per hundred resin (or 5 g of DCIP for 100 g polymer). Films were cast on quartz discs, 25 mm in diameter and 1 mm thick, using a spin coater. Thus, a few drops of casting solution were deposited on the surface of the disc, which was then spun at 2400 rpm for 15 seconds. The resultant product was then dried for 2-3 minutes at 70°C and cooled to room temperature (5 minutes) before use. Figure 3.2 illustrates a typical DCIP ink formulation and DCIP dosimeter along with an SEM image of a typical DCIP dosimeter edge on. The final UV dosimeter film product was a blue coloured, *ca.* 3.85 μm thick (as measured using a SEM see Figure 3.2) film on a quartz disc and shall be referred to forthwith as a standard DCIP film.

(a)

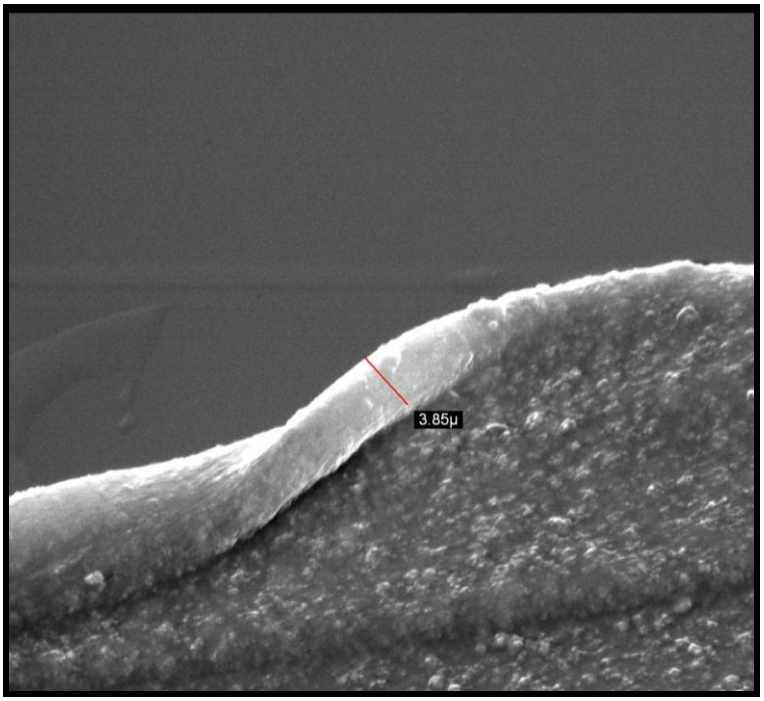

(b)

Figure 3.2 (a) A photograph of a standard DCIP ink formulation and a typical DCIP dosimeter prior to irradiation and (b) an SEM image of a typical DCIP dosimeter edge at x2,130 magnification.

3.3 Results and discussion

3.3.1 Optical characteristics of a DCIP film

A series of casting solutions were prepared comprising the standard DCIP UV-sensitive ink formulation with various components omitted, with the exception of the encapsulating polymer HEC and solvent, water. These solutions were used to cast the following films on quartz discs: HEC, Glycerol/HEC, DCIP/HEC and the typical dosimeter itself DCIP/SnO_2/Glycerol/HEC. The UV/Visible absorption spectra of these films were recorded and the results are illustrated in Figure 3.3.

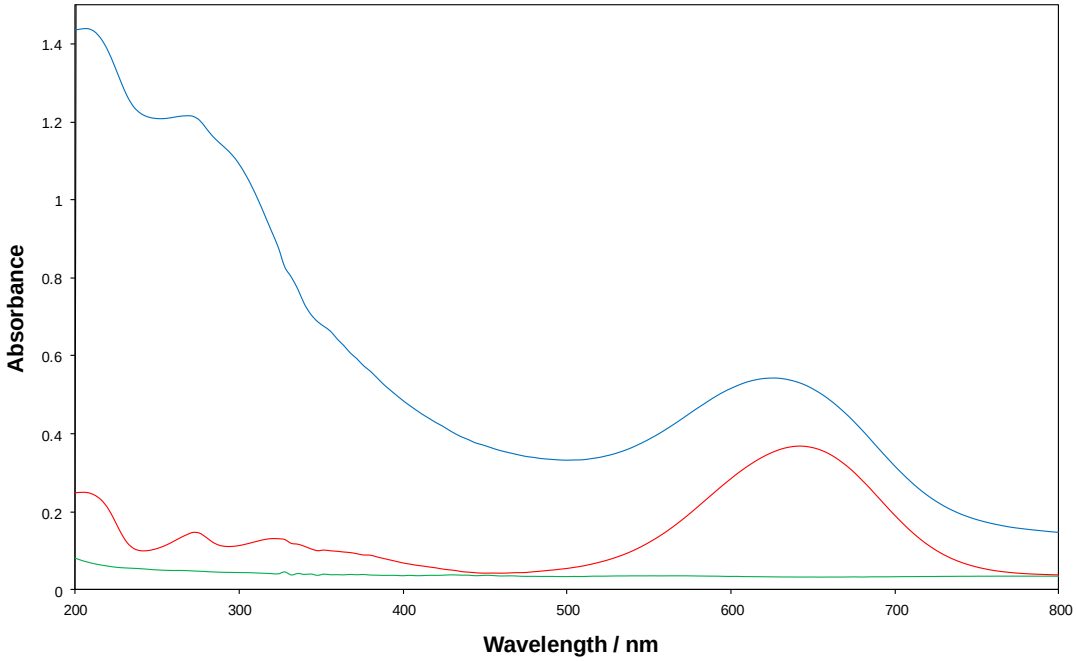

Figure 3.3 Absorption spectrum of standard DCIP film prior to irradiation. Also shown are the absorption spectra for a blank HEC film and glycerol/HEC film and also a DCIP/ HEC film.

From Figure 3.3 it is clear that the polymer (HEC), the electron donor (glycerol) and the redox dye, DCIP, do not absorb to any great extent in the UVA and UVB regions (≤ 380 nm), whereas SnO_2s absorbs significantly, especially in the UVB region. SnO_2 is a wide band-gap semiconductor (E_g = 3.5 eV *i.e.* absorption threshold

354 nm)[3] and is responsible for the broad, strong absorption band between 200 and 300 nm seen in the UV/visible absorption spectrum of the standard ink film (see Figure 3.3) The DCIP/HEC spectrum has a maximum absorption, λ_{max}, at 636 nm which gives the film its blue colour.

3.3.2 UV irradiation of a typical DCIP film

When irradiated with UVB light (λ_{max} (emission) = 315 nm) a typical DCIP film changes colour from blue to white/colourless as seen in Figure 3.4.

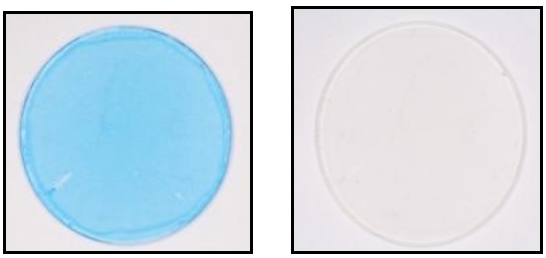

(a) (b)

Figure 3.4 Photographs of a typical DCIP film (a) before and (b) after exposure to UVB light.

This process was monitored spectrophotometrically *via* the disappearance of the absorption band due to the DCIP at 636 nm. The colour change observed arises as a result of photogenerated holes in the SnO_2 reacting with the glycerol present, a sacrificial electron donor, to yield glyceraldehdye which can then be oxidised further to glyceric acid. The photogenerated electrons are then able to reduce DCIP to its leuco-form as depicted in Figure 3.5, which is stable in air when encapsulated in HEC E^o (DCIP/leuco-DCIP) = 0.688 V.[4] These major processes are illustrated in the reaction scheme in Figure 3.6.

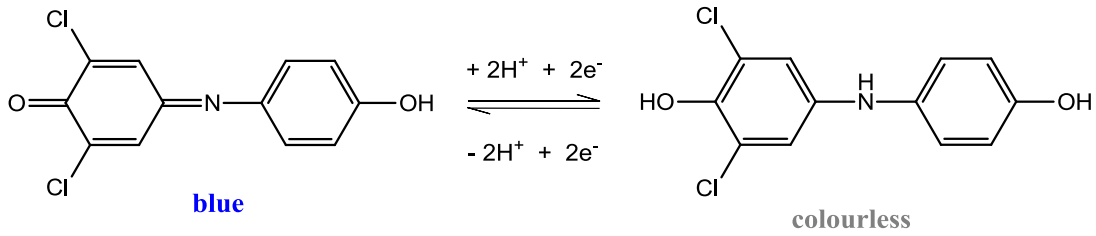

Figure 3.5 Mechanism for the reduction of DCIP (blue) to leuco-DCIP (colourless).

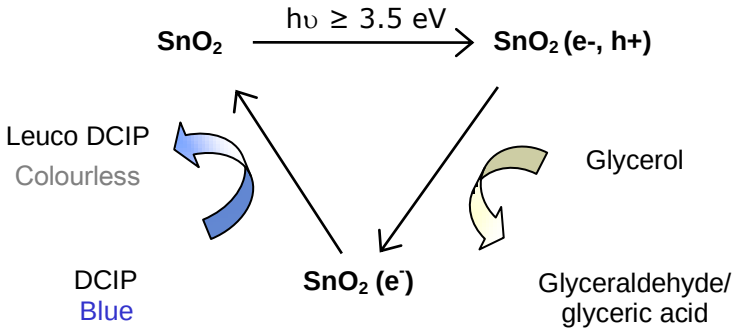

Figure 3.6 Reaction scheme illustrating the main mechanistic features of a typical DCIP/ SnO_2/Glycerol/HEC UV indicator film upon irradiation with UVB light.

A typical set of UV/visible absorption spectra recorded for a DCIP film as a function of UVB irradiation time are illustrated in Figure 3.7. Using these data, and additional results from the same experiment using 3 mW cm^{-2} UVA, it was possible to plot the variation in the change in absorbance at λ_{max} *i.e.* ΔAbs_{636} as a function of irradiation time, which is illustrated in Figure 3.8.

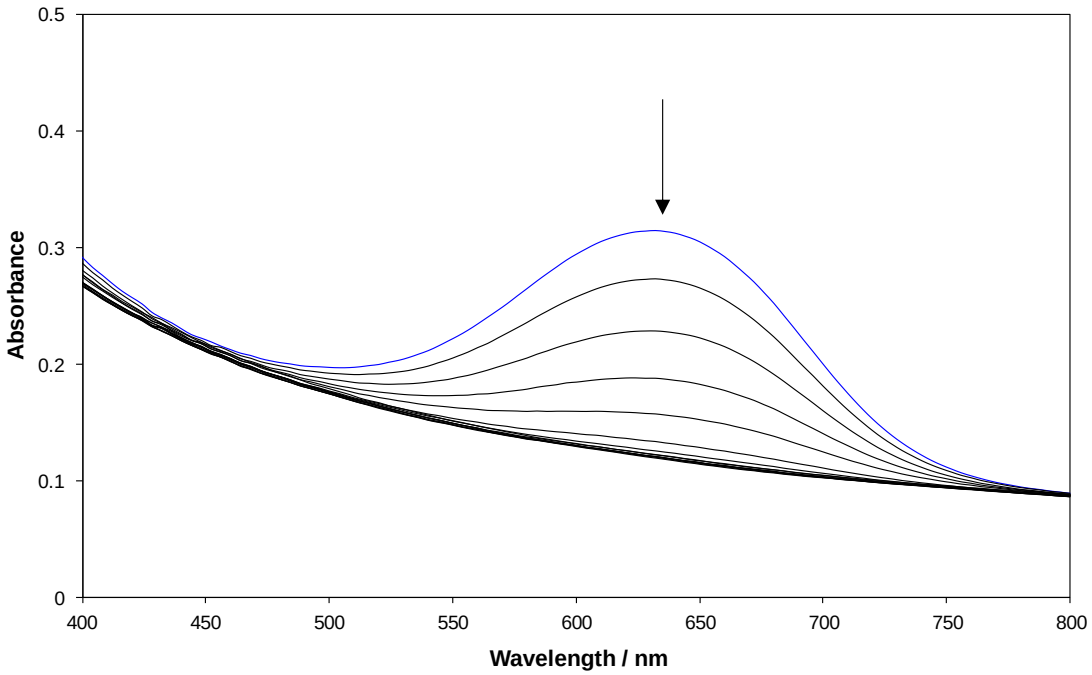

Figure 3.7 Absorption spectra of a typical DCIP film after irradiation with 3 mW cm^{-2} UVB light for 300 seconds.

The coefficient of variance associated with the films undergoing photobleaching is ± 5%; this is typical of the error for all DCIP films unless otherwise stated. A similar experiment was conducted using a film containing only DCIP and HEC (i.e. no SnO_2 or Glycerol) and 3 mW cm^{-2} UVB light and the data obtained were used to generate the third series in Figure 3.8.

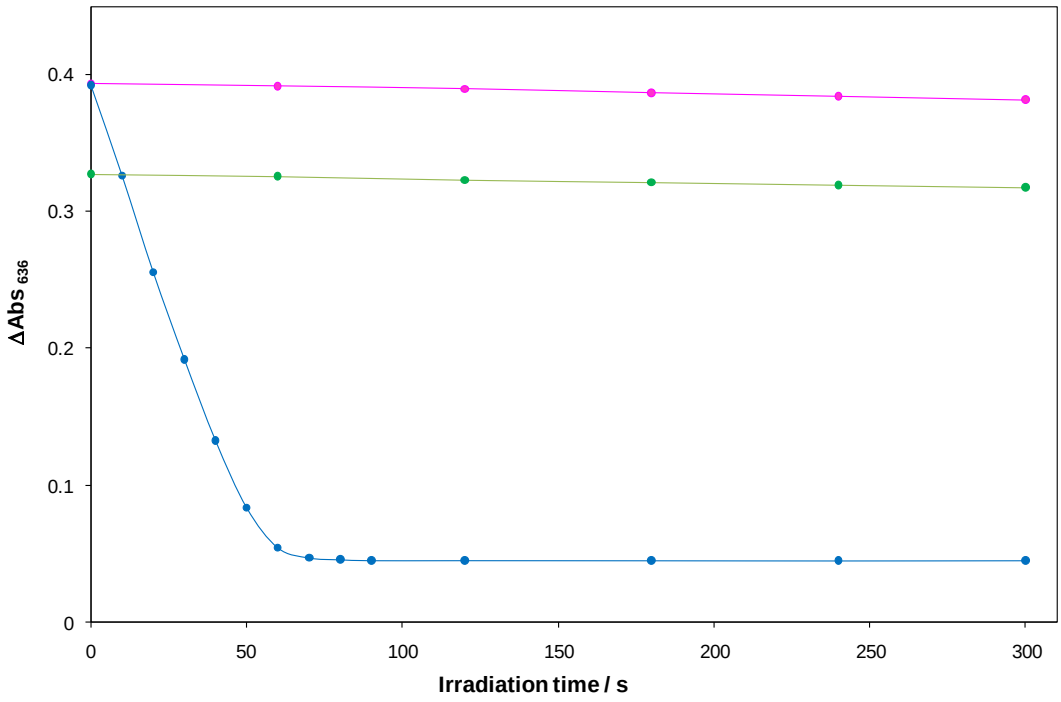

Figure 3.8 ΔAbs_{636} vs. irradiation time plot for a typical DCIP film irradiated with 3 mW cm^{-2} UVB. Also shown is the analogous plot for a typical DCIP film irradiated with 3 mW cm^{-2} UVA light and a DCIP alone film (i.e. no SnO_2) irradiated with 3 mW cm^{-2} UVB

These results show that the photo-induced decolouration of the standard DCIP film was not observed when the film was irradiated with 3 mW cm^{-2} UVA light instead of UVB, indicating that the light emitted by the UVA lamp (a black light lamp, λ_{max} (emission) = 365 nm) does not contain photons of sufficient (high) energy to create the necessary electron-hole pairs to effect the photoreaction of DCIP.

Other work showed that even when UVB light was used no decolouration occurred for a DCIP film in which the SnO_2 had been omitted (see Figure 3.8) *i.e.* the SnO_2 semiconductor sensitizer particles are essential for the DCIP film to work as a dosimeter.

3.3.3 Recovery of DCIP films

In the reaction scheme reported earlier, it was assumed that the photocatalysed bleaching of DCIP by glycerol, sensitised by SnO_2, is irreversible *i.e.* the reduced form of DCIP, colourless leuco DCIP, is not readily oxidised by ambient oxygen in the polymer/glycerol film environment. This feature is obviously necessary for the DCIP indicator to function as a dosimeter. In order to demonstrate this feature and determine the post-irradiation stability of a photobleached standard film, such a film was fully converted to its bleached form by irradiating for 10 minutes under 3 mW cm^{-2} UVB light and then monitoring the absorbance of the film at 636 nm over the following 12 hours as shown in Figure 3.9.

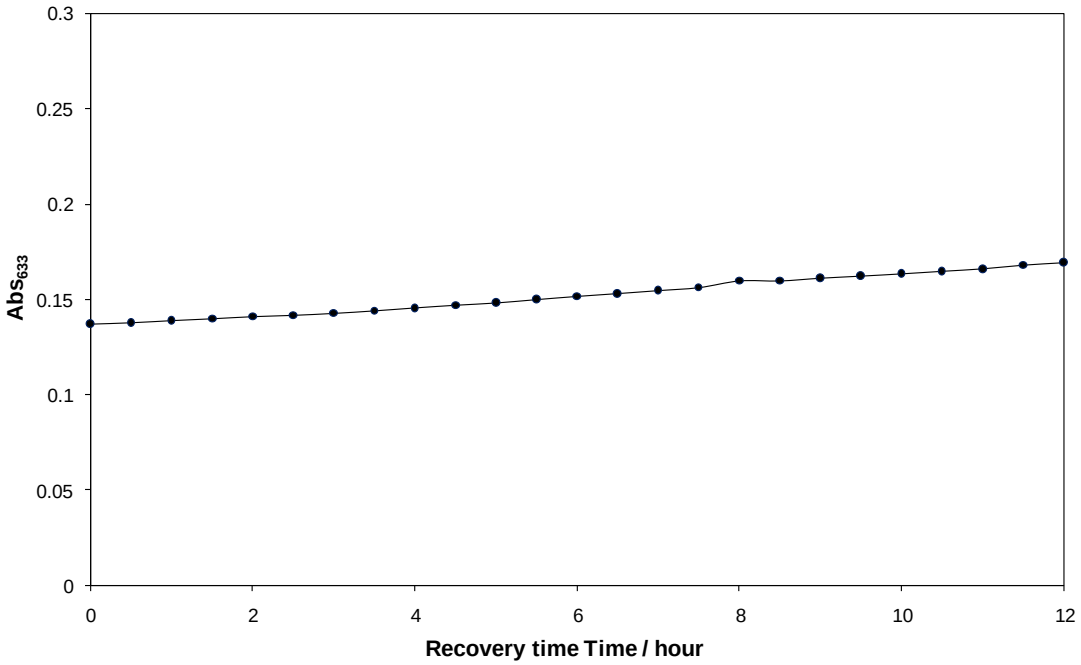

Figure 3.9 A plot of Abs_{636} against recovery time for a typical DCIP film after irradiation with 3 mW cm^{-2} UVB light for 10 minutes. Abs_{636} was recorded every 30 mins for 12 hours.

This work revealed that over this time period the film regained little (8%) of its original colour and, for the purposes of a UV dosimeter, the photobleaching of DCIP can be considered as irreversible.

3.3.4 *Kinetics of photobleaching of a DCIP film*

3.3.4.1 Irradiance

In one set of experiments, a number of standard DCIP films were exposed to different UVB irradiances ranging from 1-6 mW cm^{-2} from the UVB source with a total exposure time of 300 seconds. The absorbances (at $\lambda = 636$ nm) of the DCIP films under test were measured spectrophotometrically and the initial rate, r_i, of decolouration for each film was determined from the plot of the change in absorbance, ΔAbs_{636}, as a function of irradiation time. The results of this work are illustrated in Figure 3.10 along with the associated plot of r_i as a function of UVB irradiance in Figure 3.11.

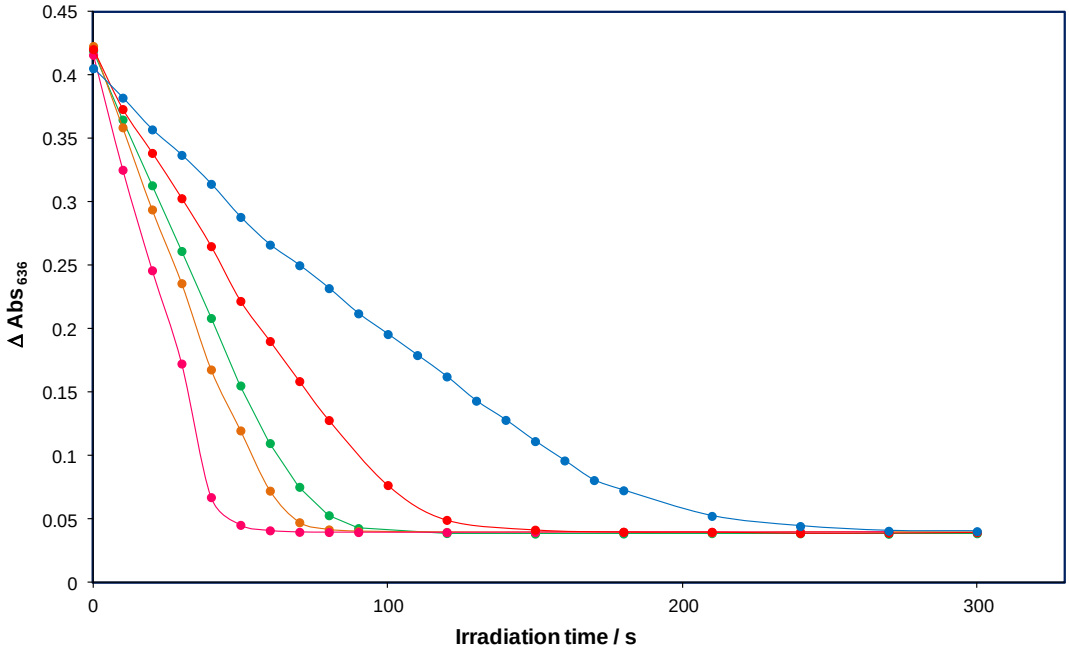

Figure 3.10 A plot of ΔAbs_{636} against irradiation time for typical DCIP dosimeter films after irradiation with 1 mW cm^{-2} , 2 mW cm^{-2}, 3 mW cm^{-2} , 4 mW cm^{-2} and 5 mW cm^{-2} UVB light.

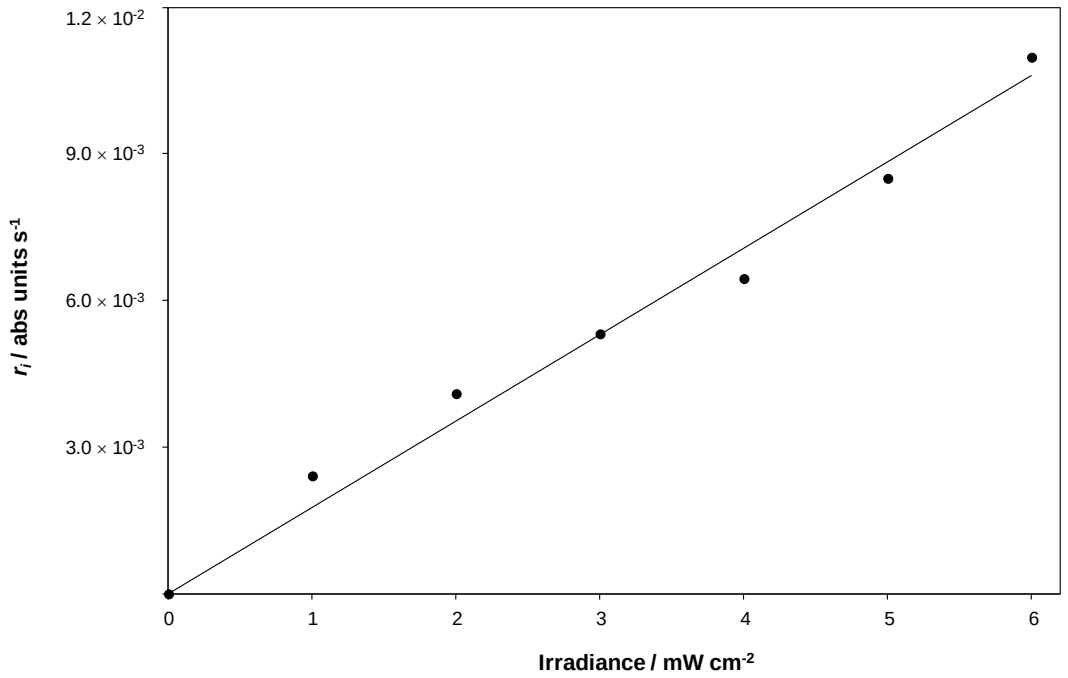

Figure 3.11 A plot showing the variation of r_i with irradiance, calculated using the data in Figure 3.10.

The observed direct dependence of r_i upon irradiance at these irradiance levels is not unusual in semiconductor photocatalysis[5,6] and, in this case, is indicative of very effective trapping of the photogenerated holes by the glycerol present. The DCIP concentration in a standard DCIP film is 0.07 M (≡ 5 phr) and film thickness is 0.00039 cm, which allows the number of moles of DCIP per cm^{-2}, *i.e.* n_o, to be determined as 6.99 x 10^{-8} moles cm^{-2}. Using this information, the gradient of the line of best fit to the data in Figure 3.11 (= 0.0018 Abs units s^{-1} mW^{-1} cm^2) and the initial ΔAbs_{636} of a DCIP film (0.405), the initial number of DCIP molecules that are photobleached cm^{-2} s^{-1}, R_i^* was determined as 7.19x10^{13} molecules cm^{-2} s^{-1}. Since the UVB lamp used in this work emitted ~1.59 × 10^{15} photons s^{-1} cm^{-2}, and the fraction of UVB light (*i.e.* light at 315 nm) absorbed by the DCIP film was determined to be 0.845), a value for the quantum yield of the photobleaching process of *ca.* 5.4% was calculated. The above data is tabulated below in Table 3.1 and the methods used to determine such values are detailed in Appendix 1.

UVR	***d***	***λ***	**Rate, R_i^***	***QE***	f_{UVR}	***QY***

	(μm)	**(nm)**	**(x10^{13}molecules/cm^2/s)**	**(molecules/photon)**		
UVB	3.9	315	7.19	0.045	0.845	0.054

Table 3.1 Optical and photocatalytic properties for DCIP dosimeter films, where d = film thickness, λ = emission wavelength from UVB source (i.e. wavelength of light being absorbed by films), QE =quantum efficiency, f_{UVR} = fraction of UVR light being absorbed by dosimeter films and QY = quantum yield.

3.3.4.2 [DCIP]

The effect of dye concentration on the kinetics of the system was investigated by preparing a series of films with varying levels of DCIP. A set of casting inks were prepared containing 1 to 20 phr DCIP, which were cast onto quartz discs and irradiated with 3 mW cm^{-2} UVB light. The r_i of decolouration for each film was determined from the plot of ΔAbs_{636} against irradiation time profiles illustrated in Figure 3.12. Note the higher [DCIP] films have larger coefficient of variations associated with them *viz.* ±10 % for 15 phr DCIP film and ±15 % for 20 phr film. A subsequent plot of r_i *vs.* [DCIP], shown as an inset in Figure 3.12, indicates that r_i does not change significantly with [DCIP] suggesting the kinetics of DCIP photobleaching are zero order. Such zero order kinetics are not uncommon in semiconductor photocatalysis, especially where coatings on photocatalytic films are involved,[28] and indicate that DCIP molecules occupy all the available photocatalytic sites. This is hardly surprising as the standard film has an effective [DCIP] of approximately 0.07 M in the film.

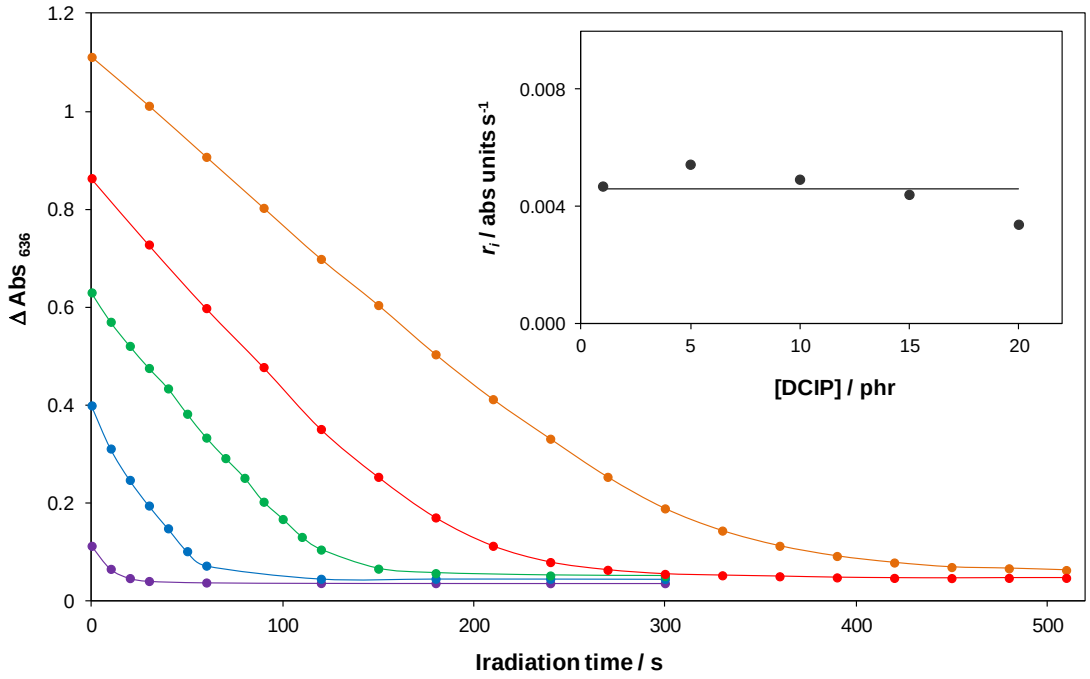

Figure 3.12 A plot of ΔAbs_{636} against irradiation time for HEC films containing 20 phr, 15 phr, 10 phr, 5 phr and 1 phr DCIP, 100 phr glycerol and 100 phr SnO_2 upon irradiation with 3 mW cm^{-2} UVB. Inset diagram shows the variation of r_i with [DCIP], calculated using the data in the main diagram.

3.3.4.3 *[SnO_2]*

The sensitivity of the standard DCIP UV dosimeter towards UVB light can be readily varied by changing the amount of UV absorbing semiconductor (SnO_2) present. Thus, a series of SnO_2/DCIP/glycerol/HEC casting inks were prepared containing 10 to 200 phr SnO_2 and used to spin-coat films on quartz discs. Using these films a series of ΔAbs_{636} versus irradiation time profiles were generated with a 3 mW cm^{-2} UVB source and the results are illustrated in Figure 3.13. The value of r_i for each film was determined from these profiles and found to be directly proportional to the level of SnO_2 present over the range studied, i.e. $r_i = 7.0 \times 10^{-5}$ [SnO_2] with a correlation coefficient value of 0.99 as seen in Figure 3.14. As it is the UVB activation of the semiconductor which initiates the reduction reaction and $r_i \propto I_{abs}$

(see Figure 3.11) which in turn depends upon [SnO_2], it was expected that an increase in [SnO_2] would in turn cause an increase in the rate of reduction.

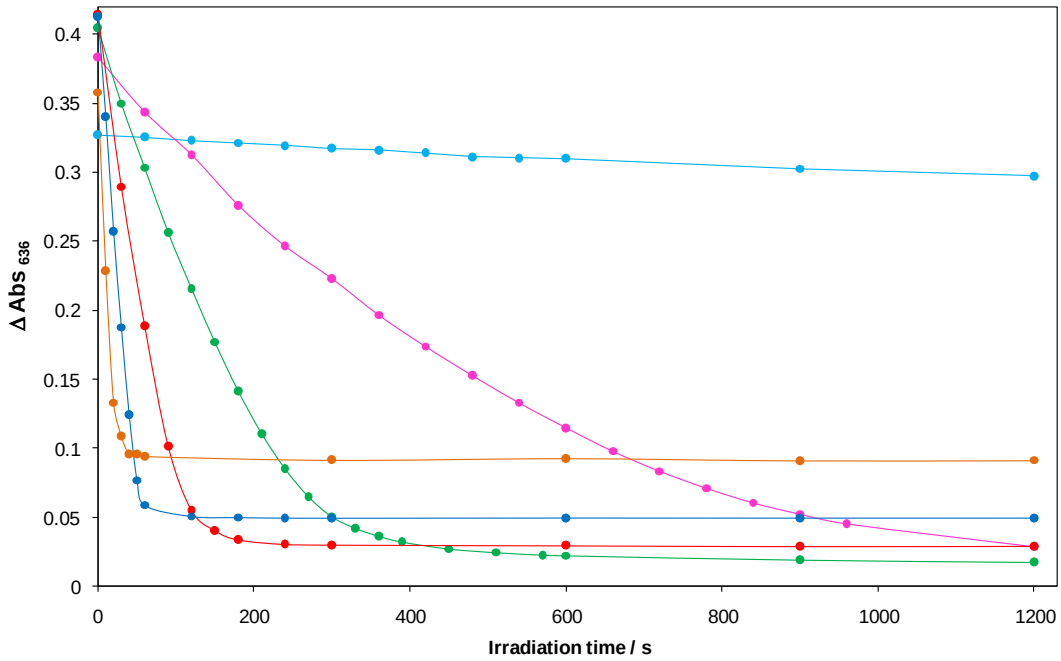

Figure 3.13 A plot of ΔAbs_{636} against irradiation time for HEC films containing 5 phr DCIP, 100 phr glycerol and 0 phr, 10 phr, 30 phr, 50 phr, 100 phr and 200 phr SnO_2 after irradiation with 3 mW cm^{-2}

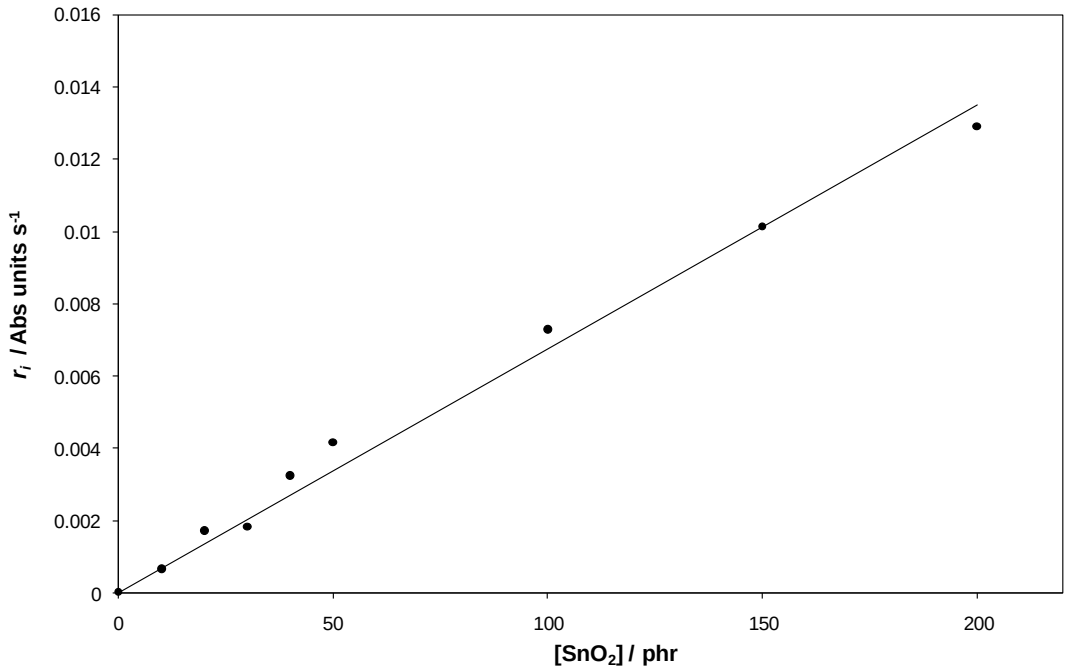

Figure 3.14 A plot of r_i against [SnO_2], r^2=0.99.

3.3.4.4 [Glycerol]

The effect of the level of glycerol present on the initial rate of DCIP film photobleaching was also investigated. As mentioned previously glycerol acts as a sacrificial electron donor, SED, trapping the photogenerated holes and thus promoting the reduction of the DCIP molecules by the photogenerated electrons. A series of casting inks were prepared, containing different loading of glycerol covering the range 0 - 300 phr; these inks were used to produce films which were then irradiated with 3 mW cm^{-2} UVB light whilst their absorbance at 612 nm was monitored. The series of ΔAbs_{612} versus irradiation time profiles arising from this work are shown in Figure 3.15, along with the variation in r_i as a function of [glycerol] that can be derived from this data, see inset diagram in Figure 3.15.

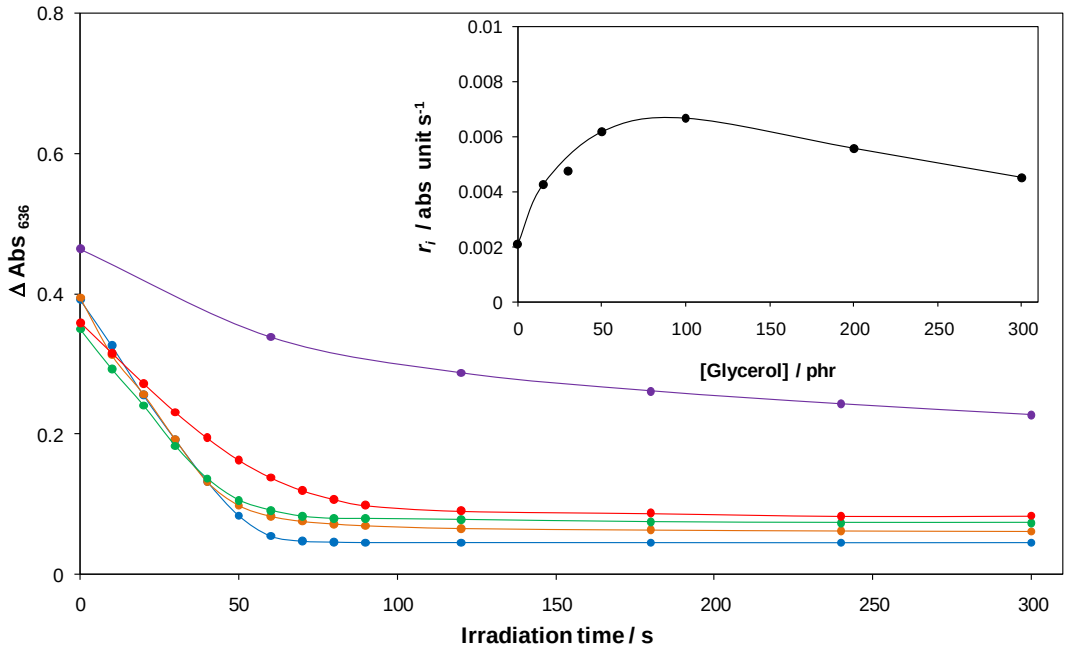

Figure 3.15 A plot of ΔAbs_{636} against irradiation time for HEC films containing 5 phr DCIP, 100 phr SnO_2 and 0 phr , 15 phr, 30 phr, 50 phr and 100 phr glycerol after irradiation with 3 mW cm^{-2} UVB. Inset diagram shows the variation of initial rate with [glycerol], calculated using the data in the main diagram and from films containing 200 phr and 300 phr glycerol which were also tested.

These results show that above a glycerol loading of 100 phr the initial rate of photobleaching of DCIP is not improved, suggesting that hole-trapping is very efficient above this level. Also of note is the observation that photobleaching of the DCIP is effected in the absence of glycerol, although at a much slower rate, implying that SnO_2 is able to utilise the polymer, HEC, as an SED.

3.3.4.5 Relative humidity

To determine if the relative humidity, RH of the surrounding environment had an effect on the response of the DCIP/SnO_2/Glycerol/HEC UV dosimeters, experiments were carried out using typical dosimeter films in high and low RH conditions. Initially a set of typical films were run in a gas cell under dry cylinder air (~0% RH)

followed by a second set that were run in 100% RH conditions. The results of these experiments are illustrated in Figure 3.16 below.

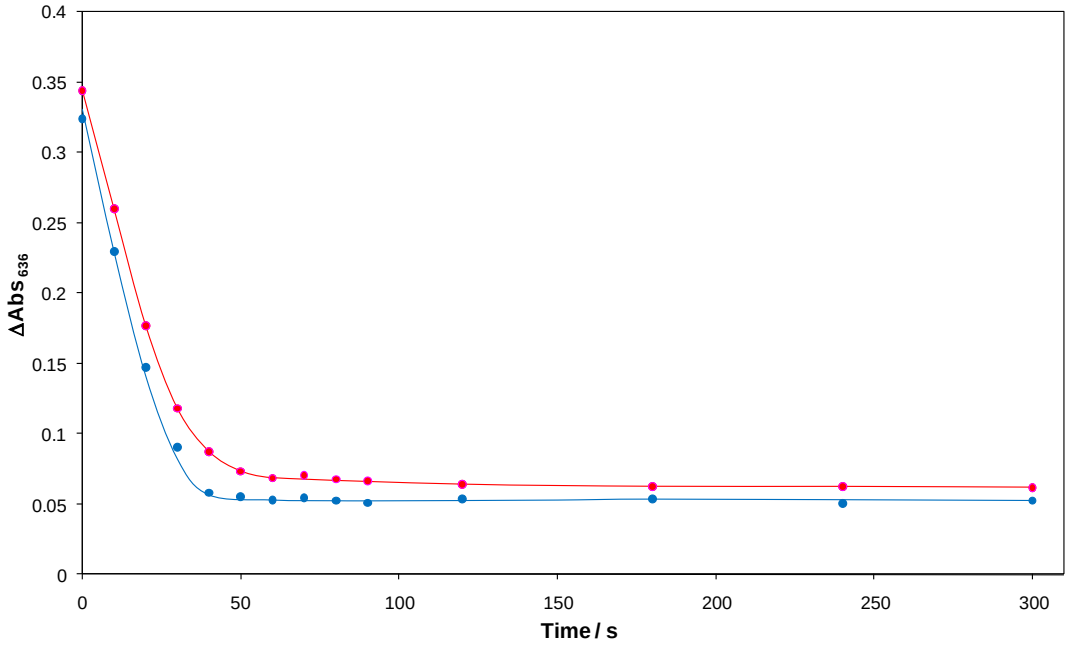

Figure 3.16 A plot ΔAb_{636} versus irradiation time for a series of typical DCIP dosimeters on exposure to 3 mW cm^{-2} UVB light under 100% RH and 0% RH conditions.

From the result in Figure 3.16 it is apparent that there is no significant effect of the relative humidity of the environment on the rate of photobleaching, with relative rates of 1:1.13 for dry and humid conditions.

3.3.5 Solar-simulator UV work using a DCIP film

In a final set of experiments UV solar simulated light (UVI 5) was used to irradiate a standard DCIP film. The observed variation of the absorbance of this film at 636 nm, *i.e.* ΔAbs_{636}, as a function of MED (for skin type II) is illustrated in Figure 3.18. These results show that a standard DCIP ink is too UV sensitive for use as an indicator of impending sunburn for someone with skin type II since it is fully bleached by MED = 0.4.

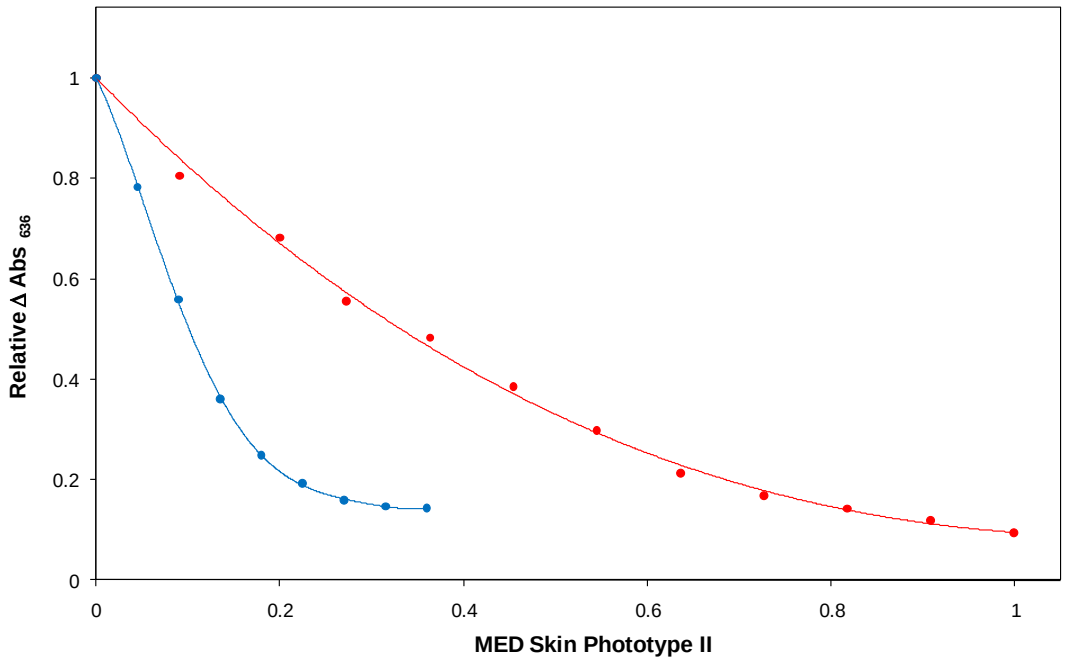

Figure 3.17 A plot of ΔAbs_{636} against MED for skin phototype II received for HEC films containing 5 phr DCIP, 100 phr glycerol with 100 phr (standard formulation) and 45 phr SnO_2, on exposure to solar simulated light at UVI 5.

However, previous work had demonstrated that the UV sensitivity of a DCIP/SnO_2/Glycerol/HEC film can be moderated by using less SnO_2 (see Figure 3.14). Thus, in a separate experiment the level of SnO_2 in the DCIP film formulation was dropped from 100 to 45 phr and its photobleaching monitored as a function of MED, the results of which are also illustrated in Figure 3.17.

These findings show that the latter film is bleached by an MED = 1 for skin phototyoe II and so is an appropriate warning indicator of a solar UV dosage sufficient to cause sunburn in a person with skin type II. By varying the levels of SnO_2 it is possible to make UV dosimeters that would indicate when sunburn is imminent for most other skin types.

3.3.6 Longevity of DCIP films

In order to be viable as a commercially available sun protection product, the DCIP dosimeter must have a reasonable shelf life, say 3 to 6 months but ideally >12 months. To test whether or not the DCIP dosimeter is sufficiently stable, a series of typical films were produced, half of which were stored in the dark under otherwise ambient conditions while the rest were refrigerated in the dark (5 ^{o}C). The films were removed periodically and their absorption spectra recorded before being returned to their dark environment. From this data a series of ΔAbs_{636} against irradiation time profiles were generated for both ambient and refrigerated samples as shown below in Figure 3.18.

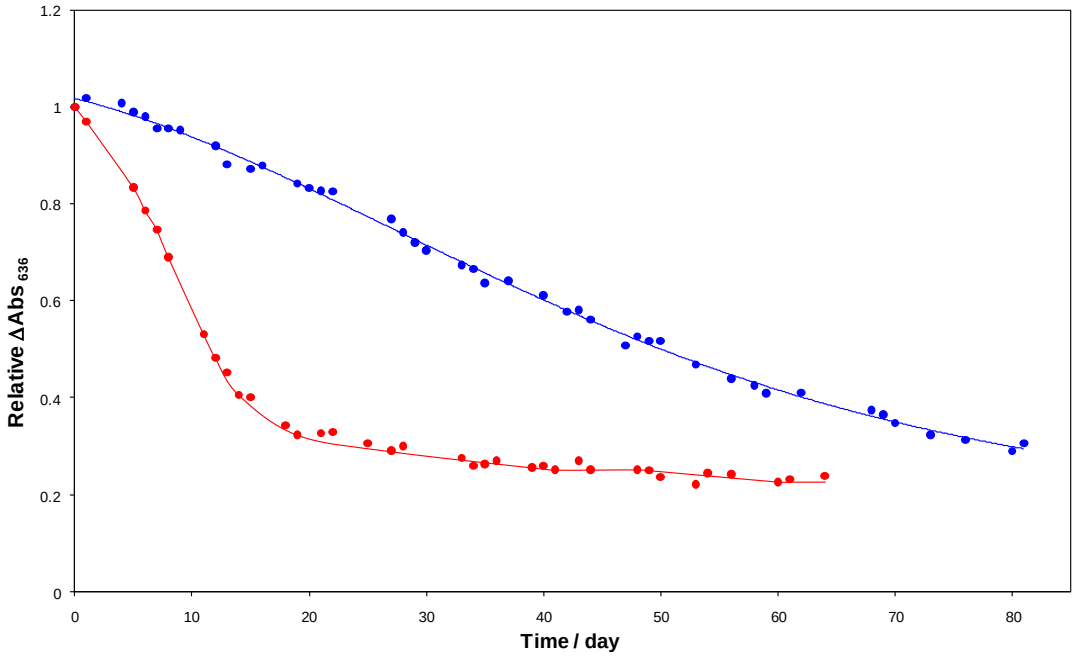

Figure 3.18 A plot ΔAb_{636} versus storage time for a typical DCIP dosimeter upon storage in the dark under ambient room temperature conditions and refrigerated at 5 ^{o}C.

Unfortunately films stored in the dark under both ambient and refrigerated conditions did not display good stability when stored for a period of 2-3 months. The dosimeters which kept at room temperature lost their blue appearance at an initial rate of 3.23×10^{-6} Abs units s^{-1} and consequently were colourless after *ca.* 25 days.

The refrigerated dosimeters were close to colourless after 80 days with the initial rate of colour loss calculated as 4.75×10^{-8} Abs units s^{-1}. The reason for this is as yet unclear, although further work carried out using HEC films containing DCIP alone experienced a similar colour loss suggesting that the instability is inherent to the dye rather than the SnO_2 or glycerol. It was also observed that after a period of a few months of storage time that the standard formulation ink changed colour to purple and developed a gel-like consistency rendering the solution useless for long term storage. Similar behaviour has been observed previously within Mills' group for DCIP/glycerol/HEC ink used for assessing photocatalytic activity of thin titanium dioxide, TiO_2, films.[7] It is thought that DCIP readily undergoes hydrolysis owing to the excellent leaving group ability of the chloride groups.[7] The result is DCIP exhibits an electronic and structural rearrangement which culminates in an insoluble red colour species.[7]

In a bid to overcome this, a similar system was generated using the redox dye Resazurin (Rz) in place of the DCIP, which, in the presence of SnO_2 and glycerol, undergoes a striking colour change from blue to pink on exposure to UVB radiation as the resazurin is reduced to resorufin (Rf). This substitution was successful with films still maintaining their initial blue colour and responding to UVB light after storage in the dark under ambient conditions for 1 year, however this system is complicated by the fact that resorufin further reduces to dihydroresorufin which is colourless. Consequently, the results of this work have not been included in the main body of this thesis but can be found in Appendix 2.

3.4 Conclusions

HEC films, containing the dye DCIP, in the presence of SnO_2 and glycerol undergo a semiconductor-activated reduction when exposed to UVB radiation. The rate at which the dosimeter film photobleaches increases with increasing UV irradiance and the system has a quantum efficiency of *ca*. 5.4%. The kinetics of photobleaching for the film are directly proportional to the level of SnO_2 and to a lesser extent the level of glycerol present but are independent of [DCIP]. The DCIP UVB dosimeter films

respond well to solar simulated light and can be tailored to be fully photobleached at different MED levels (for different skin types) by varying the level of SnO_2 present. The issue of long term stability is a very real one and is something that must be rectified if this technology were to be used to produce a commercial product and the Rz film appears promising in this area, but nevertheless this development has great potential in the role of warning of imminent sunburn for all different skin types.

3.5 References

1. A. Mills, S. Lee and M. Sheridan, *Analyst*, 2005, **130**, 1046-1051.
2. A. Mills and S. L. Hunt, *J. Photochem. Photobiol. A:Chem*, 1997, **108**, 1-35.
3. W. Liao, E. Yang, J. Chou, W. Chung, T. Sun and S. Hsiung, *IEEE Trans. Elect. Dev.*, 1999, **46**, 2278-2281.
4. J. M. Ottaway, in *Indicators*, ed. E. Bishop, Pergamon Press, Oxford, 1972.
5. A. Mills, J. Wang and M. McGrady, *J. Phys. Chem.*, 2006, **110**, 18324-18331.
6. A. Mills, G. Hill, M. Crow and S. Hodgen, *J. Appl. Electrochem.*, 2005, **35**, 641-653.
7. M. A. S. McGrady, *Novel Semiconductor Photocatalysis*, University of Strathclyde, 2012.

Chapter 4

A novel tetrazolium based UV dosimeter

4. A novel tetrazolium based UV dosimeter

4.1 Introduction

Tetrazolium salts are water-soluble organic heterocycles that can be readily reduced to form partially soluble and insoluble formazans. Tetrazoliums are generally colourless or pale yellow in solution, while formazans are highly coloured species, typically red, blue and purple. A general tetrazolium reduction reaction is as follows:

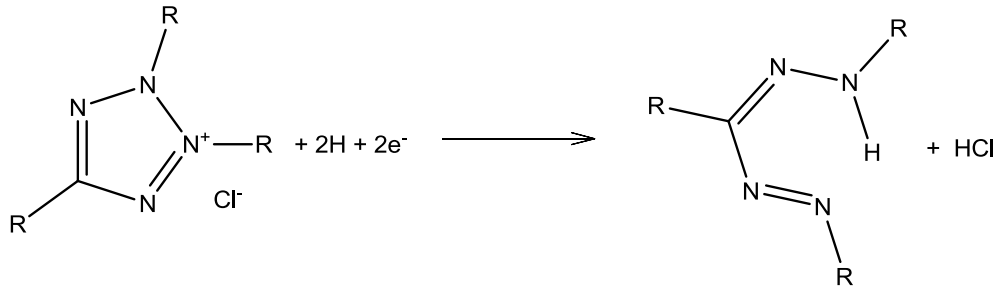

(4.1)

This colour-changing reaction has made tetrazolium salts a popular choice of indicator for the evaluation of bacterial metabolic activity[1, 2] as well as the detection of diseases such as tuberculosis.[2] The literature has numerous references to the "Tetrazolium Test" or the "Nitro Blue Test" [3-7] in which a tetrazolium dye provides a quick visual indication of cell activity *via* its addition to a cell culture. As well as occurring *via* electron transfer in biological environments, the reduction of tetrazoliums can also be induced by γ-radiation, which enables tetrazoliums to be used as dosimeters for measuring absorbed dose of radiation, in particular γ-rays. Much work in this area has been carried out using triphenyl tetrazolium chloride (TTC),[8-11] the structure of which is illustrated in Figure 4.1.

TTC based dosimeters for γ-radiation monitoring have been proposed in the form of aqueous[10, 11] and alcoholic[9] solutions, but also as agar gels.[11] Less well studied has been the use of tetrazolium dyes in films for UV dosimetry.[8, 12]

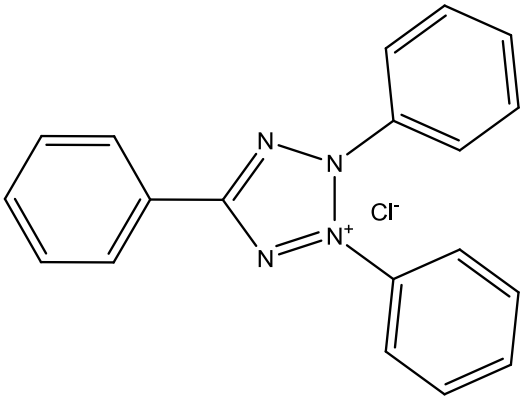

Figure 4.1 The chemical structures for triphenyl tetrazolium chloride (TTC)

The focus of this chapter is to describe a simple colorimetric indicator based on the dye neotetrazolium chloride (NTC) which can be used to indicate UV exposure dose and to warn of possible erythema, the importance of which was outlined previously. The chemical structure of NTC is illustrated in Figure 4.2.

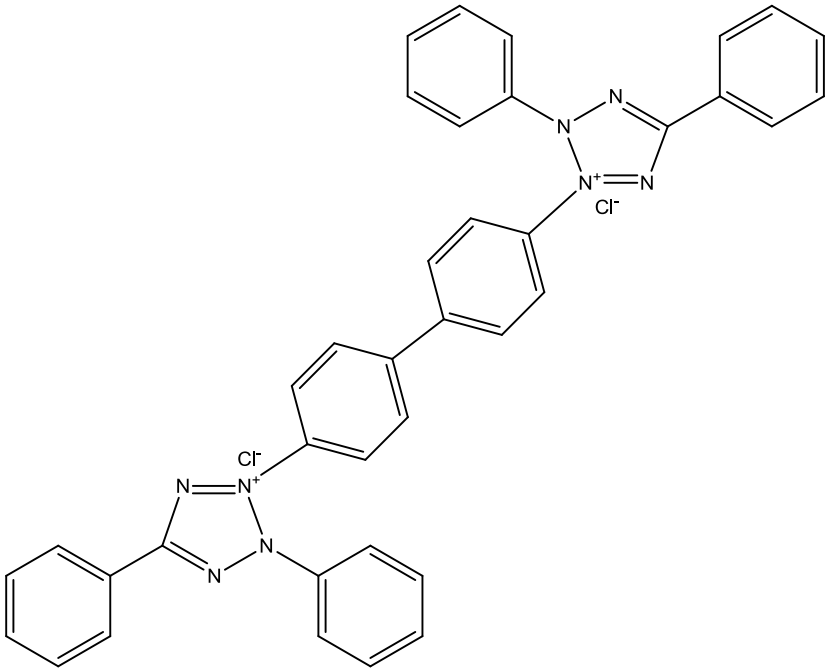

Figure 4.2 The chemical structure of neotetrazolium chloride (NTC)

4.2 Experimental

4.2.1 UV ink and dosimeter preparation

A typical NTC/PVA solution was prepared by dissolving 10 g PVA in 90 ml of water at 90 ^{o}C, which was then cooled to room temperature and stirred overnight. 20 mg of the NTC dye were then dissolved in 4 g of the PVA solution at room temperature with stirring. The casting ink was pale yellow in appearance and contained 5 phr of NTC i.e. 5 parts per hundred resin (or 5 g of dye to 100 g polymer). Films of the ink were cast onto 25 mm diameter, 1 mm thick quartz discs using a spin coater. Thus, a few drops of polymer ink solution were deposited on the surface of the disc, which was then spun at 1200 rpm for 15 seconds. The final product was then oven dried for 2 minutes at 70 $^{\circ}$C, allowed to cool to room temperature (5–10 min) and stored in the dark until used. Figure 4.3 illustrates a typical ink formulation and NTC dosimeter alone with an SEM image of a typical NTC film edge on. The final product was a

clear, colourless, *ca*. 2.5 μm thick film (as determined by SEM see Figure 4.3) on a quartz disc which will forthwith be referred to as a typical NTC film.

Work carried out using the solar simulator used films produced from a standard formulation ink but cast at 300 rpm to make the films thicker (*ca.* 8 μm) and so ensure a more striking colour change, since the absorbance changes were as a consequence *ca*. four times larger upon exposure to UV light. Such films will be referred to as typical solar NTC films.

(a)

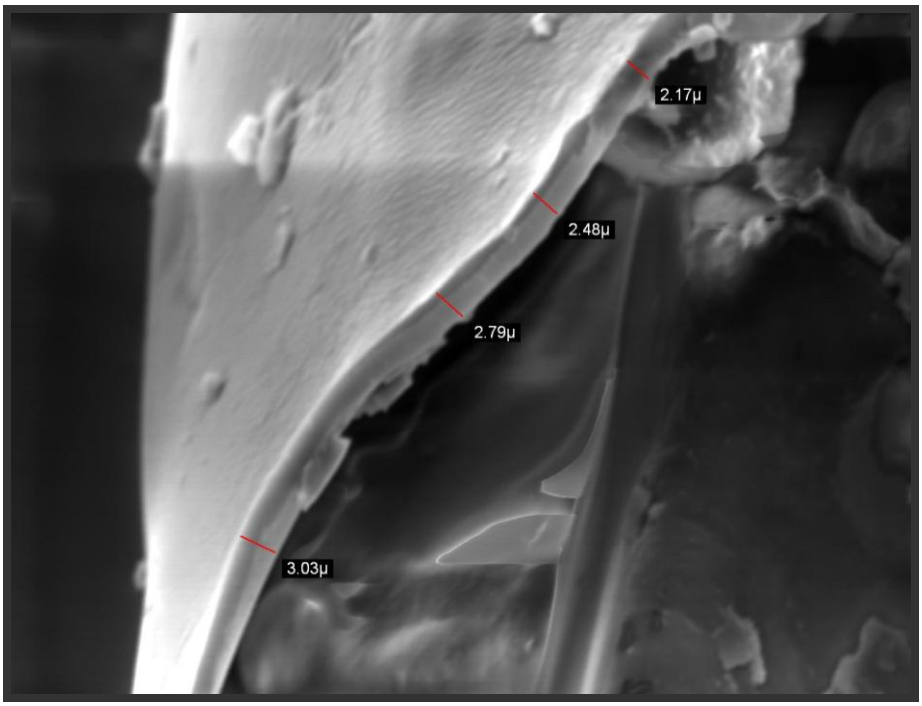

(b)

Figure 4.3 (a) A photograph of a standard NTC ink formulation and a typical NTC dosimeter prior to irradiation and (b) an SEM image of a typical NTC dosimeter edge on at x1,530 magnification.

4.3 Results and discussion

4.3.1 Optical characteristics of a NTC film

A typical NTC film was produced and the spectral fraction of light, f_A, it absorbs calculated from its absorption spectrum; the results are shown in Figure 4.4 along with the known spectral sensitivity of human skin with respect to erythema, $S(\lambda)$.[13] The film has an absorption maximum at 252 nm with a shoulder peak at 352 nm. From the data in Figure 4.4 it is clear that the NTC dosimeter, like most dye-based chemical dosimeters, has a very poor overlap with $S(\lambda)$. This renders it only appropriate as a UV dosimeter for skin erythema when calibrated using the relevant UV light source, assuming the latter's profile does not change with time. Fortunately, as noted earlier, the solar spectrum does not change significantly in shape from mid-morning to mid-afternoon, the most likely time sunburn will take place. The emission spectra of the UVA and UVB light sources and the UV solar simulator are also illustrated in Figure 4.4 to highlight their overlap with the NTC film. Note from this data it is clear that the typical NTC film dosimeter absorbs a greater proportion of UVB than UVA radiation.

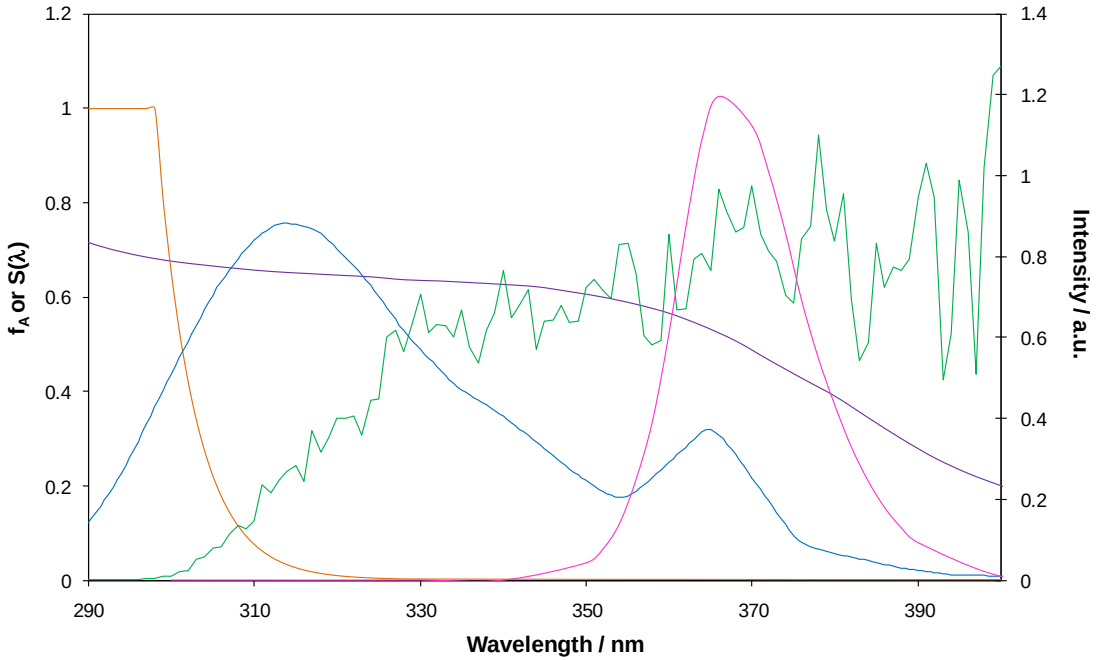

Figure 4.4 A plot of the fraction of light (f_A) absorbed by the NTC film and human skin erythemal sensitivity, $S(\lambda)$ vs. wavelength with overlays of the emission spectra of the solar simulator, UVA and UVB lamps used in this work.

The latter is a useful feature in any UV dosimeter as it is UVB in particular that is responsible for sunburn. For example on a typical summer's day approximately 6% of terrestrial light is in the UVB wavelength range (i.e. 290–320 nm) and contributes 80% towards the harmful effects associated with the sun, while the remaining 94% UVA component in sunlight (320–400 nm) contributes to the remaining 20%.[14]

4.3.2 UV irradiation of NTC film

When irradiated with either UVA or UVB light a typical NTC film develops a striking pink/red colour with time as seen in Figure 4.5, which shows photographs of such a film before and after 30 min irradiation with UVB light (4 mW cm^{-2}).

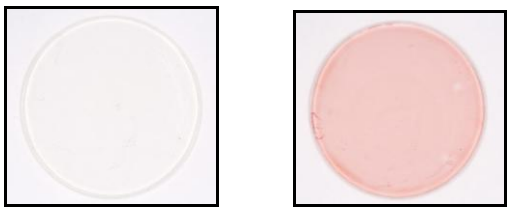

(a) **(b)**

Figure 4.5 Photographs of standard films taken before (a) and after (b) irradiation with UVB light.

This feature is further illustrated in Figure 4.6, which shows the UV/visible absorption spectral changes exhibited by this film as a function of irradiation time when irradiated with 4 mW cm^{-2} UVB light. The main diagram in Figure 4.6 illustrates the peak at 532 nm, associated with the pink/red colour growing with increasing exposure to UVB. The insert diagram in Figure 4.6 shows that the photocolouration process, as measured by the increase in absorbance at 532 nm i.e. ΔAbs_{532}, as a function of irradiation time. It also shows that for two identical NTC dosimeters the rate of photocolouration occurs at a greater rate under UVB radiation than UVA radiation of the same intensity. This difference in UV responsivity is expected given that the NTC dye absorbs a greater total fraction of UVB light (f_{UVB} *ca*. 0.60) than UVA light (f_{UVA} *ca*.0.49), as is apparent from the spectral data in Figure 4.4 and Figure 4.6.

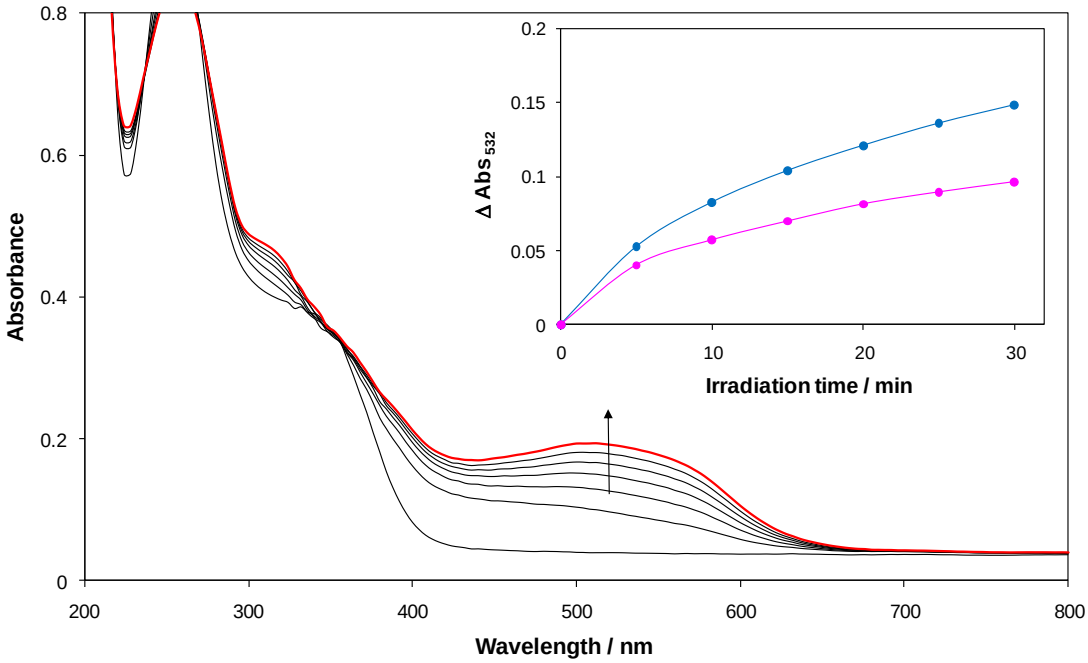

Figure 4.6 Absorption spectra of a standard NTC film after irradiation with 4 mW cm^{-2} UVB light. Insert diagram is a comparison of the ΔAbs_{532} vs. irradiation time profiles of films on exposure to 4 mW cm^{-2} UVB and 4 mW cm^{-2} UVA light.

The colour change observed arises as a result of the partial reduction of NTC to give the stable monoformazan which proceeds by means of the step-wise addition of electrons and occurs *via* a transient state consisting of one tetrazolinyl radical centre and one tetrazolium centre as detailed in Figure 4.7.[15] Further reduction of the monoformazan, λ_{max} (532 nm), can yield the diformazan form of the dye, a purple species that absorbs at a longer wavelength, λ_{max} (550 nm). [16, 17]

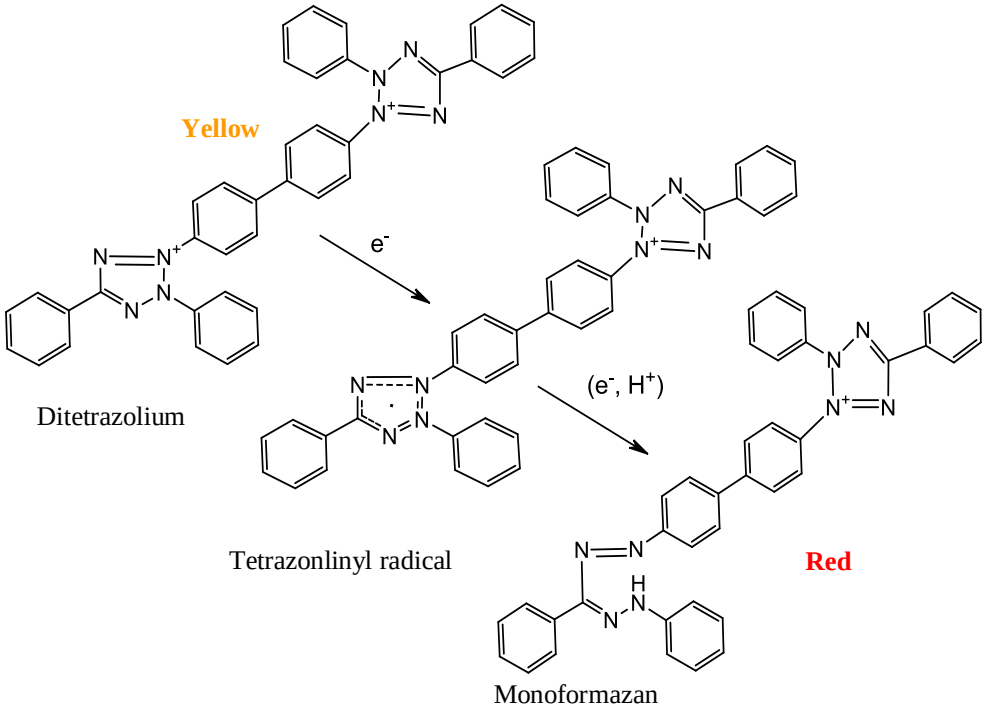

Figure 4.7 Mechanism for the reduction of ditetrazolium neotetrazolium dye (yellow) to its monoformazan (red).

4.3.3 Kinetics of colouration of an NTC film

4.3.3.1 Irradiance

In one set of experiments a series of typical NTC films were exposed to different UVA and UVB irradiances for the same length of time. Specifically 1, 2 and 3 mW cm^{-2} from the UVA source and 0.5, 1, 2 and 3 mW cm^{-2} from the UVB source, with a total exposure time of 30 min for each film. The absorbances of the NTC films under test were measured spectrophotometrically and the initial rate, r_i, of colouration for each film was determined from a plot of ΔAbs_{532} vs. irradiation time. The plot of r_i as a function of UV irradiance arising from this work is illustrated in Figure 4.8 and shows that r_i is directly related to irradiance, as might be expected for such a simple, direct photochemical process.

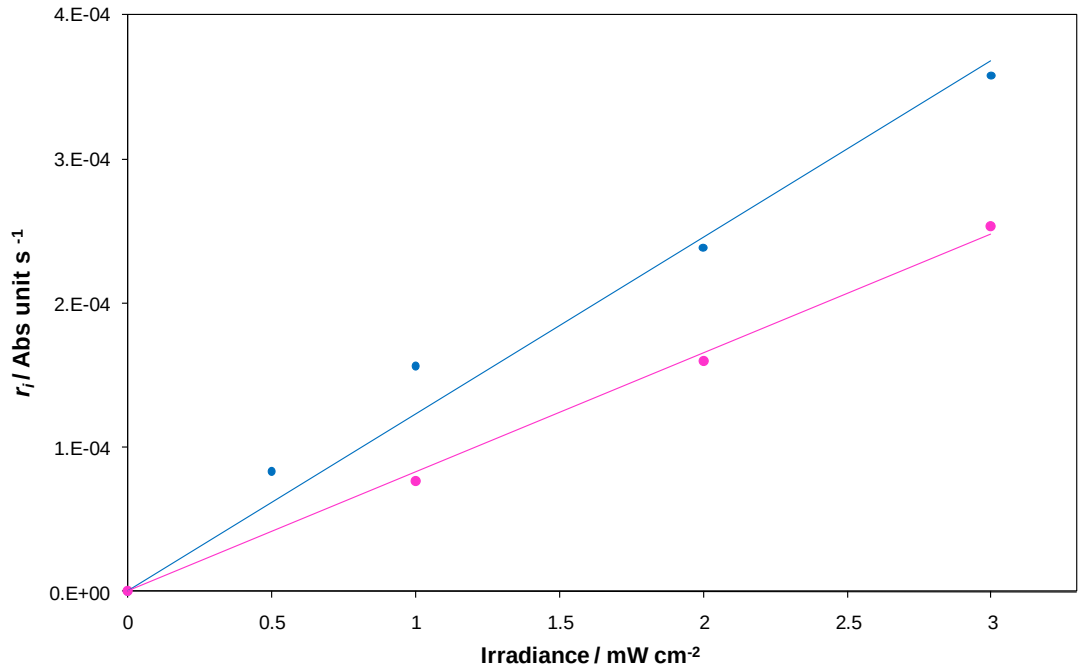

Figure 4.8 A plot of initial rate of colouration, r_i as a function of UV irradiance for typical NTC films irradiated with different intensities of UVA and UVB light**.**

From the gradient in Figure 4.8, the UVB irradiation experiment, i.e. 1×10^{-4} (Abs unit s^{-1}/ $mWcm^{-2}$), and given that the reduced NTC has a molar absorptivity of 22,000 M^{-1} cm^{-1} and a typical film is 2.5 μm thick, a formal quantum efficiency for the photoreduction of NTC in the PVA film was calculated as $(2.8\pm0.3)\times10^{-3}$ molecules/photons of UVB. Similarly a value of $(1.7\pm0.2)\times10^{-3}$ molecules/photons of UVA was calculated using the UVA irradiation data in Figure 4.8. The quantum efficiency and quantum yield data for both UVA and UVB are tabulated in Table 4.1 below and the methods used to determine such values are detailed in Appendix 1.

UVR	***D*** **(μm)**	***λ*** **(nm)**	**Rate, R_i^*** **($x10^{12}$molecules/cm^2/s)**	***QE*** **(molecules/photon)**	f_{UVR}	***QY***
UVB	2.5	315	4.45	0.00172	0.620	0.0028
UVA	2.5	365	2.27	0.00086	0.498	0.0017

Table 4.1 Optical and photocatalytic properties for NTC dosimeter films, where d = film thickness, λ = emission wavelength from UVR source (i.e. wavelength of light being absorbed by films), QE = quantum efficiency, f_{UVR} = fraction of UVR light being absorbed by dosimeter films and QY = quantum yield.

4.3.3.2 [NTC]

The sensitivity of the NTC UV dosimeter towards UV light can be readily varied by changing the amount of dye in the film formulations. Thus, a series of NTC casting inks were prepared containing 10–80 mg NTC, which were then cast onto quartz discs to produce films with NTC levels ranging from 2.5 to 20 phr respectively. Using these films a series of ΔAbs_{532} vs. irradiation time profiles were generated with a 4 mW cm^{-2} UVB light source and the results are illustrated in Figure 4.9, which shows that the initial rate increases with increasing levels of NTC, i.e. [NTC]. The initial rate of colouration, r_i, was plotted against the fraction of UVB light absorbed, f_{UVB}, by the NTC dye in each film and is shown in Figure 4.10, revealing r_i is directly proportional to f_{UVB}, as expected for a simple, direct photochemical process for which the rate of the photoreduction process is also directly proportional to the absorbed irradiance.

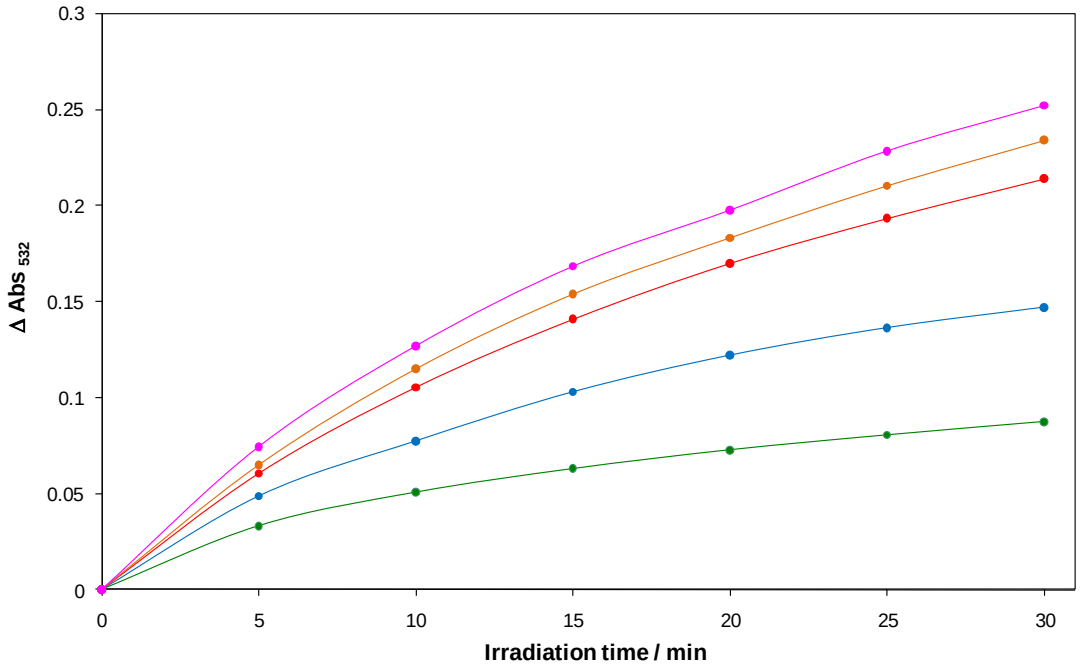

Figure 4.9 A plot of ΔAbs_{532} against irradiation time for films containing different [NTC] after irradiation with 4 mW cm^{-2} UVB light. From top to bottom concentrations are 20, 15, 10, 5 and 2.5 phr.

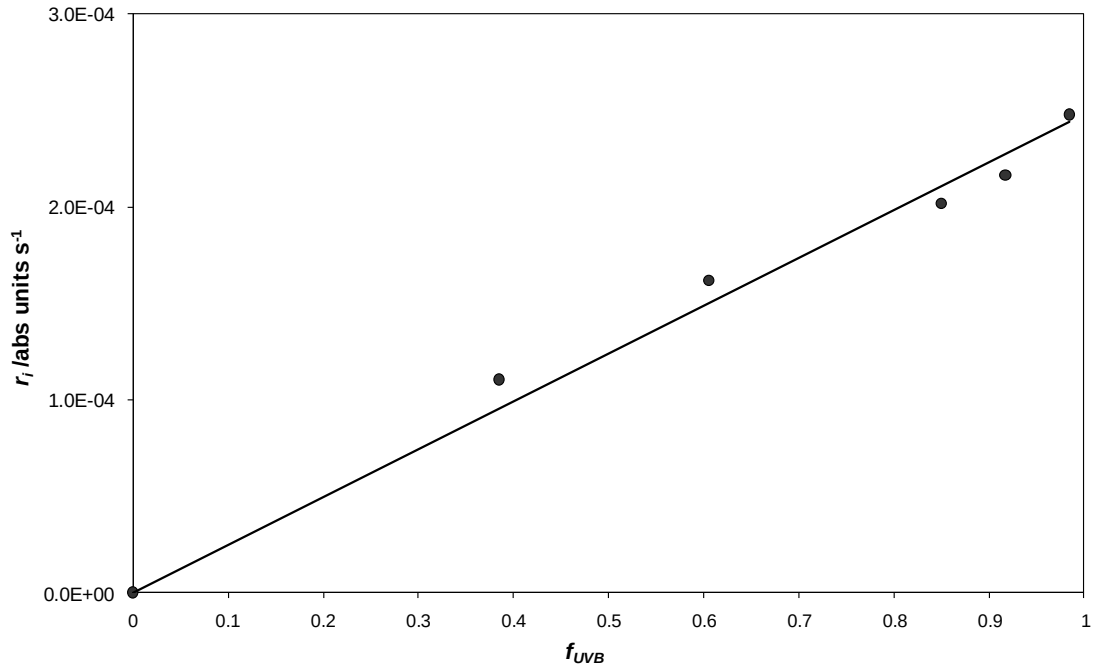

Figure 4.10 A plot of the r_i against f_{UVB} for films containing different [NTC].

4.3.3.3 Film thickness

The sensitivity of the NTC UV dosimeter towards UV light can also be readily varied by changing the thickness of the dosimeter film. Thus, a series of standard formulation NTC films were produced at 4 different spin speeds (300, 600, 900 and 1200 rpm) in order to produce films of different thicknesses. As stated earlier films produced at 1200 rpm are typically 2.5 μm thick. So, assuming Lambert's law applies, i.e. the pathlength or film thickness (μm), *d*, is equal to a constant, *k*, multiplied by the absorbance at the 352 nm shoulder minus the background absorption, then:

$$d = k\Delta Abs_{352} \tag{4.2}$$

For film spun at 1200 rpm the ΔAbs_{352} was 0.363 and the *d* value measured *via* SEM was 2.5 μm. This enabled the determination of k = 6.89 μm using equation (4.2). With this value of *k* the film thickness of the 900, 600 and 300 rpm films were calculated from their absorbance values at the 352 nm shoulder and can be found in Table 4.2.

Spin speed of film / rpm	**ΔAbs 352 (ref shoulder)**	**Calculated d / μm**
300	1.061	7.31
600	0.656	4.51
900	0.468	3.22
1200	0.363	2.50

Table 4.2 A table listing the ΔAbs_{352} and the calculated film thickness (μm) of PVA films containing 5 phr NTC spun at different spin speeds.

Using these films a series of ΔAbs_{532} vs. irradiation time profiles were generated with a 4 mW cm^{-2} UVB light source and the results are illustrated in Figure 4.11. The initial rate of colouration, r_i, was plotted against the fraction of UVB light absorbed, f_{UVB}, by the NTC dye in each film and is shown in Figure 4.12 revealing, as observed previously in the [NTC] study, r_i increases with f_{UVB}.

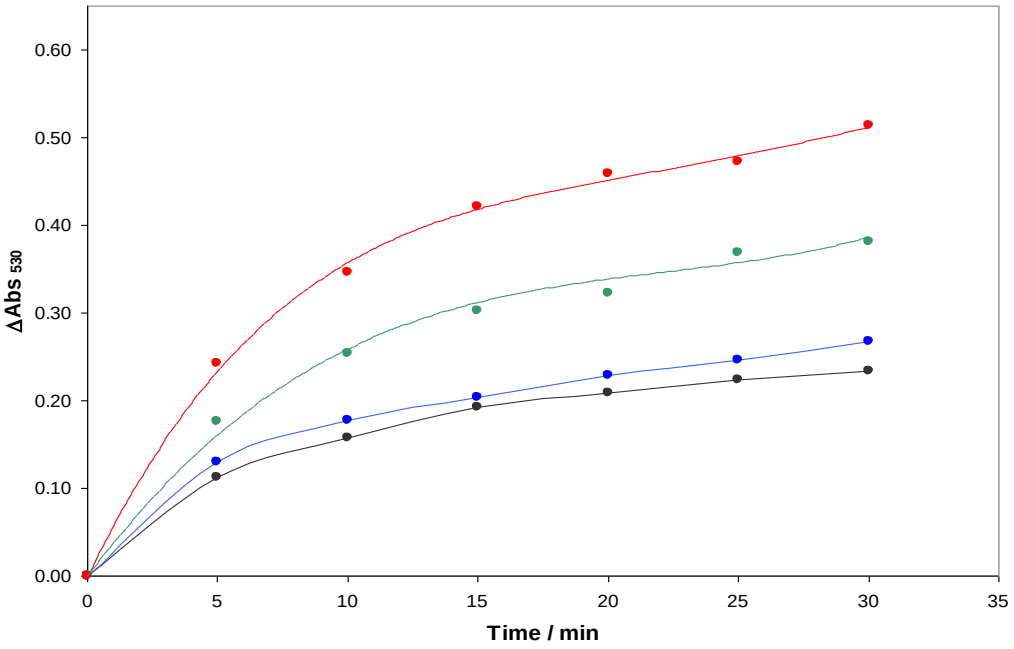

Figure 4.11 A plot of ΔAbs_{532} against irradiation time for films spun at different spin speeds (i.e. of different film thicknesses) after irradiation with 4 mW cm^{-2} UVB light. Spin speeds are from top to bottom 300 rpm (7.31 μm), 600 rpm (4.51 μm), 900 rpm (3.22 μm) and 1200 rpm (2.5 μm).

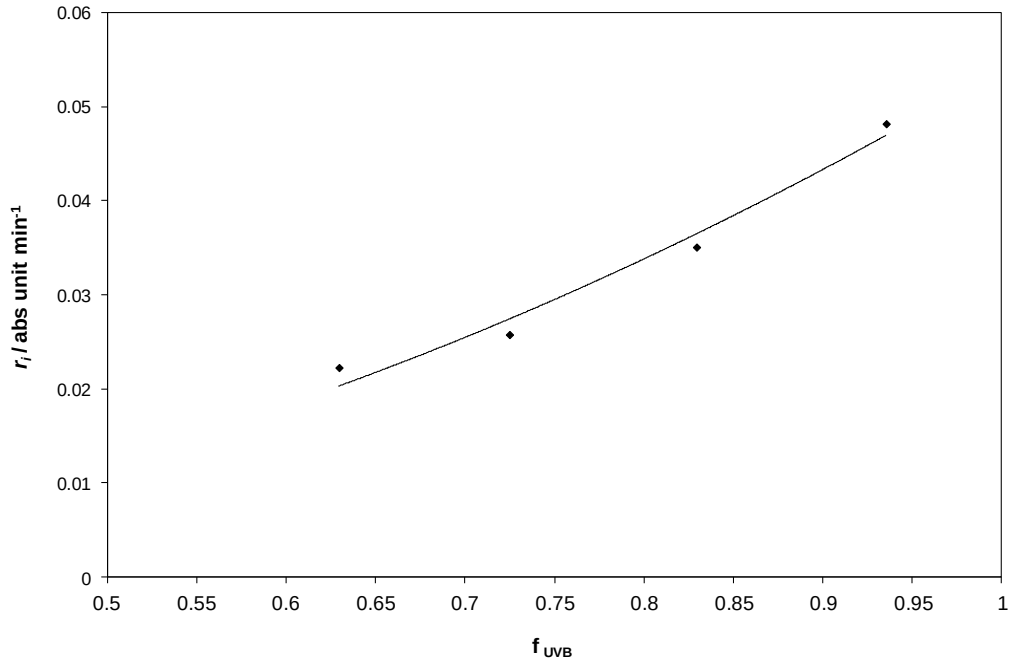

Figure 4.12 A plot of the r_i against f_{UVB} for films of different thicknesses. Line is a guide to the eye.

4.3.3.4 Relative humidity

To determine if the relative humidity, RH, of the surrounding environment had an effect on the response of the NTC UV dosimeters, experiments were carried out using typical NTC films in high and low RH conditions. Initially a set of typical films were run in a gas cell under dry cylinder air (~ 0% RH) followed by a second set that were run in 100% RH conditions at room temperature. The results shown in Figure 4.12 suggest that the RH of the environment does have a small effect on the rate at which the films change colour with the reduction to the formazan occurring slightly faster under high RH conditions. This can be rationalised by considering that in order for the reduction to occur a H^+ source is required, and the water vapour may be acting as a more readily available source of protons than the polymer.

To support the rationalisation that the presence of water in the films aids the reduction of the tetrazolium, two standard formulation films were produced, with one dried as per the standard procedure, while the other dried in the oven at 90 °C overnight. The films were then used to generate two ΔAbs_{532} versus irradiation time profiles with 4 mW cm^{-2} UVB light as shown in the inset diagram of 4.13.

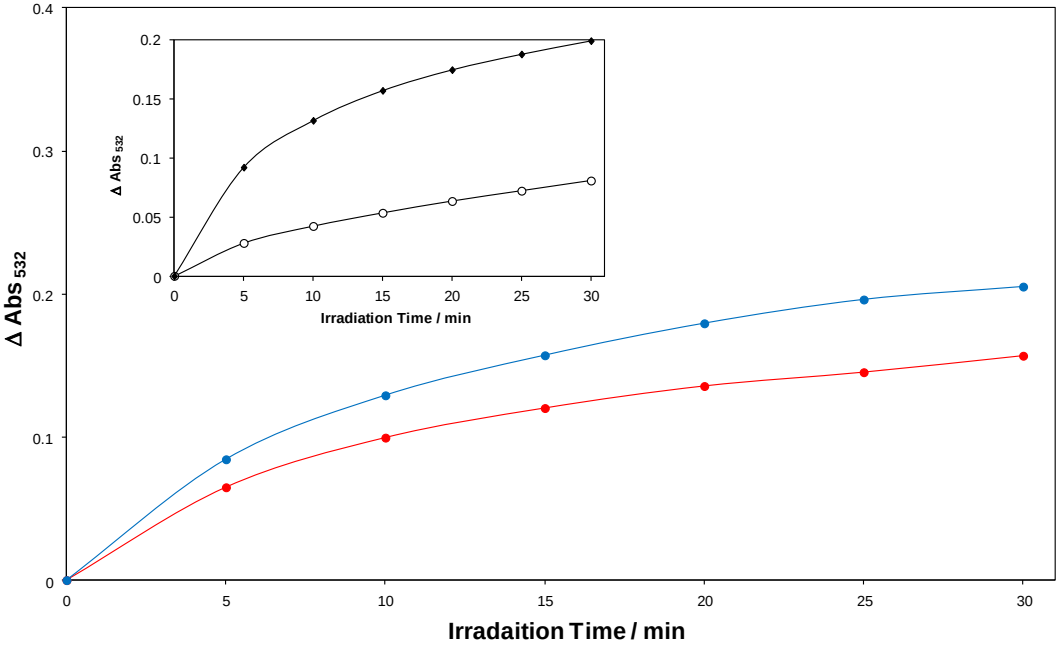

Figure 4.13 A plot ΔAbs_{532} versus irradiation time for a series of typical NTC films on exposure to 4 mW cm^{-2} UVB light under 100% RH conditions and under 0% RH dry cylinder air conditions. Inset diagram is a similar plot for a typical NTC film dried under standard conditions (–●–) *cf.* a similar film dried overnight at 90°C (–○–).

These results indicate that the films dried for longer at a higher temperature responded *ca.* 3.3 times slower than the films dried under standard conditions. Presumably, the films dried overnight have a lower water content than those dried under standard conditions, so their greatly reduced reaction rate supports the

hypothesis that H^+ present in water supports the formazan formation. It is also probable that as the film dries the polymer shrinks somewhat and thus causes a small decrease in film thickness, which would also contribute to the reduction in r_i

4.3.3.5 Temperature

Further work carried out with a small handheld UVA light source showed that the response of the NTC dosimeter is independent of the temperature over the range 20 – 40^{o}C i.e. the range most likely to be encountered under typical British/European summer holiday conditions.

4.3.4 Enhancement of photocolouration of an NTC film

The NTC UV dosimeter reported here functions *via* a UV-induced photoreduction process, in which the dye converts to its formazan form (see Figure 4.6). Since this process occurs in a polymer encapsulation medium (PVA in this case), it is presumed that the photoreduction of the NTC is accompanied by the oxidation of the polymer. It would appear likely, therefore, that the UV-induced photoreduction of NTC may be more easily effected if a more readily oxidised reagent, such as triethanolamine (TEOA) or glycerol, were present. In order to test this idea, casting solutions were prepared following the standard procedure with the addition of either 100 mg glycerol or 100 mg TEOA. Films of these inks were cast on quartz discs in the usual way and irradiated with 4 mW cm^{-2} UVB light for 30 min. The variation in the parameter ΔAbs_{532} for these films was monitored spectrophotometrically as a function of irradiation time and the results are shown in Figure 4. 14. This plot compares the response of the typical film with those films containing glycerol or TEOA, and shows that the addition of an easily oxidisable electron donor, such as TEOA or glycerol increases the initial rate at which the NTC is photoreduced by UV light. Interestingly, the film containing the glycerol develops a purple colour when irradiated with UVB light, with an absorbance peak at 550 nm, rather than that of

532 nm found for the usual red coloured formazan generated using a typical NTC film.

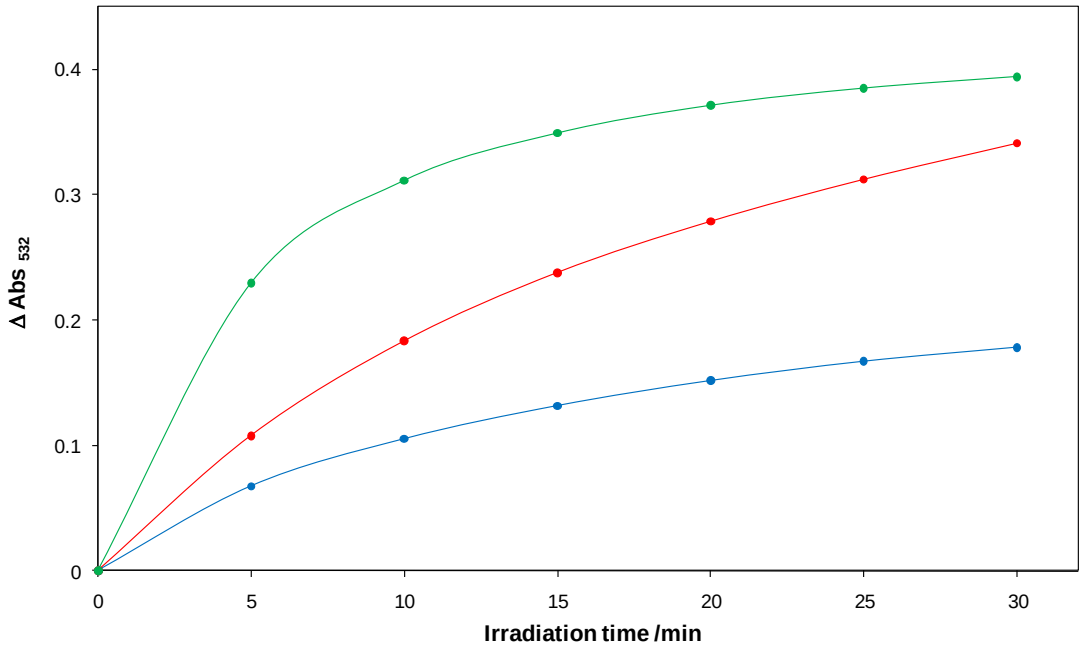

Figure 4. 14 A plot of ΔAbs_{532} vs. Irradiation time for a series of typical NTC dosimeters containing 100 mg of glycerol or 100 mg TEOA compared to the standard NTC dosimeter film after irradiation with 4 mW cm^{-2} UVB light.

These results indicate that in the presence of glycerol some of the monoformazan produced is further photoreduced to give the diformazan product, which is known to exist as an insoluble purple coloured solid absorbing at 550 nm. [16, 17]

4.3.5 Effect of UV blockers on the photocoloration of an NTC film

The initial rate of coloration of the NTC UV dosimeter, i.e. r_i, is proportional to the amount of UV radiation reaching the tetrazolium dye. Thus, it follows that if the level of UVR reaching the dye molecules were reduced, say by adding a "UV screening" agent such as 2,2-dihydroxy-4-methoxy benzophenone, DMB (whose

structure is shown in Figure 4.15), to the dosimeter system, the photocolouration would occur at a lower rate.

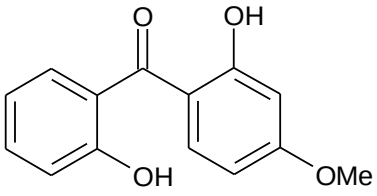

Figure 4.15 The chemical structure of 2,2-dihydroxy-4-methoxy benzophenone, DMB.

This route to varying the UV sensitivity of the NTC dosimeter films was tested by casting a 'UV-screening,' solvent-based ink on top of a typical NTC film in a bid to reduce the proportion of UVB light reaching the sample. In this experiment a series of 'UV-screening' solutions comprising of a 5% (w/w) PVB in *n*-butanol polymer solution were prepared containing different levels of 2,2-dihydroxy-4-methoxy benzophenone, DMB ranging from 40 to 100 phr. A set of standard NTC films were then each coated with a layer of one of the solvent-based 'UV-screening inks', by spin coating them on top of the standard films at 1200 rpm, and drying the final product in the oven at 70 ^{o}C. The UV/visible spectrum for a NTC film coated with a 'UV-screened' ink containing 20 phr DMB is seen in Figure 4.16. Also shown for comparison are the absorption spectra for a typical NTC dosimeter, a film containing 20 phr DMB in PVB and a film of PVB alone.

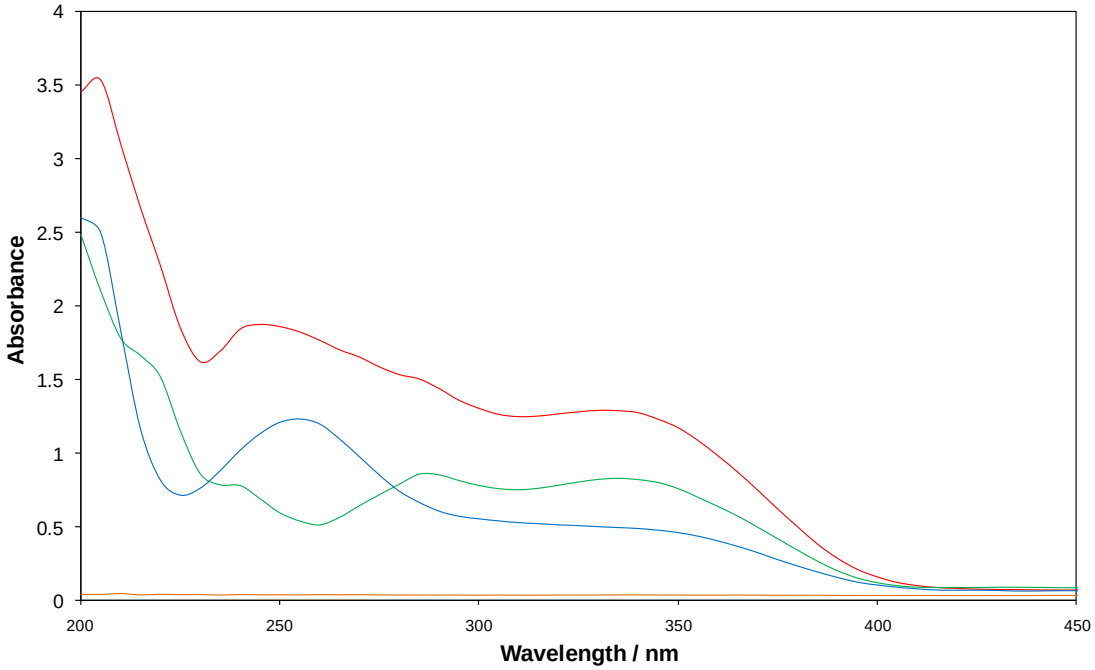

Figure 4.16 A plot of the UV/Vis absorption spectrum of a typical NTC film coated with a layer of 20 phr DMB/PVB screening ink. Also included are the UV/visible absorption spectra of a typical uncoated NTC film, a film of 20 phr DMB/PVB screening ink and a film of PVB alone.

The UV/visible spectra for the other NTC/UV-screened films are shown in Figure 4.17. The films were then irradiated with 4 mW cm^{-2} UVB light for 30 min and their UV/visible absorption spectra recorded at regular intervals. From this data a series of ΔAbs_{532} vs. irradiation time profiles were generated and are illustrated in the inset diagram of Figure 4.17 which shows that addition of such a 'UV screening layer' as anticipated decreases the r_i at which the films respond to UV light.

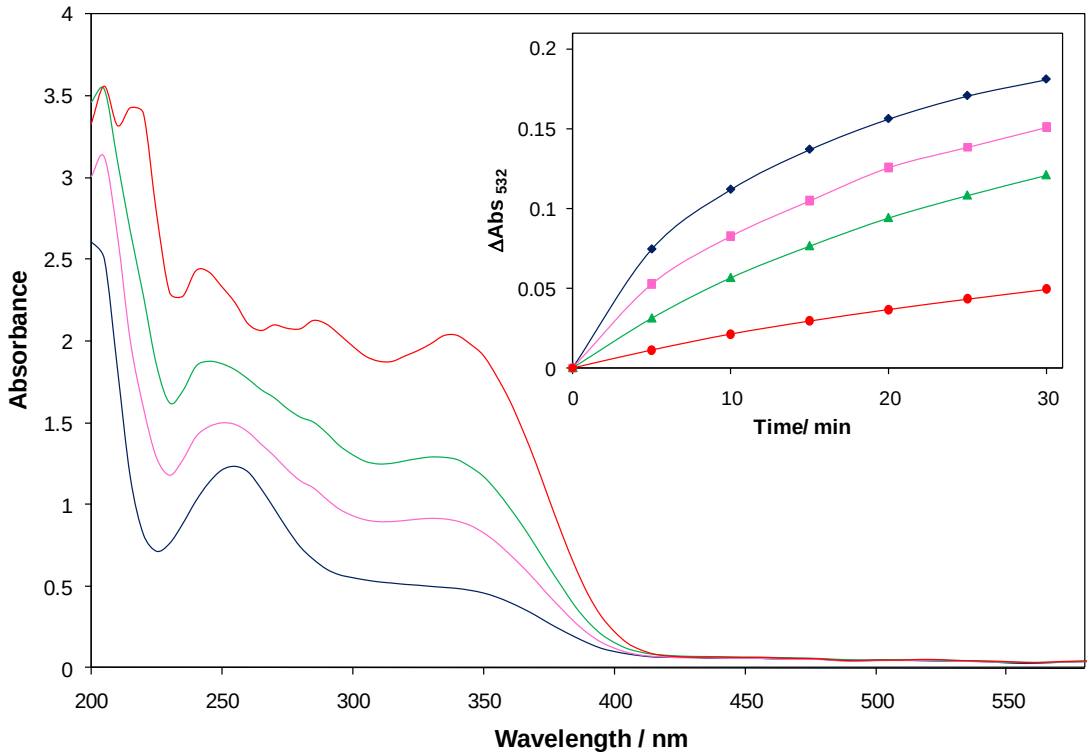

Figure 4.17 A plot of, from top to bottom, the absorption spectrum of a NTC film coated with 100 phr DMB/PVB layer, NTC film coated with 40 phr DMB/PVB layer, NTC films coated with 20 phr DMB/PVB layer and a standard NTC film with no blocker layer. The inset diagram is a plot of ΔAbs_{532} vs. irradiation time for the above mentioned films generated under 4 mW cm^{-2} UVB light conditions

In order to show that the addition of the 'UV screen layer' merely reduces the amount of UV light reaching the sample and thus reduces the rate of reaction without interfering with the photochemistry of the tetrazolium, three films, namely a typical NTC film, a 20 phr/UV screen/NTC film and 40 phr/UV screen/NTC film were irradiated with 4 mW cm^{-2} until their red colour was fully developed. The films were monitored spectrophotometrically at 532 nm and a series of ΔAbs_{532} vs. irradiation time profiles were generated as seen in Figure 4.18. The typical NTC film took 120 min, while the 20 phr/UV screen/NTC film took 320 min to achieve the same maximum absorbance (0.28) at 532 nm. The 40 phr/UV screen/NTC is

approaching a similar level having reached a ΔAbs_{532} of 0.25 after 480 min and is still increasing This feature of a UV screen top layer to reduce the UV sensitivity of a typical NTC film dosimeter suggests that such an approach could be used to adapt the NTC film to provide an indication of impending erythema for any skin type.

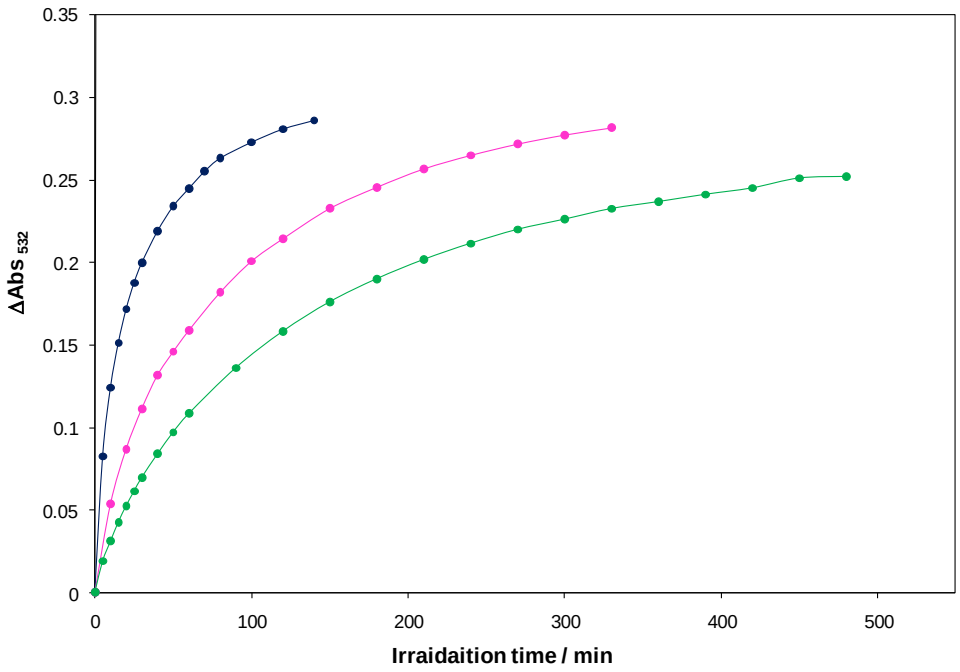

Figure 4.18 A plot of ΔAbs_{532} vs. irradiation time profile for a typical NTC film, a 20 phr/UV screen/NTC film and 40 phr/UV screen/NTC film generated with 4 mW cm^{-2} UVB light until their red colour was fully developed.

4.3.6 Solar UV work using a NTC film

In another set of experiments, UV solar-simulated light at four different UVI levels spanning the range UVI 1–8 were each used to irradiate a typical solar NTC film produced at 300 rpm. The data arising from this work allowed the UV dose for each film to be calculated in terms of MED for skin type II and plotted in the form of ΔAbs_{532} as a function of UV dose as illustrated in Figure 4.19.

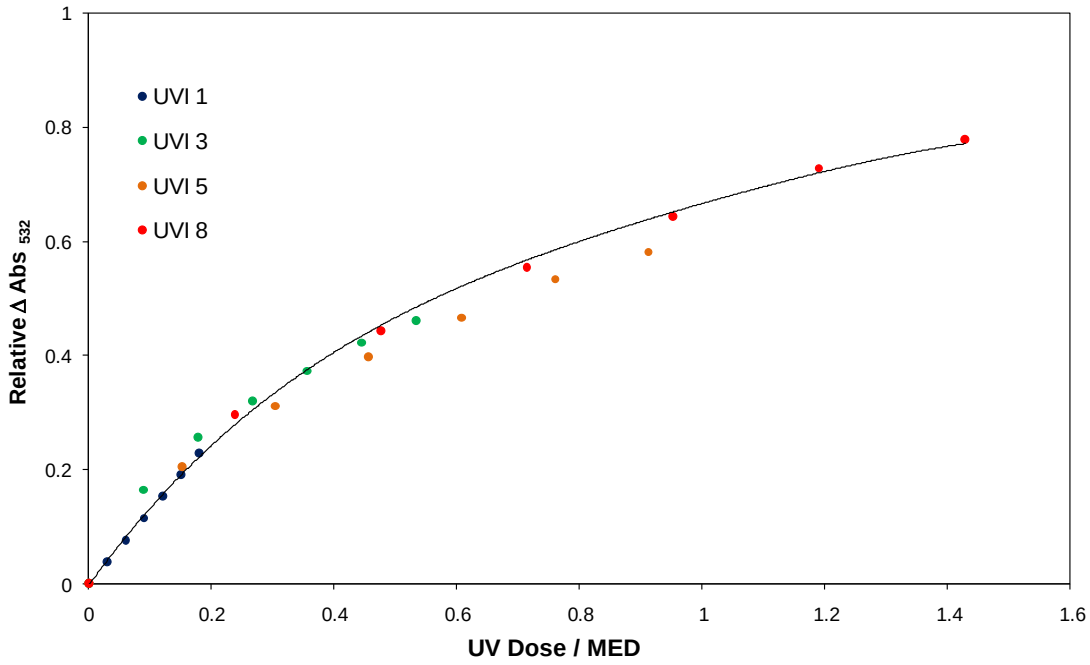

Figure 4.19 A plot of ΔAbs_{532} vs. UV dose received for skin phototype II (where 1 = MED for skin type II i.e. 250 Jm^{-2} h^{-1}) for standard formulation ink NTC films spun at 300 rpm. The solid line was calculated using equation (4.3).

The results reveal that all the data points for films exposed to UVI 1, 3, 5 and 8 lie on a common line indicating that a typical NTC film can be used as a quantitative method for assessing the solar UV dosage received. For example, if upon exposure of a typical solar NTC film a ΔAbs_{532} value of approx. 0.67 is reached this will signify an MED value of 1 has been reached for skin type II and so erythema is likely to occur. In Figure 4.19 the line of best fit to the data is given by the expression:

$$UV\ dose\ (MED) = (0.63 \pm 0.03)(\Delta Abs_{532} + \Delta Abs^2_{532} + (1.85 \pm 0.29)\Delta Abs^3_{532}) \qquad (4.3)$$

which has the same form as that reported by Diffey[18] for the polysulphone UV dosimeter. Similar ΔAbs_{532} vs. MED curves were generated using solar UV. An error analysis of the data in Figure 4.19 reveals that it is *ca*. 5% up to MED values of 0.3,

but then increases with increasing MED, reaching 7% at MED = 1. As an alternative to reading off the measured value of ΔAbs_{532} as a method of determining the MED received, a colour match card could be used to enable the user to determine when they have been exposed to 1 MED, or more, for skin type II, although this is likely to significantly increase the possible error. If an additional polymer/sunscreen layer is introduced to the system, the indicator film could be used to show when erythema is likely to occur for other (higher) skin types.

Further solar-simulator work showed that the response of the dosimeter exhibits a cosine-like response dependent upon irradiance angle. A series of typical NTC UV dosimeter films were produced and irradiated with UVI 5 solar simulated light from different angles, namely 0^o, 20^o, 30^o, 45^o, 60^o, 80^o and 90^o. The absorbance at 532 nm was monitored and used to determine relative reaction rates for each film which were then plotted against angle of irradiation. While there is some deviation from the cosine curve (data not shown) the NTC UV dosimeter does display a cosine-like response to solar simulated light similar to that observed for Quintern et al. for their *Bacillus subtilis* biofilm UV dosimeter. [19] This is expected given the geometry of the experiment.

4.3.7 Long term stability

The long term stability of the NTC UV dosimeters was investigated by producing a series of typical UV dosimeter films and storing them in a zip-lock bag in the dark. Periodically a film was removed and subjected to irradiation with 4 mW cm^{-2} UVB light and ΔAbs_{532} vs. irradiation time profiles generated as shown in Figure 4.20.

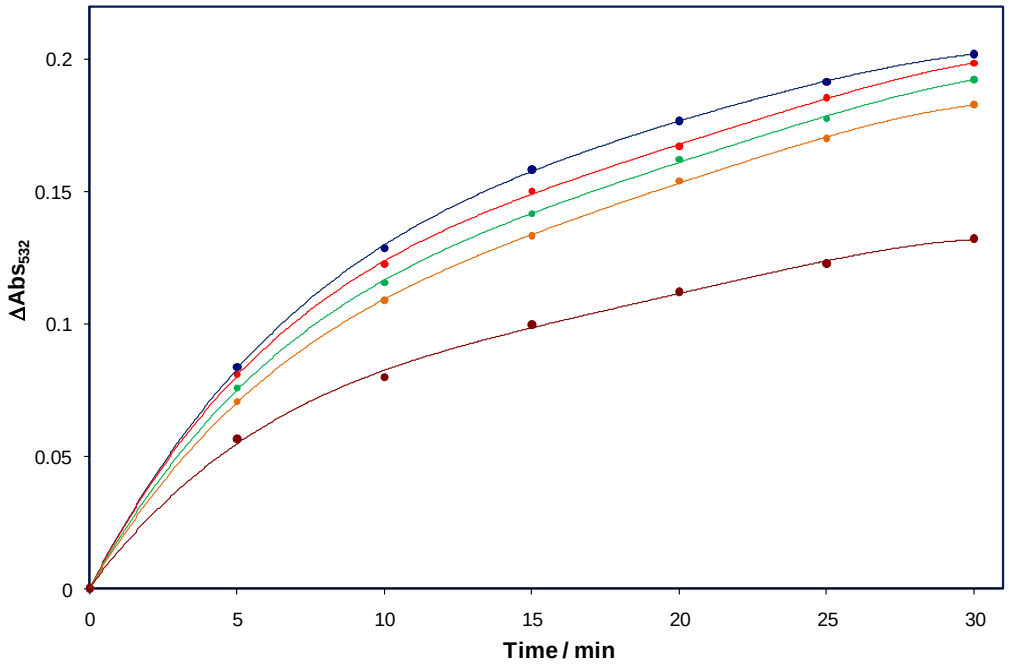

Figure 4.20 A plot of ΔAbs_{532} versus irradiation time film generated with 4 mW cm^{-2} UVB light for a series of NTC dosimeters that have been stored for increasing levels of time. Profiles are shown from top to bottom for a fresh NTC film and for NTC films after 1, 2, 3 and 12 months storage in the dark.

These profiles indicate that as the NTC UV dosimeters age the r_i of colouration and consequently the ΔAbs_{532} at t = 30 minutes are reduced, i.e. the colour change is not as marked. It is possible that this arises as a result of the polymer losing water as the film dries out with time resulting in a decrease in the r_i. As shown previously in the humidity study the presence of water aids the tetrazolium reduction thus an older and therefore drier film does not respond as well as a fresh film. After 18 months in storage in the dark the NTC UV dosimeters have developed a pink hue suggesting that some of the NTC present has converted to the formazan.

4.4 Conclusions

PVA films containing the dye NTC undergo reduction to the monoformazan form of NTC when exposed to UVA or UVB light. The rate at which the colouration of the films occurs is dependent on properties of the film, such as [NTC] and film thickness, and increases with increasing UV irradiance. The film response is temperature independent over the range 20–40^{o}C and exhibits a cosine-like response dependent upon irradiance angle. The rate of photocolouration can be reduced by the introduction of a UV screening layer on top of the standard NTC dosimeter and the dosimeter films give a consistent response to solar simulated light of different irradiances. Using this light source the NTC film dosimeter can be used to identify the point when an MED = 1 has been reached and erythema is likely to occur upon further exposure to solar UV. Although a real-time UV dosimeter, like most dye-based UV dosimeters, the NTC film has a poor match with the erythemal spectral sensitivity of skin and so can only be used as an erythemal indicator when calibrated using the UV source of interest, which in most cases is the sun. The lack of overlap is in striking contrast to several biological UV dosimeters, such as that based on *Bacillus. subtilus*, and the polysulphone UV dosimeters discussed in the introduction, although the former requires extensive processing (taking about 1 day) and the latter requires access to a UV spectrophotometer. Clearly, dye-based UV dosimeters, such as the NTC films reported here, have a long way to go before they can challenge the more established biological and chemical UV dosimeters. However, they can play a useful role in warning of sunburn when used from mid-morning to mid-afternoon.

4.5 References

1. Mshana, G. Tadesse, G. Abate and H. Miomer, *J. Clin. Microbiol.*, 1998, **36**, 1214-1219.
2. V. Creach, A. Baudoux, G. Bertru and B. L. Rouzic, *J. Microbiol. Methods*, 2003, **52**, 19-28.
3. R. L. Baehner, L. A. Boxer and J. Davis, *Blood*, 1976, 309-313.
4. M. V. Beveridge, P. M. Herst and A. S. Tan, *Biotechnol. Annu. Rev.* , 2005, **11**, 127-152.
5. A. M. Gordon, J. D. Briggs and P. R. F. Bell, *J. Clin. Microbiol.*, 1974, **27**, 734-737.
6. A. M. Gordon, R. M. Rowan, T. Brown and H. G. Carson, *J. Clin. Pathol.*, 1973, **26**, 52-56.
7. L. J. Meerhof and D. Roos, *J. Leukoc. Biol.*, 1986, 669-711.
8. A. Ebraheem, A. A. Abdel-Fattah, F. I. Said and Z. I. Ali, *Radiat. Phys Chem.*, 2000, **57**, 195-202.
9. A. Kovas, L. Wojnarovits, N. B. El-assy, H. Y. Afeefy, M. Al-sheikhly, M. L. Walker and W. L. McLaughlin, *Radiat. Phys. Chem.*, 1995, **46**, 1217-1225.
10. A. Kovas, L. Wojnarovits, W. L. McLaughlin, S. E. Ebrahim and A. Miller, *Radiat. Phys. Chem*, 1996, **47**, 483-486.
11. A. K. Pikaev and Z. K. Kriminskaya, *Radiat. Phys Chem.*, 1998, **52**, 555-561.
12. K. H. Sylvester, W. E. Franz and R. M. McGlathery, *US Pat. 349572*, 1969.
13. B. L. Diffey and P. M. Farr, *Clin. Phys. Physiol. Meas.*, 1999, **12**, 311-325.
14. B. L. Diffey, *Methods*, 2002, **28**, 4-13.
15. A. Sadeghi, M. Chaychian, M. Al-Sheikhly and W. L. McLaughlin, *Radiat. Phys. Chem.*, 2002, **64**, 13-18.
16. F. P. Altman and R. G. Butcher, *Histochemie*, 1973, **37**, 333-350.
17. R. G. Butcher and F. P. Altman, *Histochemie*, 1973, **37**, 351-363.

18. B. L. Diffey, *Radiation Measurements in Photobiology*, Academic Press Ltd., 1989.

19. L. E. Quintern, G. Horneck, U. Eschweiler and H. Bucker, *Photochem. Photobiol.*, 1991, **55**, 389-395.

Chapter 5

A novel reversible relative humidity indicator based on methylene blue

5. A novel reversible relative humidity indicator based on methylene blue

5.1 Introduction

As briefly discussed in Chapter 1, ionic dyes such as thiazine salts have been used as colorimetric relative humidity (RH) indicators. For example, methylene blue (MB)[1] and new methylene blue (NMB),[2] whose chemical structures are shown in Figure 5.1, when incorporated within a protonated mordernite zeolite (HMOR) as described by Sohrabnezhad *et al.*[1, 2] act as humidity sensors, changing colour from blue-violet when dehydrated to blue when hydrated.[1] The colour change is attributed to the protonation of the dyes during the dehydration of the HMOR by protons generated from the dissociation of water during the drying process. The absorbance spectra for a typical MB/HMOR is illustrated in Figure 5.2. The fully hydrated MB/HMOR spectrum consists of two main bands at 650 and 600 nm, see Figure 5.2 (a). The 650 nm band is associated with the monomer and the 600 nm band with the dimer aggregate. Also present at very low intensity is a peak at 754 nm which arises as a result of a small amount of the MB undergoing protonation i.e. from MB^+ to HMB^{2+}. Following dehydration the peaks at 600 and 650 nm are substantially diminished and the peak at 745 nm is greatly increased.[1] As a result the response of the MB/HMOR to changing RH conditions can be monitored at either 650 nm or 745 nm with greater sensitivity achieved at the lower wavelength.[1] The analogous NMB/HMOR humidity sensor is reported to elicit a comparable response.[2]

A similar effect has been observed by Somani *et al* for crystal violet (CV), whose structure is shown in Figure 5.1, and MB when incorporated within a polyvinyl alcohol (PVA) and phosphoric acid (H_3PO_4) system.[3,4] PVA/H_3PO_4 is a well known solid polymer electrolyte (SPE) and a good acidic proton conductor, which encourages the dye to exist in its protonated form at low RH. At high RH levels the

MB/PVA/H_3PO_4 film absorbs water, and the increase in water content causes the film to become less acidic thus causing the dye to deprotonate,[3, 4]

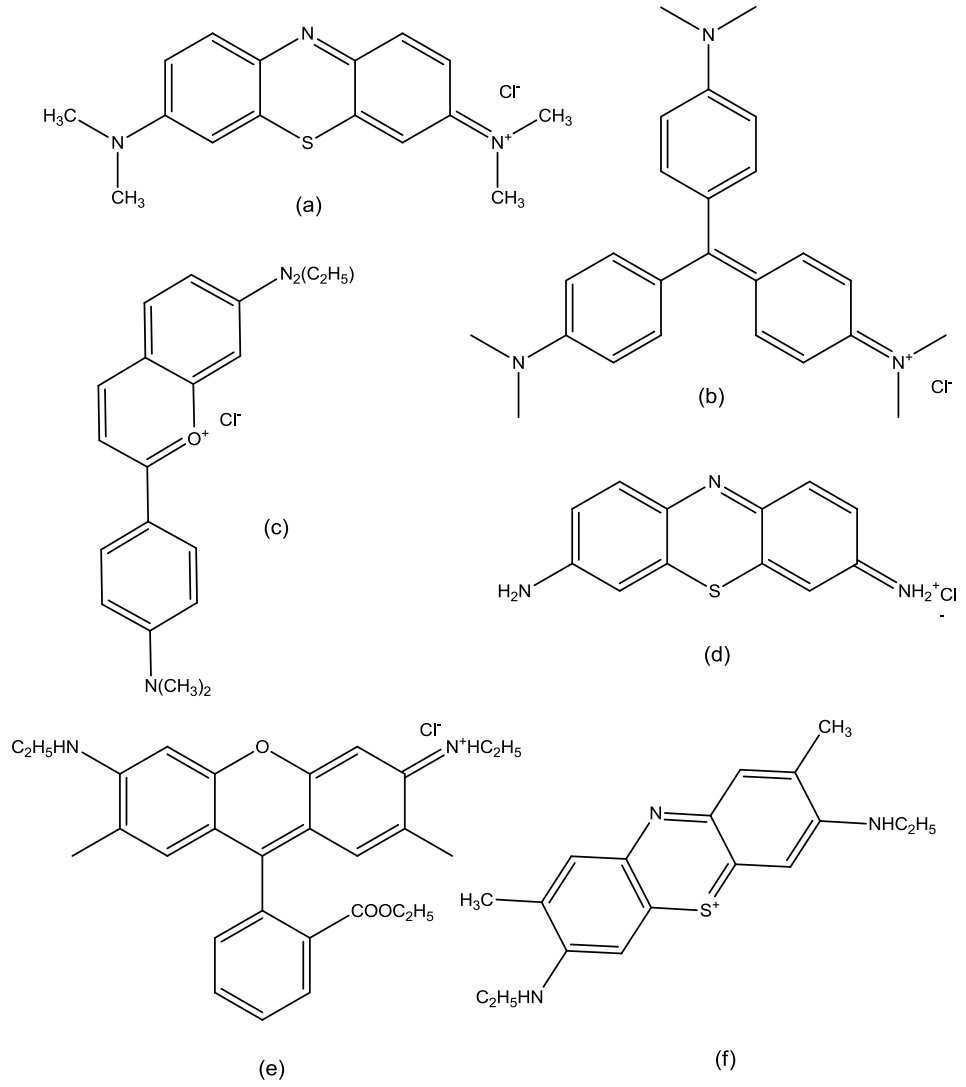

Figure 5.1 The chemical structures of (a) Methylene Blue (MB), (b) Crystal Violet (CV), (c) 7-dethylamino'-methylamionflavylium (FV), (d) Thionine (TH), (e) Rhodamine 6G (R6G) and (f) New Methylene Blue (NMB).

This process is marked by a spectral shift as illustrated in Figure 5.2 (b). Under dry conditions the UV/visible spectrum for the film has a strong peak at 600 nm, a shoulder at 670 nm and another peak at 750 nm (the MB dimer, monomer and

protonated charge transfer complex, respectively). As with Sohrabnezhad's MB/HMOR humidity sensing systems under humid conditions the peak at 750 nm disappears indicating that all of the protonated MB has deprotonated in the presence of water vapour.

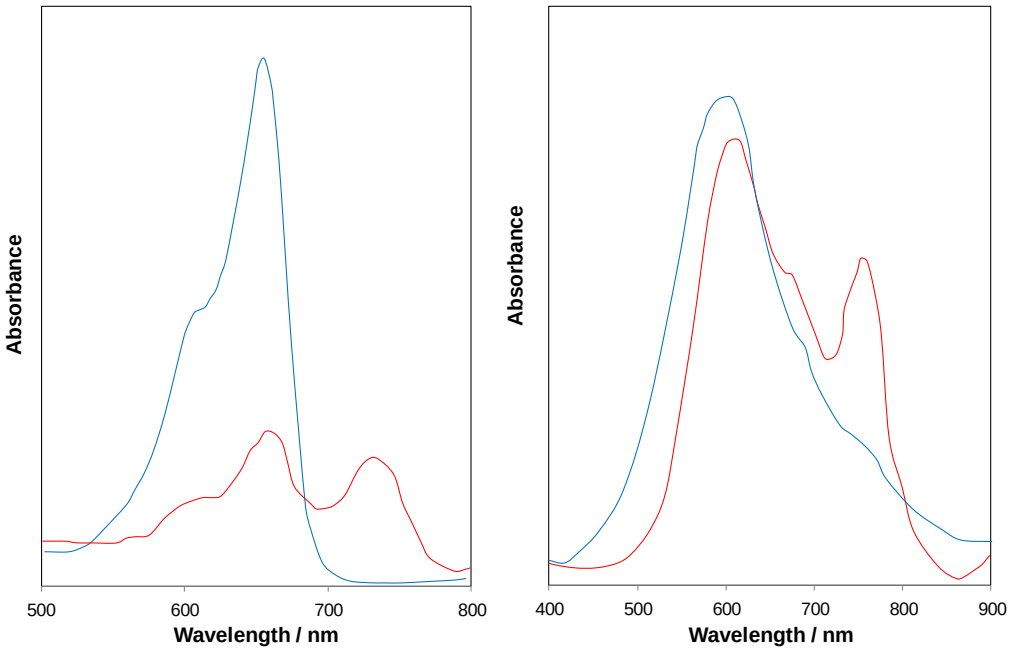

(a) (b)

Figure 5.2 The absorption spectra for (a) MB-HMOR zeolite under dry conditions (9% RH) and humid conditions (98%)[1] and (b) PVA+H_3PO_4/MB film under dry conditions (9% RH) and humid conditions (100% RH).[3]

As alluded to above, certain ionic dyes at high enough concentrations are known to undergo aggregation to form dimers and some in some cases higher aggregates. As a result of this concentration-dependant phenomena such dyes have been used as humidity indicators. Among those commonly encountered are Rhodamine 6G (R6G) and MB, whose structures are shown in Figure 5.1. Both R6G and MB have been incorporated within poly(n-vinylpyrrolidone) (PVP) films by S. Otsuki

et al.[5] to create simple reversible RH indicators based on the effect of moisture on the formation of dye aggregates. Under dry conditions the thin films of MB/PVP the MB exists predominantly in its monomeric form as illustrated by the broad UV/visible absorption at 668 nm and a smaller dimer shoulder peak at 620 nm as shown in Figure 5.3.[5]

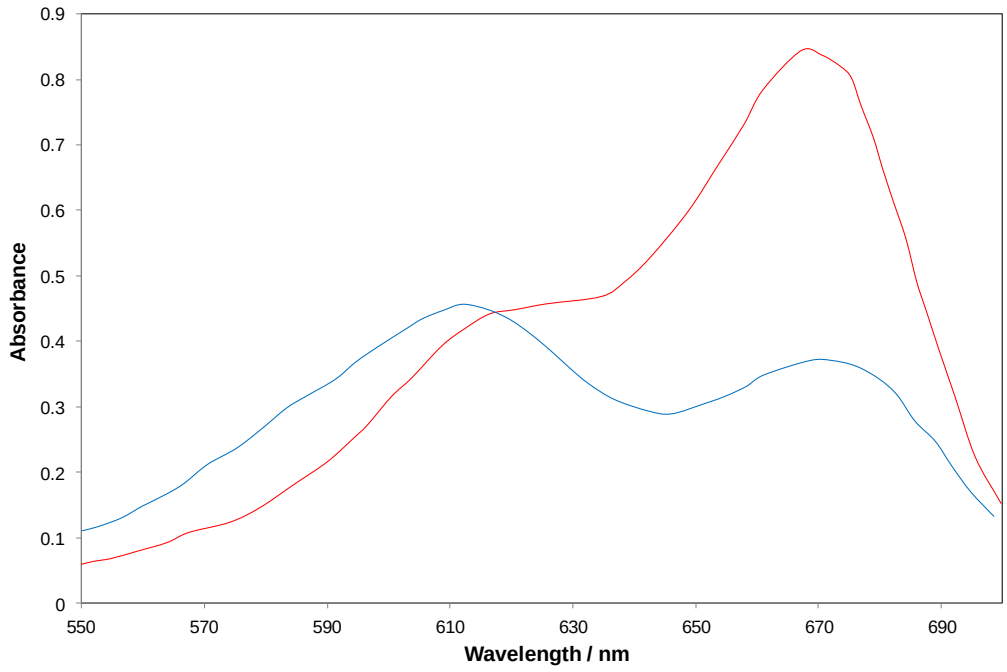

Figure 5.3 The absorption spectra for a MB/PVP film under dry conditions (0% RH) and humid conditions (88% RH).[5]

A similar effect is seen for the analogous R6G/PVP films. Otsuki rationalises this behaviour by proposing that changes in the RH humidity of the film affect the polarity of the polymer micro-environment, increasing the film's ability to support the formation of dye aggregates at increasing RH levels.[5] Otsuki also suggests the formation of water clusters at higher RH may result in the dyes (both of which are very soluble in water) concentrating in the water cluster regions, which may be a contributing factor.[5]

More recently, Matsushima *et al*. have proposed using thionine, (TH), and flavylium perchlorate (FC) salts (dye structures for which are shown in Figure 5.1) in agar and carrageenan gels as simple colorimetric humidity and temperature sensors.[6-8] These salts exhibit reversible colour changes from purple (dry) to red (humid) as a result of a change in RH. This has been attributed to the absorption of water vapour by the gel in humid conditions which encourages the dye to form dimers and so leads to a shift in λ_{max} absorbance ($\approx$ 20-30 nm) to a lower wavelength. The UV/visible absorption for (a) a TH/carageenan gel[6] and (b) a FC/carageenan gel[8] under dry and humid conditions are shown in Figure 5.4. The explanation offered by Matsushima for the dye's tendency to form dimers under high RH conditions is that water has the potential to stabilise the aggregates of charged dyes as a result of its high dielectric constant and hydrogen bonding capabilities. Consequently the TH and FC dimers are more stable than the monomer equivalents in the presence of water vapour.[8] Matsushima also reports similar behaviour for an MB-doped film.[8]

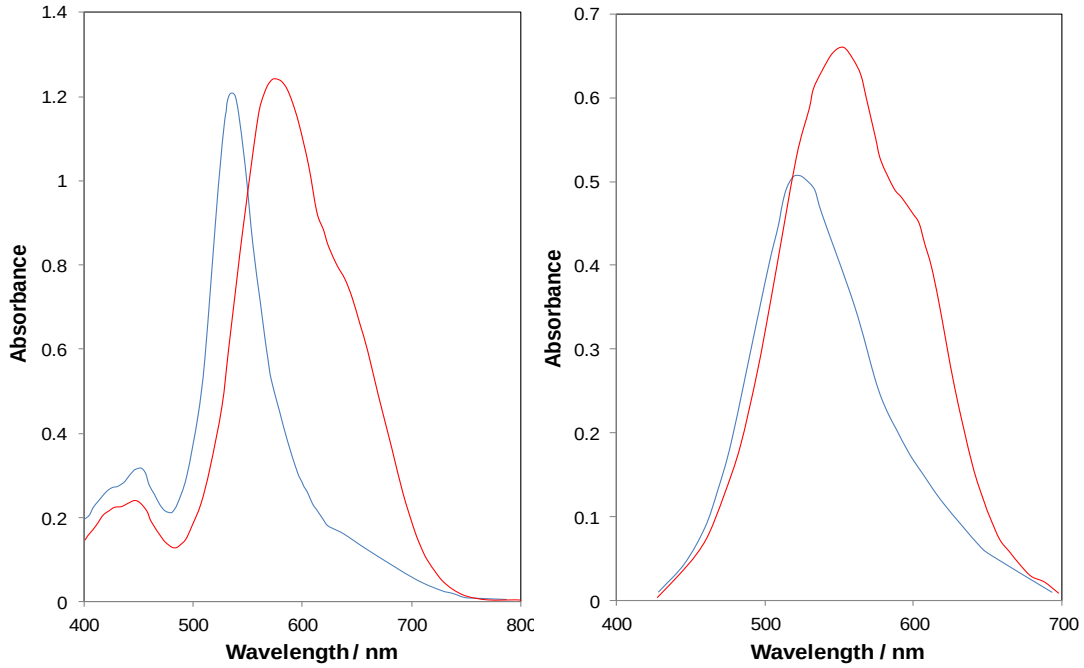

(a) (b)

Figure 5.4 The absorption spectra for (a) TH-carrageenan gel film under dry conditions and humid conditions[6] and (b) FC-carrageenan gel film film under dry conditions and humid conditions.[8]

The purpose of this chapter is to expand on this work by investigating the behaviour of methylene blue in a polymer with and without urea (a deliquescent material) as an additive and its potential application as a humidity-indicating device.

5.2 Experimental

5.2.1 Materials

All chemicals were purchased from Sigma Aldrich Chemicals unless specified. The water used to produce the inks was double distilled and deionised and the

polymer used to produce the humidity sensors in this work was hydroxy ethyl cellulose (HEC) (medium viscosity) purchased from Fluka.

5.2.2 *Preparation of MB/HEC relative humidity indicators*

A typical MB/HEC RH indicator casting ink was prepared by dissolving 5 mg of MB in 2 g of a 5% w/v HEC polymer solution. The solution was well stirred to ensure dissolution of the dye. The blue-coloured casting solution contained 5 phr of MB *i.e.* 5 parts per hundred resin (or 5 g of MB for 100 g polymer). Films were cast on quartz discs, 25 mm in diameter and 1 mm thick, using a spin coater. Thus, a few drops of casting solution were deposited on the surface of the disc, which was then spun at 3500 rpm for 30 seconds. The resultant product was then dried for 2-3 minutes at 70°C and cooled to room temperature (for 5 minutes) before use. Figure 5.5 (a) illustrates a typical MB/HEC ink formulation and MB/HEC RH indicator. The final RH indicator product was a blue coloured film on a glass disc under ambient conditions (40-60% RH, T=20^{o}C), which will be referred to forthwith as a typical MB/HEC indicator film.

5.2.3 *Preparation of MB/Urea/HEC relative humidity indicators*

A typical MB/Urea/HEC casting ink was prepared by dissolving 5 mg of MB and 100 mg of urea in 2 g of a 5% w/v HEC polymer solution. The solution was well stirred to ensure dissolution of the dye and urea. The blue-coloured casting solution contained 5 phr of MB *i.e.* 5 parts per hundred resin (or 5 g of MB for 100 g polymer) and 100 phr urea. Films were cast on quartz discs, 25 mm in diameter and 1 mm thick, using a spin coater. Thus, a few drops of casting solution were deposited on the surface of the disc, which was then spun at 3500 rpm for 30 seconds. The resultant product was then dried for 2-3 minutes at 70°C and cooled to room temperature (for 5 minutes) before use. Figure 5.5 (b) illustrates a typical MB/urea/HEC ink formulation and MB/urea/HEC RH indicator. The final RH indicator product is a pink, opaque, highly crystalline

film (*ca*. 1.7 μm thick) on a glass disc under ambient conditions (40-60% RH, T=20^{o}C), which will be referred to forthwith as a typical MB/urea/HEC indicator film.

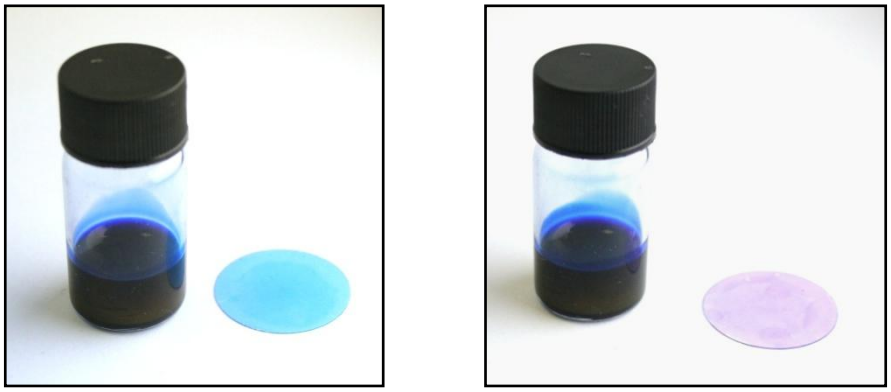

(a) (b)

Figure 5.5 Photographs of (a) a typical MB/HEC ink and film and (b) a typical MB/Urea/HEC ink and film.

5.2.4 Methods

a) UV/visible spectrometry

UV/visible absorption spectra for sample films were recorded using a Cary Model 50 UV/visible spectrophotometer. Typically, a MB humidity sensor was exposed to a stream of 100% RH water vapour (air bubbled through a Drechsel bottle containing water) at 2 l min^{-1} for 1 minute followed by a stream of dry air for 1 minute. The absorbance spectrum of the film was recorded every 6 seconds. In order to carry out this work, all films tested were housed in a gas cell through which a humid air stream was passed.

b) Humid air stream generation

Air streams containing different RH% vapour were generated by passing air through two Drechsel bottles containing 150 ml of,water fitted with a glass sintered tip to ensure the effective dispersion of the carrier gas as bubbles and their saturation with water vapour. The humid air stream was then blended with a dry nitrogen stream to generate different RH levels which were measured with a Thermo Hygrometer (Hanna HI 9564). In this work, all relative humidities quoted are at T=20^{o}C unless otherwise stated.

5.3 Results and discussion

5.3.1 MB in solution

(a) MB in water

A series of dilute aqueous solutions of MB were prepared with concentrations ranging from 0.125 x 10^{-5} to 1 x 10^{-5} M. Their UV/visible absorption spectra were recorded in a 1 cm cell. A saturated solution of MB in water was also prepared and a small amount was sandwiched between two 25 mm diameter borosilicate glass cover slips and its UV/visible absorption spectra recorded. The spectral data for both are shown below in Figure 5.6.

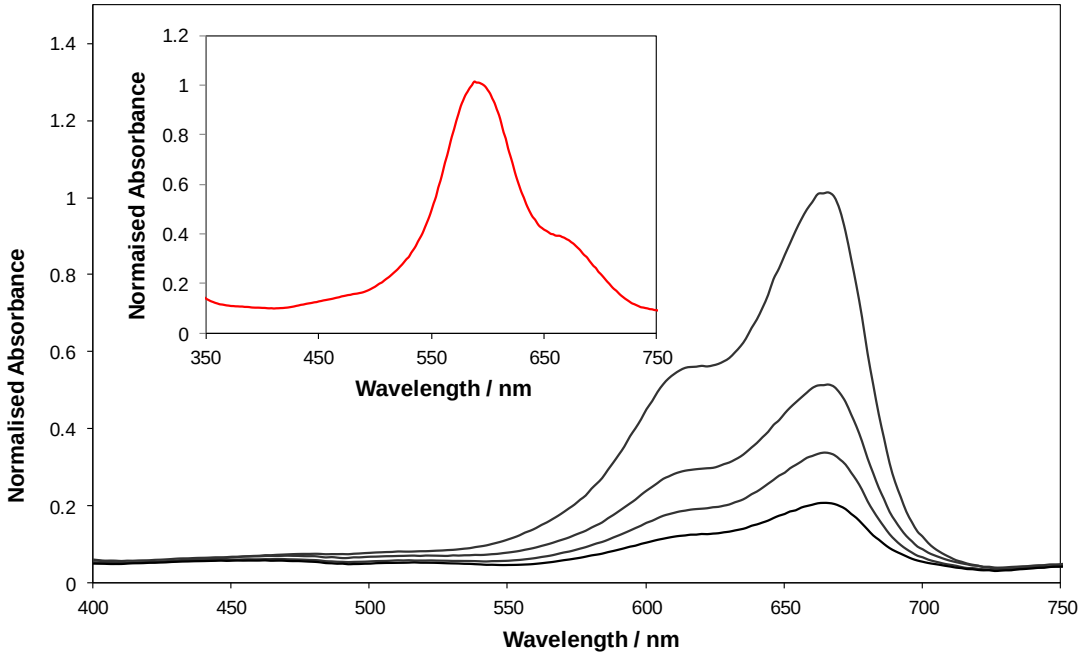

Figure 5.6 The UV/visible absorption spectra for a series of dilute MB solutions in a 1 cm cell. MB concentrations are from top to bottom 10^{-5} M, 0.5×10^{-5} M, 0.25×10^{-5} M and 0.125×10^{-5} M. The inset diagram is the UV/visible absorption spectrum of a few drops of a saturated aqueous solution of MB between two glass cover-slips.

It is clear that the spectra of dilute MB solutions differ greatly from that of a highly concentrated saturated solution. The former has a λ_{max} at 660 nm and a shoulder at 620 nm while the latter has a λ_{max} at 587 nm and a shoulder at 665 nm. This deviation from Beer's law with increasing concentration is commonly reported for MB systems and is explained by assuming that in dilute solution the MB molecules exist mainly in their monomer form which absorbs at 660 nm; however, if the levels are increased significantly the molecules will tend towards their dimeric and trimeric structures, the spectra for which are shown in Figure 5.7 below, which absorb at lower wavelengths.[9, 10]

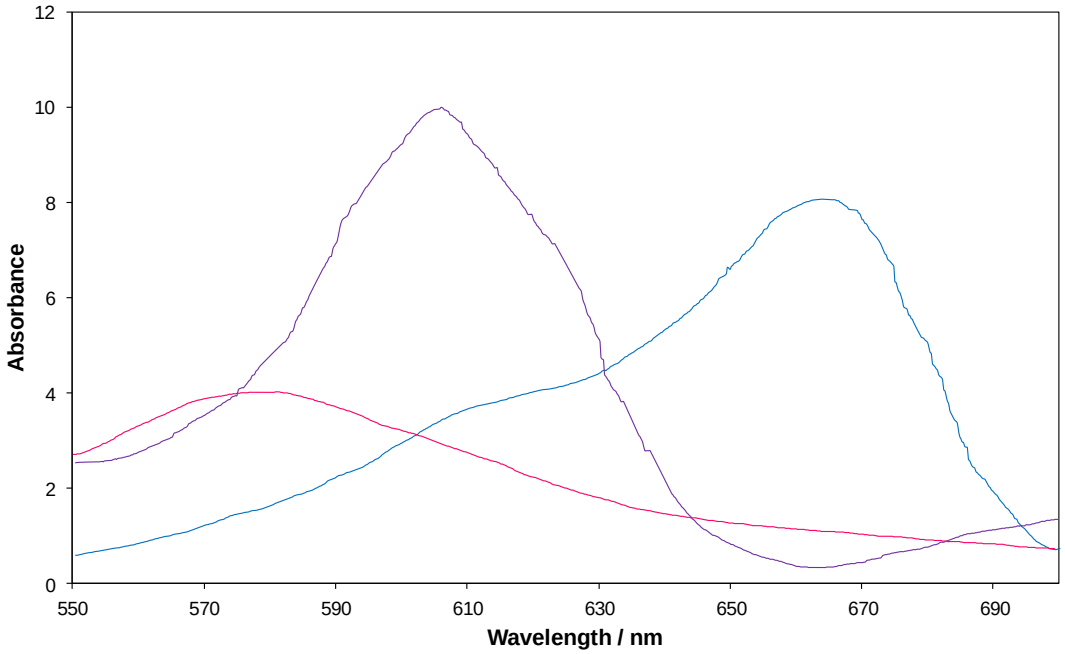

Figure 5.7 Absorption spectra of the MB aggregates present in aqueous solutions of MB: curve (a) is the monomer (λ_{max} at 665 nm), curve (b) is the dimer (λ_{max} at 605 nm), and curve (c) is the trimer (λ_{max} at 578 nm). [9, 10]

(b) MB in aqueous urea solution

It has been previously reported that the addition of urea to water can increase its solubility characteristics towards organic molecules including dyes.[11-13] The exact mechanism by which urea does this is unclear. Some authors have suggested that as urea is a known 'water structure breaker' i.e. breaks up the hydrogen bonds in water, it is able to destroy water clusters which reduces polarity of the water and thus its dielectric constant. [11-13] These conditions are less favourable for dimer formation resulting in the dye reverting back to its monomer formation. Thus it is presumed that urea's ability to change the micro-environment surrounding the dye molecules is responsible for the increased solubility towards dyes. [11-13] To confirm this, a series of aqueous solutions containing 1.2 x 10^{-4} M MB and varying concentrations of urea (0-8 M) were prepared. Their absorption spectra were recorded in a 1 mm quartz cell

and these results are shown in Figure 5.8 below. These results show that at [MB] = 1.2 x 10^{-4} M in the absence of urea there are two distinct peaks present in the MB spectra, one at 665 nm (the monomer peak) and the other at 610 nm (the dimer peak). As the concentration of urea is increased the peak at 665 nm is increased while at the same time the peak at 610 nm is lowered. This is indicative of the presence of urea in the system and its ability to increase the solvent power of water and encourage disaggregation of the MB molecules as discussed above.[11-13] Consequently, more of the MB can be dissolved in its monomeric form and thus the increasing intensity of the monomer peak.

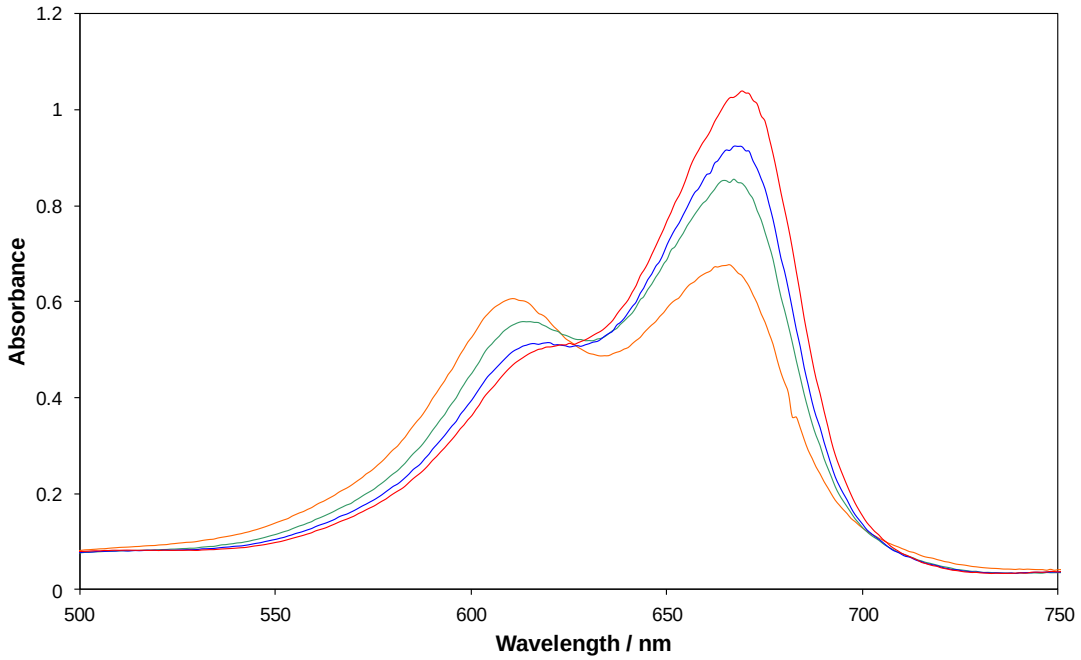

Figure 5.8 Effect of urea on the absorption spectrum of MB in aqueous solution. Spectra determined in a 1 mm cell. The concentration of MB is 1.2x10^{-4} M while the concentration of urea from top to bottom is 8 M, 4 M, 2 M and 0 M.

5.3.2 MB/HEC films

After observing the behaviour of MB in aqueous solutions, a typical MB/HEC

humidity indicator was prepared and exposed to a stream of 100% RH air. The colour change was observed and recorded photographically as illustrated in Figure 5.9, which shows the MB/HEC film before and after exposure to humid air. The colour change is subtle but noticeable from blue under ambient conditions to dark purple under high RH conditions.

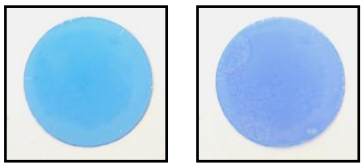

(a) (b)

Figure 5.9 Photographs of a typical MB/Urea/HEC humidity indicator (a) before (blue) and (b) after (purple/blue) exposure to 100% humid air.

In order to observe the colour change on a spectroscopic level a typical MB/HEC film was housed in a gas cell and exposed to a stream of 100% RH for 1 min. The UV/visible absorbance spectra of the dry and humid film were recorded and are illustrated in Figure 5.10. The UV/visible absorption spectra for the MB monomer (λ_{max} = 665 nm), dimer (λ_{max} = 605 nm) and trimer (λ_{max} = 578 nm) in aqueous solution were shown previously in Figure 5.7.[9]

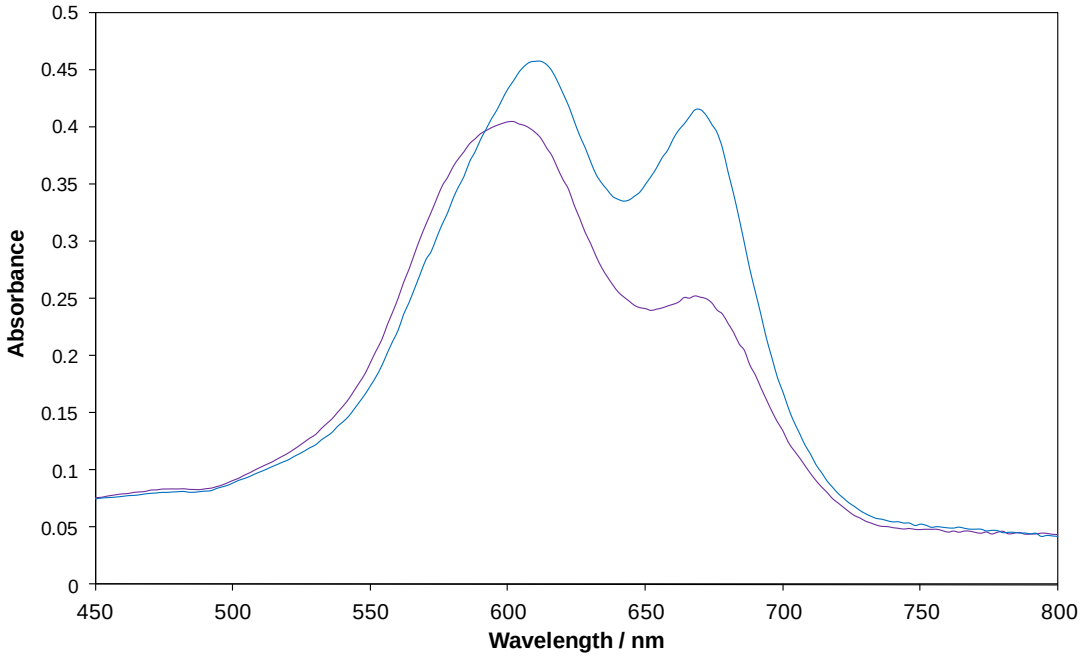

Figure 5.10 The UV/visible absorption spectra of a MB/HEC film. The blue line indicates the initial spectrum of the dry film with λ_{max} at 610 nm and 668 nm. The purple line illustrates the effect of exposure to 100% humid air for 1 minute, with λ_{max} at 600 nm and 668 nm.

The MB/HEC film was blue under ambient conditions and rapidly changed to purple/blue when exposed to 100% RH humid air as is evident by the spectral shift from 610 nm (dry/ambient) to 600 nm (humid). This effect has been observed previously by Matsushima *et al.*[6-8] who suggest that under humid conditions the adsorption of water vapour by the film encourages MB monomers to form dimers as illustrated in equation (5.1), with λ_{max} at 605 nm, thus causing the absorption peak to shift to a lower wavelength and the monomer peak (665 nm) height to decrease.

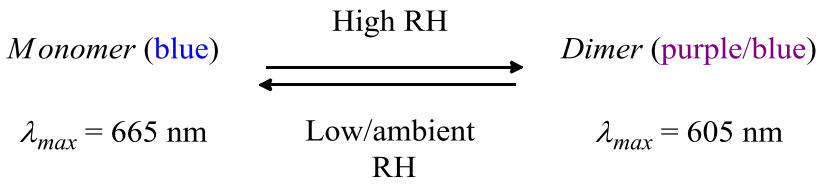

(5.1)

5.3.3 MB/Urea mixture

During the investigation of the MB/HEC humidity indicator system, while experimenting with different encapsulation materials, it was discovered that the incorporation of urea, a crystalline material that deliquesces at RH = 80% at T = 18°C[14], into the system yields some unusual results. A polymer-free system, where a small amount of MB was mixed together with an excess of urea, produced a pale pink/purple powder, which on exposure to 100% RH air rapidly was rendered blue-coloured. This intriguing process was recorded photographically as illustrated in Figure 5.11 which clearly shows the progression of the blue colour on increasing exposure to 100% RH air. The process was also monitored spectrophotometrically using diffuse reflectance measurements.

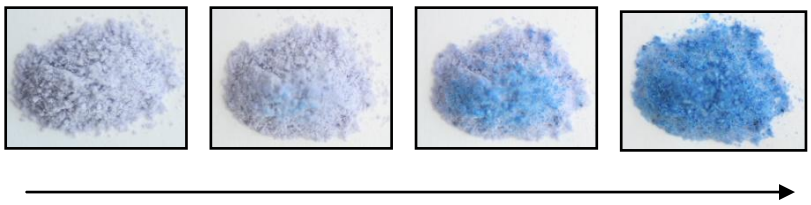

Exposure to 100% RH air

Figure 5.11 Photographs of ground MB/Urea powder changing colour from pink/purple (left) to blue (right) upon exposure to 100 % RH air.

The reflectance data gathered, R, was used to determine the Kubelka-Munk function, f(R), which is an absorbance-like function, using equation (5.2) which was plotted against wavelength to generate Figure 5.12.

$$f(R) = \frac{(1-R)^2}{2R} \qquad (5.2)$$

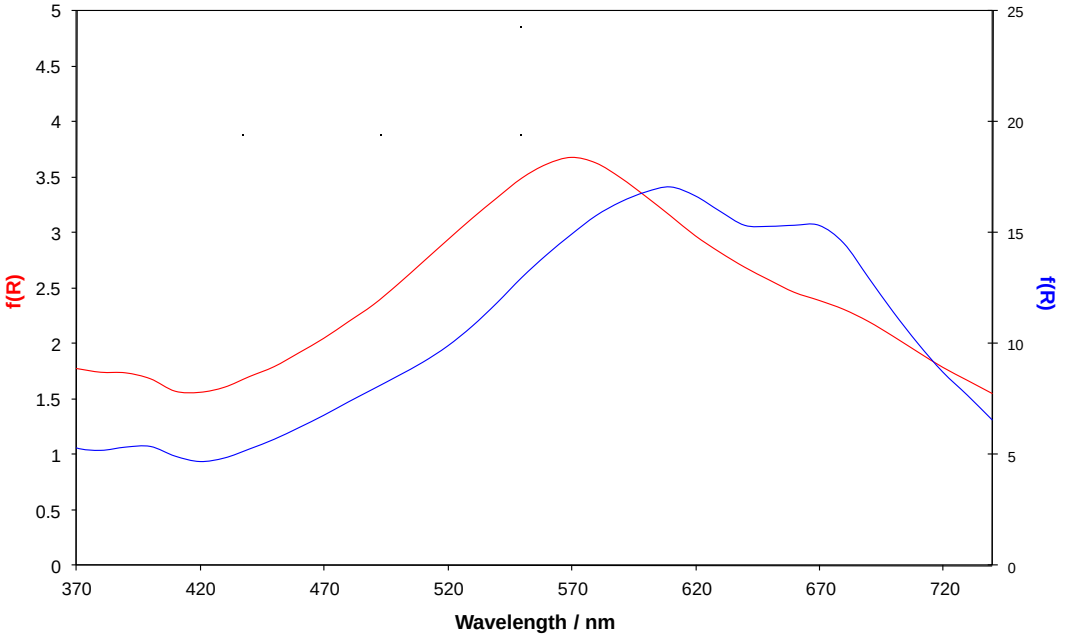

Figure 5.12 A plot of f (R) against wavelength determined from the diffuse reflectance data (not shown) for the MB/Urea powder when dry with λ_{max} at 570 nm, and on exposure to humid air with λ_{max} at 610 and 670 nm.

The resulting spectra shows a spectral shift in the *opposite* direction from those observed by Matsushima *et al* [6-8] and from the MB/HEC films discussed above. The initial spectra for the dry pink/purple mixture has a λ_{max} at 570 nm and on exposure to high RH air the powder changes to a blue colour which has a λ_{max} at 610 nm with a shoulder at λ_{max} at 670 nm.

At first glance the cause of the colour change is not immediately clear. The initial spectrum of the dry mixture (λ_{max} = 570 nm) does not resemble that of the monomer and dimer, and is if anything like that of the MB trimer spectrum shown previously in Figure 5.7 (λ_{max} = 578 nm), which on exposure to high RH air is converted to the

MB dimer with a λ_{max} at 605 nm. In support of this, it is well known that urea is a hygroscopic compound which deliquesces under high RH conditions >80% RH at 18 ^{o}C.[14-16] Urea, as shown earlier in Figure 5.9, is also known for its ability to encourage the formation of lower aggregate MB species in aqueous solutions.[11-13] Under high RH conditions it is possible that the monomer form of MB exists in the humid mixture causing the absorption at 670 nm; however, perhaps a more plausible explanation for this, given the amount of MB present, is that the MB forms not only the usual sandwich type, H-aggregates dimers in the urea (λ_{max} = 605) but also the less common J-aggregates, i.e. end-to-end type dimers which are contributing to the apparent monomer peak.[10] H- and J-aggregate dimers are illustrated in Figure 5.13 below:

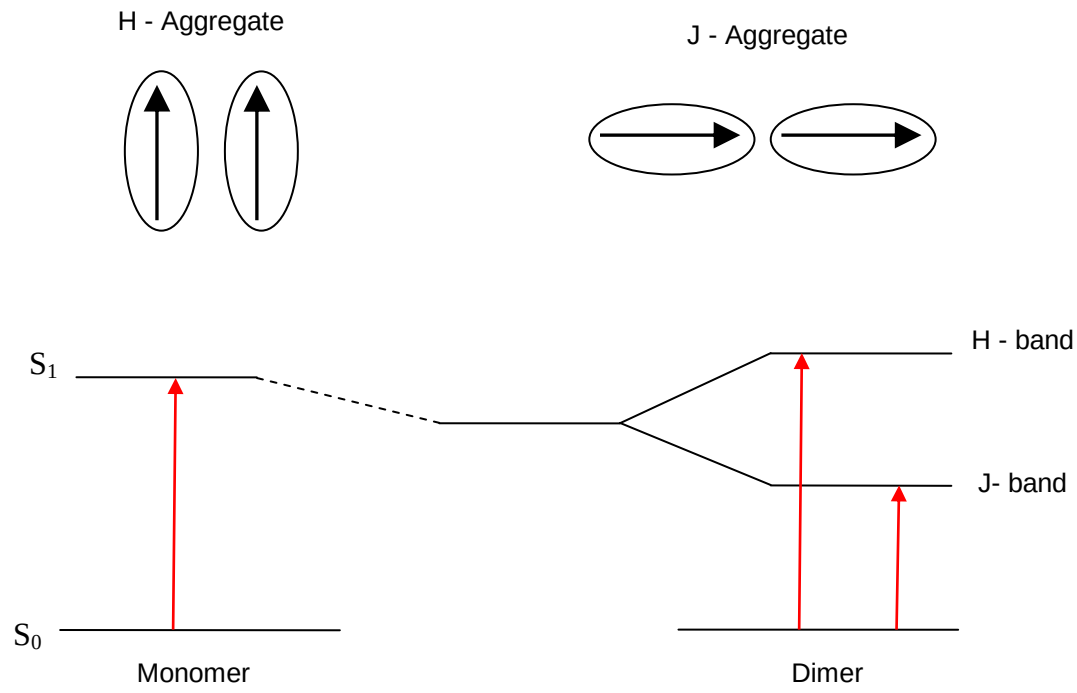

Figure 5.13 Energy diagram for monomer and H- and J-aggregate dimers.

A. Ghanadzadeh *et al.* have proposed that J-type aggregates of MB exist in aqueous and alcoholic dye solutions, the calculated spectral profile for which has a λ_{max} similar to that of the monomer as shown in Figure 5.14.[10]

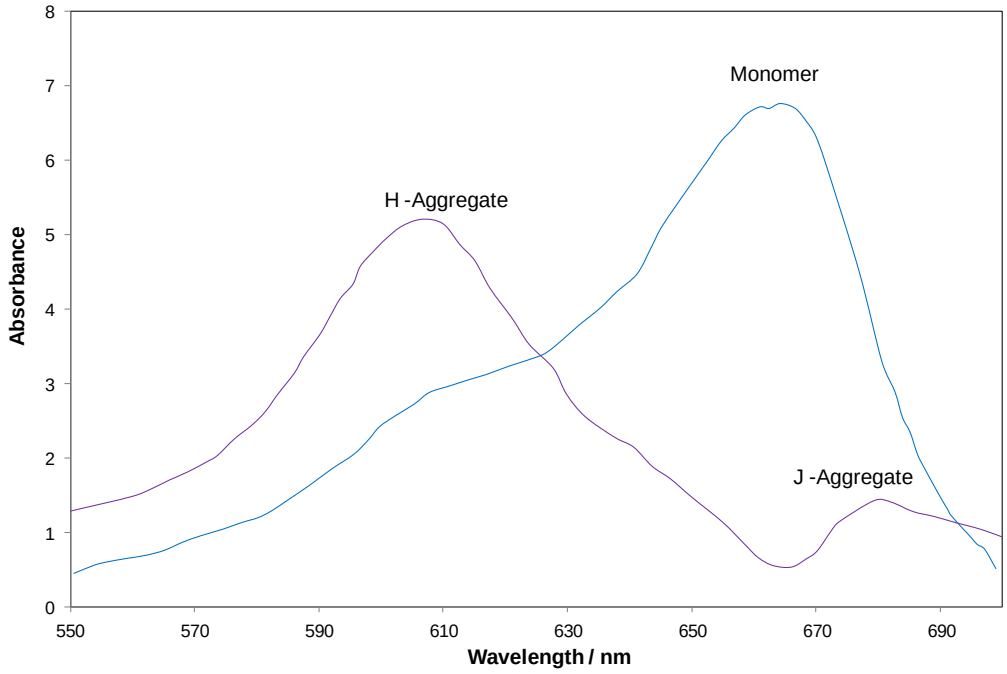

Figure 5.14 Monomer and dimer absorption spectra of MB in aqueous solution as calculated by Ghanadzadeh.[10]

A similar set of spectra have been obtained by K. Patil *et al.* during their investigation on the aggregation on MB in aqueous urea solutions.[13]

5.3.4 MB/Urea/HEC RH indicators

(a) Optical characteristics

When MB is encapsulated within a polymer such as hydroxyethyl cellulose (HEC) with a notable (20 time wt/wt more than MB) excess of urea, the product,

a typical MB/Urea/HEC ink, is blue. This casts as a thin, opaque pink film under ambient conditions (RH = 60%, T = 20^{o}C) or dry (RH ~ 0%) conditions, As observed with the MB/Urea mixture, the indicator rapidly and reversibly is rendered blue (λ_{max} = 600 nm) and clear when exposed to RH values >85%. The process was recorded by subjecting a typical MB/Urea/HEC film to 100% RH and taking a series of photographs with (a) a hand held digital camera and (b) a microscope mounted camera. The images gathered from both are illustrated in Figure 5.15 and show clearly the distinct change in colour (from pink to blue) but also the change in opacity (from highly opaque to clear) under high RH conditions. The coefficient of variance associated with the MB/Urea/HEC humidity indicator colour change is ± 1.5%; this is typical of the error for all MB/Urea/HEC humidity indicators

Exposure to 100% RH air

(a)

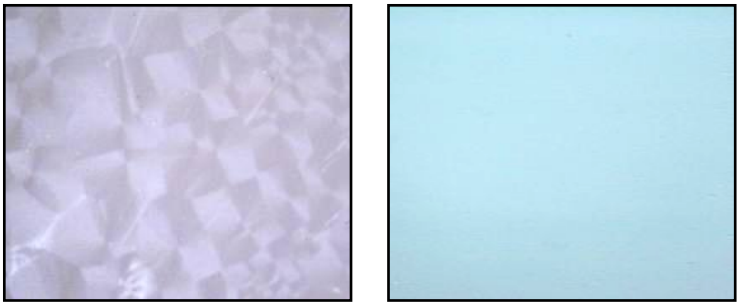

(b) (c)

Figure 5.15 (a) Photographs of a typical MB/Urea/HEC humidity indicator on increasing exposure to 100% humid air. Images of a typical MB/HEC/Urea film at x40 magnification (b) at ambient conditions and (c) after exposure to 100% RH air.

Note the observed colour changes are once again the *opposite* of those observed by Matsushima *et al*.[6-8] for their gel films and observed by ourselves for MB/HEC (i.e. no urea) films, but do match those observed for the MB/Urea mixture. This colour changing process was also followed spectrophotometrically by subjecting a typical MB/Urea/HEC film, mounted in a gas cell, to a stream of 100% RH air for 1 min followed by a stream of dry air for 1 min. The UV/visible absorption spectra of a typical MB/Urea/HEC film in dry and humid conditions are illustrated in Figure 5.16 and show a similar spectral shift from λ_{max} = 570 nm (pink) under dry condition to λ_{max} = 600 nm (blue) under humid condition as seen for the MB/Urea mixture. This curious process occurs rapidly with response and

recovery times of 10 and 60 seconds and is also highly reversible as shown by the data in Figure 5.17 which illustrates the response and recovery profile of a typical MB/Urea/HEC relative humidity indicator film on exposure to repeated 1 minute cycles of humid (100% RH) and dry air.

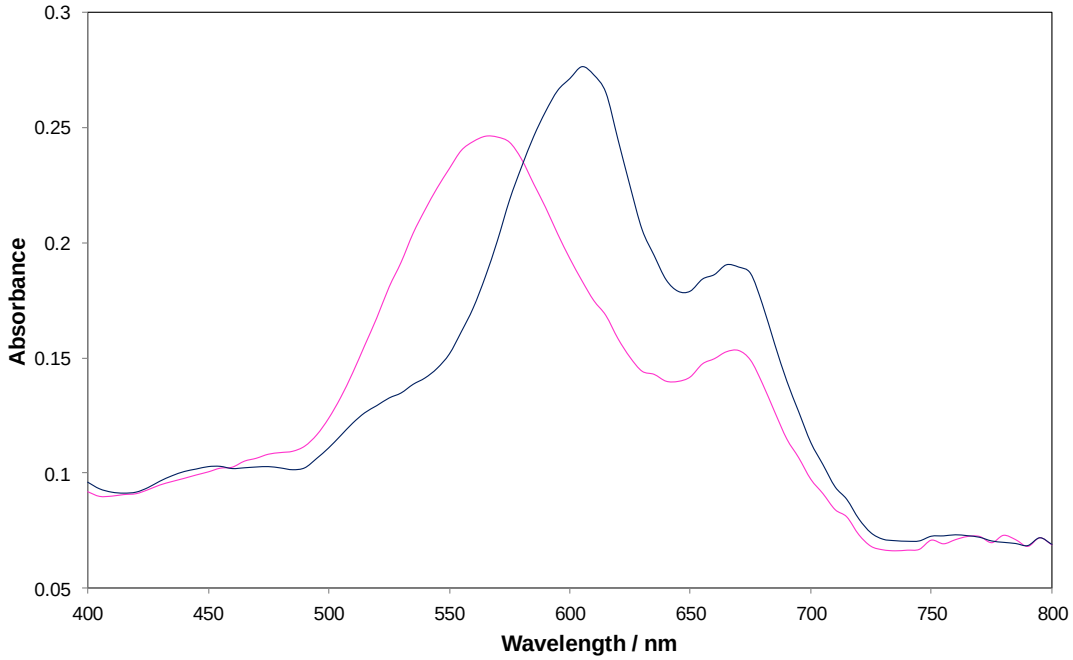

Figure 5.16 The UV/visible absorption spectra of a typical MB/Urea/HEC film. The pink line indicates the initial spectrum of the dry film with λ_{max} at 570 and 665 nm. The blue line illustrates the effect of exposure to 100% humid air for 1 minute, with λ_{max} at 600 and 670 nm.

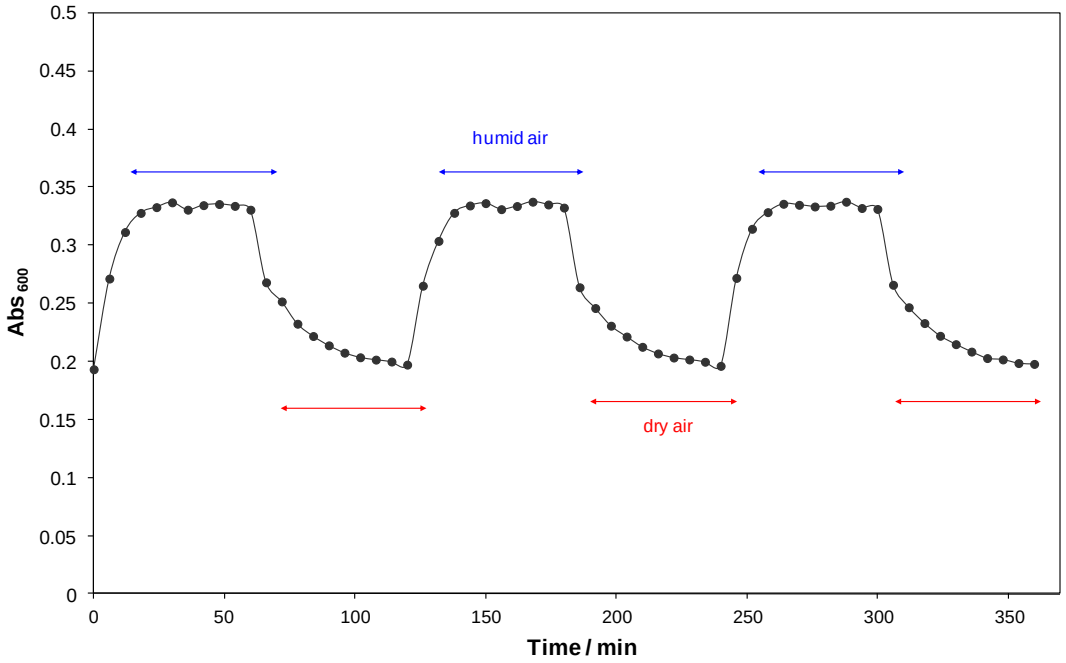

Figure 5.17 A plot of Abs_{600} against time for a MB and Urea polymer film exposed to humid air for 1 min and then to dry air for 1 min. This was repeated for 3 cycles. Absorbance recorded every 6 seconds.

The initial spectrum of the dry film (λ_{max} = 570 nm, see Figure 5.16) under ambient conditions, as with the MB/Urea mixture, is like that of the MB trimer (λ_{max} = 578 nm, see Figure 5.7.[9, 18]) and, as with the MB/Urea mixture, when exposed to a high RH air stream the urea crystals dissolve, releasing the MB into its more stable MB dimer form (λ_{max} = 605 nm). The shoulder at 670 nm again is indicative of the presence of some MB monomers and/or any J-type dimers in the dissolved urea system.[10, 13]

Further work shows that urea forms highly crystalline, optically opaque films with a characteristic XRD peak at $2\theta = 22.25^{o}$ at moderate and low RH. This compares well with the previously reported urea XRD data.[17] The XRD data in Figure 5.18 are for a typical MB/Urea/HEC humidity indicator and show that initially for a dry opaque film the urea crystallites' peak at 22.25^{o} is clearly

visible and that on exposure to high relative humidities these crystallites are rapidly dissolved rendering a clear film with no XRD peak. The urea XRD peak reappears when the opacity change is reversed by blowing dry air over the film or placing the film in the oven (70^{o}C for a few minutes). Thus, it appears that the colour change associated with the MB in the humidity indicator film (pink (dry) $\longleftrightarrow$ humid (blue)) is linked with the change in crystallinity of the urea when exposed to high relative humidities.

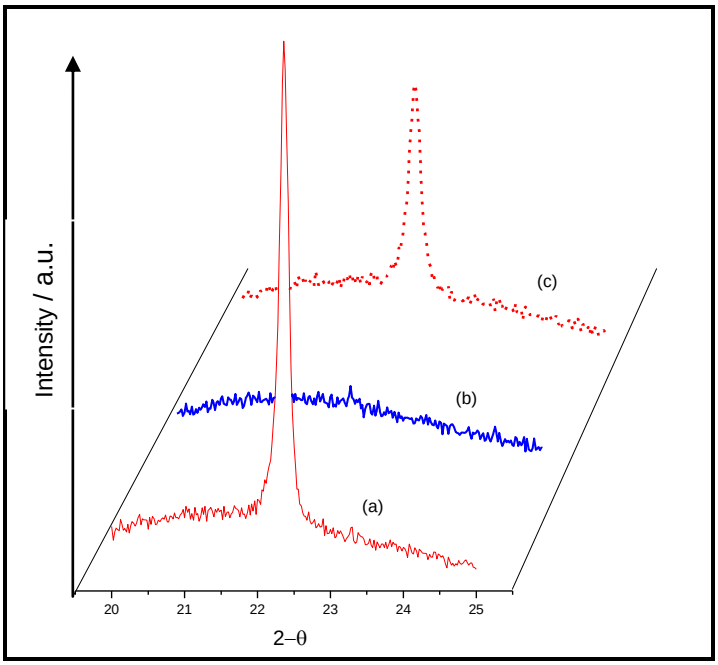

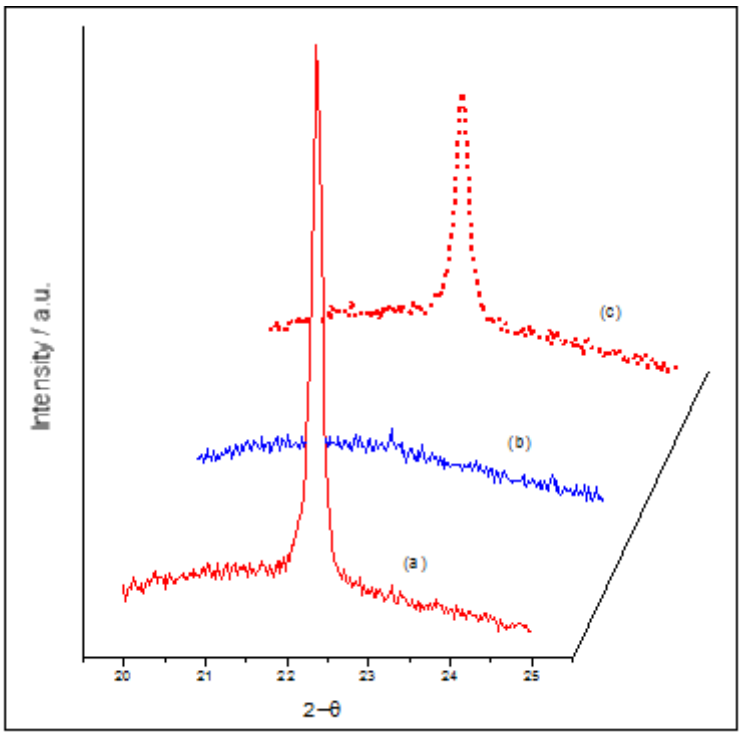

Figure 5. 18 XRD data for a typical MB/Urea/HEC film (a) initially, (b) on exposure to 100% RH air and (c) after drying again in oven for few minutes.

(b) Relative humidity

To determine the minimum % RH to which the films would respond (i.e. change colour from pink to blue), a typical MB/Urea/HEC film was exposed to gas streams of different RH levels. The UV/visible absorption spectra of the film were recorded initially and after exposure to a humid air stream for 10 minutes. The same film was used for each RH level and was removed from the gas cell and "reset" by exposing to 100% RH air and then oven drying until the film had reverted back to its pink form. The % RHs tested were 35%, 49%, 61%, 67%, 73%, 80%, 86%, 91% and 100% and the absorption spectra of the film after exposure to each RH level are shown in Figure 5.20. Using this data, it was possible to plot the variation in the change in absorbance at λ_{max}, ΔAbs_{605} (i.e. $Abs_{605} - Abs_{800}$), as a function of %RH to generate the inset diagram in Figure 5.19.

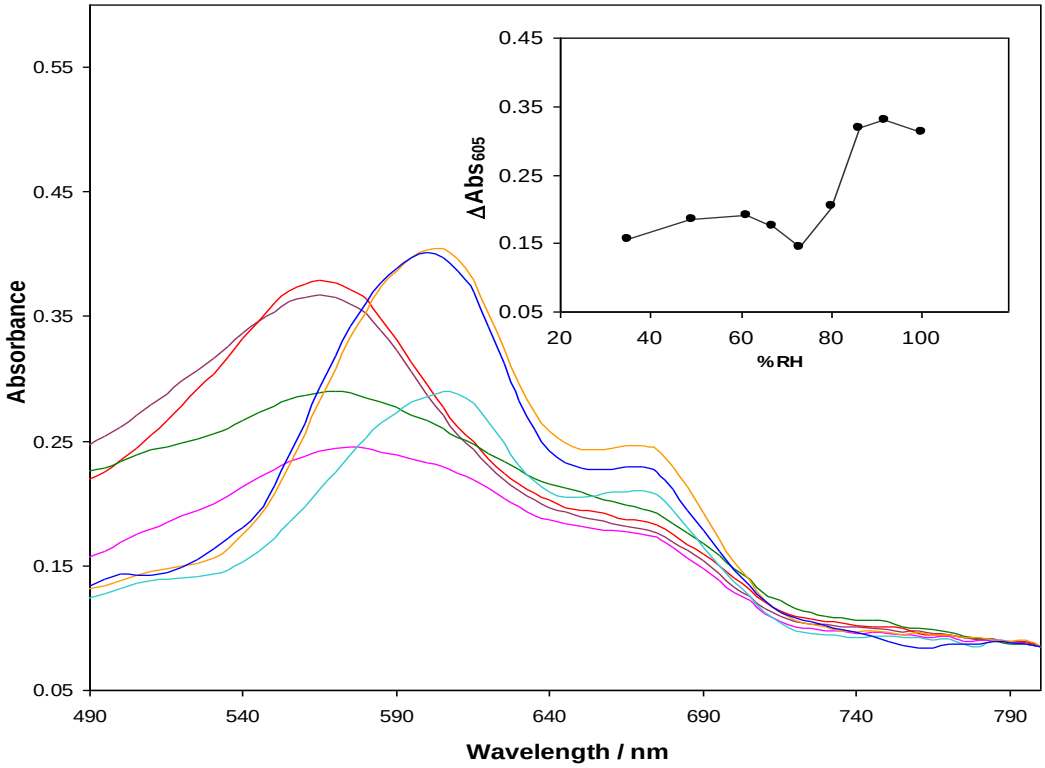

Figure 5.19 The absorption spectra for a typical MB/Urea/HEC film on exposure to increasing RH levels: 49% RH, 61% RH, 67% RH, 73% RH, 80% RH, 86% RH and 100% RH. Inset diagram is a plot of ΔAbs_{605} against % RH for the film at different % RH levels.

RH (%)	**Colour when dry (λ_{max})**	**Colour of exposure to humid air (λ_{max})**
35	Pink (565 nm, 665 nm)	Pink (565 nm, 665 nm)
49	Pink (565 nm, 665 nm)	Pink (565 nm, 670 nm)
61	Pink (565 nm, 665 nm)	Pink (565 nm, 670 nm)
67	Pink (565 nm, 665 nm)	Pink/purple (br 565 nm, 670 nm)
73	Pink (565 nm, 665 nm)	Pale blue/ pink patches (br 565 nm, 670 nm, wk sh 605 nm)
80	Pink (565 nm, 665 nm)	Blue (605 nm, 670 nm)
86	Pink (565 nm, 665 nm)	Blue (605 nm, 670 nm)
91	Pink (565 nm, 665 nm)	Blue (605 nm, 670 nm)
100	Pink (565 nm, 665 nm)	Blue (605 nm, 670 nm)

Table 5.1 The colours and λ_{max} values for a standard MB/Urea/HEC film on exposure to different % RH levels.

These results indicate that at a RH lower than 80% RH there is no significant colour change observed. Such a result is hardly surprising as the RH levels in the ambient lab environment can typically vary from 40-60% RH and these typical MB/Urea/HEC humidity indicator films remain pink under lab conditions. At RH levels of 80% and above the film undergoes a striking colour change from pink to blue with the greatest change in absorbance observed for >86% RH.

(c) Different polymers

The polymer used, in this case HEC, does not appear to have any effect on the colour or opacity change, but merely acts as an encapsulation agent. This was confirmed by observing a similar effect in different polymers *viz*. polyvinyl alcohol, PVA and polyethylene oxide, PEO. This is hardly surprising as previously discussed results show the same colour change is observed in a polymer free MB/Urea environment.

The colour changes observed for MB/Urea/PVA and MB/Urea/PEO are illustrated below in Figure 5.20 and mirror those observed for typical MB/Urea/HEC films.

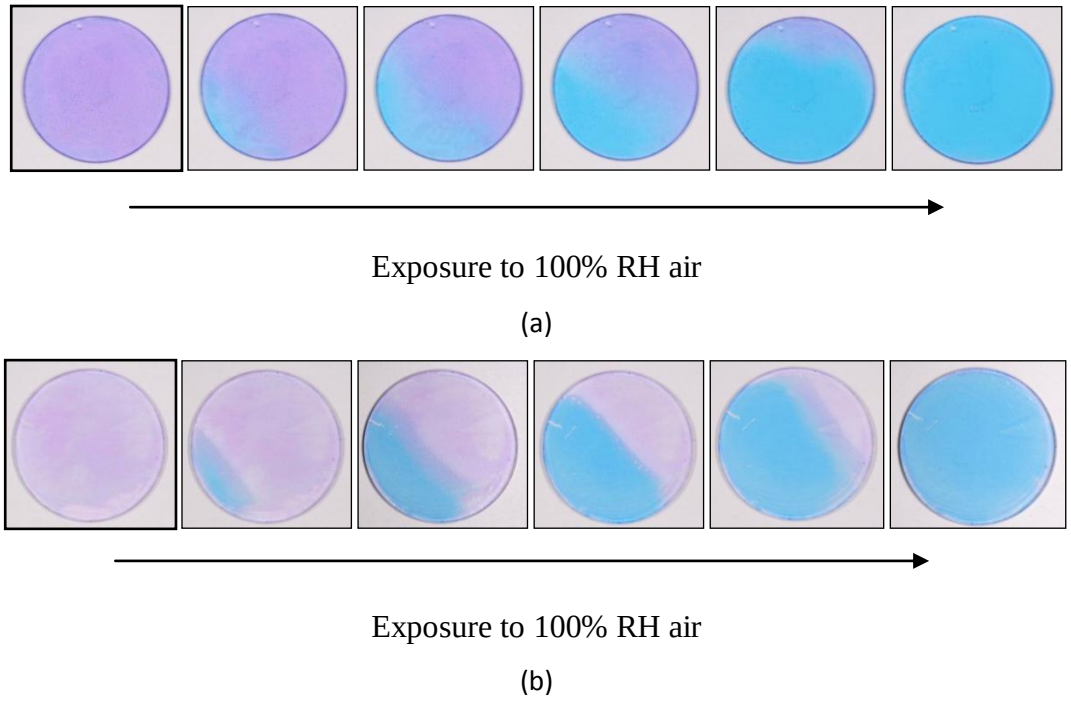

Figure 5.20 Photographs of (a) a MB/Urea/PVA humidity indicator and (b) a MB/Urea/PEO humidity indicator on increasing exposure to 100% humid air.

(d) Urea-like compounds

To determine if other urea-like compounds behaved in a similar manner when incorporated in polymer films with MB, a series of films were prepared containing 5 phr MB and 100 phr of the urea in question in 2 g of 5% wt/wt aqueous HEC. The urea-like compounds tested were thiourea, methyl urea, n,n`dimethyl urea, hydroxy urea and hydroxyethyl urea and their chemical structures are shown in Figure 5.21.

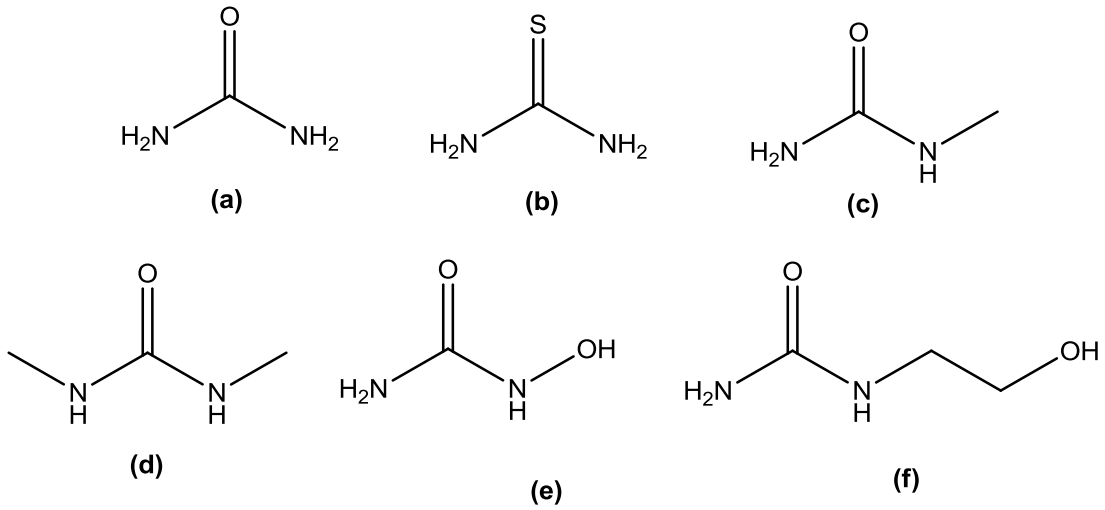

Figure 5.21 The chemical structures for (a) urea, (b) thiourea, (c) methylurea, (d) N,N`dimethyl urea, (e) hydroxyurea and (f) hydroxyethylurea.

The humidity indicator films were exposed to 100 % RH air and any observed colour changes noted. Results are tabulated below in Table 5.2.

Urea	**Deliquescence RH / %**	**Colour - dry**	**Colour - humid**
Urea	80.1	Pink	Blue
Thiourea	N/A*	Pink/purple	Blue
Hydroxy urea	N/A*	Pink/purple	Blue
Methyl urea	70.0	Blue	Blue – no colour change
N,N`Dimethyl urea	62.5	Blue	Blue – no colour change
Hydroxyethyl urea	N/A*	Blue	Blue – no colour change

Table 5.2 Response of MB/HEC films containing different ureas to humid and dry air. Deliquescence data taken from Clow's paper.[14]

* indicates data not available.

Under lab conditions (RH ~ 50-60%), the only films to behave in a similar manner to the urea-based films, i.e. pink under dry lab conditions and rapidly rendered blue under 100% RH conditions, were the thiourea and the hydroxy urea films. Although there is no data available for the deliquescence RH % is it assumed to be higher than 62.5 to 70% RH given that the methyl urea and n,n`-dimethyl urea films remain blue under lab conditions. Likewise the hydroxyethyl urea films are also blue under ambient lab conditions with no visible colour change on exposure to 100 % RH air.

In a bid to expose the three latter films to less than ambient RH% conditions (i.e. < 70% RH) these urea-type films were stored under vacuum for approximately 18 hours before being further dried in an oven at 70^{o}C for 1 hour. After removal from the oven the films were exposed to a stream of 100% RH air and any observed colour changes are noted in table 5.3 below.

Urea	**Colour - vacuum / oven dried**	**Colour - humid**
N,N`-Dimethyl urea	Pale pink	Pale blue
Hydroxyethyl urea	Pink patches	Pale blue
Methyl urea	Blue (crystalline/opaque)	Blue (clear)

Table 5.3 Response of oven dried MB/HEC films containing different ureas to humid air and oven drying.

The films containing n,n`-dimethyl urea and hydroxyethyl urea are beginning to show similar behaviour to that of the typical MB/Urea indicator albeit in small localised areas of the film rather than uniformly across the whole film. It may be possible that an increase in the concentration of the relevant urea and a prolonged exposure of the film to low RH conditions would be sufficient to ensure a uniform colour change from pink to blue is achieved. Unfortunately time did not permit the undertaking of this experiment. Arguably the more interesting result is the lack of observed colour change for the film containing methyl urea. From Table 5.2 it is noted that the deliquescent RH level for methyl urea is 70% RH. As the additional drying measures (i.e. vacuum and oven storage) were sufficient to reduce the RH of the environment such that a partial colour change is observed for the n,n`-dimethylurea film which has a deliquescence RH of 62.5% RH it is anticipated a colour change would be observed for the methyl urea film. This is not the case, despite the film appearing opaque and highly crystalline under dry conditions the film remains blue at all times. The exact reason for this is as yet unknown. Presumably the crystalline structure of the methyl urea is such that is discourages the formation of the MB trimer and as such the pink colour is not observed.

(e) Longevity

To determine the long term stability and storage capabilities of MB/Urea/HEC films a series was prepared and stored in zip-lock bags in the dark. Over a period of a few

months the films were found to retain their colour and after being "reset" by exposure to humid air and dried with dry air, the films exhibited a similar response to fresh films. Figure 5.22 shows a plot of ΔAbs_{600} against time for a newly prepared MB/Urea/HEC film and for that of an 11-week-old film. The latter is slightly slower to respond initially but does achieve the same degree of colour change seen in fresh films and appears from the figure below to have good recovery and reproducibility, not unlike the fresh films. This result is encouraging and suggests that the interaction of the urea and MB has a stabilising effect on the MB that is not seen in films of MB and HEC alone.

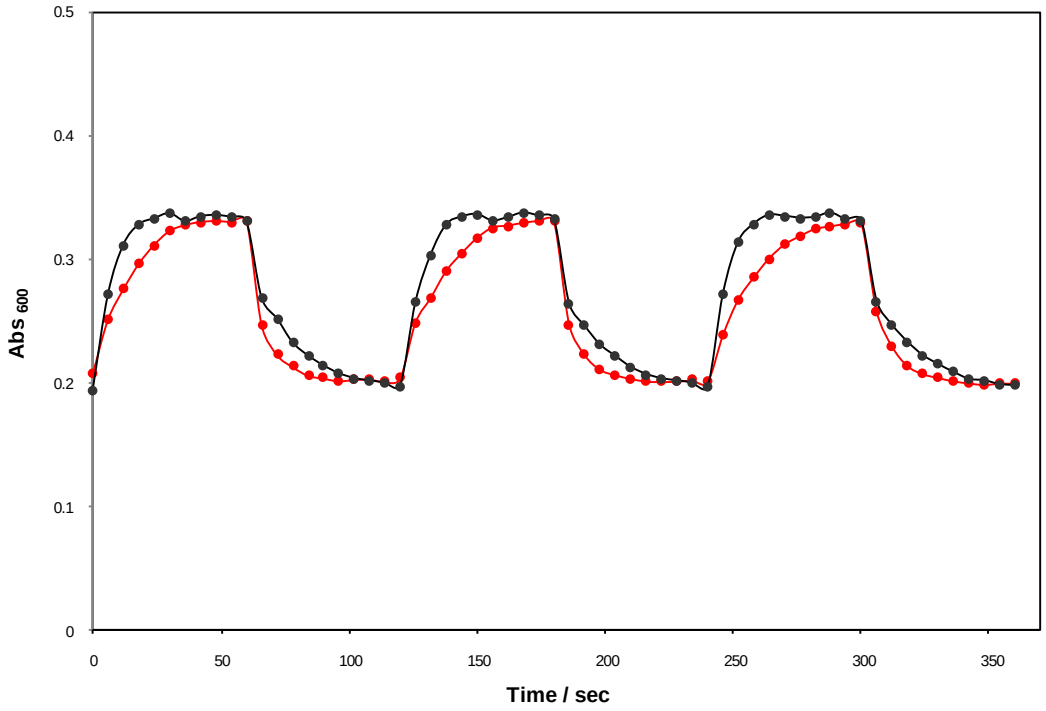

Figure 5.22 A plot of Abs_{600} against time for a fresh MB/Urea/HEC film and one which is 11 weeks old exposed to humid air for 1 minute followed by dry air for 1 minute. This was repeated for 3 cycles. Absorbance recorded every 6 seconds.

5.3.4 Urea/HEC films

In addition to the MB/Urea/HEC system a dye-free relative humidity indicator based on optical clarity can be simply created using just urea in a polymer, such as HEC. Figure 5.23 shows such a film is opaque at medium and low (<80%) RH levels, but clear at RH values >80% as the hygroscopic urea deliquesces. This process is entirely reversible and can be monitored spectrophotometrically at any visible wavelength. Figure 5.24 is a plot of the absorbance at 600 nm versus time for a typical dye-free humidity indicator on exposure to 1 min cycles of 100% RH humid air and dry air, and shows that in the absence of any dye the absorbance level decreases when the film is clear (i.e. humid conditions) and increases when opaque (i.e. dry conditions), thus confirming that the degree of opacity is linked to the RH level.

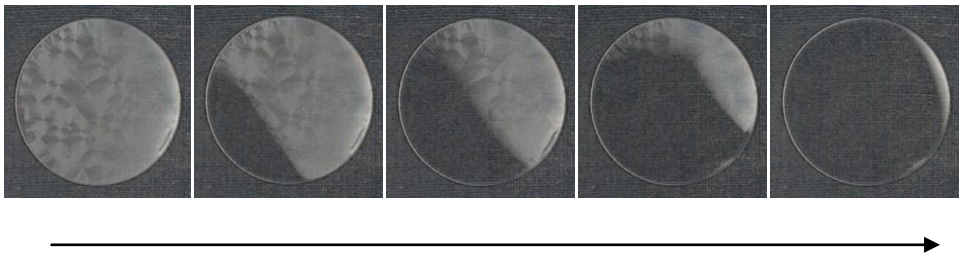

Exposure to 100% RH air

(a)

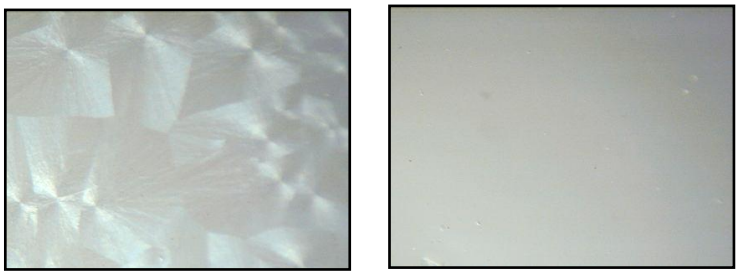

(b) (c)

Figure 5.23 (a) Photographs of a Urea/HEC humidity indicator on increasing exposure to 100% humid air. Images of a Urea/HEC film at x40 magnification (b) at ambient conditions and (c) after exposure to 100% RH air.

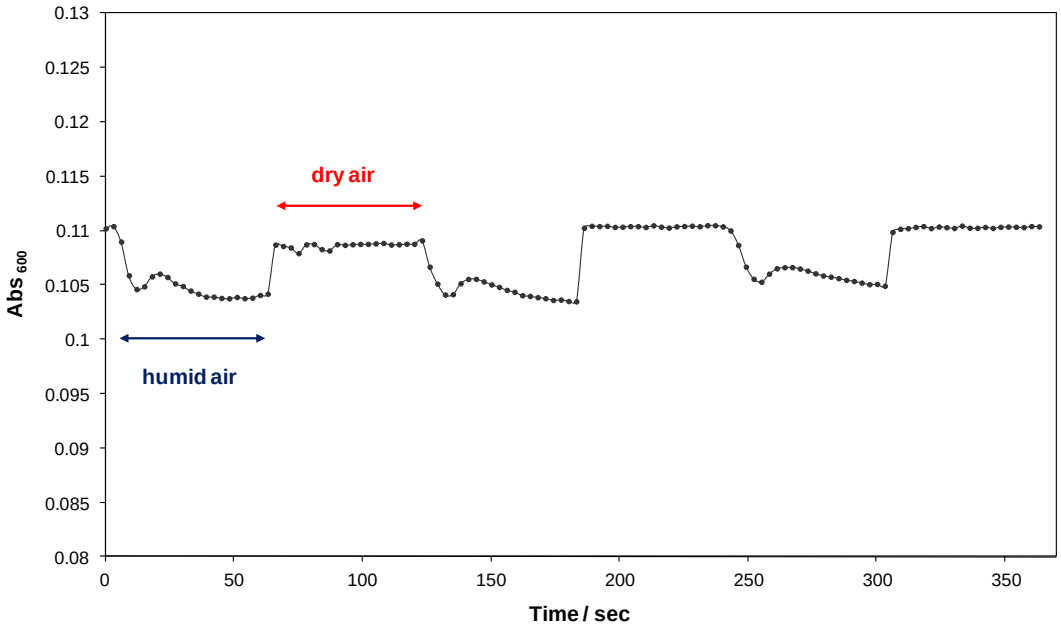

Figure 5.24 A plot of Abs_{600} against time for a Urea/HEC film containing no MB. Film was exposed to humid air for 1 min followed by dry air for 1 min. This was repeated for 3 cycles. Absorbance spectra recorded every 3 seconds.

5.4 Conclusions

The most notable features of this type of relative humidity indicator are not only that it can be used exclusively for monitoring high (>86%)RH levels, but it is quick to respond, highly reversible and has good long term stability. As it stands such a >85% RH humidity indicator has a potential application for ensuring the correct relative humidity conditions for the storage and ripening of fruit[19] for example. There is scope for further developing this system using a series of hygroscopic, possibly urea-related compounds which undergo deliquescence at different relative humidities (e.g. N,N´dimethyl urea deliquesces at RH >63% at 18 ^{o}C) to generate a set of relative humidity indicators for providing a sharp register of different relative humidity levels for a range of applications.

5.5 References

1. M. A. Zanjanchi and S. Sohrabnezhad, *Sens. Acuat. B*, 2005, **105**, 502-507.
2. S. Sohrabnezhad, A. Pourahmad and M. A. Sadjadi, *Mater. Lett.*, 2007, **61**, 2311-2314.
3. P. R. Somani, A. K. Viswanath, R. C. Aiyer and S. Radhakrishnan, *Sens. Acuat. B Chem.*, 2001, **80**, 142-148.
4. P. R. Somani, A. K. Viswanath, R. C. Aiyer and S. Radhakrishnan, *Org. Electron.*, 2001, **2**, 83-88.
5. S. Otsuki and K. Adachi, *Polym. J.*, 1995, **27**, 655-658.
6. R. Matsushima, N. Nishimura, K. Goto and Y. Kohno, *Bull. Chem. Soc. Jpn.*, 2003, **76**, 1279-1283.
7. R. Matsushima, A. Ogiue and S. Fujimoto, *Chem. Lett.*, 2000, 590-591.
8. R. Matsushima, A. Ogiue and Y. Kohno, *Chem. Lett.*, 2002, 436-437.
9. E. Brasswell, *J. Phys. Chem.*, 1968, **72**, 2477-2483.
10. A. Ghanadzadeh, A. Zeini, A. Kashef and M. Moghadam, *J. Mol. Liq.*, 2008, **138**, 100-106.
11. J. D. Hamlin, D. A. S. Phillips and A. Whiting, *Dyes and Pigments*, 1999, **41**, 137-142.
12. P. Mukerjee and A. K. Ghosh, *J. Phys. Chem.*, 1963, **67**, 193-197.
13. K. Patil, R. Pawar and P. Talap, *Phys. Chem. Chem. Phys*, 2000, **2**, 4313-4317.
14. A. Clow, *Nature*, 1940, **146**, 26.
15. J. R. Adams and A. R. Merz, *Ind. Eng. Chem.*, 1929, **21**, 305-307.
16. E. A. Werner, *Nature*, 1937, **139**, 512.
17. P. B. V. Prasad, *Cryst. Res. Technol.*, 1992, **27**, 457-461.
18. Z. Zhao, *Appl. Spec.*, 1999, **53**, 1567-1574.
19. C. Vazquez-Salinas and S. Lakshminarayana, *J. Food Sci*, 1985, **50**, 1646-1648.

Chapter 6

Ammonia and volatile amine indicators

6. Ammonia and volatile amine indicators

6.1 Introduction

Ammonia (NH_3) is a caustic, hazardous gas with a pungent characteristic odour. It is widely used both directly and indirectly in the production of explosives, fertilisers, pharmaceuticals, household cleaning products and as an industrial coolant. Ammonia and other volatile amines also give spoiled fish its 'off' taste and smell, as these are produced as fish meat decays.[1] After fish are caught and killed micro-organisms present on the skin and scales known as specific spoilage organisms (SSO) start to increase. SSOs produce ammonia and volatile amines including trimethylamine (TMA) and dimethlyamine (DMA) from the amino acids present as the fish starts to spoil.[1] These microbial degradation products are collectively known as total volatile basic nitrogen (TVB-N).[1] As part of the EU Directive 95/149/EC[2] these volatile amines are legally defined as indicators of seafood spoilage[3] and maximum limits of TVB-N are defined for different categories of fish.

Cat.	**Family/*Species***	**Example**	**25 mg N / 100 g fish**	**30 mg N / 100 g fish**	**35 mg N / 100 g fish**
A	*Sebastes* spp.	Rockfish	✓		
A	*Helicolenus dactylotepterus*	Blackbelly rosefish	✓		
A	*Sebastichthys capensis*	Cape redfish	✓		
B	Pleuronectidaea (except halibut: *Hippoglossus* spp.)	Plaice Lemon sole		✓	
C	*Salmo salar*	Atlantic salmon			✓
C	Merluccidae	Hake			✓

Cat.	Family/*Species*	Example	25 mg N / 100 g fish	30 mg N / 100 g fish	35 mg N / 100 g fish
C	Gadidae	Cod, Haddock, Whitting, Pollock			✓

Table 6.1 EU Directive 95/149/EC TVB-N limits for certain fish species.[2]

There are a number of different techniques used to monitor ammonia and TVB-N detailed in literature as discussed in Chapter 1.[1,4-29] The majority of these techniques are based on simple indicator systems that undergo a visible colour change in the presence of ammonia and/or volatile amines (A/VA). Such indicators are typically based on intelligent inks and indicating solutions. These are usually pH-sensitive dyes dissolved in polymer solutions[4-6, 15, 21, 23, 25, 26, 30, 31] or solvents.[9, 14, 18, 24, 27, 28, 32] The resulting inks and solutions can be cast as thin films[4-7,18,21,23,25,32] or encapsulated within a support matrix such as filter paper,[9, 31] porous tape[24] or optical fibres.[15, 28, 30] For fish freshness applications such indicators would most likely be mass produced and be fixed to the packaging material prior to use. The need to attach the indicator leads to an increase in manufacturing costs and time, both of which are highly undesirable. As a result there is a growing interest in developing 'smart packaging materials' with food spoilage indicators incorporated into the packaging material itself.

The aim of this chapter is to investigate the possibility of expanding work carried out previously within the group on a solvent-based ammonia indicator by developing A/VA sensitive pigments.[23] It is hoped that such pigments can be incorporated into flexible thermoplastics and used as smart packaging for monitoring fish spoilage.

A pigment is a substance that is mixed with media in which it is relatively insoluble, creating a suspension, and used especially to impart colour to coating materials (as

paints) or to inks, plastics, and rubber. This differs from a dye which is mixed with a substance with which is it souble. Pigments are traditionally used to colour plastics by mixing the powdered colorants with the polymer resins prior to heating and moulding or extruding. Thermoplastic is the term used to describe polymers that liquefy when heated and cool to form a glass-like state that can be readily re-melted and remoulded.[33] Polyethylene (PE) is the most widely used thermoplastic and possesses several desirable qualities including low cost, good flexibility and strength.[33] Of particular interest in this work is low density polyethylene which is used to make films and packaging materials.[34] PE is a popular choice in the food industry because it is compliant with all relevant safety regulations, is lightweight and can be extruded into thin yet durable films which minimise the packaging materials required.[35]

The pigments described in this chapter are similar to those concurrently developed within the group for CO_2 indicating intelligent pigments for modified atmosphere packaging (MAP) leakage indicators that resulted in paper and published patent.[36, 37] They are comprised of a hydrophobic inorganic substrate which is coated with an A/VA sensitive dye which is then dispersed within thin PE films.

6.2 Theory

Ammonia (NH_3) is readily soluble in water; NH_3 molecules dissolve in solution as NH_3 (aq). The ammonia molecules react with water to give ammonium NH_4^+ and hydroxide OH^- ion:

$$NH_3\,(aq) + H_2O \rightleftharpoons NH_4^+(aq) + OH^- \qquad (6.1)$$

The resulting solution is weakly basic which increases the pH. As the partial pressure of the NH_3 gas, $P_{NH3,}$ is increased the pH of the aqueous solution will increase. If a pH indicating dye was present in the solution this change in pH may (depending on the pK_a of the dye) register as a change in colour as a result of the

deprotonation of the dye. Ideally the extent of the observed colour change would be proportional to the level of NH_3 i.e. a more striking colour change with increasing $P_{NH3.}$

$$NH_3(aq) + H^+ \underset{}{\overset{K_{amm}}{\rightleftharpoons}} NH_4^+ \tag{6.2}$$

$$HD\ (\text{colour A}) \underset{}{\overset{K_a}{\rightleftharpoons}} D^- + H^+\ (\text{colour B}) \tag{6.3}$$

The pK_a of any dye is unique to that dye and will determine the pH range over which the colour change (colour A to colour B) occurs given:

$$pK_a = -\log_{10} K_a \tag{6.4}$$

$$pH = pK_a + \log \frac{[D^-]}{[HD]} \tag{6.5}$$

such that when the pH = pK_a, the ratio of the protonated [HD] and deprotonated [D^-] of the dye is 1:1. This means that both species are present in equal amounts, thus the resulting colour will be a mixture of that of both A and B. When the pH < pK_a the [HD] is greater than [D^-] and consequently the dominant colour will be colour A, similarly when the pH > pK_a [D^-] is greater than [DH] and colour B will dominate. Consequently different dyes will respond in different ways to the same P_{NH3}.

For example Bromophenol blue (BPB) and Bromocresol Green (BCG) are two pH indicating dyes whose dye properties and structures are found in Table 6.2 and Figure 6.1 below:

Dye	pK_a	pH range	Colour change
BPB	4.10	3 - 4.6	Yellow to blue
BCG	4.9	3.8 - 5.4	Yellow to blue

Table 6.2 Properties of pH indicators

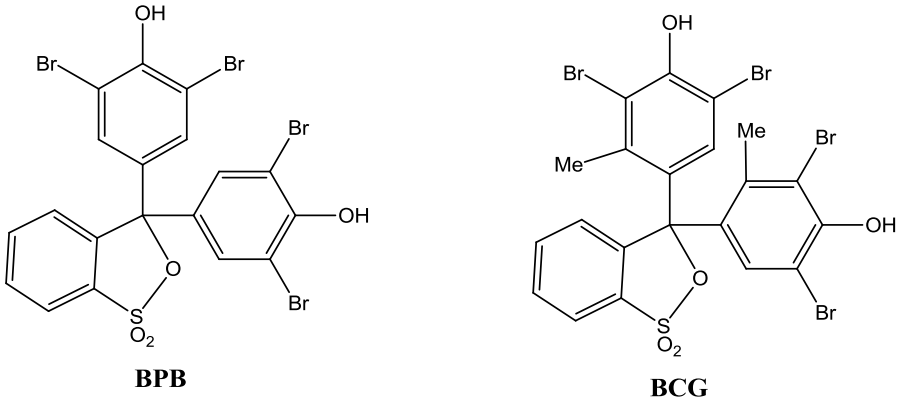

Figure 6.1 Chemical structures of BPB and BGC.

They belong to the same family of dyes, hydroxyl triarylmethanes, and undergo the same colour change and have overlapping working pH ranges for the detection of ammonia. For example if both of these dyes were exposed to the same P_{NH3} level at the same time, the BPB would exhibit the greater response because of its lower pK_a which makes it more sensitive to the increasing pH of its surrounding environment. Conversely if an NH_3 rich environment was purged with nitrogen to reduce the $[NH_3]$ in the presence of both indicator dyes BCG with its higher pK_a would change colour first, i.e. BCG would be less sensitive than BPB to the presence of ammonia.

Previous work carried out within the Mills group has shown that similar features can be expected for a largely hydrophobic solid-state ammonia indicator.[23] In this work a reaction occurs between a pH indicating dye and 'ammonia dissolved in the plastic film' i.e.[23]

$$NH_3(g) \overset{K_H}{\rightleftharpoons} NH_3(dis) \tag{6.6}$$

$$HD + NH_3(dis) \overset{K_4}{\rightleftharpoons} NH_4^+D^- \tag{6.7}$$

Here, K_H is Henry's constant for the dissolved ammonia gas in the plastic film and K_4 is an 'ion-pair formation constant' for the formation of the $NH_4^+D^-$ ion, whose value will depend strongly on the dyes acidity constant, K_a.[23] In this scenario the plastic film sensors 'behave as direct sensors, i.e. sensors in which there is a 1:1 equilibrium reaction between the analyte and the immobilised reagent'.[23] From Henry's law the partial pressure of the ammonia P_{NH3} can be defined as:

$$P_{NH_3} = \frac{[NH_4^+D^-]}{\{K_4K_H[HD]\}} = \frac{P_B(\%NH_3)}{100} \tag{6.8}$$

where P_B is the barometric pressure, which is taken as 1 atm for this work.[23]

The colour change was monitored spectrophotometrically at the maximum absorbing wavelength of the deprotonated $NH_4^+D^-$ i.e. 600 nm, thus allowing the ratio, *R*, of the protonated and deprotonated dye to be determined;

$$R = \frac{[NH_4^+D^-]}{[DH]} = \frac{\{Abs(NH_4^+D^-) - Abs(NH_4^+D^-)_0\}}{\{Abs(NH_4^+D^-)_\infty - Abs(NH_4^+D^-)\}} \tag{6.9}$$

where $Abs(NH_4^+D^-)_0$ is the absorbance of the film in absence of ammonia i.e. 0% NH_3, and $Abs(NH_4^+D^-)_\infty$ is the absorbance of the film when the dye is fully converted to the deprotonated form.

This chapter outlines a new method for producing novel ammonia and volatile amine indicators by incorporating an intelligent ammonia and volatile amine-indicating pigment for use in a fish freshness system, made by coating ammonia sensitive dyes onto white, inert hydrophobic support material, into a flexible, hydrophobic,

thermoplastic polymer, which is expected to have similar features to one detailed above. This work was carried out in collaboration with Graham Skinner who developed an analogous carbon dioxide indicator.[37]

The bulk of the work was carried out using BPB, as this pigment was found to respond to key levels of ammonia, undergoing a clear, distinct colour change on exposure to 1000 ppm ammonia and was also the dye used in the solvent-based ammonia sensitive sensors produced previously by the group.[23]

6.3 Experimental

6.3.1 Materials

The silica used in the A/VA pigments was fumed hydrophobic silica, Aerosil R812 (specific surface area = 260 ± 30 m^2/g, average particle size = 7 nm) supplied by Degussa/Evonik. Hydrophobic silica is prepared by the manufacturer by treating silica with dimethyldichlorosliane, a procedure that converts silanol groups (Si-OH) to hydrophobic Si-Me groups, see Figure 6.2

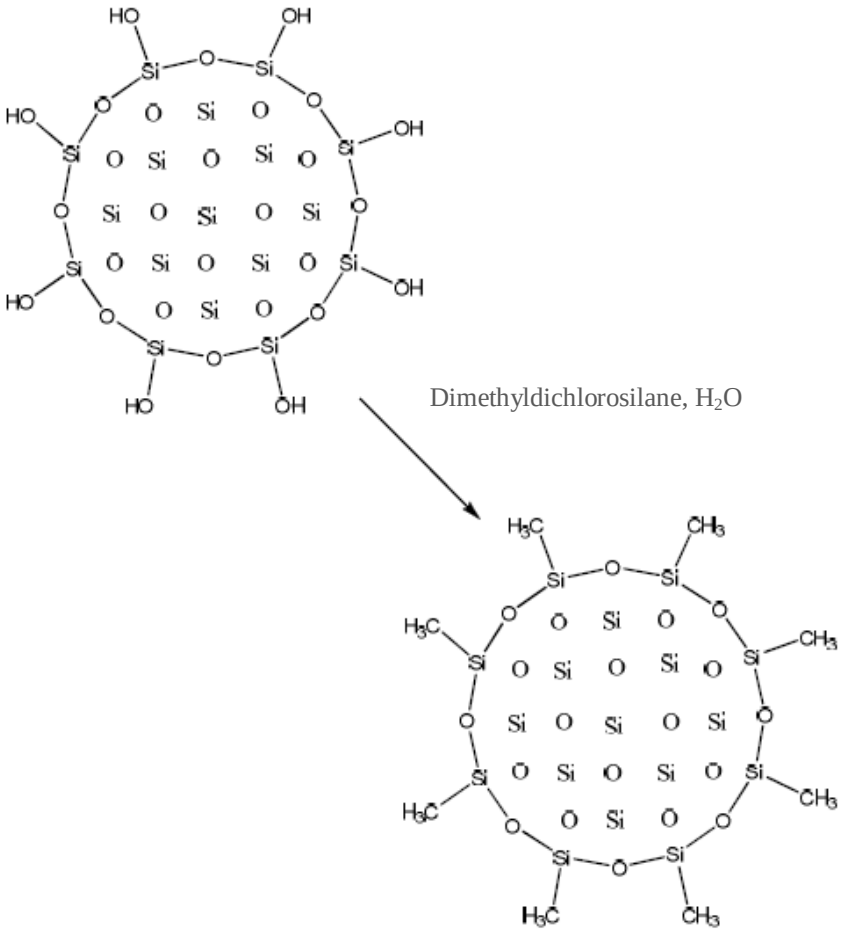

Figure 6. 2 Preparation of hydrophobic silica.

6.3.2 Preparation of A/VA indicator pigments

A typical BPB amine/volatile amine (A/VA) pigment was prepared by adding 0.4 g of bromophenol blue (BPB) to a beaker containing 2 g of hydrophobic silica and approx. 80 ml methanol. The mixture was well stirred and sonicated in an ultrasonic bath for 15 min to ensure dissolution of the dye and good coating of the silica. The resulting solution was transferred to a round-bottomed flask. The methanol was then removed with the aid of a rotary evaporator at 30°C under reduced pressure. The dye coated silica product was removed and ground into a fine orange powder that will be referred to forthwith as the pigment BPB A/VA pigment as illustrated in Figure 6.3.

Figure 6. 3 A photograph of a BPB A/VA pigment.

A similar method was used to produce a series of A/VA pigments using a range of different organic dyes listed in Table 6.3. The chemical structures for these dyes are shown in Figure 6.4

Dye	**Abbreviation**	**Dye family**	**pK_a**
Bromophenol Blue	BPB	Hydroxy triarlymethane	4.10
Bromocresol Green	BCG	Hydroxy triarlymethane	4.90
Bromocresol Purple	BCP	Hydroxy triarlymethane	6.8
Bromothymol Blue	BTB	Hydroxy triarlymethane	7.0
Thymol Blue	TB	Hydroxy triarlymethane	1.65
m-Cresolpurple	MCP	Hydroxy triarlymethane	1.6
Phloxine B	PB	Fluorone (fluorescein derivative, xanthene)	?

Table 6.3 Names, dye classes and pK_a of dyes used in pigment preparations

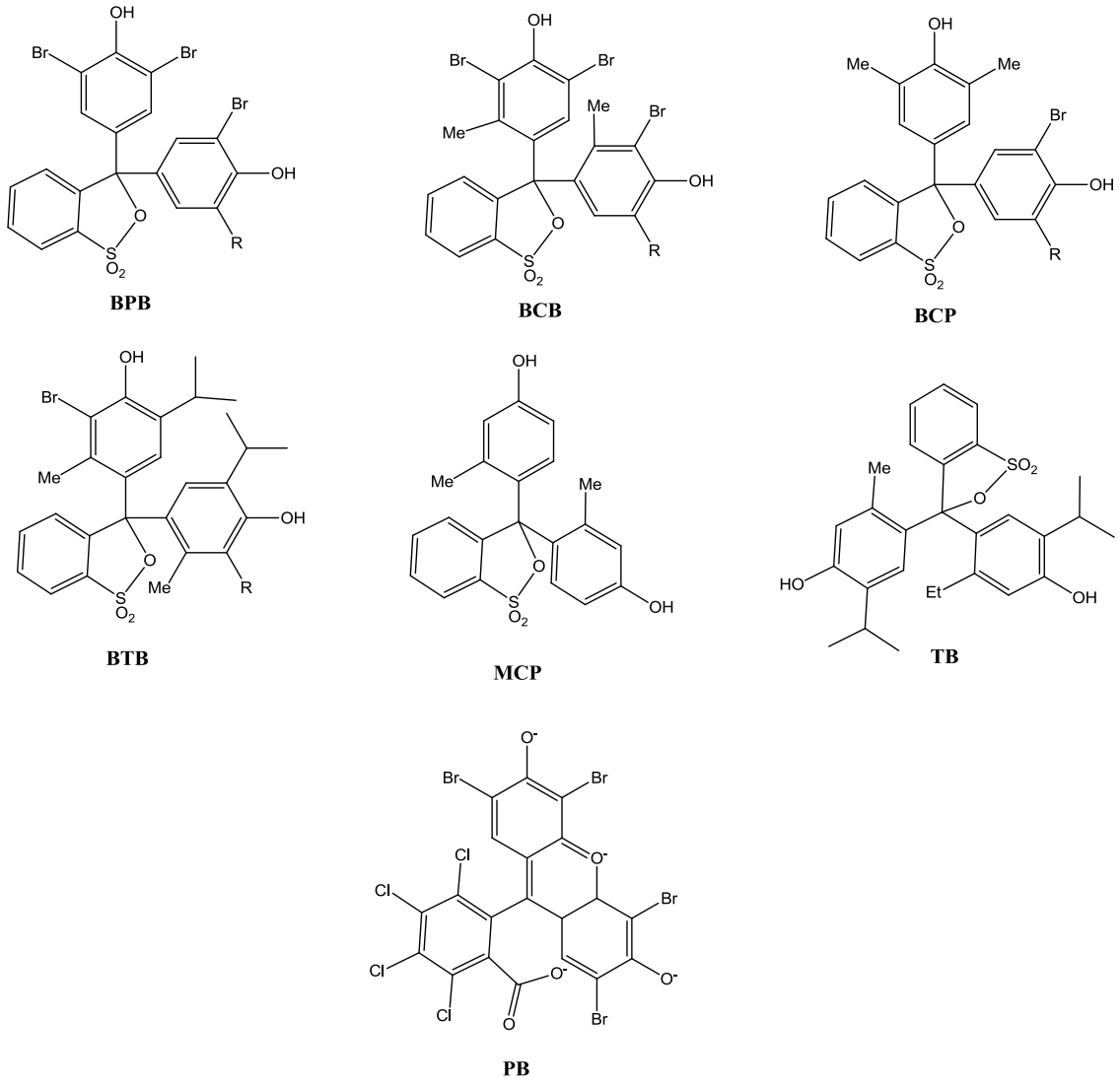

Figure 6.4 The chemical structures for pH dyes.

6.3.3 Preparation of A/VA plastic indicator films

A typical BPB amine/volatile amine indicator film was prepared by adding 0.4 g of the hydrophobic BPB A/VA pigment to 2 g of powdered polyethylene (Alfa Aesar, LDPE, 100 μm) and ground together using a mortar and pestle, until the colour was homogeneous. A small amount of the hydrophobic pigment/polymer mixture (*ca.* 0.3-0.4 g) was heat pressed, between two discs of aluminium foil, using a Specac Atlas^{TM} Series Heated Platens at 115^{o}C. The result is a thin (0.1 mm thick), yellow coloured plastic film, which has a typical composition, in terms of parts per hundred resin (phr), PE/pH dye/SiO_2 = 100/5/20 as illustrated in Figure 6.5 and shall be referred to forthwith as a typical BPB/PE A/VA film

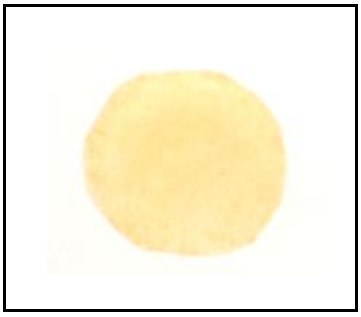

Figure 6.5 A photograph of a BPB A/VA pigment based PE film.

6.4 Results and discussion

6.4.1 A/VA indicating pigments

6.4.1.1 Properties

All of the dyes used to prepare the pigments, with the exception of Phloxine B, (PB) are hydroxy triarylmethane dyes. More specifically they belong to a class of dyes knows as sulfonephthaleins. These are pH indicator dyes which when placed in a sufficiently basic environment deprotonate. The result of this is a bathochromic shift

in the maximum wavelength of the absorption spectrum (λ_{max}). The main dye used was bromophenol blue, (BPB), whose structure is shown in Figure 6.6. It has a pK_a of 4.10 and undergoes a shift in λ_{max} from 430 nm (the yellow acidic form of the dye at pH 3.0) to 600 nm (the blue basic form of the dye at pH 4.6). Phloxine B is a fluorone derived from the xanthene dye fluorescein, and is widely used as an additive for food colouring and as a biological stain for fluorescence microscopy. Phloxine B can also be used as a pH indicator as it undergoes a pH-related deprotonation between pH 2.1 (colourless) and 3.3 (pink).

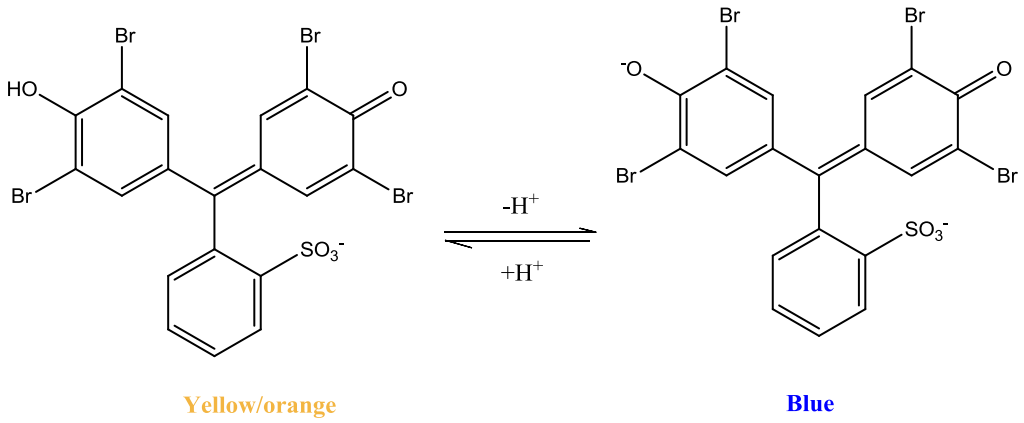

(a)

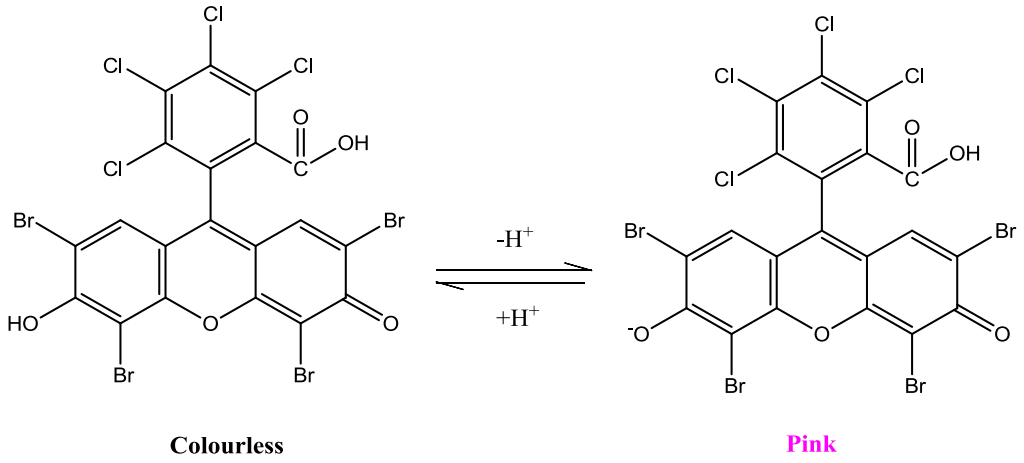

(b)

Figure 6. 6 The structure of the protonated and deprotonated forms of (a) bromophenol blue (BPB) and (b) phloxine B (PB).

6.4.1.2 Response to ammonia

On exposure to the gaseous ammonia (the headspace above a 25% ammonium hydroxide solution) the standard BPB A/VA pigment changes colour from orange, through green to blue as the ammonia diffuses through the sample. This process is documented in the photographs below in Figure 6.7. Despite the colour change

occurring gradually, the overall effect is visually striking and as such is ideally suited for an optical indicator.

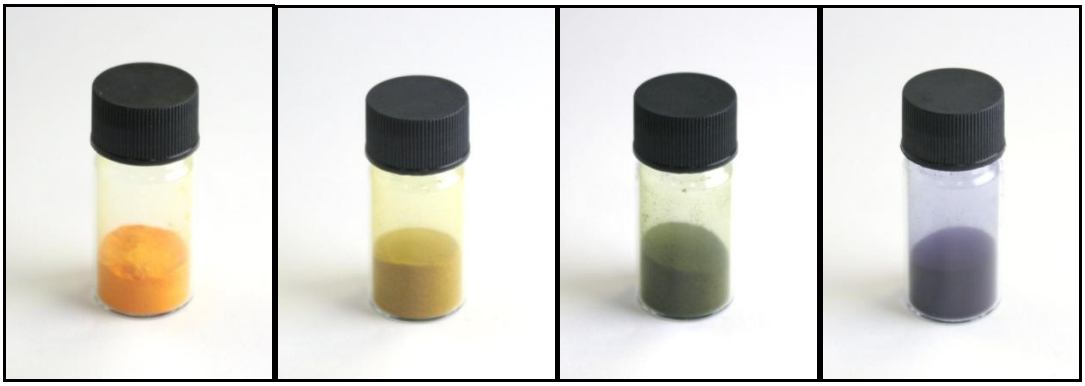

Figure 6.7 Photographs of the standard BPB A/VA pigment before (orange) and on increasing exposure to the headspace above a 25% ammonium hydroxide solution (green to blue) delivered *via* a Pasteur pipette.

Figure 6.7 illustrates clearly the distinct colour change which occurs within the pigment on a 'bulk' scale. The same effect can be illustrated on a magnified scale as seen in Figure 6.8 which shows images of the BPB hydrophobic silica pigment before and after exposure to ammonia (headspace above a 25% ammonium hydroxide solution delivered *via* a Pasteur pipette), captured using an Olympus SZ11 microscope fitted with a DP12 digital camera. Here is observed that the silica particles are coated with the BPB dye, which changes colour from yellow to blue on exposure to ammonia. Particle cluster sizes range from 10 to 150 μm

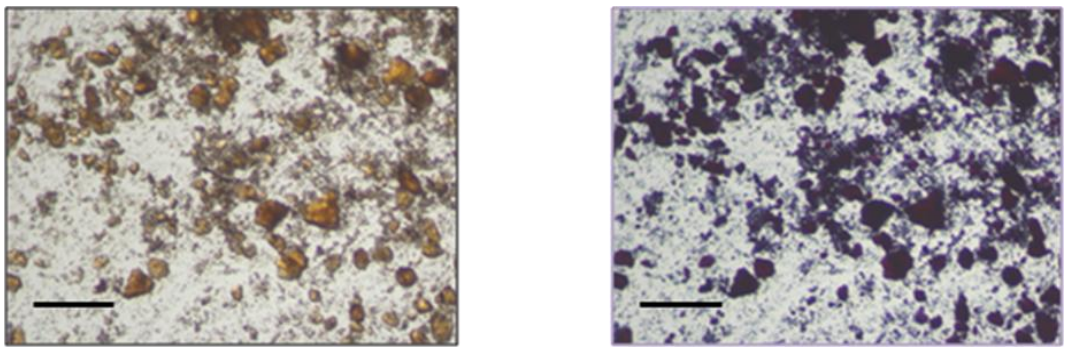

(a) (b)

Figure 6.8 Photograph of BPB A/VA sensitive pigment on hydrophobic silica at x110 magnification (a) before and (b) after exposure to ammonia (headspace above a 25% ammonium hydroxide solution delivered *via* a Pasteur pipette). Particle size typically 10-150 μm. Scale bar = 400 μm.

A similar pigment was prepared using hydrophilic silica. These crystals have a more uniform particle size and as such the colour change is more readily observed, as illustrated in Figures 6.9 and 6.10 below.

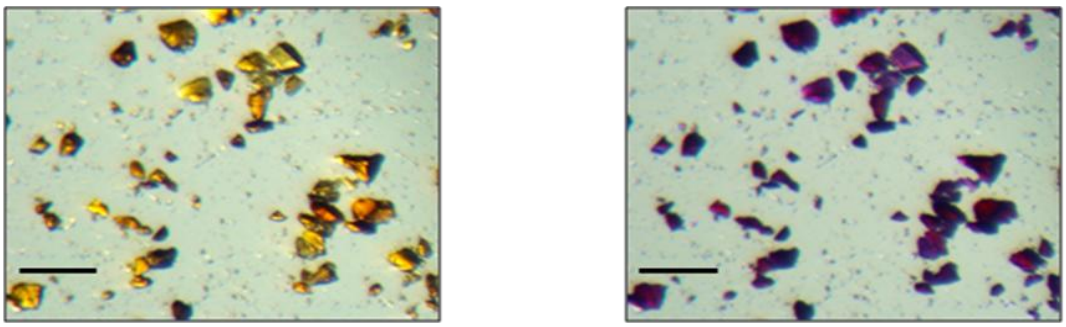

(a) (b)

Figure 6.9 Photograph of the hydrophilic BPB A/VA sensitive pigment at x 220 magnification (a) before and (b) after exposure to ammonia (headspace above a 25% ammonium hydroxide solution delivered *via* a Pasteur pipette). Particle size typically 50-100 μm. Scale bar = 20 μm.

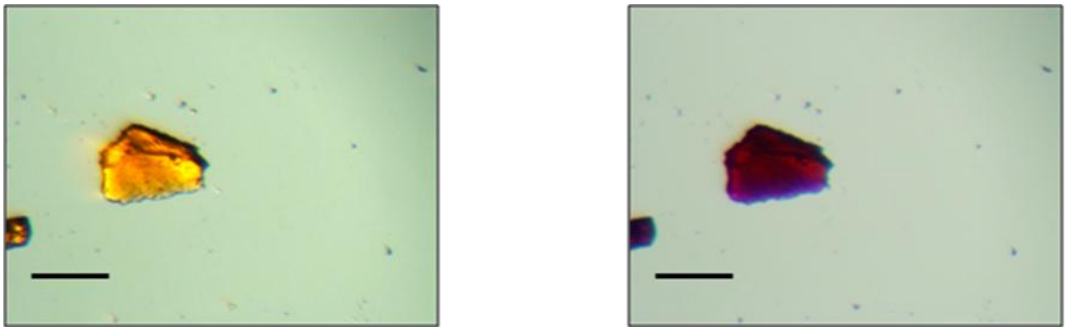

(a) (b)

Figure 6.10 Photographs of a large (*ca.* 250 μm) hydrophilic BPB A/VA sensitive pigment particle at x 220 magnification (a) before and (b) after exposure to ammonia (headspace above a 25% ammonium hydroxide solution delivered *via* a Pasteur pipette). Scale bar = 200 μm

6.4.2 A/VA indicator films

6.4.2.1 Optical characteristics of an A/VA BPB/PE film

A typical BPB/PE film was prepared and its UV/visible absorption spectrum recorded as shown in Figure 6.11. Note that it is the hydrophobic BPB A/VA sensitive pigment that is used in the A/VA BPB/PE film because of the hydrophobic nature of the PE. Also included in Figure 6.11 are the absorption spectra for a PE film and a PE film containing non dye-coated hydrophobic silica. While the PE does absorb to an extent in the UV and lower visible wavelength region, the pigment is the only species which absorbs significantly in the visible region with a broad peak at 430 nm which is consistent with its yellow/orange colour.

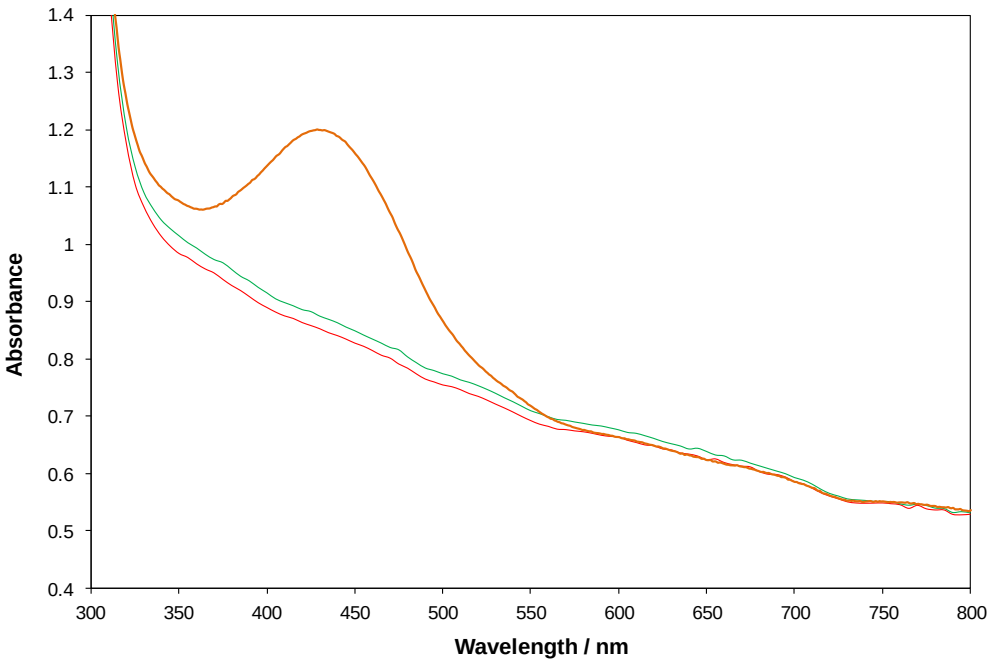

Figure 6.11 The UV/visible absorption spectra of a typical BPB/PE A/VA indicator film, a PE and hydrophobic silica film and a PE alone film.

6.4.2.2 Conditioning of BPB/PE A/AV films

In order to achieve the maximum performance from the hydrophobic BPB/PE A/VA indicator films, each film was "conditioned" with ammonia prior to use. This can be achieved by exposing the films to 1000 ppm ammonia at 300 ml min^{-1} for 1 hour. This will result in the film changing colour from yellow to blue. The film is 'reset' by being placed in an oven at 70°C for 2 hours, after which time the film will be yellow in colour. The UV/visible spectra in Figure 6.12 below illustrated the effect of this "conditioning" step on the film.

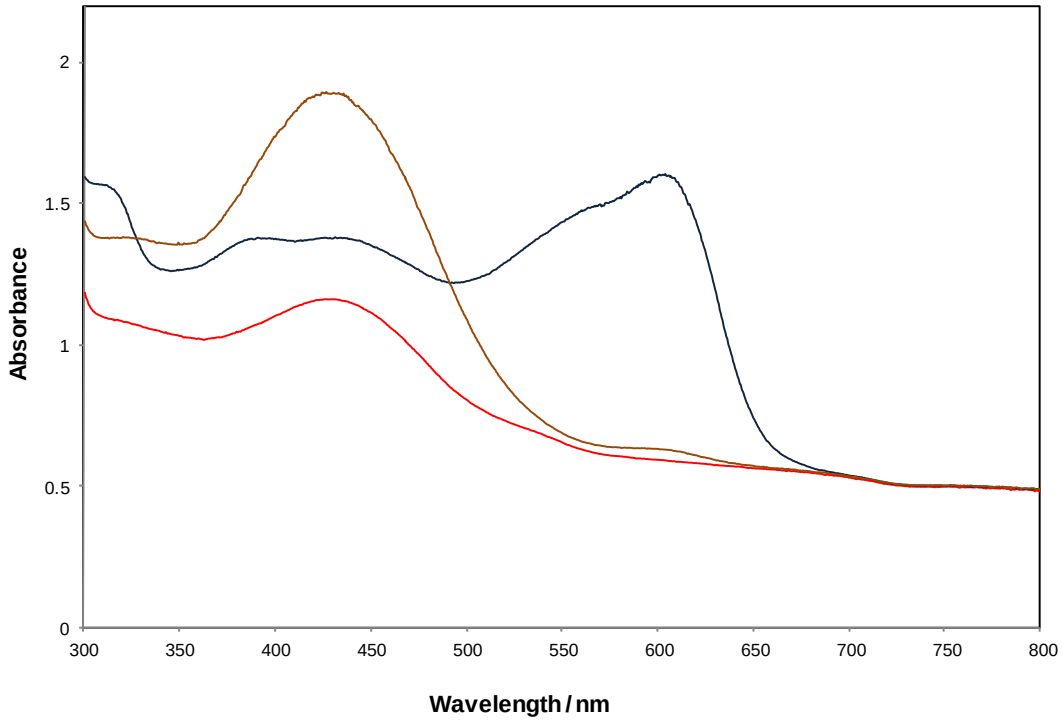

Figure 6.12 The UV/visible absorption spectra of a typical unconditioned PBP/PE film, the same film on exposure to 1000 ppm ammonia, and the thermally recovered "conditioned film".

These results show that the spectrum of the recovered "conditioned" film absorbs much more strongly a λ_{max} 430 nm than the initial spectrum of the film. The reason for this is not immediately clear, but it would appear that the "conditioning cycle"

allows more of the dye to be solubilised in the film. Given ammonia's affinity for water it is likely that there is water vapour in the ammonia gas phase that dissolves in the PE film along with the ammonia, which helps solubilise the dye, increasing the absorbance of the peak at 430 nm. Further experiments exposing a typical unconditioned BPB/PE A/VA indicator film to humid air show a similar effect. Figure 6.13 shows the UV/visible absorption spectra of a film before and after sitting above a vial of water for 8 and 24 hours. The observed increase in the absorbance peak at 430 nm in the presence of water supports the above hypothesis that the water vapour in the ammonia gas stream is responsible for solubilising the BPB.

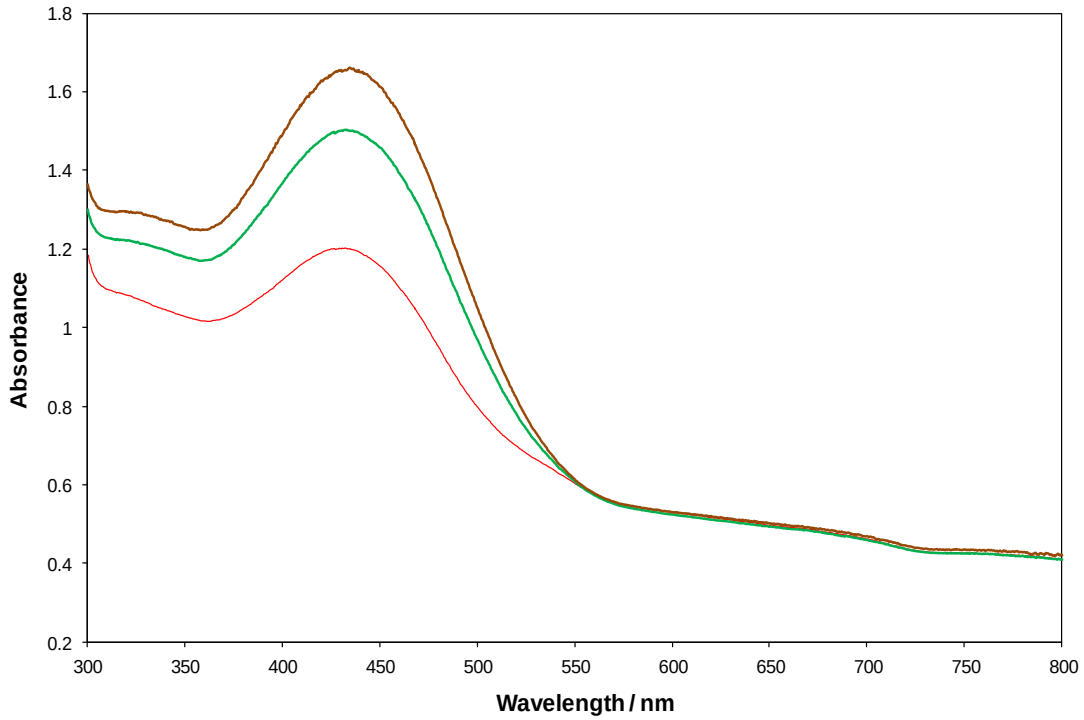

Figure 6.13 The UV/visible absorption spectra of a typical unconditioned PBP/PE film, the same film after exposure to water vapour for 8 hours and 24 hours.

6.4.2.3 Response of a BPB/PE film to ammonia

When exposed to a gas stream containing 1000 ppm ammonia at 300 ml min^{-1} for 300 minutes a typical "conditioned" hydrophobic BPB/PE film undergoes a gradual but striking colour change from its acidic form, yellow, towards its basic form, blue, as illustrated in Figure 6.14 below.

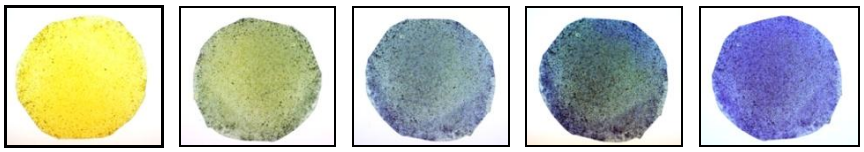

0 min 30 min 60 min 180 min 300 min

Figure 6.14 Photographs of a standard BPB/PE A/VA sensor on exposure to 1000 ppm ammonia for 300 minutes.

This feature is further illustrated in Figure 6.15 which shows the UV/visible absorption spectral changes exhibited by a typical BPB/PE A/VA film as a function of exposure time when exposed to 1000 ppm ammonia at 300 ml min^{-1} for 300 minutes. The inset diagram illustrates the progress of the colour change, as measured by the increase in absorbance of the basic blue form of the dye, λ_{max} = 600 nm, i.e. ΔAbs_{600} as a function of exposure time. These results reveal that the rate at which the ammonia dissolves in the film, and hence the rate at which the pH of the encapsulation polymer becomes sufficiently basic to effect the colour change is much slower than that of its CO_2 equivalent which reaches its final colour change after 30 seconds.[38]

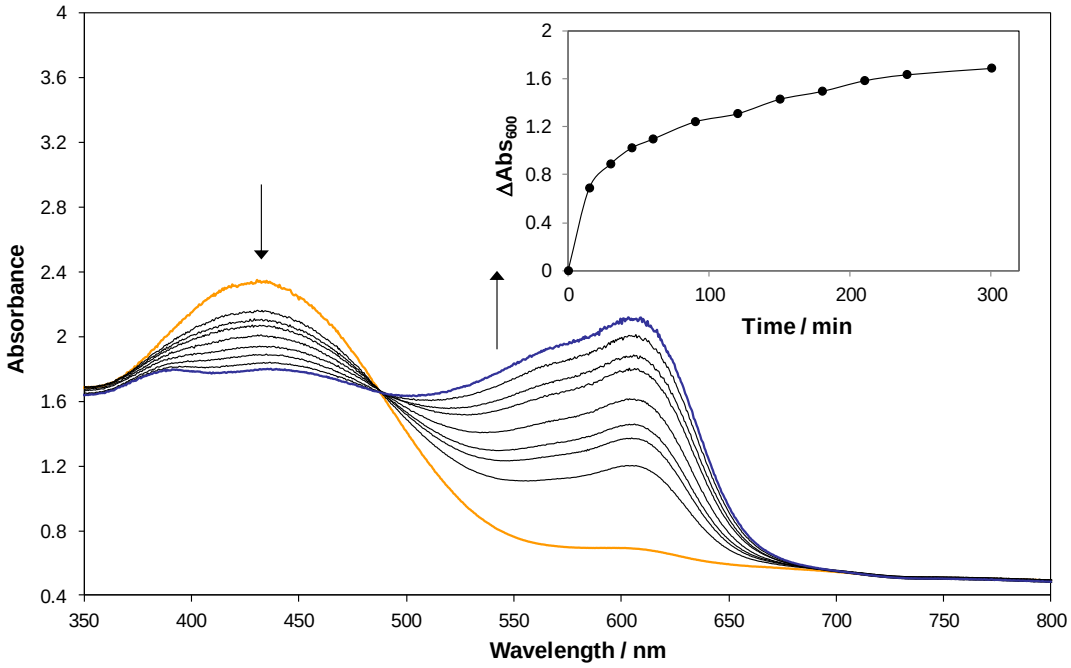

Figure 6.15 Absorbance spectra of a standard BPB/PE A/VA indicator film on exposure to 1000 ppm ammonia at 300 ml min^{-1} for 300 minutes. Inset diagram is a plot of ΔAbs_{600} vs. time.

6.4.2.4 Ambient recovery a BPB/PE film

Typical BPB/PE A/VA indicator films are slow to recover under ambient ammonia-free conditions as observed in the figures below. The UV/visible absorption spectra for the recovering film and accompanying photographs illustrating the colour changes of the film are found in Figures 6.16 and 6.17. The inset diagram in Figure 6.16 is a plot of ΔAbs_{600} against time for a BPB/PE A/VA indicator that was left to recover under ambient lab conditions following exposure to 1000 ppm ammonia for 300 minutes and it is clear that even after a couple of weeks the film has not fully recovered.

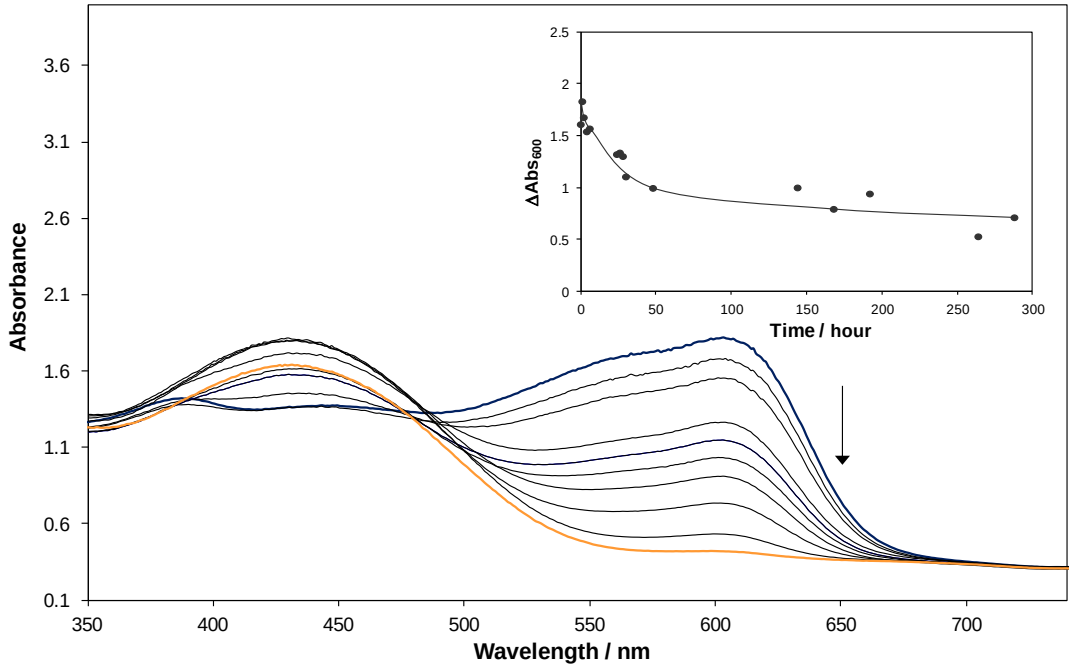

Figure 6.16 Absorption spectra of a standard BPB/PE A/VA film recovering under ambient conditions after exposure to 1000 ppm ammonia for 300 minutes. Inset diagram is a plot of ΔAbs_{600} against recovery time based on data from main diagram.

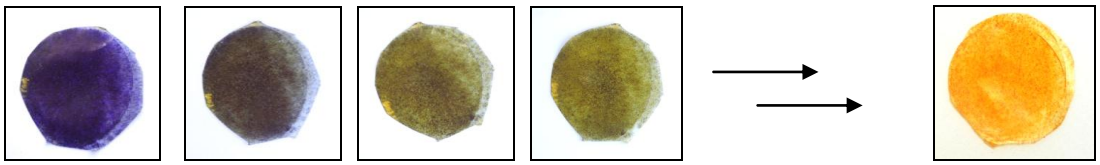

Initially 6 hours 1 day 1 week 8 weeks

Figure 6.17 Photographs of a typical BPB/PE A/VA indicator film recovering under ambient conditions following exposure to 1000 ppm ammonia for 300 minutes.

6.4.2.5 Thermal recovery a BPB/PE film

The recovery period can be greatly reduced by heating the films. For example a typical BPB/PE A/VA indicator film was prepared and exposed to 1000 ppm ammonia for 60 min. The same film was then placed in an oven at 70°C and removed periodically to take note of its colour. After a period of 2 hours the film had regained its yellow appearance i.e. had fully recovered. The corresponding UV/visible absorbance spectra are shown in Figure 6.18 below.

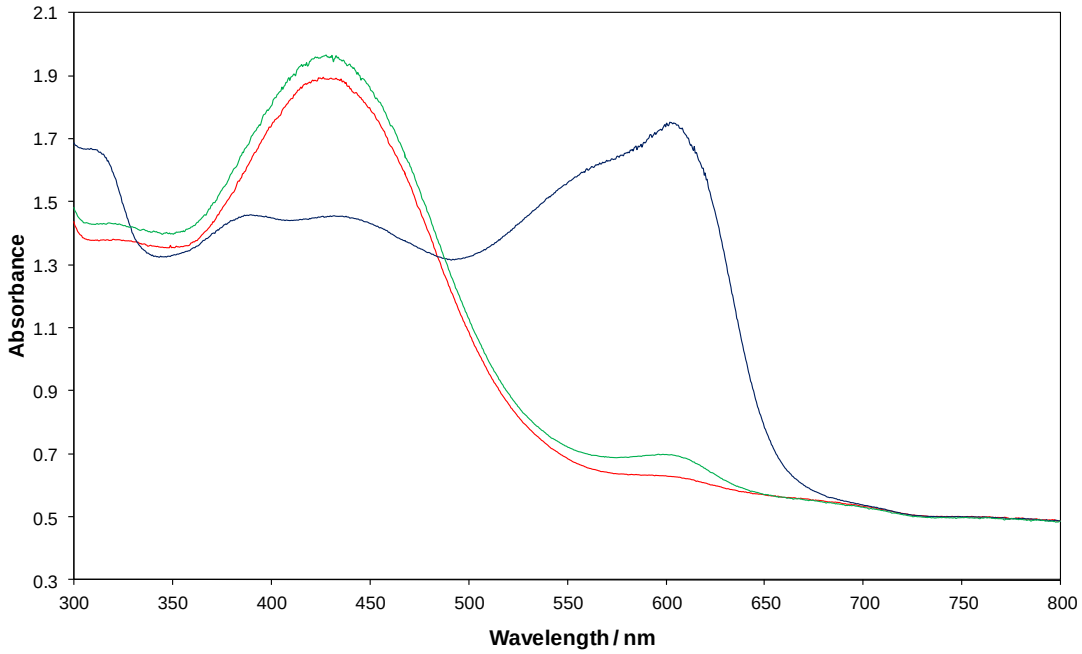

Figure 6.18 The UV/visible absorption spectra of a typical conditioned PBP/PE film, the same film on exposure to 1000 ppm ammonia, and then thermally recovered.

These results show that after 2 hours at 70°C the spectrum of the film resembles that of a film allowed to recover under ambient lab conditions after ~ 8 weeks. This is a far more desirable recovery period and is on a par with the typical ambient recovery period for the comparable CO_2 sensors.[38] This result is not surprising as work carried out previously on a BPB ink-based A/VA indicator film[23] show that the concentration of ammonia in the film (see equation 6.6) and K_4 (see equation 6.7) decrease with increasing temperature. Consequently heating the film to 70°C will

not only aid in the dissociation of $NH_4^+D^-$ moiety but will also drive off the dissolved ammonia within the film, rapidly increasing the recovery of the film.

BPB/PE A/VA films are not only fully reversible by thermal means but they give good reproducibility on repeated ammonia exposure. Following on from this a typical BPB/PE A/VA indicator film was prepared and exposed to repeat cycles of 1000 ppm ammonia at 300 ml min^{-1} for 1 hour followed by heating at 70 ^oC for 2 hours to recover. The process was monitored spectrophometrically at 600 nm and the Abs_{600} versus time plot is shown in Figure 6.19 which shows that BPB/PE A/VA films can be repeatedly used and recovered thermally without any loss in performance.

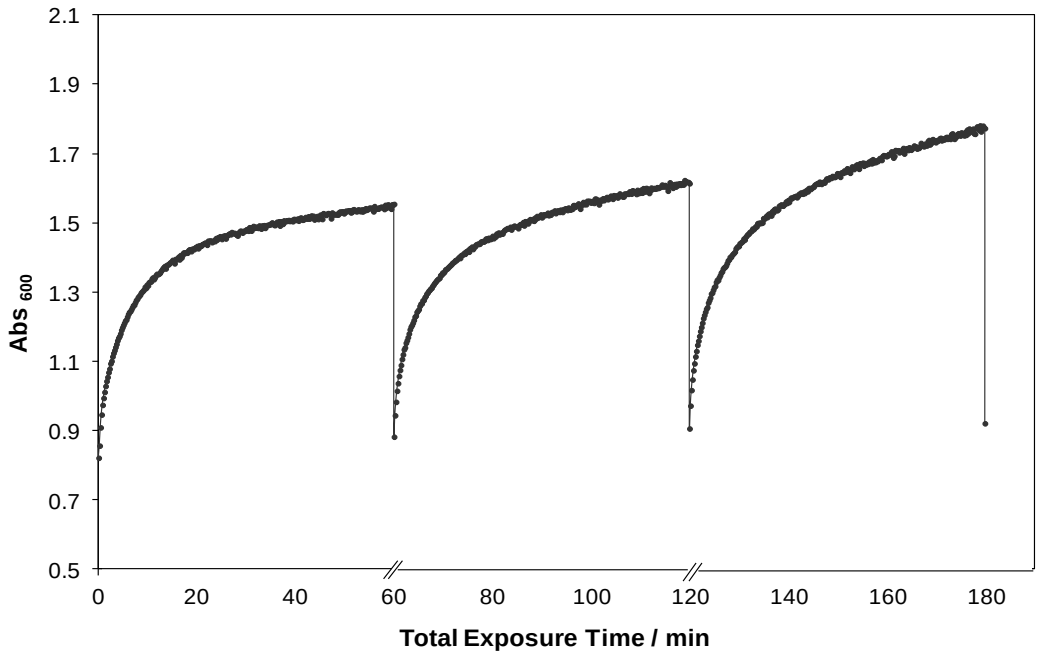

Figure 6.19 A plot of Abs_{600} against time for a typical BPB/PE A/VA film on exposure to repeat cycles on 1000 ppm ammonia for 60 minutes and thermal recovery for 2 hours at 70^oC (no data shown).

6.4.2.6 Response to varying %NH_3

The UV/visible absorption spectra of a typical BPB/PE A/VA indicator film as a function of the %NH_3 at ambient temperature were recorded as shown in Figure 6.20.

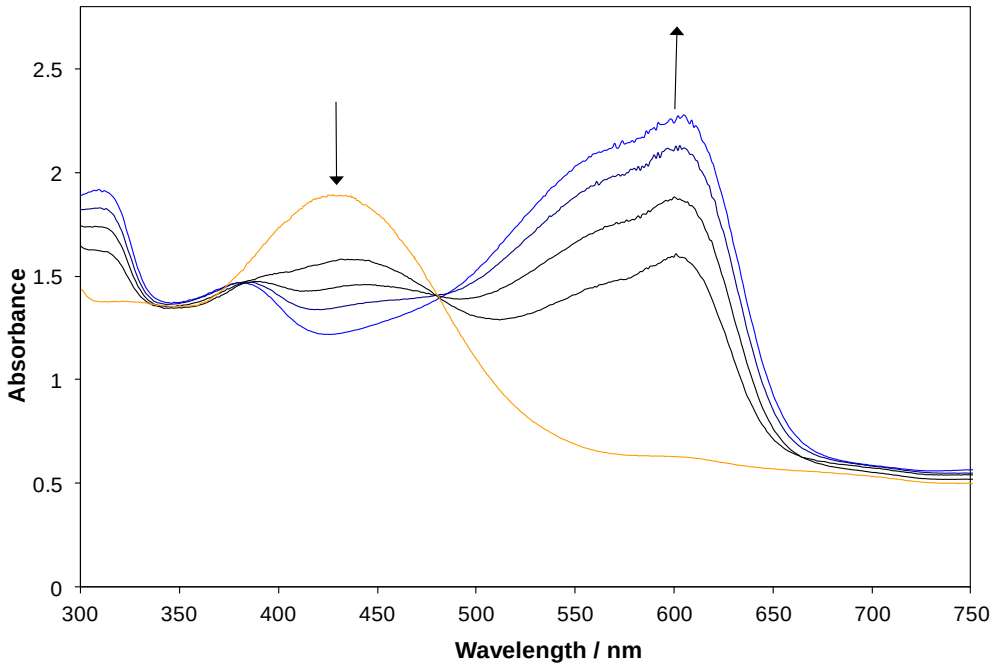

Figure 6.20 The UV/visible absorption spectra of a BPB/PE A/VA indicator film as a function of %NH_3, from top to bottom 0.01, 0.005, 0.002 and 0.001% NH_3. The film was exposed to each increasing NH_3 level for 300 minutes.

The variation in ΔAbs_{600} with %NH_3 is illustrated in Figure 6.21. From equations 6.8 and 6.9 as discussed previously, a direct ammonia optical indicator should yield a linear plot of R vs. P_{NH3} (or %NH_3) with a zero intercept and a gradient of:

$$\alpha = K_4 K_H / 100 \qquad (6.10)$$

Here α can be used as a measure of the film's sensitivity to A/VA. This linear relationship between R and %NH_3 is illustrated in the inset diagram in Figure 6.21.

These results show that the BPB/PE A/VA indicator film appears to give a reasonably straight line at low $\%NH_3$ ($\alpha = 1054 \pm 37$) levels with an intercept close to zero as predicted. Table 6.4 lists the coefficients of a least squares analysis of the line of best fit.

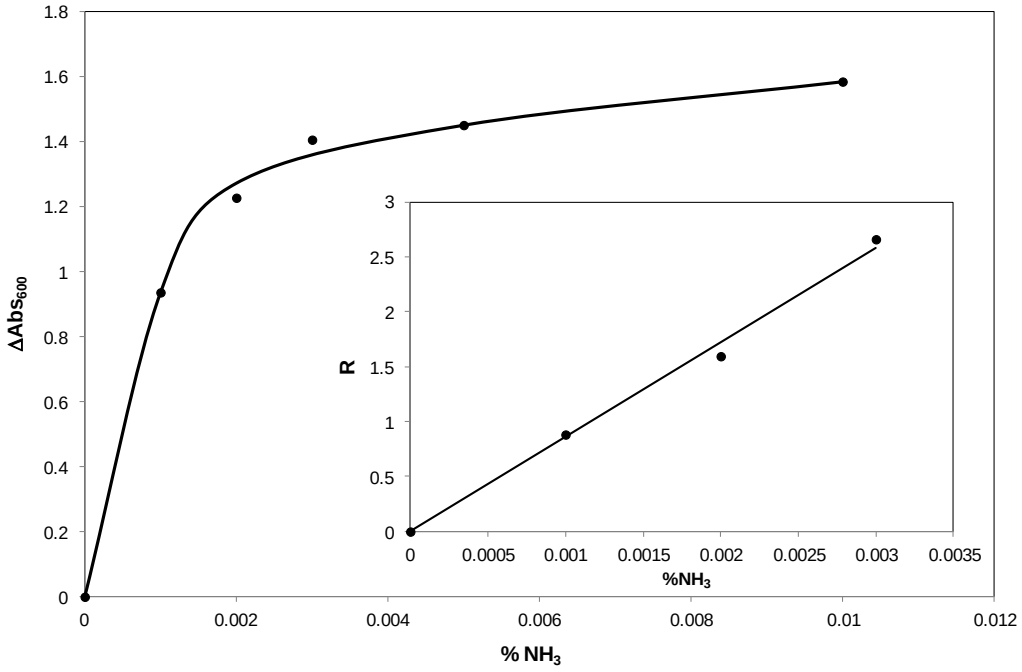

Figure 6.21 A plot of ΔAbs_{600} versus $\%NH_3$ for a typical BPB/PE A/VA indicator film. Inset diagram is the corresponding R versus $\%NH_3$ plot.

Plot*	m/α	c	r^2
BPB/PE A/VA indicator film R *vs.* NH_3 *(0-0.003%* NH_3*)*	1054 ± 37	-0.029 ± 0.069	0.9954

Table 6. 4 Response characteristics of A/VA indicators.

*the terms m, c and r^2 refer to the results of a least squares analysis of the line of best fit where m = gradient, c = intercept and r^2 = correlation coefficient.

6.4.2.7 Volatile amines

Given that the BPB/PE A/VA indicator films respond to changes in pH until now it has been assumed the films will respond not only to ammonia as discussed above but to many other volatile amines, including the biogenic amines putrascein and cadaverine i.e. 1,4- and 1,5-diamino butane respectively which are associated with food spoilage. To confirm this, a simple test was carried out by placing standard BPB/PE A/AV indicator films above a sample vial containing a few drops of a range of volatile amines for 3 minutes. Photographs of the films were taken before and after to document any observed colour change and are shown below in Figure 6.22.

It is clear that typical BPB/PE A/VA indicator films are not only responsive to ammonia but change colour on exposure to other volatile amines. This desirable feature increases the versatility of such indicators and extends their possible applications.

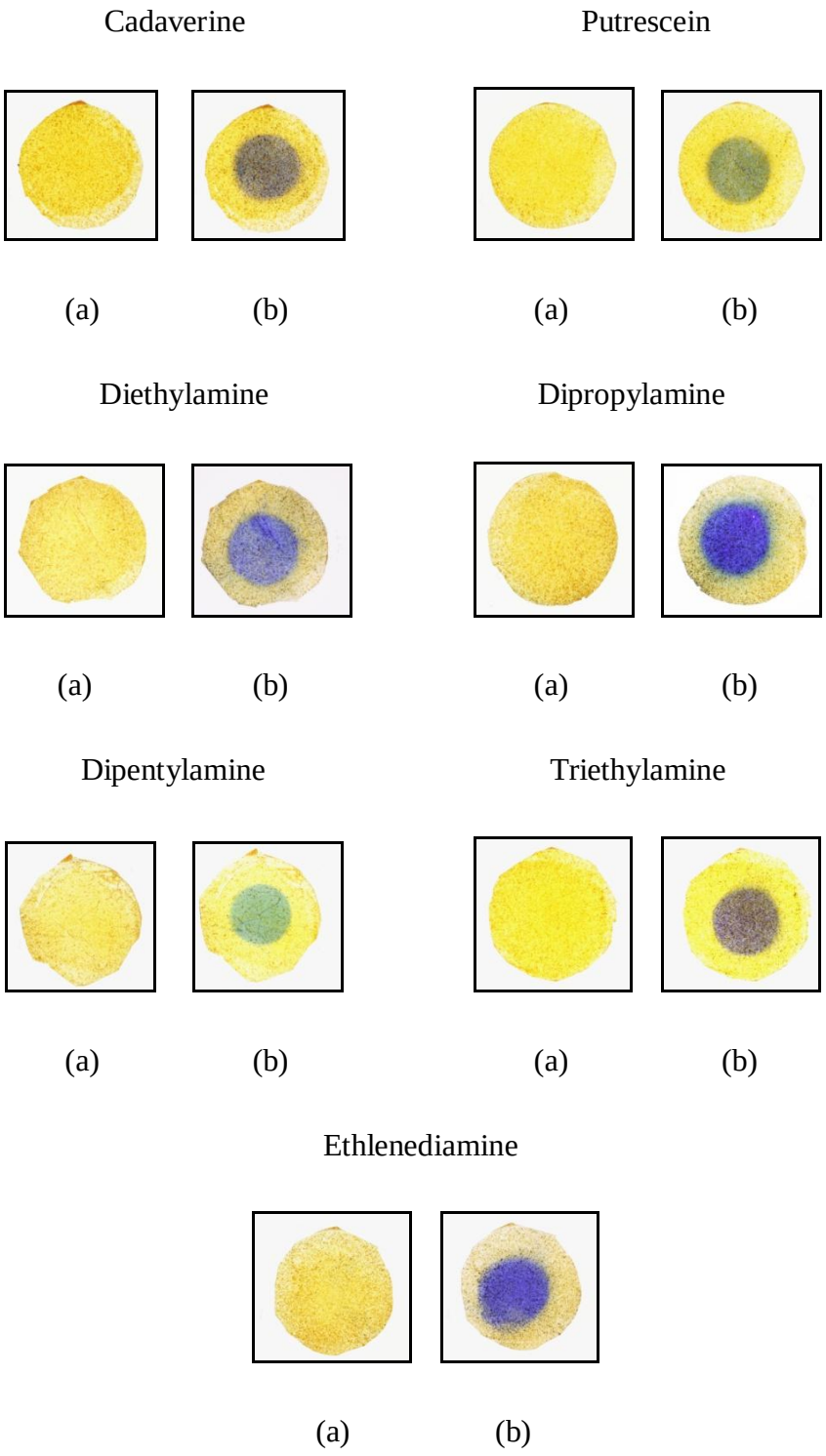

Figure 6.22 Photographs of typical BPB films (a) before and (b) after exposure to the headspace above a few drops of neat amine solutions for 3 minutes.

6.5 Application

The A/VA indicator films discussed here were designed with a particular application in mind *viz*. fish freshness indicators. By incorporating an A/VA pigment into a plastic commonly used for food packaging e.g. polyethylene, there is the potential to develop 'intelligent packaging' capable of informing the consumer of the quality of their seafood prior to purchase and consumption *via* a simple colour change. This application is demonstrated in Figure 6.23. Two BPB/PE A/VA indicators have been packaged with fresh haddock fillets and sealed with an industrial heat sealer. Immediately after packaging, sample 1 was refrigerated (~ 5^{o}C) while sample 2 was left at room temperature (~ 20^{o}C). Both samples were examined 24 hours later and as seen below the indicator in sample 2 has undergone a striking colour change from yellow to blue indicating that the unrefrigerated sample is no longer safe to eat. This was confirmed by a sensory evaluation of sample 2 which had a strong amine odour and a slimy appearance. The indicator in sample 1, however, showed no colour change and very little odour indicating as expected after refrigeration for 24 hours the haddock was still fit for consumption. It should be noted that these type of indicators are known to have a temperature dependence such that their sensitivity increases with decreasing temperature.[23] Despite this increase in sensitivity the levels of amine in the refrigerated sample after 24 hours are still low enough to not cause a visible colour change. It is hoped that further research and development on this will lead to the development of a plastic packaging material which incorporates an A/AV pigment without the need for an additional indicator strip. Further tests should be carried out to ensure that the indicator is tuned to respond to the specific A/VA levels associated with fish spoilage and temperature studies should be carried out to characterise the sensitivity of the films at less than ambient temperature as fish samples are typically iced or refrigerated during transportation and storage.

Sample 1

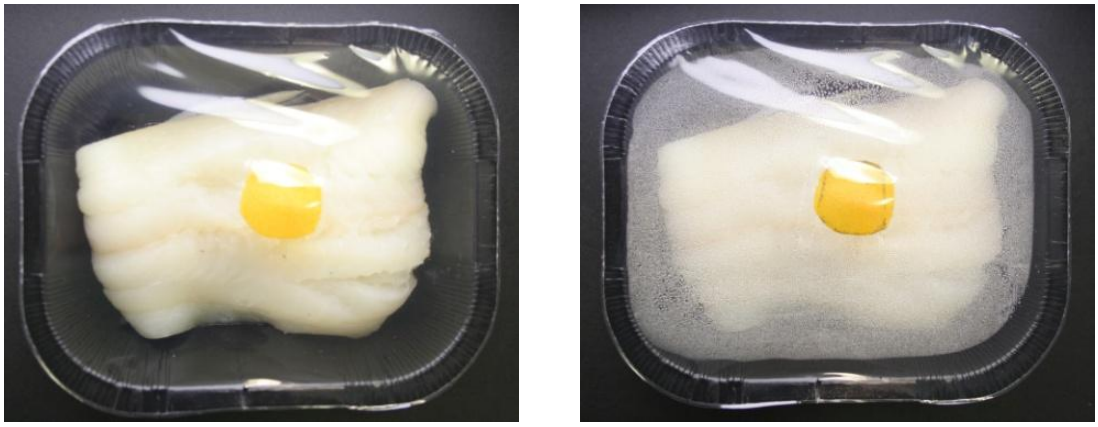

(a) (b)

Sample 2

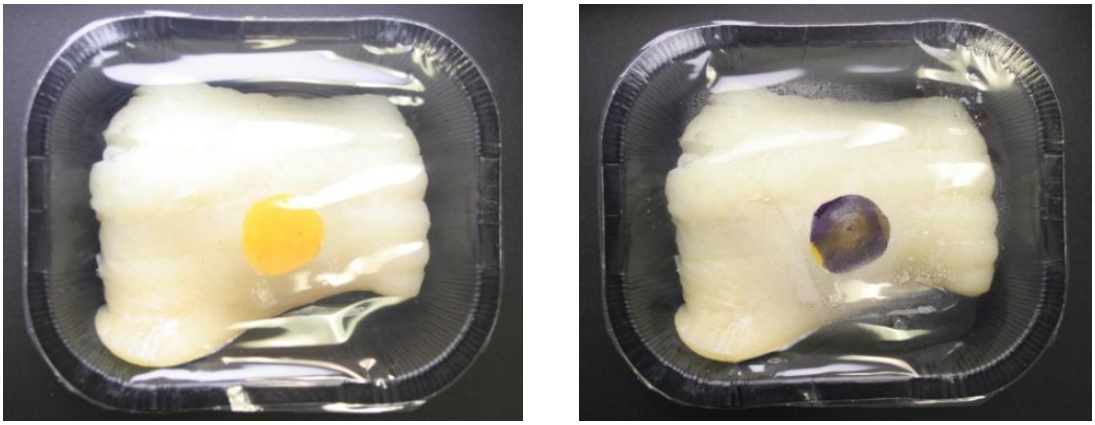

(a) (b)

Figure 6. 23 Photographs of packaged fish samples containing typical BPB/PE A/VA indicators (a) immediately and (b) after 24 hours. Sample 1 was refrigerated at ~ 5 ^{o}C while Sample 2 was stored at room temperature.

6.6 Alternative A/VA pigments and plastic indicator films

6.6.1 Alternative A/VA pigments

As the initial studies appeared promising the possibility of developing alternative A/VA pigments with different pH dyes was investigated. A literature and patent review of fish freshness and A/VA indicators highlighted a series of dyes commonly adopted which are listed in Table 6.5. Hydrophobic pigments were prepared using a method similar to the one outlined previously and each pigment was exposed to a 1000 ppm ammonia stream and also the headspace above an ammonium hydroxide solution. The observed colour changes are detailed below.

Dye	**pK_a**	**Initial colour**	**1000 ppm NH_3**	**NH_4OH headspace**
Bromophenol Blue (BPB)	4.1	Orange	Blue	Blue
Bromocresol Green (BCG)	4.6	Orange	Green/Blue	Blue
Bromocresol Purple (BCP)	6.3	Orange	Green	Blue
Bromothymol blue (BTB)	7.0	Yellow	Dark Yellow/Green	Blue
Phloxine B* (PB)	?	Pale pink/colourless	Bright pink	Bright pink
Phenol Red (PR)	7.9	Orange	Orange/Red	Red
Methyl Red (MR)	5.06	Red	Orange/Red	Orange/yellow

Table 6.5 Properties of alternative A/VA pigments.

*no pK_a value available but colour change occurs in pH range 1.1-3.3.

In order to be effective for food packaging applications the A/VA pigments must give a response readily visible to the human eye i.e. a striking colour change. Not surprisingly the dyes with lower pK_a values yielded the best colour changes i.e. BCG and BCP along with PB and as such they were selected for further investigation. For comparison's sake BTB was also considered.

6.6.2 Alternative A/VA plastic indicator film

Selected A/VA pigments were incorporated into PE films using the method described previously. The response characteristics for each film on exposure to 1000 ppm ammonia at 300 ml min^{-1} for 1 hour and the accompanying photographs of the films are found in Figures 6.24-6.30 below. The first alternative film tested was the BCG/PE A/VA indicator. The film which is initially yellow in colour is green in appearance after an hour's ammonia exposure. This colour change while still striking is not as distinct as the BPB/PE A/VA film at the ammonia level under test, see Figure 6.24 and 6.25.

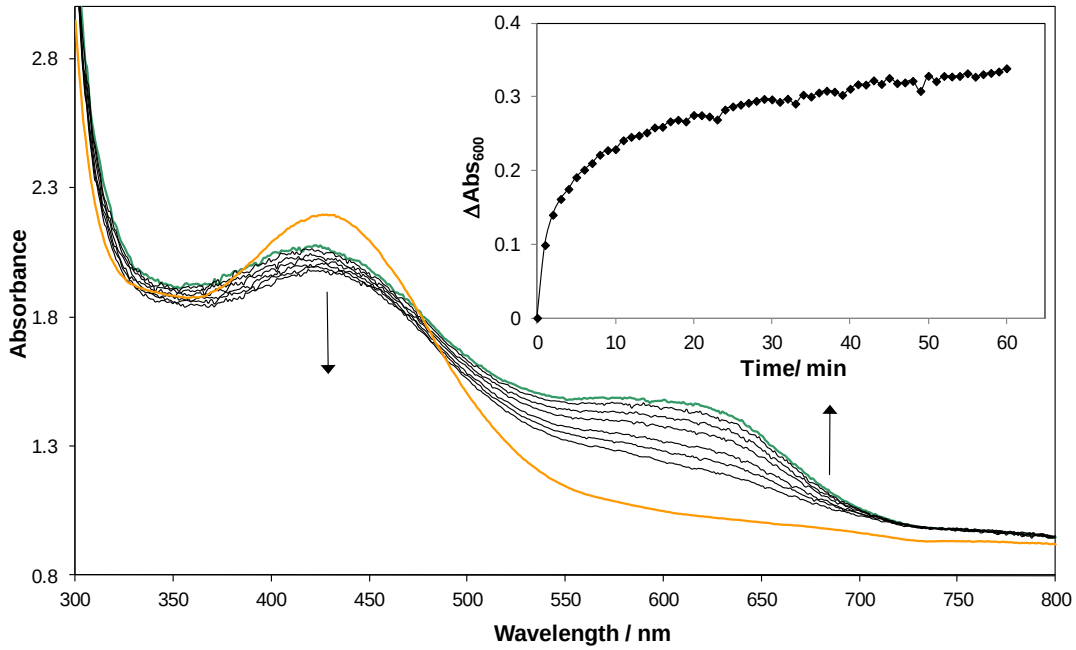

Figure 6.24 Absorbance spectra of a standard BCG/PE A/VA indicator film on exposure to 1000 ppm ammonia at 300 ml min^{-1} for 60 minutes. Inset diagram is a plot of ΔAbs_{600} versus time.

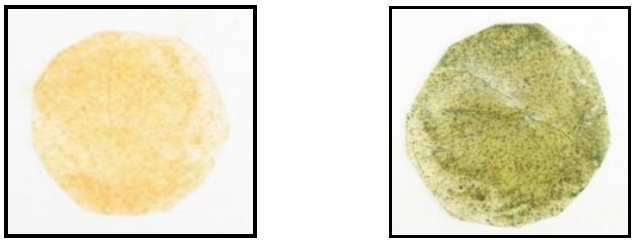

(a) (b)

Figure 6.25 Photographs of a standard BCG/PE A/VA indicator film (a) before and (b) after exposure to 1000 ppm ammonia at 300 ml min^{-1} for 60 minutes.

A similar level of performance is observed for the second indicator film tested *viz*. BCP/PE A/VA indicator film, which also undergoes a similar yellow to green colour change.

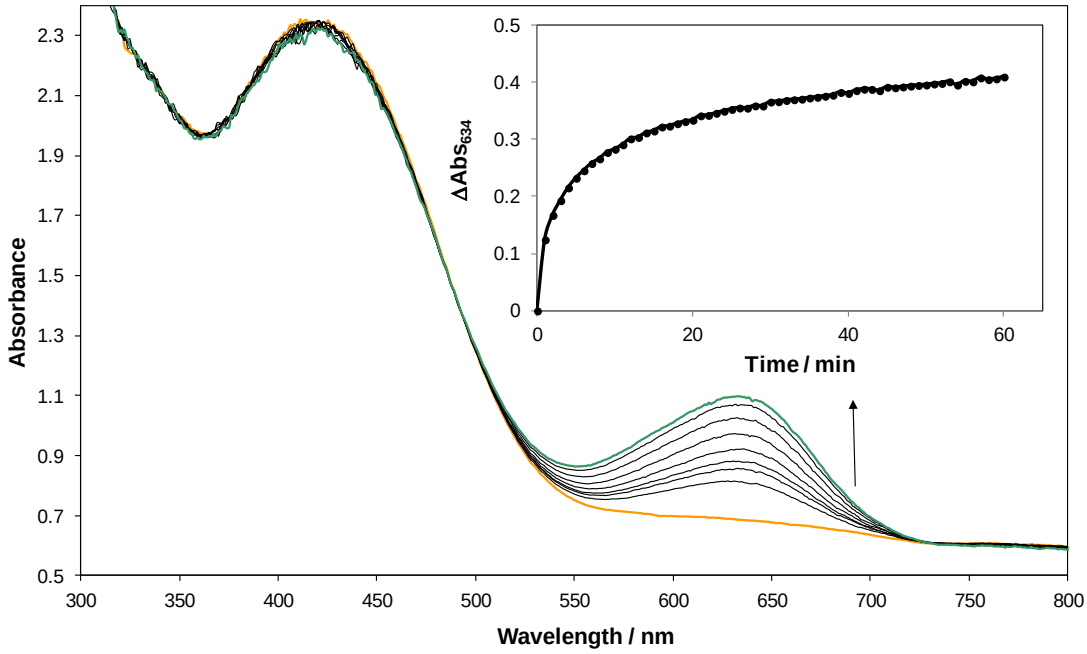

Figure 6.26 Absorbance spectra of a standard BCP/PE A/VA indicator film on exposure to 1000 ppm ammonia at 300 ml min^{-1} for 60 minutes. Inset diagram is a plot of ΔAbs_{634} versus time.

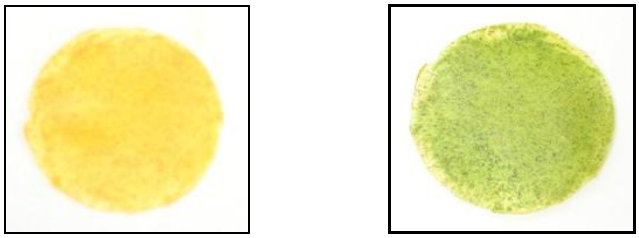

(a) (b)

Figure 6.27 Photographs of a standard BCP/PE A/VA indicator film (a) before and (b) after exposure to 1000 ppm ammonia at 300 m l min^{-1} for 60 minutes.

The most striking colour change occurred with the only fluorone-based film tested, the PB/PE A/VA indicator film. As illustrated in Figures 6.28 and 6.29 below this film is transformed from a pale pink to a vivid magenta in the presence of ammonia.

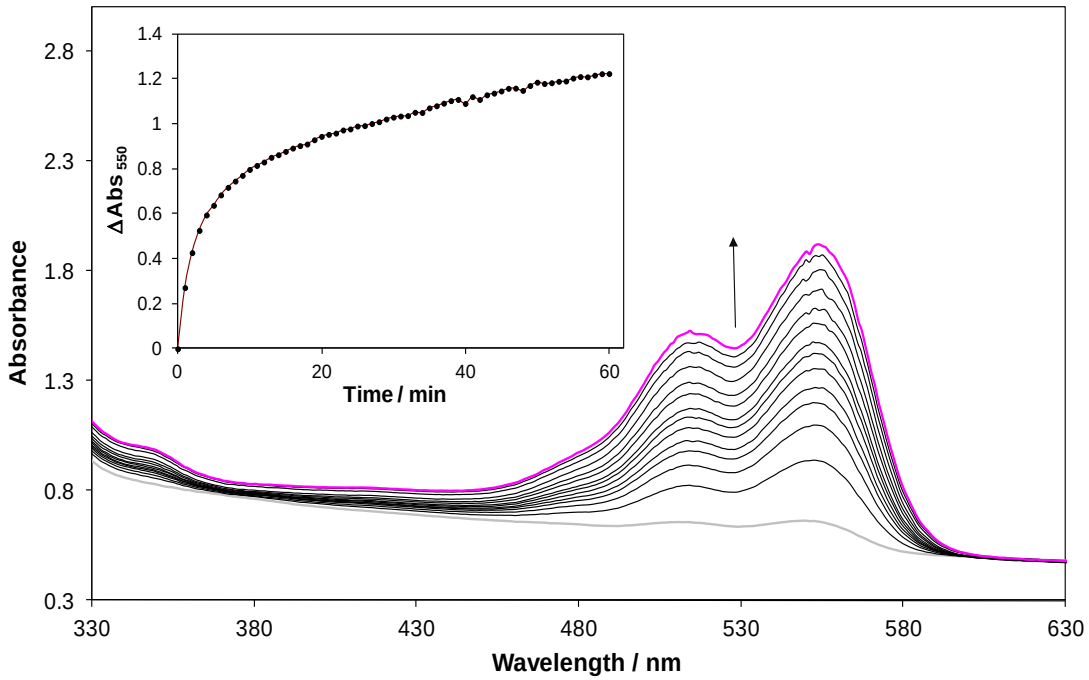

Figure 6.28 Absorbance spectra of a standard PB/PE A/VA indicator film on exposure to 1000 ppm ammonia at 300 ml min^{-1} for 60 minutes. Inset diagram is a plot of ΔAbs_{550} versus time.

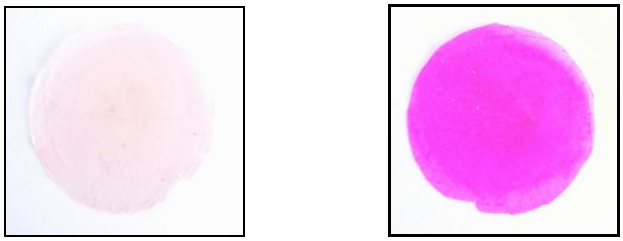

(a) (b)

Figure 6.29 Photographs of a standard PB/PE A/VA indicator film (a) before and (b) after exposure to 1000 ppm ammonia at 300 ml min^{-1} for 60 minutes.

For comparison purposes a BTB/PE A/VA was also prepared and exposed to 1000 ppm ammonia. As shown below in Figure 6.30:

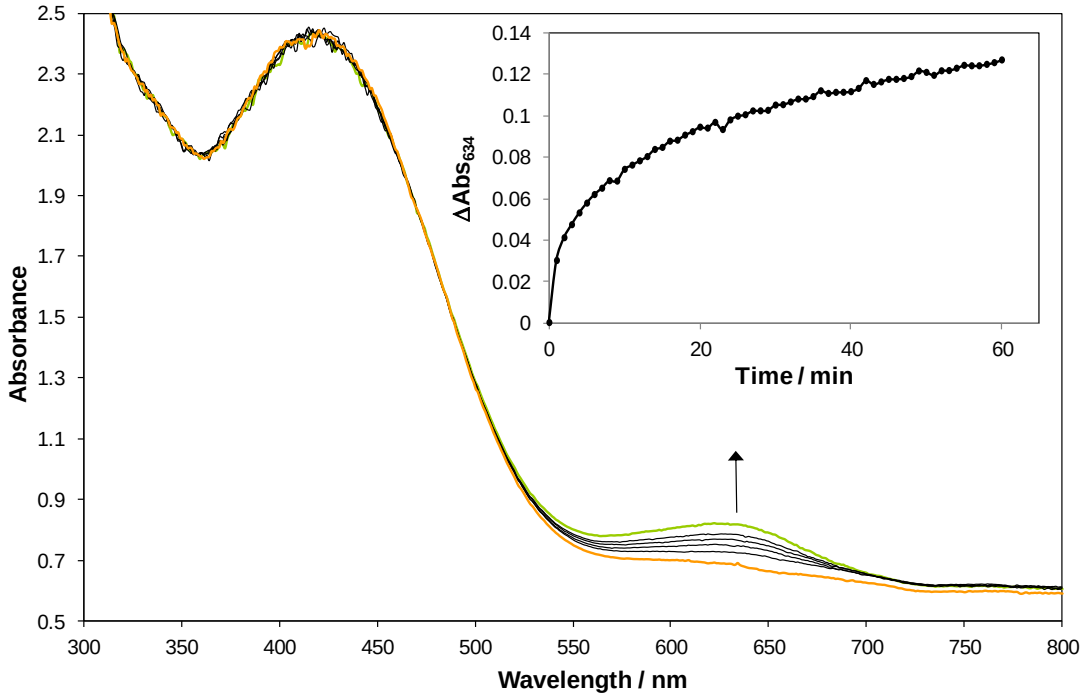

Figure 6.30 Absorbance spectra of a standard BTB/PE A/VA indicator film on exposure to 1000 ppm ammonia at 300 ml min^{-1} for 60 minutes. Inset diagram is a plot of ΔAbs_{634} versus time.

Of all the alternative pigments tested PB is the most promising as it resulted in a high quality film that undergoes a very striking colour change on exposure to 1000 ppm of assumed the value will fall within the pH range associated with the colour change i.e.1.1-3. A dye with such a low pK_a would be more sensitive to changing $\%NH_3$ and thus more of the dye is converted to its basic pink $NH_4^+D^-$ form. It is the opinion of the author that the PB pigment should be considered for further work along with the original BPB pigment.

BCG and BCP pigments which are structurally very similar to BPB pigment undergo less striking but still very distinct colour changes on exposure to 1000 ppm NH_3

owing to their higher pK_a values. It is clear from looking at the UV/visible absorption spectra that a large portion of the starting acidic yellow DH is present (see large peaks at 430 nm in Figures 6.23 and 6.25). It is possible that if they were incorporated within a more permeable thermoplastic than PE that the resulting films may have increased sensitivity.

6.7 Conclusion

Plastic indicator films for A/VA monitoring can be readily produced by incorporating an A/VA sensitive pigment into a PE film using a heat press method. Such sensors give a reproducible response that is fully reversible by thermal means. The sensitivity of the A/VA films is dictated by the pK_a of the associated dye and thus the analogous pigment also. The potential application for A/VA indicator films as fish freshness sensors has been demonstrated and such films have demonstrated a response to a range of volatile amines. Due to time constraints during this work the proposed A/VA indicators discussed here have not been fully characterised and there is room for further work. Given the previously observed temperature dependence of both the ink-based BPB ammonia sensors[23] and the analogous CO_2 indicating pigments and plastics[37] it is necessary to carry out a temperature study to determine how the sensitivity of the A/VA indicator films varies with temperature. It would also be prudent to carry out a humidity study to determine what effect, if any, humidity has on the A/VA indicator film's response.

Since completing this work additional funding was made available to continue the development of these A/VA pigments and plastics for the food packaging industry. In recent years these pigments along with the analogous CO_2 indicating pigments[37] have been used to prepare dye-coated polymer beads which can then be melted and extruded to produce thin films more akin to food packaging materials. This work has attracted much interest from the media[38] and food packaging industry and great steps have been taken towards generating a viable commercial product.

6.8 References

1. A. Pacquit, K. Crowley and D. Diamond, in *Smart Packaging Technologies for Fast Moving Consumer Goods*, eds. J. Kerry and P. Butler, John Wiley & Sons, Ltd, West Sussex, 2008, pp. 77-98.
2. *Comission Decision 95/149/EC*, (OJ L97, p84, 29/04/1995).
3. M. Smolander, in *Smart Packaging Technologies for Fast Moving Consumer Goods*, eds. J. Kerry and P. Butler, John Wiley & Sons, Ltd, West Sussex, 2008, pp. 115-118.
4. A. Pacquit, J. Frisby, D. Diamonmd, K. T. Lau, A. Farrell, B. Quilty and D. Diamond, *Food Chem.*, 2007, **102**, 466-470.
5. A. Pacquit, K. T. Lau and D. Diamond, IEEE Sensors, Vienna, Austria, 2004.
6. A. Pacquit, K. T. Lau, H. McLaughlin, J. Frisby, B. Quilty and D. Diamond, *Talanta*, 2006, **69**, 515-520.
7. L. Byrne, K. T. Lau and D. Diamond, *Analyst*, 2002, **127**, 1338-1341.
8. A. Lobnik and O. S. Wolfbeis, *Sens. Acuat. B*, 1998, **51**, 203-207.
9. M. Loughran and D. Diamond, *Food Chem.*, 2000, **69**, 97-103.
10. L. Pivarnik, P. Ellis, X. Wang and T. Reily, *J. Food. Sci*, 2001, **66**, 945-952.
11. D. W. Miller, *WO 99/061399*, 1999.
12. D. F. H. Wallach, *WO 02/061399 A1*, 2002.
13. J. Williams and K. myers, *WO 2005/071399 A1*, 2005.
14. J. Williams and K. Myers, *WO 2006/032025 A1*, 2006.
15. T. Grady, T. Butler, B. D. MacCraith, D. Diamond and M. A. McKervey, *Analyst*, 1997, **122**, 803-806.
16. G. E. Khalil, D. L. Putnam and T. W. Hubbard, *WO 01/035057 A2*, 2000.
17. K. T. Lau, S. Edwards and D. Diamond, *Sens. Acuat. B*, 2004, **98**, 12-17.
18. C. J. Liu, J. T. Lin, S. H. Wang, C. J. Jiang and L. G. Lin, *Sens. Acuat. B*, 2005, **108**, 521-527.
19. C. J. Lui, J. T. Lin, S. H. Wang, J. C. Jiang and L. G. Lin, *Sens. Acuat. B*, 2005, **108**, 521-527.
20. K. I. Oberg, R. Hodyss and J. L. Beauchamp, *Sens. Acuat. B*, 2006, **115**, 79-85.

21. W. Qin, P. Parzuchowski, W. Zhang and M. E. Meyerhoff, *Anal. Chem.*, 2003, **75**, 332-340.
22. T. Yagi, N. Kuboki, Y. Suzuki, N. Uchino, K. Nakamura and K. Yoshida, *Opt. Rev,*, 1997, **4**, 596-600.
23. A. Mills, L. Wild and Q. Chang, *Mikrochim. Acta.*, 1995, **121**, 225-236.
24. N. Nakano, Y. Kobayashi and K. Nagashima, *Analyst*, 1994, **119**, 2009-2012.
25. C. Perininger, G. J. Mohr, I. Klimant and O. S. Wolfbeis, *Anal. Chim. Acta*, 1996, **334**, 113-123.
26. R. A. Potyrailo, S. P. Golubkov, P. S. Borsuk and P. M. Talanchuk, *Analyst*, 1994, **119**, 443-448.
27. P. Caglar and R. Narayanaswamy, *Analyst*, 1987, **112**, 1285-1288.
28. M. R. Shahriari, Q. Zhou and G. H. Sigel, *Opt. Lett.*, 1988, **13**, 407-409.
29. Q. Zhou, D. Kritz, L. Bonnell and G. H. Sigel, *App. Opt.*, 1989, **28**, 2022-2025.
30. C. Malins, M. Landl, P. Simon and B. D. MacCraith, *Sens. Acuat. B*, 1998, **51**, 359-367.
31. D. P. Muller, *WO 99/04256*, 1999.
32. C.-H. J. Liu and W.-C. Lu, *J. Chin. Inst. Chem. Engin.*, 2007, **38**, 483-488.
33. R. M. Harris, *Colouring Technology for Plastics*, Plastic Design Library, Norwich, NY, 1999.
34. http://www.packagingtoday.com/introplasticexplosion.htm, Accessed 15/07/2012.
35. http://www.borealisgroup.com/industry-solutions/advanced-packaging/pp-aids-air-quality/food-challenge-rigid-packaging/, Last Accessed 15/17/2012.
36. A. Mills, P. Grosshans and G. A. Skinner, *WO 2011/045572*, 2011.
37. A. Mills, G. A. Skinner and P. Grosshans, *J. Mat. Chem.*, 2010, **20**, 5008-5010.
38. http://www.bbc.co.uk/news/uk-scotland-glasgow-west-12128120, Last Acessed 15/07/2012.

Chapter 7

Hydrogen peroxide vapour indicator

7. Hydrogen peroxide vapour indicator

7.1 Introduction

Hydrogen peroxide, H_2O_2, is a pale blue liquid, slightly more viscous than water. It is a weak acid with strong oxidising properties and is inexpensive and readily available for use as a common bleaching agent and disinfectant.[1] Its widespread use is in part due to its environmentally friendly nature, given that it decomposes to produce water and oxygen. Popular uses include as a disinfectant for medical equipment and surfaces[2] and for sterilising surgical instruments.[3,4] Hydrogen peroxide has been used in the standard method for cleaning and storing many types of soft contact lenses since 1990.[5] Further applications include the chemical treatment of water systems to control diseases such as Legionnaires' disease in hospitals,[6] a slurry disinfectant,[7] and as a bleach for paper production in the wood pulp industry.[8]

A more recent use of hydrogen peroxide is in the production of "kitchen sink" explosives by terrorists. As the name suggests these improvised explosive devices are usually made with common household ingredients. One such example is triacetone triperoxide (TATP). TATP has been used in several, well-publicised terrorist attacks in recent years, including the July 2005 London bombings and the attempted bombing by Richard Reid, the 'shoe bomber', of a trans-Atlantic flight in December 2001.[9] TATP itself is a white crystalline material with a low chemical stability that is highly sensitive to mechanical stress and open flames.[10] It is very volatile, losing 68% of its weight within 14 days at room temperature,[11] and has an explosive power comparable with that of TNT.[10]

TATP can be easily synthesised by mixing acetone, hydrogen peroxide and a strong acid catalyst using ingredients that are readily available for purchase in the public domain. For example, H_2O_2 can be purchased from a pharmacy as a disinfectant at 6 wt. % in water and concentrated down to *ca.* 30 wt. % for TATP synthesis,[9,11]

acetone is available over the counter in the form of nail polish remover, and many household drain cleaners contain sulphuric acid. Not only are the ingredients cheap and readily accessible but as TATP is sufficiently easy to prepare there are concerns it could be prepared *in situ.i.e.* at the target site from otherwise apparently innocuous materials.

Of all the key ingredients, hydrogen peroxide is the most difficult to detect. It is very soluble in water and has a high boiling point (150^{o}C), thus there is very little present, *ca*. 360 ppm, above the headspace of even a highly concentrated (50 wt. %) aqueous solution.[12] Such solutions are effectively odourless and cannot be easily sensed, even by sniffer dogs.

With the increased threat of terrorist attacks at airports and on aircraft, there is a real need for a simple and easy to use hydrogen peroxide vapour indicator that will alert security officials to its presence in any liquids that are carried on board. Ideally the indicator should be cheap to produce, easy to use, non-invasive (i.e. responds when held over suspect liquid), and undergoes a clear response, such as a striking colour change, when exposed to hydrogen peroxide vapour. Obviously, other possible applications of such an indicator include the detection of H_2O_2 vapour in sterilisers and water disinfectant units in hospitals, or in fact wherever H_2O_2 is used.

Hydrogen peroxide is a common oxidising agent capable of generating highly reactive hydroxyl radicals, which are able to oxidise many complex organic compounds, including dyes.[13-17] Previous studies have shown that alkaline, aqueous solutions of triarylmethane dyes such as phenolphthalein (PP) and lissamine green (LG) (see Figure 7.1) undergo rapid oxidative degradation, accompanied by bleaching, upon the addition of H_2O_2, although under neutral or acidic conditions this reaction is usually very slow.[18-23] Intriguingly, initial work showed that the triarylmethane dye, lissamine green (see Figure 7.1), is particularly vulnerable to oxidative bleaching by H_2O_2 vapour when encapsulated in a largely neutral, polymeric environment. Thus, this chapter details the characterisation of a simple

colorimetric H_2O_2 vapour indicator, comprising the triarylmethane dye, LG, in the polymer, polyvinyl alcohol (PVA).

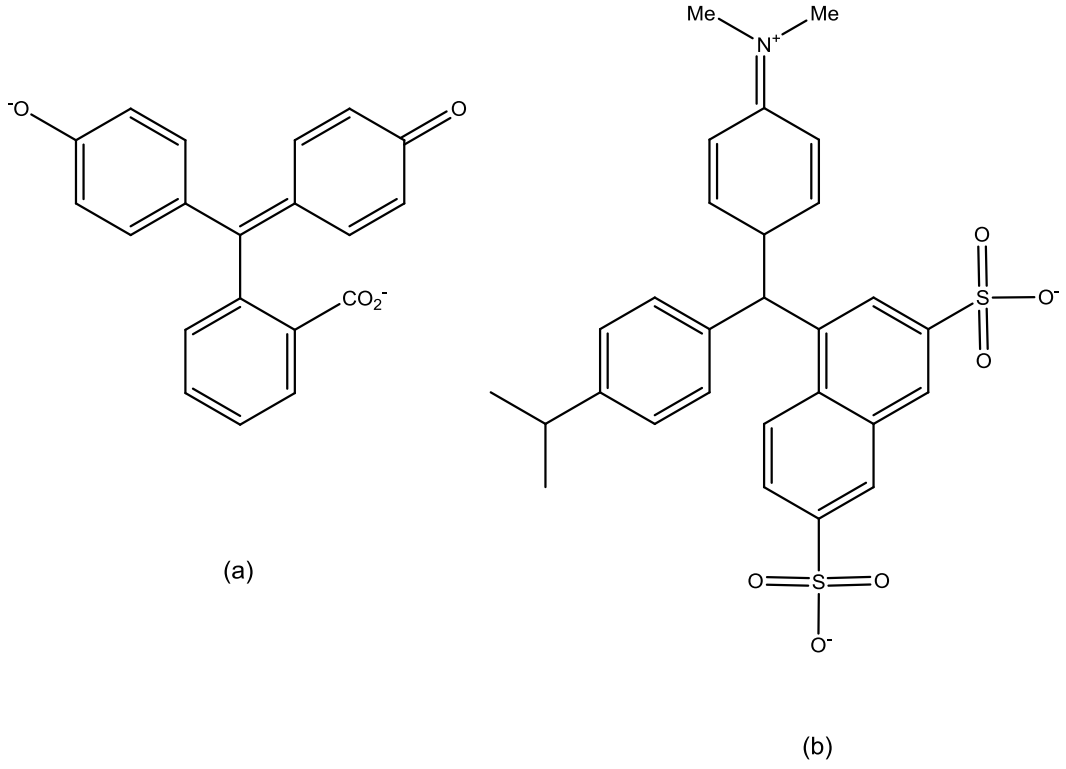

Figure 7.1 The chemical structures for (a) phenolphthalein, (PP) and (b) lissamine green (LG).

7.2 Experimental

7.2.1 Materials

All chemicals were purchased from Sigma Aldrich Chemicals and used as received unless specified. The water used to produce the casting inks was double distilled and deionised, and the polymer used to produce the films was average Mol. Wt 124,000–186,000, 98–99% hydrolysed polyvinyl alcohol. The hydrogen peroxide solutions were prepared from a 50 wt% aqueous hydrogen peroxide stock solution.

7.2.2 Preparation of LG ink and films

A typical LG/PVA ink solution was prepared as follows: 10 g of PVA were dissolved in 90 ml of water at 90°C, cooled to room temperature and stirred overnight. 40 mg of LG dye were then dissolved in 4 g of the PVA solution at room temperature with stirring to generate an ink with LG present at 10 phr (≡ 0.21 M). The ink (pH 5.7) was dark green/blue in appearance. Films of the ink were then cast onto 25 mm diameter borosilicate glass discs, using a spin coater. Thus, a few drops of casting ink were deposited on to the surface of the disc and then spun at 2400 rpm for 25 s. The product was dried for 2 min in an oven at 70°C and allowed to cool to room temperature before use. Figure 7.2 illustrates a typical ink formulation and a typical LG film along with an SEM image of a typical LG film edge on. The final product was a green/blue film, typically *ca*. 1.1 μm thick (as measured by SEM see Figure 7.2) on a glass disc and is referred to henceforth as a typical LG film.

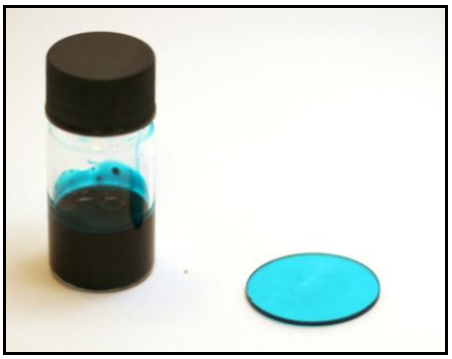

(a)

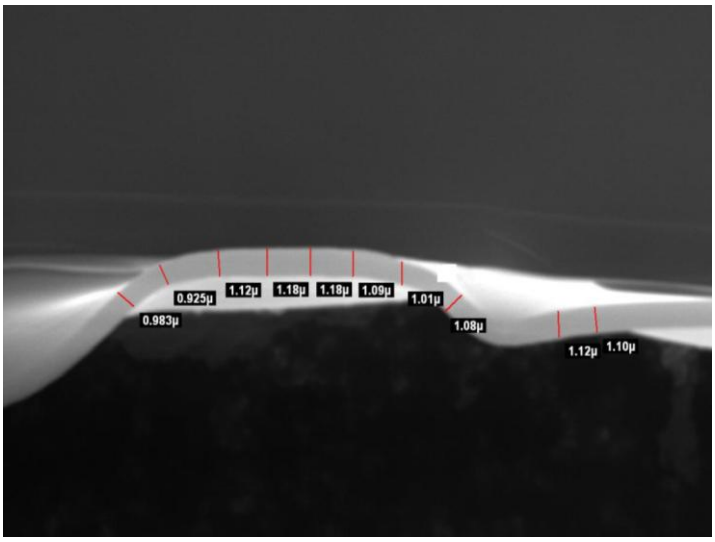

(b)

Figure 7.2 (a) A photograph of a standard LG ink formulation and a typical LG film (b) an SEM image of a typical LG film edge on at x 2,960 magnification.

The LG/PVA films, when stored in a cool dark place under otherwise ambient conditions, appear largely unchanged and active for over 1 year.

7.2.3 UV/visible spectrometry

In a H_2O_2-containing solution well equilibrated with its headspace, the vapour pressure due to the H_2O_2, pH_2O_2 , is directly proportional to the concentration of H_2O_2 in the solution, i.e. $[H_2O_2]$.[12] Thus, gas streams containing different levels of hydrogen peroxide vapour were generated by passing air (flow rate = 2 l min^{-1}) through 150 ml of aqueous solutions of H_2O_2 of different concentrations contained in a Drechsel bottle, fitted with a glass sintered tip to ensure the effective dispersion of the carrier gas as bubbles and their saturation with H_2O_2 vapour.

UV/visible spectra for sample films were recorded using a Cary Model 50 UV/visible spectrophotometer. Typically, upon exposure of a LG film to H_2O_2 vapour, the absorbance spectrum of the film was recorded every 30 s until the film was fully bleached. In order to carry out this work, any film under test was housed in a gas cell through which was flowed the gas stream containing the H_2O_2 vapour under test, typically derived from a 1 wt% H_2O_2 solution (pH_2O_2 = *ca.* 7 ppm) for most work.

7.3 Results and discussion

7.3.1 Bleaching of LG in aqueous solution

Solutions of 1.7×10^{-5}M LG were prepared in water (pH 6.3 blue/green, λ_{max} 636 nm) and in a pH 9.2 borate buffer (blue, λ_{max} 614 nm). Each of these LG solutions were then mixed with 50 wt% aqueous H_2O_2 in a glass cuvette in a ratio of 30:3 (v:v) to produce an approx. 5 wt% H_2O_2 aqueous solution, and the bleaching followed spectrophotometrically *via* the decay in the absorbance of LG at 636 nm. The results of this work, plotted in the form of the relative change in absorbance with time, are illustrated in Figure 7.3 and reveal that LG is bleached slowly ($t_{1/2}$ = 96 min) at pH 6.3, but much more rapidly (>340 times; $t_{1/2}$ = 17 s) at pH 9.2.

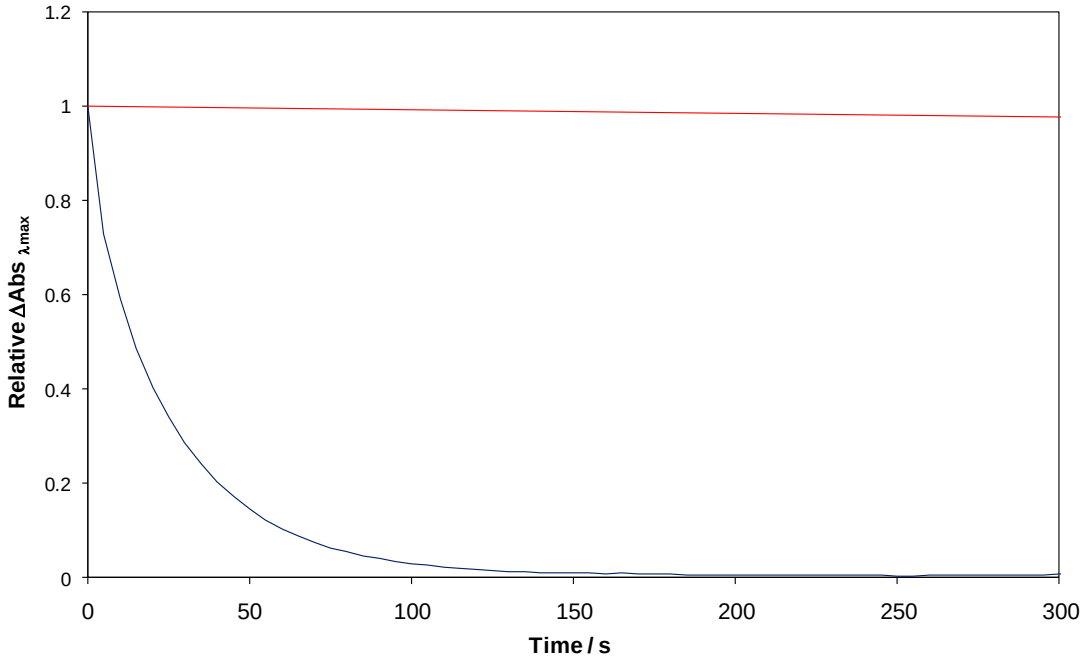

Figure 7.3 A comparison of the bleaching of 1.7×10^{-5} M LG (aq) at pH 6.3 where $t_{1/2}$ = 96 min, and at pH 9.2 where $t_{1/2}$ =17 s.

These results are consistent with the work of Thompson *et al.*[22] in their study of the oxidation of aqueous phenolphthalein by H_2O_2, who also noted that oxidative bleaching of such triarylmethane dyes in solution is comparatively very slow at neutral or acidic pHs. These results lend support to the proposal by these workers that bleaching in aqueous solution occurs *via* nucleophilic attack by the peroxy anion, HOO^-, at the central carbon of the triarylmethane unit as depicted in Figure 7.4. Thus, at pHs significantly below the pK_a of H_2O_2 (11.75), the rate of trialkylmethane dye oxidation (LG or PP) is very low.

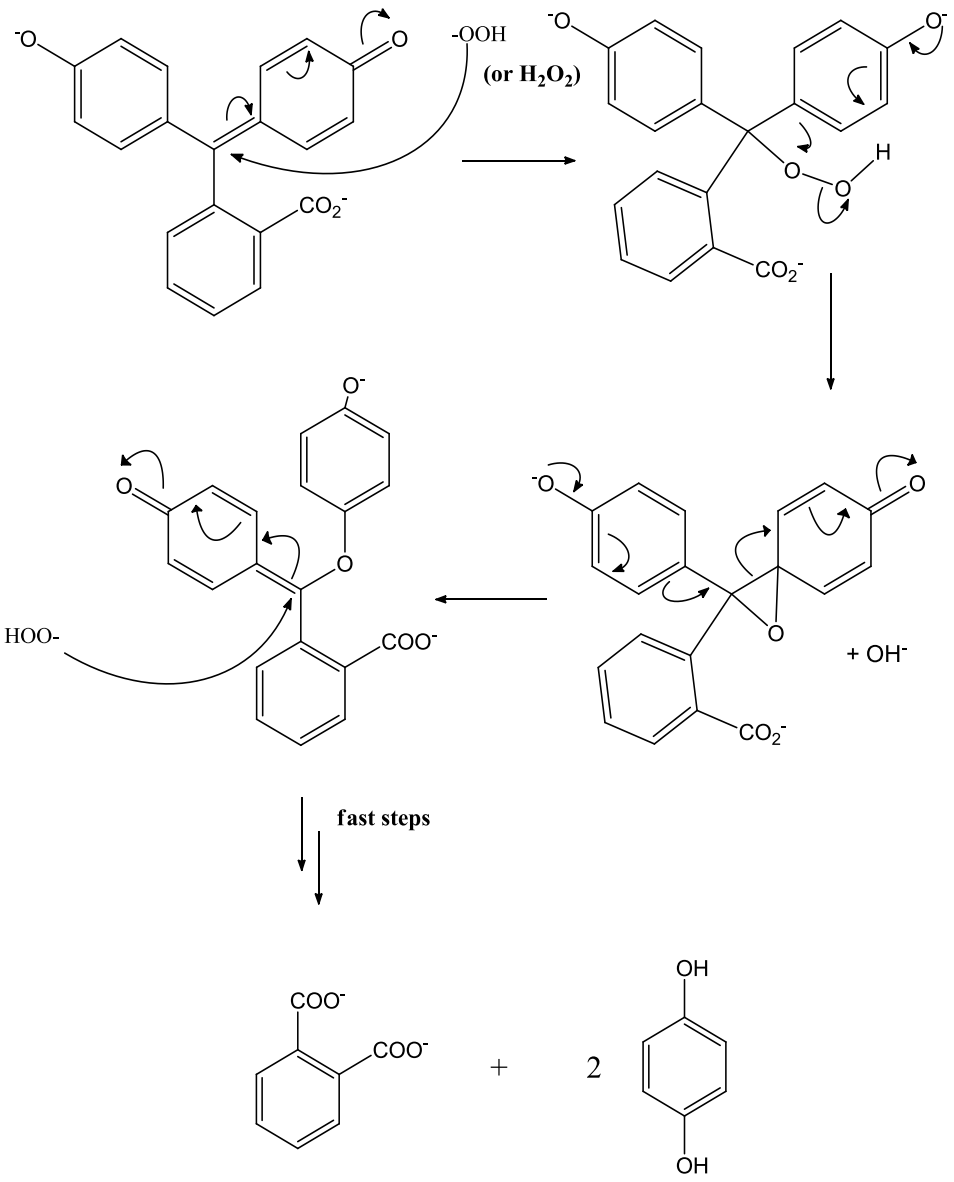

Figure 7.4 The proposed mechanism of the bleaching of phenolphthalein by hydrogen peroxide.[22]

7.3.2 Visual bleaching of standard LG films

The above results in aqueous solution indicate it is very unlikely a typical LG/PVA film (where the pH of the casting ink = 5.7) will be bleached rapidly by the H_2O_2 vapour above even a strong (50 wt %) H_2O_2 solution, not only because the amount of

H_2O_2 in the vapour phase is so low (*ca*. 360 ppm), but also because the reaction rate is so slow in a neutral or acidic medium, such as aqueous solution at pH 6.3 ($t_{1/2}$ = 96 min). However, in practice, and for reasons that as yet remain unclear, the bleaching kinetics of LG in polymer films by H_2O_2 vapour are rapid. For example, when a typical LG film was placed on top of a sample vial containing 5 ml of 50 wt % H_2O_2 water, film side down, the H_2O_2 vapour above the solution (*ca*. 360 ppm) caused the LG film to bleach within minutes, as illustrated by the photographs in Figure 7.5.

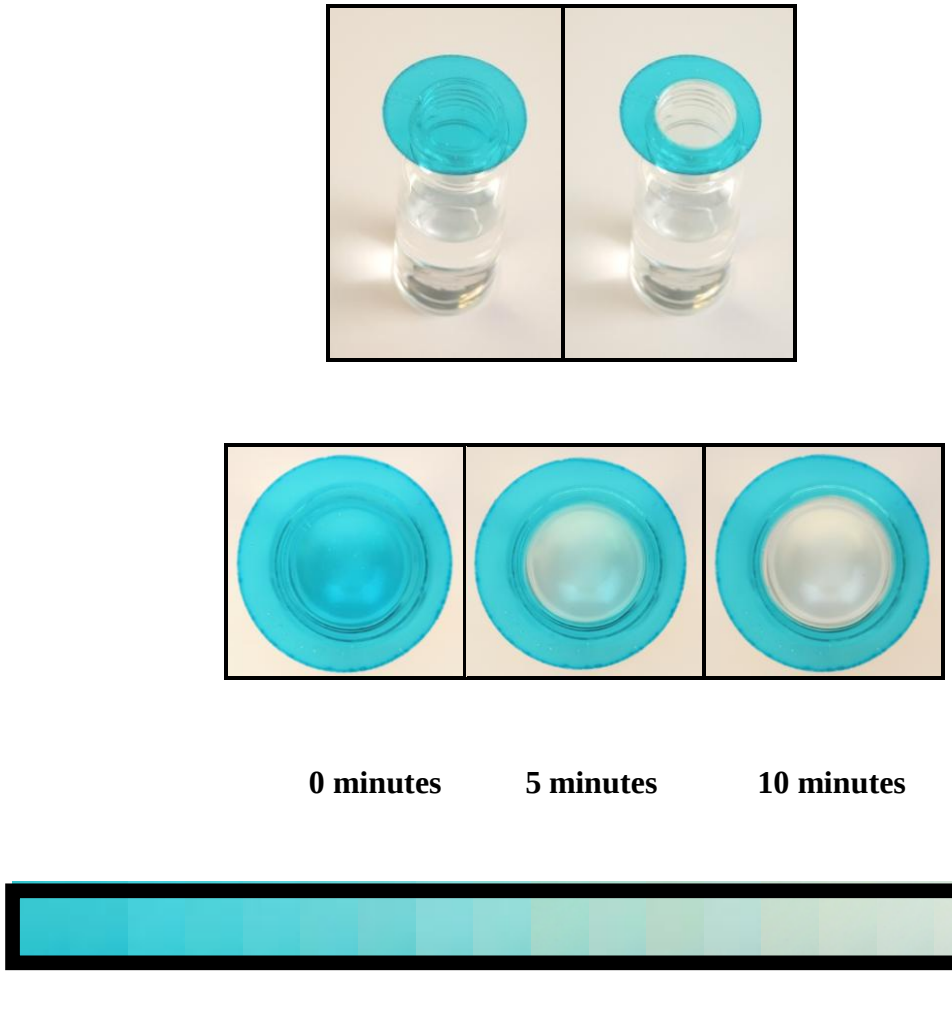

Figure 7.5 Photographs illustrating the chemical bleaching of a typical LG film when placed above a 50 wt % aqueous H_2O_2 solution.

7.3.3 Spectral and response characteristics of a LG film

An aqueous solution of LG (10^{-5} M) has a peak in its absorption spectrum at 636 nm, whereas in a PVA film not only is the peak slightly broader, with a shoulder emerging at 605 nm, but it is red-shifted to 650 nm, most probably due to the formation of dimers, which is not surprising given [LG] in films = 0.21 M. Indeed, a 0.1 M LG aqueous solution has a λ_{max} at 640 nm and a shoulder peak at 601 nm, also implying dimer formation at high dye concentrations. It is possible that such dimers are more vulnerable to oxidative attack by hydrogen peroxide. The absorption spectra for a 10^{-5} M LG solution (in a 10 mm cell), a typical LG/PVA film and a 0.1 M LG solution (a small drop of solution sandwiched between two glass cover slips) are shown below in Figure 7.6.

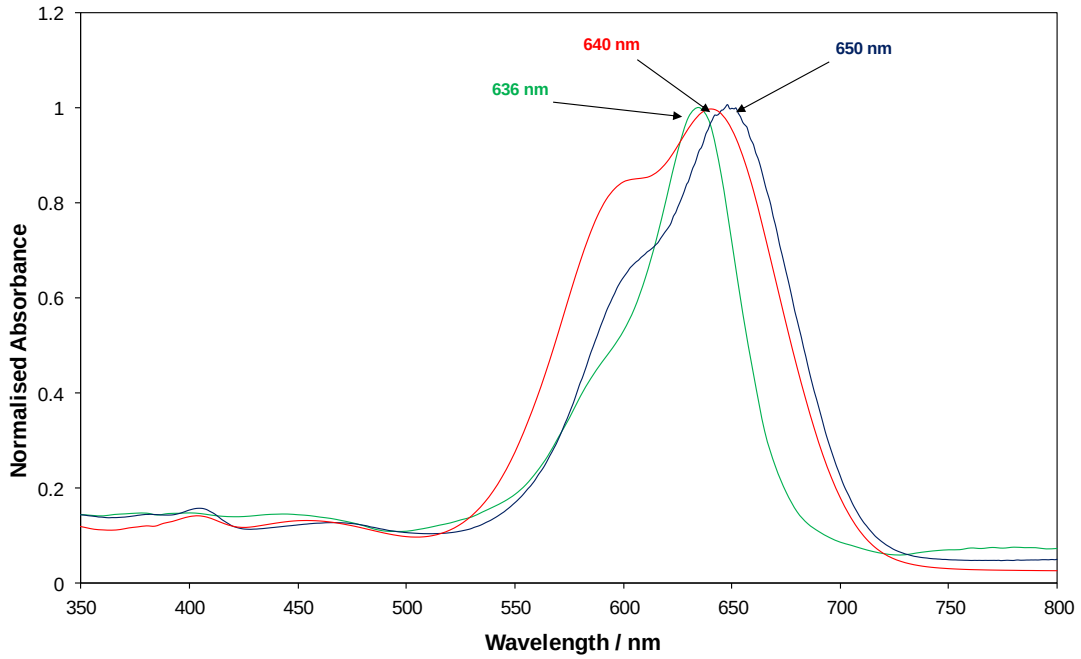

Figure 7.6 The absorption spectra for a 10^{-5} M LG solution (in a 10 mm cell), a typical LG/PVA film and a 0.1 M LG solution (a drop of solution sandwiched between two glass cover slips).

It is also possible that a change in microenvironment polarity is responsible for the significant increase in reactivity of LG with H_2O_2 vapour when the dye is encapsulated in a PVA film.

A typical LG film was mounted in gas cell and exposed to H_2O_2 vapour from a 1 wt% aqueous H_2O_2 solution. The loss of colour of the LG film was followed spectrophotometrically, and the results are displayed in Figure 7.7. Using this data, a plot of the change in absorbance at λmax, i.e.ΔAbs_{650}, against time was generated as seen in Figure 7.8 and revealed that, after a slight initial delay, possibly due to an experimental artefact associated with gas switching, the kinetics of LG bleaching by H_2O_2 vapour above a 1 wt% aqueous H_2O_2 solution give a reasonable fit (r^2 = 0.996) to a first order bleaching process ($t_{1/2}$ = 3.5 min). The coefficient of variation with the LG film bleaching is ± 6%; this is typical of the error for all LG films unless otherwise stated.

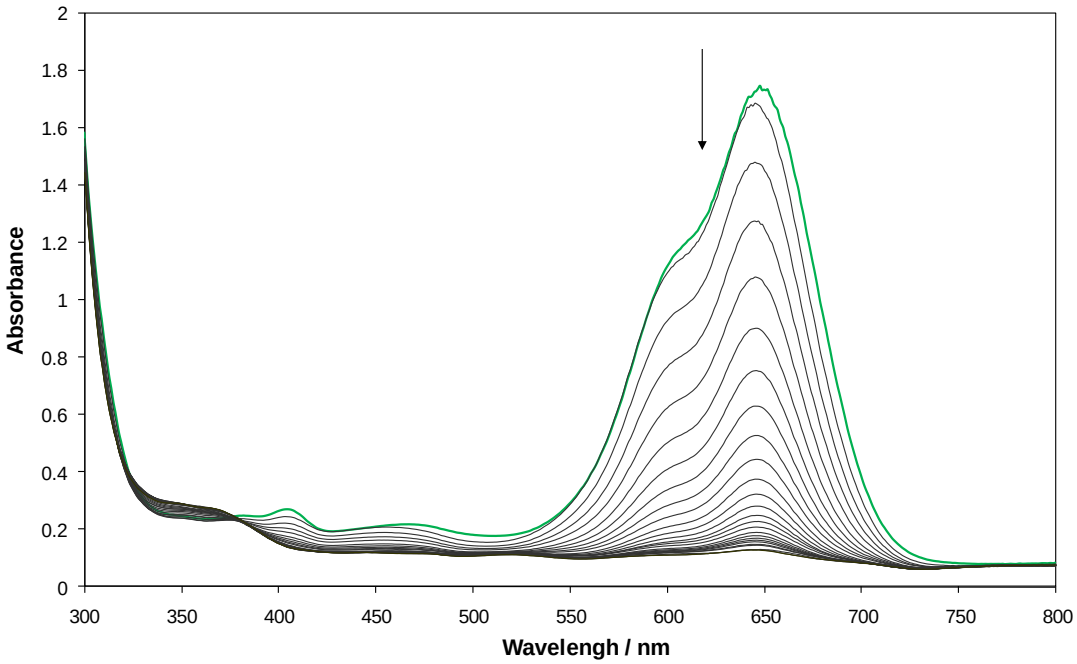

Figure 7.7 The absorption spectra of a standard LG film on exposure to hydrogen peroxide vapour from a 1 wt% H_2O_2 solution at a flow rate of 2 l min^{-1}. Spectra recorded at 1 min intervals.

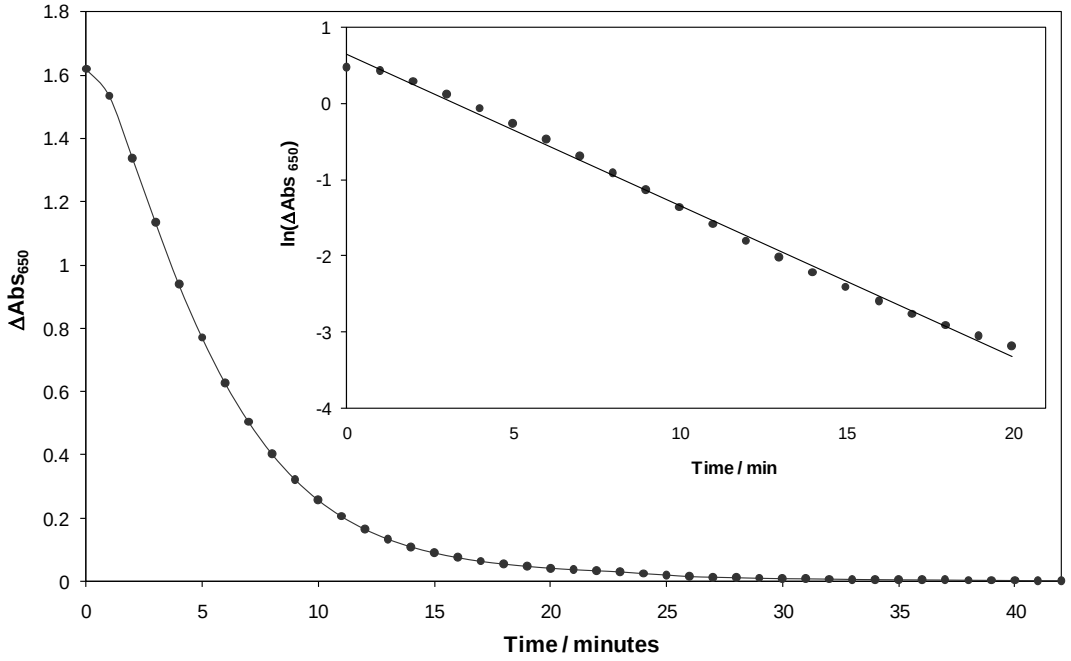

Figure 7.8 A plot of ΔAbs_{650} against time for a typical LG film exposed to the vapour from a 1% wt. H_2O_2 solution at a flow rate of 2 l min^{-1}. Inset shows a first order kinetic plot of ln(ΔAbs_{650}) versus time, for the first 2 half-lives of the same typical LG film, (r^2 = 0.9962).

7.3.2 Kinetics of a LG film

7.3.2.1 [H_2O_2]

Extending the above study, the kinetics of LG bleaching in a typical LG/PVA film were studied as a function of the H_2O_2 vapour pressures above different aqueous [H_2O_2] solutions over the range of 0–20 wt%, and the results are illustrated in Figure 7.9 as a plot of ΔAbs_{650} against time. First order kinetics analysis of these results generated the plots of k_1 versus wt% H_2O_2, illustrated in Figure 7.10, where k_1 is the first order rate constant.

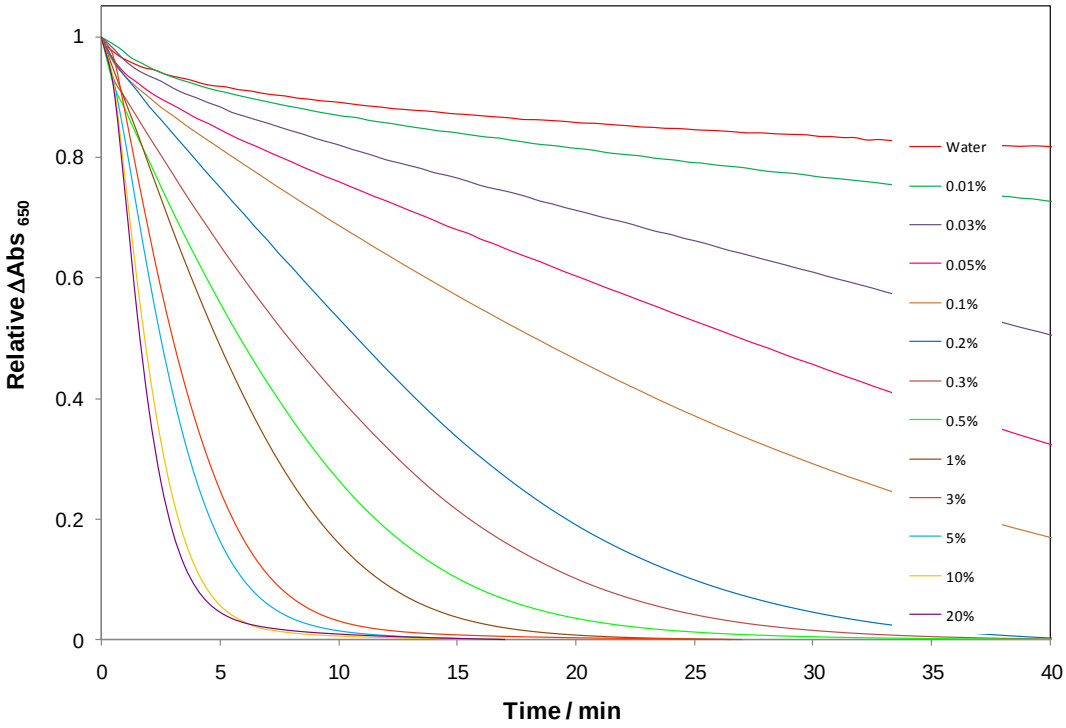

Figure 7.9 A normalised plot of ΔAbs_{650} against time for typical LG films exposed to H_2O_2 vapours from solutions of different $[H_2O_2]$ at a flow rate of 2 l min^{-1}. The concentrations of aqueous H_2O_2 solutions used to produce the different vapours are, from top to bottom: 0, 0.01, 0.03, 0.05, 0.1, 0.2, 0.3, 0.5, 1, 3, 5, 10 and 20 wt %.

As noted earlier, previous work has established that the kinetics of the bleaching of PP in aqueous alkaline solution by H_2O_2 are first order kinetics with respect to $[H_2O_2]$ and [PP] and we find similar kinetics apply to LG in aqueous solution (see Figure 7.3).[22]

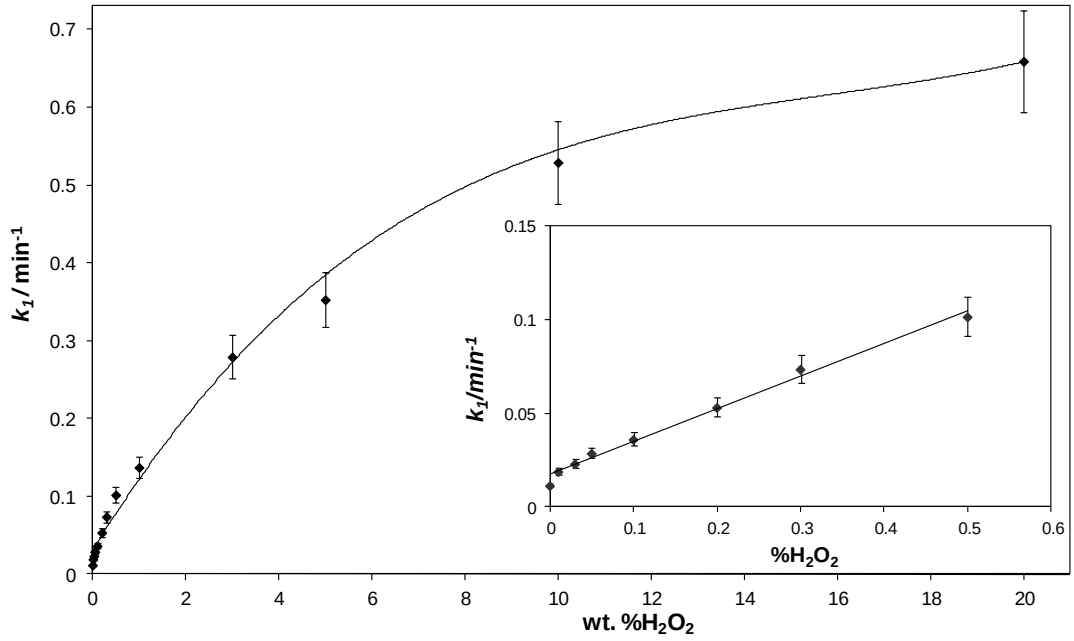

Figure 7.10 A plot of k_1 vs. wt% H_2O_2. Inset diagram shows an expanded view of the region from 0 to 0.5 wt% H_2O_2.

The results illustrated in Figure 7.9 indicate that the kinetics of LG bleaching in a LG/PVA film are first order with respect to [LG], and those in Figure 7.10 indicate they are also first order with respect to [H_2O_2] at $p$$H_2O_2$ below 0.5 wt% [H_2O_2]. However, above *ca.* 0.5 wt% H_2O_2 the value of the apparent first order rate constant, k_1, appears to level off with increasing [H_2O_2] (see Figure 7.10), possibly due to the heterogeneous nature of the polymer environment, which often results in a distribution of reaction rate constants. For example, this feature is typical of luminescent quenching by O_2 of oxygen-sensitive luminescent dyes encapsulated in polymer films including PVA.[23]

7.3.2.2 Flow rate

Further work revealed that the kinetics of dye bleaching in the LG/PVA films are independent of the gas flow rate at or above the gas flow rate used in this work

(typically 2 l min^{-1}), indicating that the kinetics are independent of the mass transfer of the H_2O_2 in the vapour to the LG/PVA film.

7.3.2.3 Film thickness

In the study of kinetics of LG bleaching as a function of film thickness, *d*, a slightly modified LG/PVA ink casting solution, containing 2.5 phr (rather than 10 phr) LG, was prepared by dissolving 5 mg (instead of 20 mg) of LG in 2 g of 10 wt% PVA in water. This lower [LG] was used in order to allow much thicker films, with higher absorbances, to be prepared using slower spin speeds. From this slightly less coloured LG/PVA ink, a series of films of different thicknesses were produced using a spin coater by varying the spin speed from 600 to 2500 rpm. These films were then exposed to H_2O_2 vapour from a 1 wt% aqueous H_2O_2 solution. As before, bleaching of the samples was monitored spectrophotometrically at 650 nm and a plot of the ΔAbs_{650} against time was generated for each film spin speed and the collected decay profiles are shown in Figure 7.11.

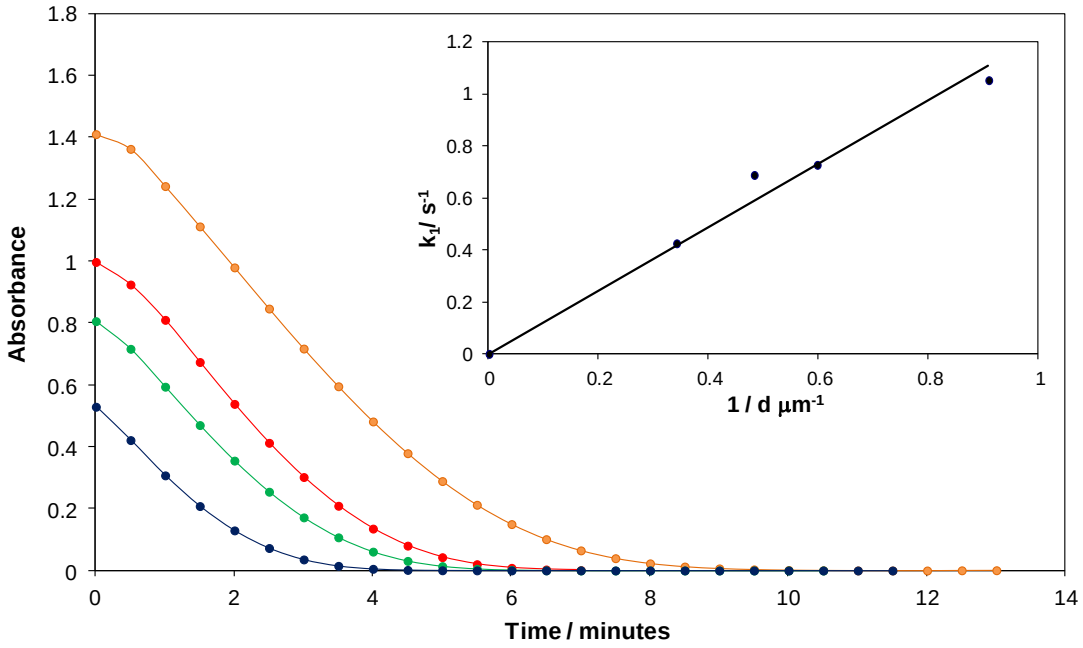

Figure 7.11 A plot of ΔAbs_{650} against time for 5 phr LG films generated at different spin speeds (from top to bottom 600, 800, 1200 and 2500 rpm) upon exposure to H_2O_2 vapour from a 1 wt% H_2O_2 aqueous solution. The flow rate used was 2 l min^{-1}. Inset diagram shows a plot of k_1 vs. 1/d, with m = 1.22 and a correlation coefficient of 0.961.

A plot of $\ln(\Delta Abs_{650})$ against time yielded a set of k_1 values. If the kinetics of LG bleaching were dependent solely upon diffusion of H_2O_2 through the film it would be expected that $k_1 \propto 1/d^2$ whereas in practice it appears that they are approximately proportional to $1/d$ as seen from the inset in Figure 7.11.[25,26] Thus, the kinetics of LG bleaching in LG/PVA films appear to be only partially controlled by the diffusion of the H_2O_2 through the PVA film.

7.3.2.4 Encapsulating polymer

The effect of the encapsulation polymer and thus the microenvironment polarity of the LG was investigated by preparing a series of LG films in different polymers, namely polyvinyl alcohol (PVA), polyethylene oxide (PEO) and hydroxyethyl

cellulose (HEC). The films were exposed to a H_2O_2 vapour stream generated from a 1 w% [H_2O_2] solution and the initial rates determined. The relative rates of bleaching by H_2O_2 vapour were found to be 1.6:1:0.6 for HEC, PVA and PEO respectively. From looking at the structures of each of the polymers shown in Figure **7.12**, these results indicate the more polar the polymer environment encapsulating the LG molecules the faster the rate, supporting the notion that it is the change in micropolarity that is responsible for the significant increase in reactivity of LG with H_2O_2 vapour when the dye is encapsulated in a PVA film observed in Figure 7.6.

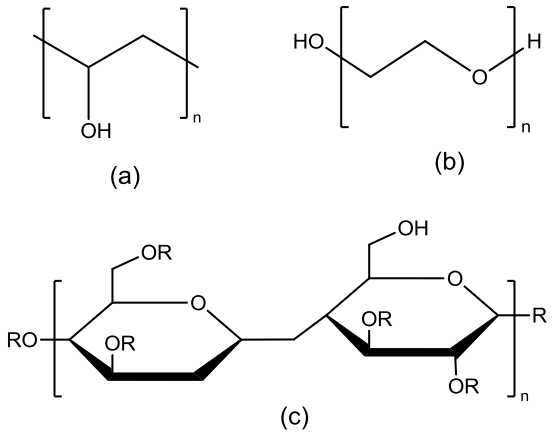

Figure 7.12 The chemical structures for the three encapsulating polymers tested: (a) Polyvinyl alcohol (PVA), (b) Polyethylene oxide (PEO) and (c) Hydroxyethyl cellulose (HEC).

7.3.3 Enhancement of bleaching

7.3.3.1 NaOH

As the rate of peroxide bleaching of LG in solution is increased in the presence of NaOH (i.e. under basic conditions), a series of standard LG/PVA inks was prepared that contained 0-5 phr of sodium hydroxide (NaOH) and used to produce a series of films. The LG/NaOH/PVA films were exposed to a 1% H_2O_2 vapour stream and their absorbance at 650 nm recorded. The addition of NaOH to the casting inks

rendered blue rather than green/blue inks and films, which accounts for the shift in λ_{max} from 650 nm to 620 nm as noted in Figure 7.13 below.

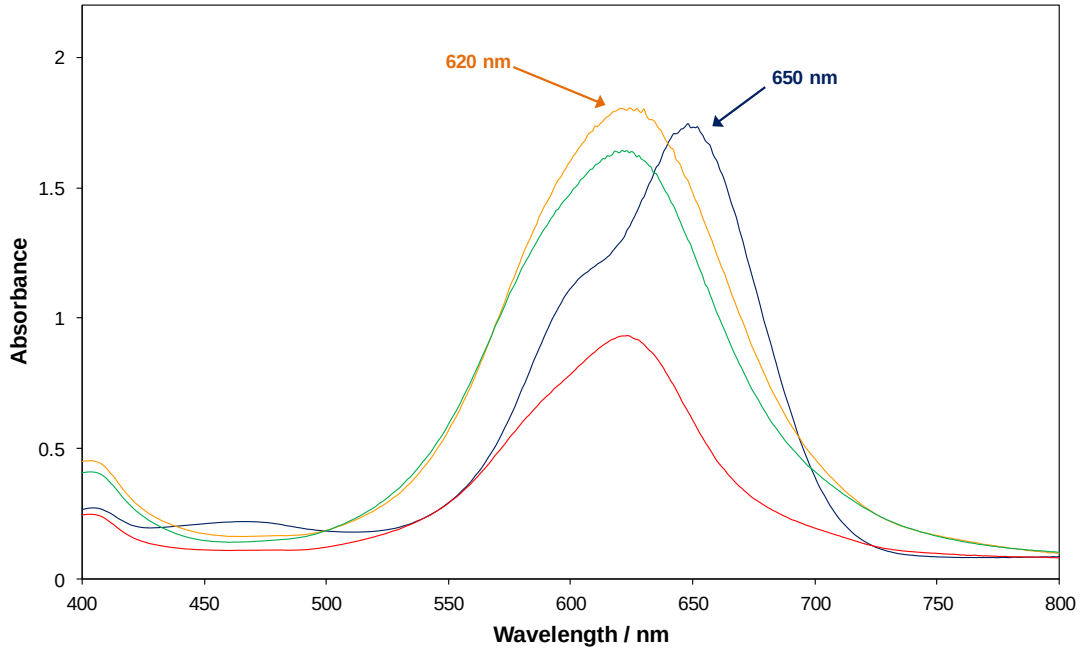

Figure 7.13 The absorption spectra of a typical LG/PVA film containing 0 phr, 0.5 phr, 2.5 phr and 5 phr, NaOH.

It is also apparent from Figure 7.13 that as the level of NaOH increases the initial starting absorbance of the film decreases. It was found that films containing 1 phr did bleach marginally faster than the typical LG/PVA films but did not show a significant enhancement in the rate of bleaching (relative rates 1:1.1). The film containing 2.5 phr NaOH when compared to the typical LG/PVA film had a relative rate ratio of 1:1.5. The film containing 5 phr NaOH, despite having a lower initial absorbance, took almost twice as long as a typical LG/PVA film to photobleach. Upon examination of the 5 phr solution it was noted that the ink was not its usual consistency, rather it appeared thick and glutinous and was beginning to change colour from blue to dark green. This suggests that the inclusion of NaOH in the ink has compromised the integrity of the system, presumably by reacting with the polymer. One suggestion is that under alkaline conditions the PVA strands undergo

cross-linking to form a water-insoluble gel, as a similar effect has been observed in the dechlorination of PVC under mildly alkaline conditions, the product of which is a non water-soluble PVA product.[26]

7.3.4 Longevity

The longevity of the typical LG films was monitored throughout the course of this study. A series of typical LG films stored in zip-lock bags were kept in the dark at room temperature (*ca*. 22 ^{o}C), with a second set of identical films refrigerated (*ca*. 5 ^{o}C) in the dark. Over the course of 12 weeks both sets of films gradually lost some of their colour, with the films stored at room temperature dropping from an average initial λ_{650} of 2.0 to 1.5, i.e. a 25% reduction in absorbance. As absorbance is a logarithmic scale this difference is not a striking as it initially appears. The films stored at the lower temperature saw a smaller decease in absorbance maxima, from 2.01 to 1.78 i.e. 12.1%.

To determine whether older films were still active, 3 standard LG films of different ages were tested and their response to a 1% wt H_2O_2 solution compared. The films used were a fresh film prepared from a new solution, a 12- and a 24-month-old film, which had been stored in a zip-locked bag at room temperature (*ca*. 22^{o}C). The respective plots of ΔAbs_{650} against time are found below in Figure 7.14. These decay curves confirm as noted above that films lose some of their colour during storage. What is also apparent is that the older films are bleached by H_2O_2 at a slower rate as indicated in Table 7.1 below. The reason for this is unknown but may be indicative of polymer shrinkage, reducing the films porosity and thus the rate at which the H_2O_2 is able to diffuse through the film. This is not ideal, however it should be noted that the rates for a 12-month-old film and a 24-month-old film are comparable and that bleaching on the film is achievable albeit at a reduced rate.

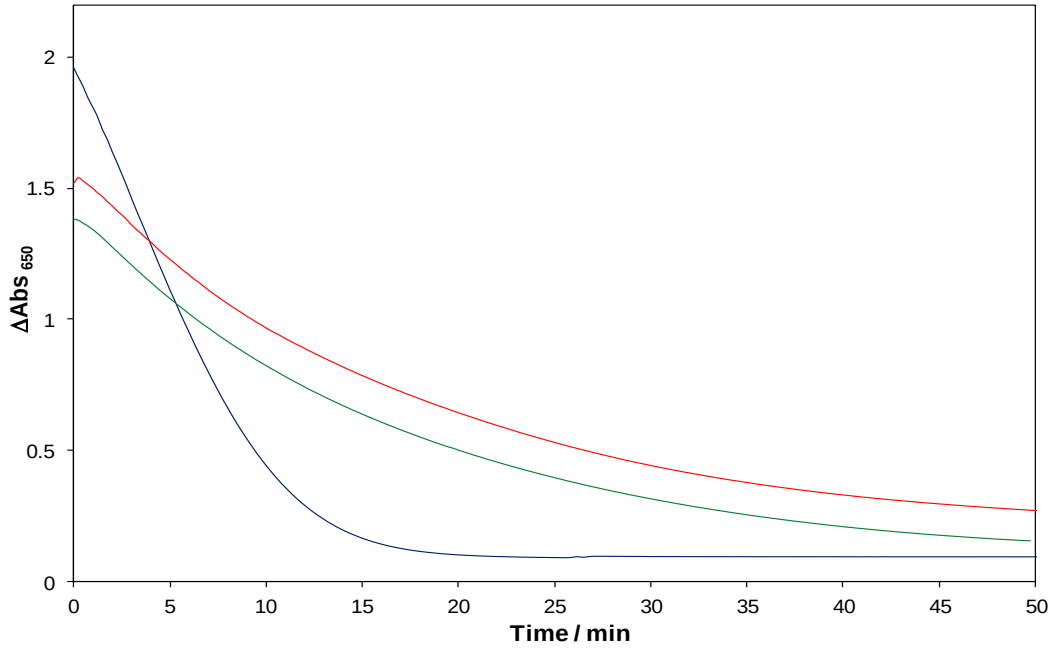

Figure 7.14 A plot of ΔAbs_{650} against time for typical LG films of different ages, including a fresh film, a 12-month-old film and a 24-month-old film, upon exposure to H_2O_2 vapour from a 1 wt% H_2O_2 aqueous solution. The flow rate used was 2 l min^{-1}.

Age of film	**Relative Rate of Bleaching**
Fresh	1
12 months	0.36
24 months	0.38

Table 7.1 A comparison of the relative reaction rates of bleaching of LG films with 1 wt% H_2O_2 aqueous solution.

7.3.5 Comparison of LG films with starch-iodide paper

A commonly employed indicator of the presence of strong oxidising agents such as H_2O_2 is, of course, starch-iodide paper. However, this very effective indicator needs to be damp in order to allow the dark blue starch–iodide complex to be formed.[24] If water is not present the less colourful straw-yellow colour of iodine is generated. Figure 7.15 (a) and (b) illustrate the typical colour responses of both dry and damp commercial starch-iodide paper when placed above a 50 wt% aqueous H_2O_2 solution.

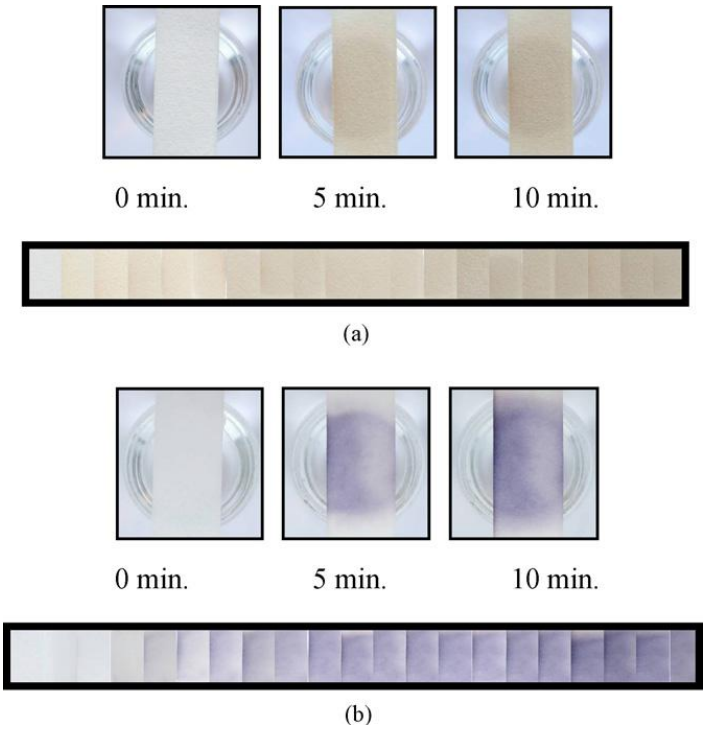

Figure 7.15 Photographs illustrating the colouration of (a) dry and (b) wet starch-iodide paper when placed above a 50 wt% aqueous H_2O_2 solution.

The response times of dry and damp starch-iodide paper are similar to that of a LG film, but only the damp starch-iodide paper produces a striking colour response. Although an attractive method for detecting the presence of a strong oxidising agent, such as H_2O_2, in many cases the need to wet the indicator makes the starch-iodide paper test less convenient that the LG film-based indicators.

7.3.6 Selectivity

To determine whether or not the LG/PVA hydrogen peroxide sensors would photobleach with other peroxide and hypochlorite based bleaching agents a selection of common household bleaching agents were purchased and used to test a series of typical LG/PVA films by sitting a typical film over the opening of a sample vial containing the bleaching agent under test and time observing what, if any bleaching occurs. The bleaching agents used are found below with their key ingredients listed as well:

1. Domestos Thick Bleach, Original

   - Sodium Hypochlorite (4.9g per 100g)

   - Less than 5% Chlorine based bleaching agents and Non-ionic surfactants.

2. Flash with Bleach

   - Sodium Hypochlorite and Anionic surfactants (<5%)

3. Vanish Oxi-Action Stain Remover

   - Oxygen based bleaching agent, Phosphonate and Anionic surfactants (<5%)

4. Care+ Hydrogen Peroxide Solution 6% BP (Thompson & Ross)

   - 6% w/v H_2O_2

   - Phosphoric acid, Phenacetin

5. Blond Cream Peroxide, 40 vol. 12% (Jerome Russell)

   - Hydrogen Peroxide,

   - Centimonium Chloride, Cetyl alcohol, Ceteth-2-Ceteareth-25, Phosphoric acid, Oxiquinadline sulphate

6. Hydrogen Peroxide solution 50% w/v (Aldrich)

7. Solution containing 2.5 ml 50% H_2O_2 and 2.5 ml 0.1 M NaOH (25% H_2O_2 and 0.05 M NaOH)

The results are found in Table 7.2 below, and not surprisingly indicate that all hydrogen peroxide based agents are able to fully bleach within 40 minutes. The hypochlorite based bleaches underwent a degree of bleaching but also produced a red coloured compound whose identity is not yet known.

Product	**5 mins**	**10 mins**	**20 mins**	**40 mins**	**16 hours**
1. Domestos Thick Bleach	No change	No change	Slight bleaching	Slight bleaching	Fully bleached with red colour formed
2. Flash with Bleach	No Change	No change	No Change	No Change	Slight bleaching, with red colour forming
3. Vanish Oxi Action	Slight Bleaching	Further Bleaching	Further Bleaching	Fully Bleached	Fully Bleached
4. 6% H_2O_2 solution	Slight Bleaching	Further Bleaching	Further Bleaching	Fully Bleached	Fully Bleached
5. Blonde Cream Peroxide (12%)	Bleaching	Further Bleaching	Fully Bleached	Fully Bleached	Fully Bleached
6. 50% H2O2 solution	Bleaching	Fully Bleached	Fully Bleached	Fully Bleached	Fully bleached
7. 25% H_2O_2, 0.05M NaOH	Bleaching	Fully Bleached	Fully Bleached	Fully Bleached	Fully Bleached

Table 7.2 Bleaching times of and effects to typical LG/PVA films after exposure to common household bleaching products.

An ideal H_2O_2 vapour indicator is one which responds specifically to H_2O_2 vapours; however, both the conventional starch-iodide paper and the LG film-based indicators respond not only to H_2O_2 vapours but also to other volatile strong oxidising agents, such as ozone, chlorine or nitrogen dioxide. This lack of selectivity is obviously undesirable, although the detection of such vapours would be indicative of a liquid

containing a strong oxidising agent and so the ability to detect such agents is still useful.

7.4 Conclusions

LG/PVA films are stable over many months and, in contrast to starch-iodide paper, need no wetting to respond rapidly to the vapour associated with aqueous H_2O_2 solutions that could be used to make so-called 'kitchen sink' explosives *in situ*, i.e. 30 wt% in water. In a flowing gas stream the kinetics of the bleaching process are first order with respect to [LG] and $[H_2O_2]$ at low concentrations $[H_2O_2]$ (<0.5 wt%), but tend to zero-order with respect to $[H_2O_2]$ as the latter is increased above this level. The kinetics of LG bleaching are also dependent upon the film thickness (α 1/*d*), indicating some degree of diffusion control. Overall, these LG/polymer indicators appear promising for the detection of H_2O_2 vapour and other volatile, strong oxidising agents, and so, amongst other things, may find application in the detection of peroxide-based terrorist bombs.

7.5 References

1. G. McDonnell and A. D. Russell, *Clin. Microbiol. Rev.*, 1999, **12**, 149-155.
2. B. M. Andersen, M. Rasch, K. Hochlin, F.-H. Jenson, P. Wismar and J.-E. Fredriksen, *J. Hosp. Infect.*, 2006, **62**, 149-179.
3. G. Fichet, K. Antloga, E. Comoy, J. P. Deslys and G. McDonnell, *J. Hosp. Infect.*, 2007, **67**, 278-286.
4. D. M. Reid, *US Pat. 6,790,411*, 2004.
5. J. Gavin, N. F. Button, I. A. Watson-Craik and N. A. Logan, *Int.Biodeterior. Biodegrad.*, 1995, **36**, 431-440.
6. B. R. Kim, J. E. Anderson, S. A. Mueller, W. A. Gaine and A. M. Kendall, *Water Res.*, 2002, **36**, 4433-4444.
7. A. Tofant, M. Vucemilo, Z. Panic and D. Minic, *Livestock Sci.*, 2006, **102**, 243-247.
8. R. J. Michalowski, S. H. Christiansen, J. Myers and D. A. Wilson, *US Pat. 4,732,650*, 1988.
9. D. F. Laine, C. W. Roske and I. F. Cheng, *Anal. Chim. Acta*, 2008, **608**.
10. F. Dubnikova, R. Kosloff, J. Mlmog, Y. Zeiri, R. Boese, H. Itzkaky, A. Alt and E. Keinan, *J. Am. Chem.*, 2007, **127**, 1146-1159.
11. J. Yinion, *Forensic and Envrionmental Detection of Explosives*, John Wiley&Sons Ltd., 1999.
12. J.J. Van Laar, *Z. Physik. Chem.*, 1910, **72**, 723-751.
13. M. E. Abdelsalam and P. R. Birken, *Phys. Chem. Chem. Phys.*, 2002, **4**, 5340-5345.
14. J. R. Darwent and A. Lepre, *J. Chem. Soc., Faraday Trans.*, 1986, **282**, 1457-1468.
15. S. Das, P. V. Kamat, S. Padmaja, V. Au and S. A. Madison, *J. Chem. Soc., Faraday Trans.*, 1992, 1219-1223.
16. K. Dutta, S. Bhattacharjee, B. Chaudhuri and S. Mukhopadhyay, *J. Environ. Monit.*, 2002, **4**, 754-760.
17. V. Nadtochenko and J. Kiwi, *J. Chem. Soc., Faraday Trans.*, 1997, **93**, 2373-2378.

18. D. M. Davies and A. U. Moozyckine, *J. Chem. Soc., Perkins Trans.2*, 2000, **2**, 1495-1503.
19. P. H. d'Hausen, C. N. Tait and D. M. Davies, *J. Chem. Soc., Perkins Trans.2*, 2002, **2**, 389-403.
20. A. U. Moozyckine and D. M. Davies, *Green Chem.*, 2002, **4**, 4452-4458.
21. K. M. Thompson, W. P. Griffith and M. Spiro, *J. Chem. Soc., Faraday Trans.*, 1993, **89**, 1203-1209.
22. K. M. Thompson, W. P. Griffith and M. Spiro, *J. Chem. Soc., Faraday Trans.*, 1994, **90**, 1105-1114.
23. A. Mills, *Platinum Met. Rev.*, 1997, **41**, 115-127.
24. H. N. McMurray, *J. Mater. Chem.*, 1992, **2**, 401-406.
25. A. Mills and Q. Chang, *Analyst*, 1992, **117**, 1461-1466.
26. T. Yoshinaga, M. Yamaye, T. Kito, T. Ichiki, M. Ogata, J. Chen, H. Fujino, T. Tanimura and T. Yamanobe, *Polym. Deg. Stabil.*, 2004, **86**, 541-547.

Chapter 8

Summary

8. Summary

This author set out to develop novel colorimetric optical sensors for a range of analytes including UV radiation, humidity, hydrogen peroxide and ammonia and other volatile amines. The development and characterisation of each of these indicators has been detailed in the previous chapters. Here follows a short summary of each investigation.

8.1 UV radiation

An investigation into an existing polymer encapsulated UVA specific indicator and dosimeter based on the photocatalytic reduction of a redox dye in the presence of a semiconductor results in the development of a UVB specific dosimeter for use as a sunburn warning indicator. This dosimeter, which responds to the component of UV light responsible for solar-induced biological damage such as sunburn, was well characterised and its sensitivity was found to increase with increasing semiconductor concentration. Thus, its response was tailored to suit specific skin phototypes. Furthermore the redox dye adopted, DCIP, was found to be less susceptible to re-oxidation by ambient O_2 than the MB previously reported for the UVA specific dosimeter. This simplifies the dosimeter production by negating the need for a separate O_2 barrier making it more commercially viable. Unfortunately this dosimeter did not display good shelf-life stability when stored for a period of 2-3 months, gradually decoloring within 25 days.

Previously tetrazoliums dyes had been well characterised in literature for their applications as indicators for the evaluation of bacterial metabolic activity and for γ-radiation monitoring. Less well studied was their potential application for UV dosimetry. Various tetrazoliums were explored and NTC selected as the preferred choice. Further investigation led to the development of a polymer based UV dosimeter containing NTC which undergoes a UV induced reduction to the monoformazan form on NTC. The novel UV dosimeter, whose response

characteristics are dependent on the dye concentration and film thickness but are independent of temperature across the normal operating range, undergoes a striking colour change upon increasing exposure to UV radiation. This factor coupled with the ability to coat the dosimeter with different levels of UV-screening layers to reducing the rate of UV-induced colouration enabled the dosimeter to be tailored for use as a sunburn warning indicator for different skin phototypes.

8.2 Relative humidity

An investigation into existing MB based relative humidity indicators based on monomer and dimer aggregates was performed and some unusual phenomena discovered. When MB was encapsulated within a polymer such as HEC with a notable excess of urea (20 times w/w more than MB), the product ink was blue, but cast as a thin, opaque pink film under ambient (RH 60%, T 20^{o}C) or dry conditions. This film was then rapidly and reversibly rendered blue coloured and clear when exposed to RH values >85%. Notably the observed colour changes for MB/urea/HEC films were the opposite of those observed previously for MB based RH indicators, suggesting the dimer and trimer aggregates were responsible for the observed colour changes. Alternative formulations containing other deliquescent urea-like compounds were also investigated with limited success.

8.3 Ammonia and volatile amines

A range of novel intelligent pigments were developed by coating inorganic substrates with pH sensitive dyes. By dispersing such pigments in thin films of an extrudable thermoplastic polymer a range of intelligent plastics were developed. The films of varying sensitivity were characterised with respect to ammonia and other volatile amines including some of those associated with food spoilage. Their application as potential indicators of fish spoilage was successfully demonstrated.

8.4 Hydrogen peroxide vapour

LG/PVA films for the detection of H_2O_2 were developed and found to be stable over many months. In contrast to starch-iodide paper, they need no wetting to respond rapidly to the vapour associated with aqueous H_2O_2 solutions that could be used to make so-called 'kitchen sink' explosives *in situ*, i.e. 30 wt% in water. In a flowing gas stream the kinetics of the bleaching process are first order with respect to [LG] and $[H_2O_2]$ at low concentrations $[H_2O_2]$ (<1 wt%), but tend to zero-order with respect to $[H_2O_2]$ as the latter is increased above this level. The kinetics of LG bleaching are also dependent upon the film thickness (α 1/*d*), indicating some degree of diffusion control. Overall, these LG/polymer indicators appear promising for the detection of H_2O_2 vapour and other volatile, strong oxidising agents, and so, amongst other things, may find application in the detection of peroxide-based terrorist bombs.

8.5 Further Work

- The issue of long term stability with the DCIP/SnO_2/Glycerol/HEC UVB specific dosimeters is a very real one and is something that must be rectified if this technology were to be used to produce a commercial product. Further work was carried out on a similar dosimetric system using the more stable dye Rz as detailed in Appendix 2. While this system appears promising in this area, this system is complicated by the ability of Rz to undergo a 2 stage reduction first to Rf and then to dihydroresorufin and as a result further investigation is required to fully characterise this dosimetric system. Furthermore as the encapsulation media, HEC, is water soluble, this is highly unsuitable for use as a sunburn warning indicator. Further work is required to take this technology to the next stage and develop a printable solvent-based ink that could be used to print commercial sunburn warning indicators in the form or wristbands or stickers etc.

- The NTC/PVA UV dosimeter, while an effective system does have its drawbacks, among which is the ability to cost-effectively source NTC. This tetrazolium was discontinued from known suppliers during the course of this research and prior to that was only available in small quantities at a relatively high cost. This is less than ideal for the batch production of sunburn warning indicators for retail purposes. It was proposed that the cheaper, more readily available triphenylotetrazolium chloride, TTC, might be a suitable alternative. Further work was carried out on this modified dosimetric system by Dr Michael McFarlane working on a Proof of Concept (POC) programme funded by Scottish Enterprise. Not only did substituting the NTC for TTC produce a castable dosimeter ink with similar response characteristics to the one described in this thesis this work was further extended to incorporate the TTC within a thin extrudable plastic.

- There is scope for further developing the MB/Urea/HEC high RH indicating system, particularly with regards to utilising other hygroscopic, possibly urea-related compounds which undergo deliquescence at different relative humidities (e.g. N,N´dimethyl urea deliquesces at RH >63% at 18 ^{o}C) to generate a set of relative humidity indicators for providing a sharp register of different relative humidity levels for a range of applications. It may also be worthwhile to investigate other ionic dyes which are known to undergo dye aggregation to see if a similar phenomenon occurs or if this process in unique to MB.

- As mentioned in Chapter 6 due to time constraints during the work on A/VA indicators, the indicators discussed were not able to be fully characterised and there is considerable room for further work. Given the previously observed temperature dependence of both the ink-based BPB ammonia sensors and the analogous CO_2 indicating pigments and plastics it is necessary to carry out a temperature study to determine how the sensitivity of the A/VA indicator films varies with temperature. It would also be prudent to carry out a humidity study to determine what effect, if any, humidity has on the A/VA

indicator films' response. Since completing this work additional funding was made available to continue the development of these A/VA pigments and plastics for the food packaging industry. In recent years these pigments along with the analogous CO_2 indicating pigments have been used to prepare dye-coated polymer beads which can then be melted and extruded to produce thin films more akin to food packaging materials. This work which was carried out by Dr Graham Skinner and Dr Julie Bardin has attracted much interest from the media and food packaging industry and great steps have been taken towards generating a viable commercial product.

Appendices

A1. Quantum efficiency and quantum yield calculations

The quantum efficiency of a photochemical system is equivalent to the ratio of the output from the system to the input into the system. In these examples, the output is the rate at which the UV induced reduction is occurring and the input is the number of photons striking the UV dosimeters every second. Below is a detailed outline of the calculation performed for the DCIP dosimeter.

The first step in determining the quantum efficiency is to calculate the concentration of the dye causing the colour change.

This calculation assumes that there is no solvent present and the only material that the dye is dispersed in is the polymer for NTC, and the polymer and glycerol for DCIP. It is further assumed that as the dye is present at such a low concentration, and is dissolved in the polymer its contribution to the volume will be negligible. The calculation for DCIP is shown below.

The concentration of DCIP present was calculated using the following equation:

$$[DCIP] = \left(\frac{\frac{(mass_{DCIP}(g))}{MW_{DCIP}}}{\left(\frac{mass_{HEC}(g)}{\rho_{HEC}(g/mL)}\right) + \left(\frac{mass_{GLYC}(g)}{\rho_{GLYC}(g/mL)}\right)} \right) * 1000 \qquad \text{(A1.1)}$$

Where the mass $_{DCIP}$ = 0.005 g, MW $_{DCIP}$ 290.09, mass $_{HEC}$ = 0.1 g, ρ_{HEC} = 0.6 g/mL, mass $_{GLYC}$ = 0.1 g and ρ_{GLYC} = 1.25 g/mL. Resulting in [DCIP] = 0.0699 M.

The next step is to convert the initial rate of the DCIP reduction under 1 mW cm^{-2} UVB radiation, determined from the slope of the plot of initial rate against irradiance (Figure 4.5) from Abs units s^{-1} mW^{-1} cm^2 to molecules cm^{-2} s^{-1}.

For DCIP this was done as follows,

Slope of the plot of initial rate against irradiance (r_i) = 0.0018 Abs units s^{-1} mW^{-1} cm^2

ΔAbs_{636} (i.e. absorbance at 636 nm – background absorbance) = 0.4055

Measured film thickness (d) = 0.000385 cm

The number of moles of dye (n_o) was calculated using equation (A1.2)

$$n_o = \frac{[DCIP]}{1000} * d \qquad \text{(A1.2)}$$

So that n_o = 2.690 x10^{-8} moles.

Next, the number of moles cm^{-2} s^{-1} (R_i) was determined using equation (A1.3)

$$R_i = \frac{r_i}{\Delta Abs_{636}} * n_o \qquad \text{(A1.3)}$$

This value can them be converted to molecules cm^{-2} s^{-1} (R_i*) using equation (A1.4)

$$R_i^* = R_i \text{ x } N_A \qquad \text{(A1.4)}$$

Where N_A is Avogadro's constant, 6.023×10^{23} molecules mol^{-1} and as such $R_i^* = 7.193 \times 10^{13}$ molecules cm^{-2} s^{-1}.

To determine the amount of incident photons from a 1 mW cm^{-2} UVB lamp striking the surface of the dosimeter per second, the energy associated with the wavelength of the UV source (E) has to be calculated. For a UVB lamp the main emission peak is present at 315 nm, so using equation A1.5, $E = 6.306 \times 10^{-19}$ J.

$$E = \frac{hc}{\lambda} \tag{A1.5}$$

Where h is Planks constant = 6.626×10^{-35} J s^{-1}, and c is the speed of light in a vacuum = 2.998×10^{8} m s^{-1}.

For a 1 mW cm^{-2} lamp, the no? of incident photons (N_p) can be calculated using equation A1.6 below,

$$Np = \frac{0.001}{E} \tag{A1.6}$$

Such that 1.58×10^{15} photons hit the surface every second.

Thus, the quantum efficiency can be calculated using equation A1.7,

$$QE = \frac{R_i^*}{N_p} \tag{A1.7}$$

The quantum efficiency for the DCIP film = 0.118 molecules $photon^{-1}$.

As not all the UVB light is absorbed by the DCIP film it is perhaps more meaningful to calculate the quantum yield, using equation A1.8

$$QY = \frac{R_i^*}{N_p * f} \quad \text{(A1.8)}$$

Where the fraction of UVB light being absorbed, f is defined as:

$$f = (1 - 10^{\Delta Abs315,\ t=0}) \quad \text{(A1.9)}$$

The ΔAbs at 315 nm for a standard DCIP film prior to irradiation is 0.811, which gives a quantum yield equal to 0.0536.

A similar method was used to determine the quantum efficiency and quantum yield for the NTC dosimeters. The only difference in the procedure is the calculation of the concentration of the formazan. As the amount of formazan present in the film at the end of the irradiation is not known, [formazan] was estimated using equation A1.10

$$[formazan] = \frac{Abs}{\varepsilon l} \quad \text{(A1.10)}$$

Where $\Delta Abs_{532,}$ at t=30 minutes was equal to 0.112, the pathlength, l, is equal to the film thickness, 2.3 μm and the molar extinction coefficient is taken as that of the monoformazan in ethanol, ε = 22,000 dm^3 mol^{-1} cm^{-1} as reported by Altman *et al.*[1] This last step assumes that ε of the formazan is the same in a PVA film as it is in ethanol and allows the approximate [formazan] to be calculated. Based on this assumption for the NTC dosimeter films QE = 0.0021 molecules $photon^{-1}$, and QY = 0.0034.

The assumption that ε is the same in ethanol as it is in PVA films may not hold true as it is possible that at the high concentrations found within the dosimeter, formazan dimers are formed. If this were to occur the ε would be smaller, which would result

in a higher [formazan] and consequently a higher quantum efficiency and yield would result, e.g. if ε = 11,000 dm^3 mol^{-1} cm^{-1} (i.e. half the assumed value) then the new *QE* = 0.0042 molecules $photon^{-1}$ and *QY* = 0.0069.

A1 References

1. F. P. Altman and R. G. Butcher, *Histochemie*, **37**, 1973, 333-350.

A2. UV dosimeter based on resazurin and tin(IV)oxide

A2.1 Introduction

In a recent paper we reported a colorimetric UV indicator and dosimeter that utilises semiconductor photocatalysis.[1] Photocatalysis is a term used to describe the "acceleration of a photoreaction by presence of a catalyst" where the phrase "photoreaction" is synonymous with the terms "photo induced" or "photo activated" reaction.[2]

The UVA indicator[1] comprised a hydroxy ethyl cellulose film containing the redox dye, methylene blue (MB), the sacrificial electron donor triethanolamine (TEOA) and titania nano particles (TiO_2). The TiO_2 nanoparticles absorb the UV light and photo-oxidise the TEOA. The trapped photogenerated electrons are then able to reduce the redox dye from its highly coloured (blue) oxidised form, i.e. MB, to its colourless form, leuco methylene blue, LMB. Oxygen present in air reacts rapidly with the LMB, re-oxidising it to MB. As a result the degree of bleaching exhibited by a naked MB film is directly dependent upon the level of UVR, due to a dynamic equilibrium between the photoreduction process (MB→LMB) and the dark re-oxidation process (LMB + O_2→MB). When covered with an O_2 impermeable barrier, such as glass or regenerated cellulose, the latter step is not possible and the covered MB film is able to act as a UV dosimeter.

In the above UV indicator/dosimeter the titania particles absorb light of wavelengths ≤ 380 nm thus are very responsive to both UVA and UVB light. However, as noted earlier, it is mostly the UVB component of solar UV that is responsible for solar-induced biological damage, such as sunburn. Clearly what is required is a semiconductor photocatalyst that has a larger band gap than titania (3.2 eV) and so is more effective in absorbing UVB light, than UVA. In addition, a more attractive alternative to MB as a redox indicator would be a dye that is not only readily reduced by the photogenerated electrons generated on the semiconductor photocatalyst

particles but, unlike MB, has a reduced form that is not readily re-oxidised by ambient O_2. Such a feature would avoid the need for an O_2 barrier and make fabrication of this UVB sensitive dosimeter relatively simple. In this chapter the characteristics of such an improved UV dosimeter, using tin(IV)oxide, SnO_2, as the large band-gap, UVB-absorbing semiconductor (3.5 eV) and Resazurin (Rz) as the O_2-insensitive redox indicating dye will be described.

A2.2 Experimental

A2.2.1 Materials

The tin(IV)oxide (SnO_2) used in the Rz dosimeter films was >100 nm nanopowder purchased from Aldrich Chemicals, with particle sizes typically ranging from 10-70 nm as determined using SEM and TEM, see Figures A2.1.

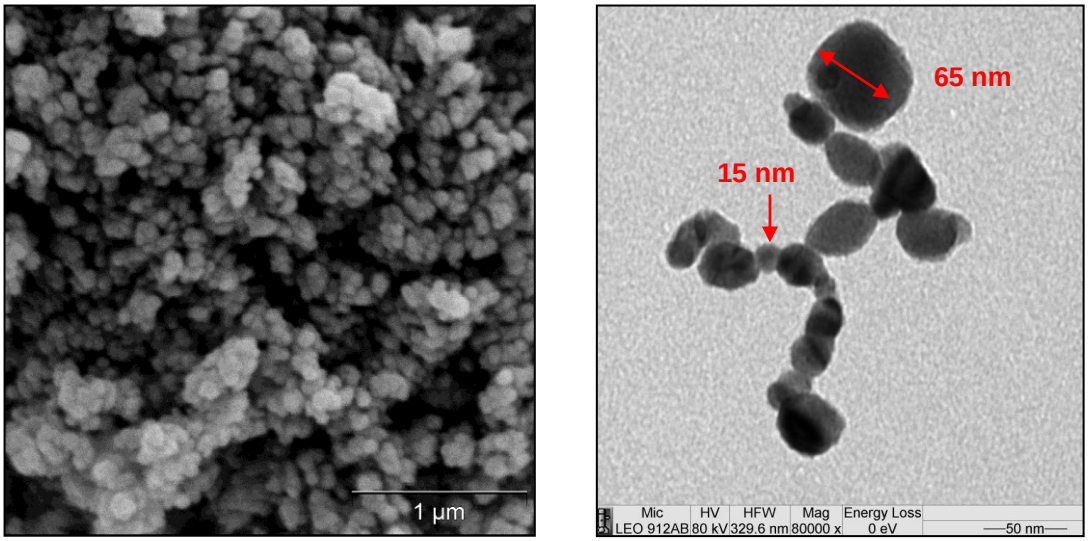

Figure A2.19 (a) SEM Image of SnO_2 nanopowder at x30,000 magnification and (b) TEM Image of SnO_2 nanopowder at x80,000 magnification.

A2.2.2 UV ink and dosimeter preparation

A typical UV dosimeter casting ink was prepared by dissolving 5 g of HEC in 95 ml water at room temperature, followed by stirring for 24 hours. 5 mg of Rz, 100 mg SnO_2 and 100 mg glycerol were then added to 2 g of the HEC polymer solution. The solution was well stirred to ensure dissolution of the dye and the dispersion of the SnO_2. The blue-coloured casting solution contained 5 phr of Rz *i.e.* 5 parts per hundred resin (or 5 g of Rz for 100 g polymer). Films were cast on quartz discs, 25 mm in diameter and 1 mm thick, using a spin coater. Thus, a few drops of casting solution were deposited on the surface of the disc, which was then spun at 2400 rpm for 15 seconds. The resultant product was then dried for 2-3 minute at 70°C and cooled to room temperature (5 minutes) before use. The final UV dosimeter film product was a blue coloured, *ca.* 3.85 μm thick film on a quartz disc and shall be referred to forthwith as a standard Rz film.

A2.3 Results and discussion

A2.3.1 Optical characteristics of a Rz film

A series of casting solutions were prepared comprising the standard Rz UV sensitive ink formulation with various components omitted, with the exception of the encapsulating polymer HEC and solvent, water. These solutions were used to cast the following films on quartz discs: HEC, Glycerol/HEC, Rz/HEC and the typical dosimeter itself Rz/SnO_2/Glycerol/HEC. The UV/Visible absorption spectra of these films were recorded and the results are illustrated in Figure A2.2.

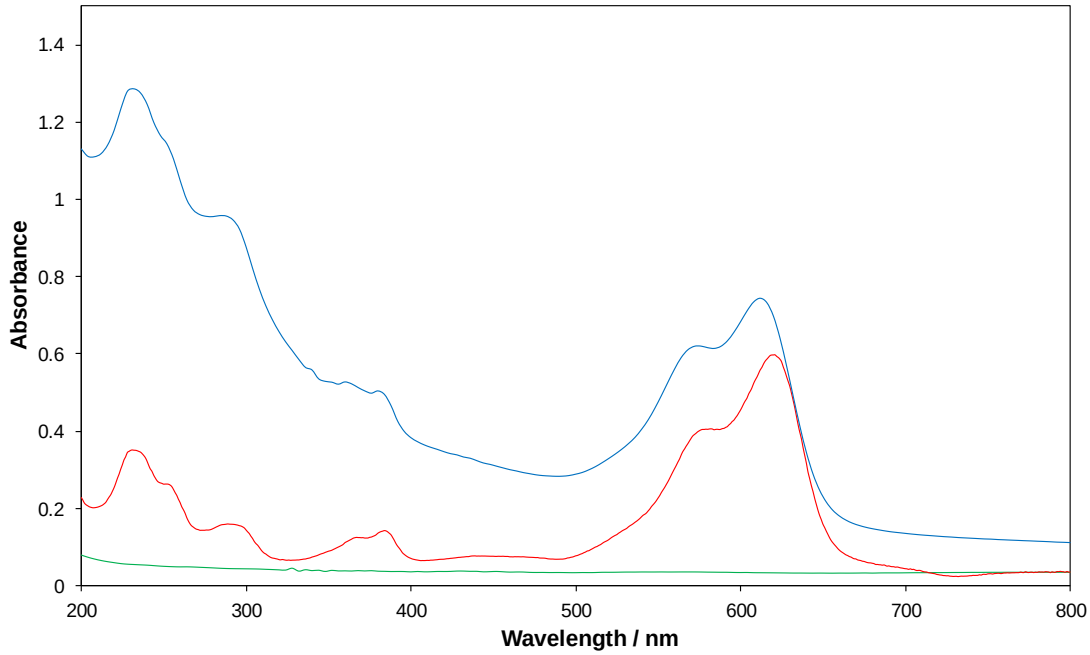

Figure A2.20 Absorption spectrum of standard Rz film prior to irradiation. Also shown are the absorption spectra for a blank HEC film and glycerol/HEC film and also a Rz/ HEC film.

From Figure A2.2 it is clear that the polymer (HEC), the electron donor (glycerol) and the redox dye, RZ, do not absorb to any great extent in the UVA and UVB regions (≤ 380 nm), whereas SnO_2 does absorb significantly, especially in the UVB region. SnO_2 is a wide band-gap semiconductor (E_g = 3.5 eV *i.e.* absorption threshold 354 nm)[6] and is responsible for the broad, strong absorption band between 200 and 300 nm seen in the UV visible absorption spectrum of the standard ink film (see Figure A2.2). The standard Rz film spectrum has a maximum absorption, λ_{max}, at 612 nm which gives the film its blue colour.

When irradiated with UVB light (λ_{max} (emission) = 315 nm) a typical Rz film changes colour from blue to pink as seen in Figure A2.3.

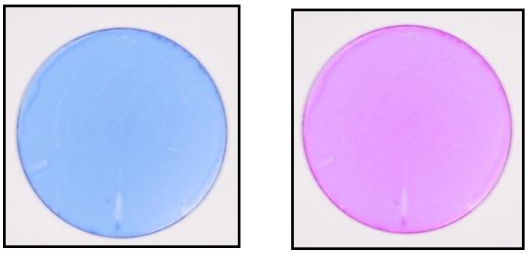

(a) (b)

Figure A2.21 Photographs of a typical Rz film (a) before and (b) after exposure to UVB light.

This process was monitored spectrophotometrically *via* the disappearance of the absorption band due to the Rz at 612 nm. The colour change observed arises as a result of photogenerated holes in the SnO_2 reacting with the glycerol present, a sacrificial electron donor, to yield glyceraldehdye which can then be oxidised further to glyceric acid. The photogenerated electrons are then able to reduce Rz to its pink form Resorufin (Rf) as depicted in Figure A2.4. With prolonged exposure the photogenerated electrons can further reduce the resorufin to dihydroresorufin. These major processes are illustrated in the reaction scheme in Figure A2.5.

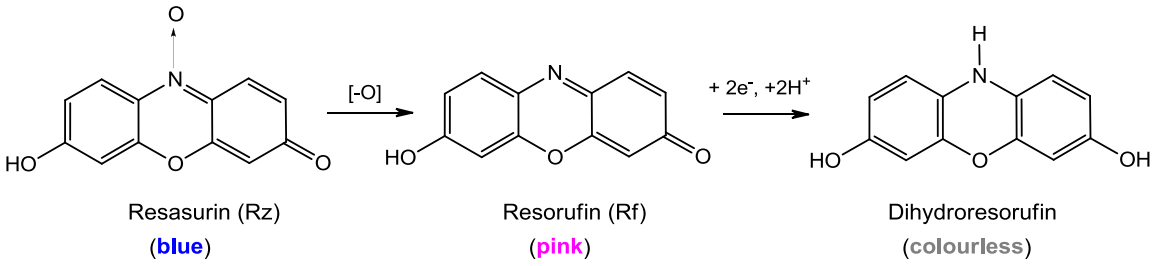

Figure A2.22 Mechanism for the reduction of Rz (blue) to Rf (pink) and dihydroreserufin (colourless).

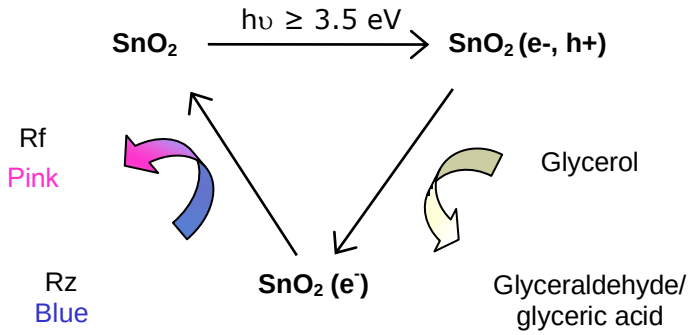

Figure A2.23 Reaction scheme illustrating the main mechanistic features of a typical Rz/ SnO_2/Glycerol/HEC UV indicator film, upon irradiation with UVB light.

A typical set of UV/visible absorption spectra recorded for a Rz film as a function of UVB irradiation time are illustrated in Figure A2.6. Using these data, and additional results from the same experiment, using 3 mW cm^{-2} UVA it was possible to plot the variation in the change in absorbance at λ_{max} *i.e.* ΔAbs_{636}, as a function of irradiation time, which is illustrated in the in Figure A2.7.

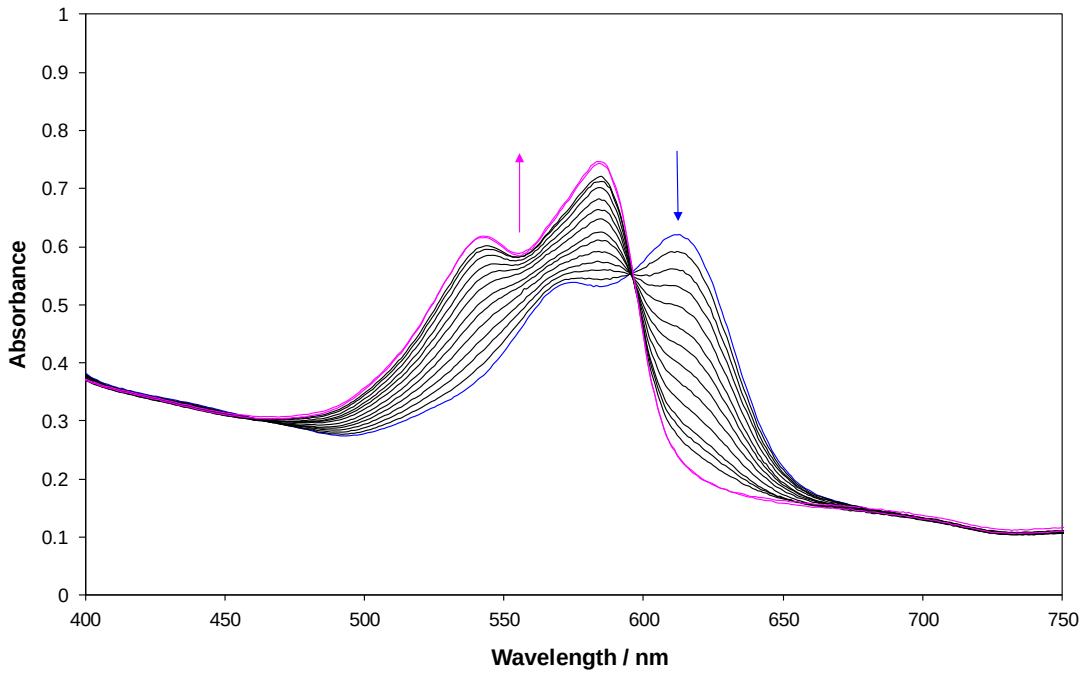

Figure A2.24 Absorption spectra of a typical Rz film after irradiation with 3 mW cm^{-2} UVB light

A similar experiment was conducted using a film containing only Rz and HEC (i.e. no SnO_2 or Glycerol) and 3 mW cm^{-2} UVB light and the data obtained used to generate the third series in Figure A2.7.

These results show that the photo-induced reduction of the standard Rz film was not observed when the film was irradiated with 3 mW cm^{-2} UVA light, rather than UVB, indicating that the light emitted by the UVA lamp (a black light lamp, λ_{max} (emission) = 365 nm) does not contain photons of sufficient (high) energy to create the necessary electron-hole pairs to effect the photoreaction of Rz. Other work showed that even when UVB light was used no decolouration occurred for a Rz film in which the SnO_2 had been omitted (see Figure A2.7) *i.e.* the SnO_2 semiconductor sensitizer particles are essential for the Rz film to work as a dosimeter.

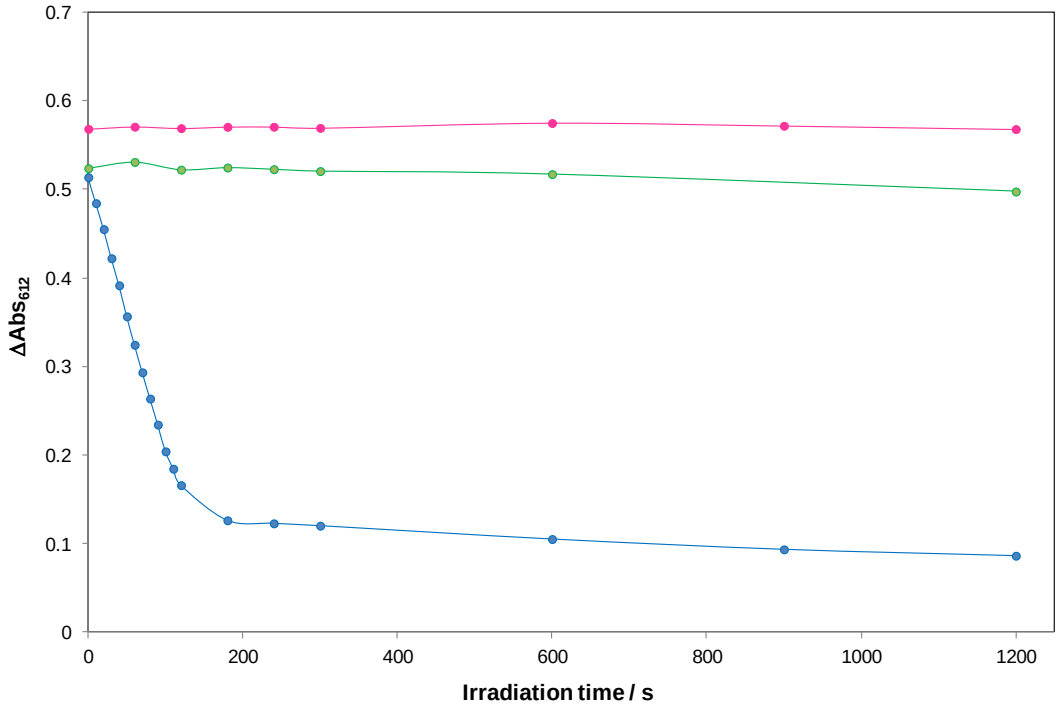

Figure A2.25 ΔAbs_{612} vs. irradiation time plot for a typical Rz film irradiated with 3 mW cm^{-2} UVB. Also shown is the analogous plot for a typical Rz film irradiated with 3 mW cm^{-2} UVA light and a Rz alone film (i.e. no SnO_2) irradiated with 3 mW cm^{-2} UVB.

A2.3.2 Kinetics of photobleaching of a Rz film

A2.3.2.1 Irradiance

In one set of experiments, a number of standard Rz films were exposed to different UVB irradiances ranging from 1-6 mW cm^{-2} from the UVB source with a total exposure time of 300 seconds. The absorbances (at $\lambda = 612$ nm) of the Rz films under test were measured spectrophotometrically and the initial rate, r_i, of decolouration for each film was determined from the plot of the change in absorbance, ΔAbs_{612}, as a function of irradiation time. The results of this work are illustrated in Figure A2.8 along with the associated plot of r_i as a function of UVB irradiance in Figure A2.9.

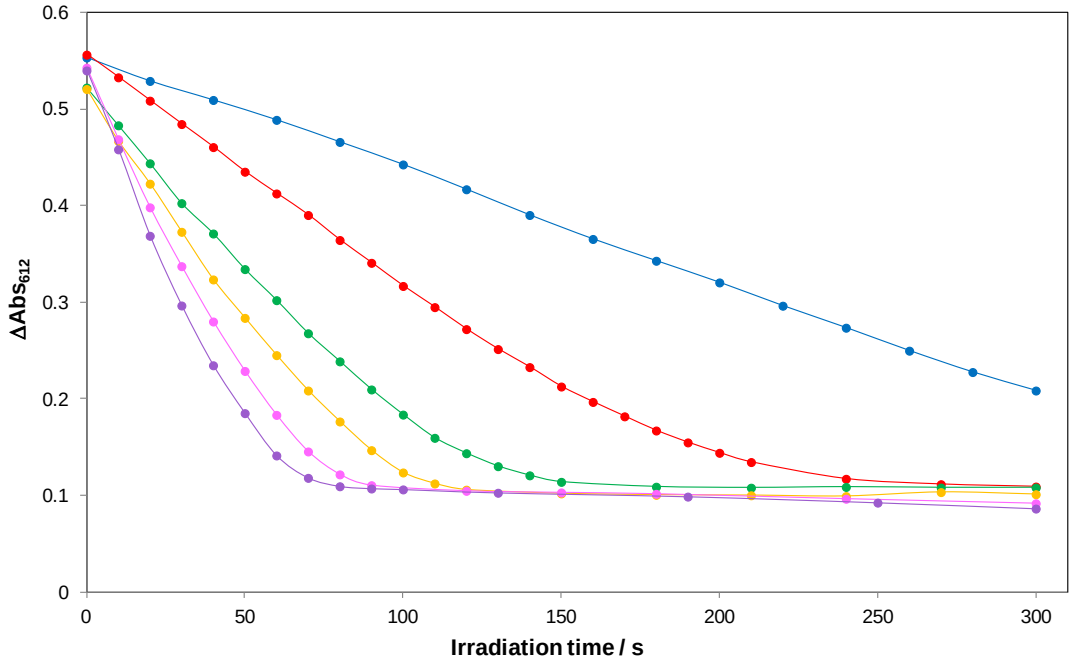

Figure A2.26 A plot of ΔAbs_{636} against irradiation time for typical Rz dosimeter films after irradiation with 1 mW cm^{-2} , 2 mW cm^{-2}, 3 mW cm^{-2}, 4 mW cm^{-2}, 5 mW cm^{-2} and 6 mW cm^{-2} UVB light.

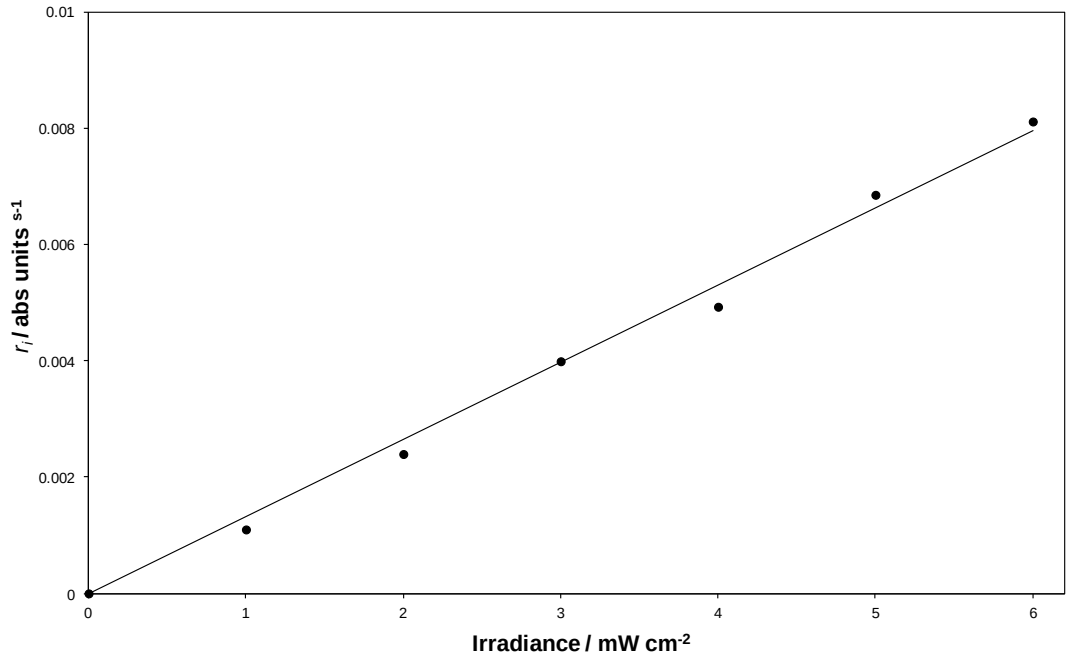

Figure A2.27 A plot showing the variation of r_i with irradiance, calculated using the data in Figure A2.8.

The observed direct dependence of r_i upon irradiance at these irradiance levels is not unusual in semiconductor photocatalysis[8,9] and, in this case, is indicative of very effective trapping of the photogenerated holes by the glycerol present. The Rz concentration in a standard Rz film is 0.08 M (≡ 5 phr) and film thickness is 0.0003 cm, which allows the number of moles of Rz per cm^{-2}, *i.e.* n_o, to be determined as 2.81 x 10^{-8} moles cm^{-2}. Using this information, the gradient of the line of best fit to the data in Figure A.19 (= 0.0013 Abs units s^{-1} mW^{-1} cm^2) and the initial ΔAbs_{612} of a Rz film (0.573), the initial number of Rz molecules that are photobleached cm^{-2} s^{-1}, R_i^* was determined as 3.95 x 10^{13} molecules cm^{-2} s^{-1}. Since the UVB lamp used in this work emitted ~1.59x10^{15} photons s^{-1} cm^{-2}, and the fraction of UVB light (*i.e.* light at 315 nm) absorbed by the Rz film was determined to be 0.734), a value for the quantum yield of the photobleaching process of *ca.* 3.4% was calculated. The above data is tabulated below in Table A2.1 and the methods used to determine such values are detailed in Appendix 1.

UVR	d (μm)	λ (nm)	Rate, R_i^* (x10^{13}molecules/cm^2/s)	QE (molecules/photon)	f_{UVR}	QY
UVB	3.5	315	3.95	0.025	0.734	0.0339

Table A2.1 Optical and photocatalytic properties for RZ dosimeter films, where d = film thickness, λ = emission wavelength from UVB source (i.e. wavelength of light being absorbed by films), QE =quantum efficiency, f_{UVR} = fraction of UVR light being absorbed by dosimeter films and QY = quantum yield.

A2.3.2.2 [Resazurin]

The effect of dye concentration on the kinetics of the system was investigated by preparing a series of films with varying levels of Rz. A set of casting inks were prepared containing 1 to 20 phr Rz, which were cast on to quartz discs and irradiated with 3 mW cm^{-2} UVB light. The r_i of decolouration for each film was determined from the plot of ΔAbs_{612} against irradiation time profiles illustrated in Figure A2.10. A subsequent plot of r_i *vs.* [Rz], shown as an inset in Figure A2.10, indicates that r_i does not change significantly with [Rz] suggesting the kinetics of Rz photobleaching are zero order. Such zero order kinetics are not uncommon in semiconductor photocatalysis, especially where coatings on photocatalytic films are involved,[28] and indicates that Rz molecules occupy all the available photocatalytic sites. This is hardly surprising as the standard film has an effective [Rz] of approximately 0.08 M in the film.

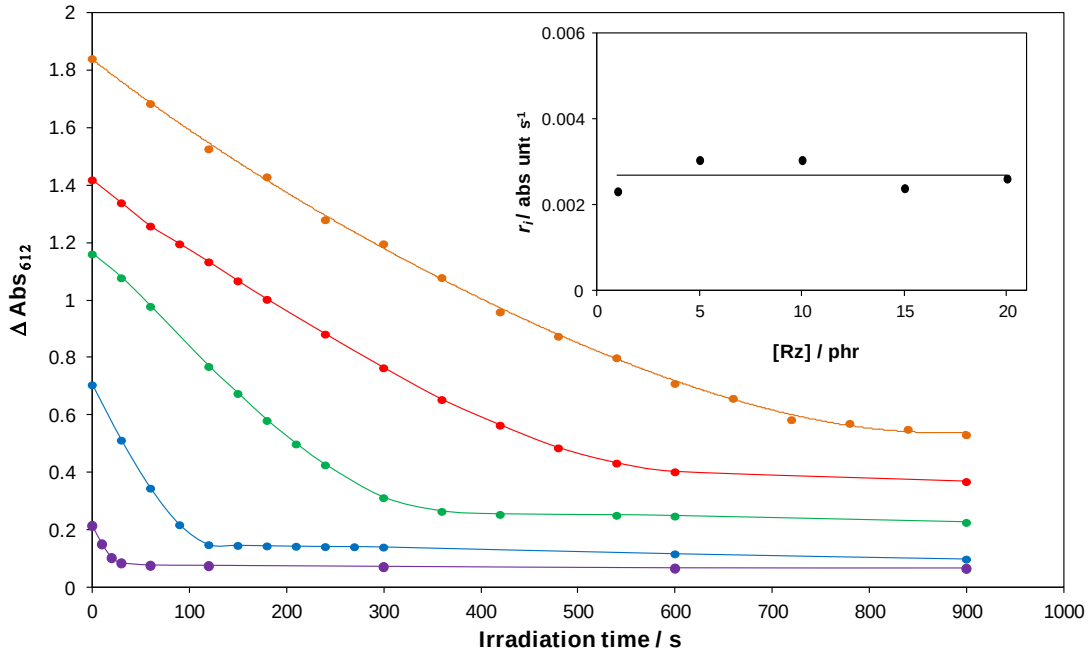

Figure A2.28 A plot of ΔAbs_{636} against irradiation time for HEC films containing 20 phr, 15 phr, 10 phr, 5 phr and 1 phr Rz, 100 phr glycerol and 100 phr SnO_2 upon irradiation with 3 mW cm^{-2} UVB. Inset diagram shows the variation of r_i with [Rz], calculated using the data in the main diagram.

A2.3.2.3 [SnO_2]

The sensitivity of the standard Rz UV dosimeter towards UVB light can be readily varied by changing the amount of UV absorbing semiconductor (SnO_2) present. Thus, a series of SnO_2/Rz/glycerol/HEC casting inks were prepared containing 10 to 200 phr SnO_2 and used to spin-coat films on quartz discs. Using these films a series of ΔAbs_{636} versus irradiation time profiles were generated with a 3 mW cm^{-2} UVB source and the results are illustrated in Figure A2.11. The value of r_i for each film was determined from these profiles and found to be directly proportional to the level of SnO_2 present over the range studied, i.e. $r_i = 4.78 \times 10^{-5} [SnO_2]$ with a correlation coefficient value of 0.988 as seen in Figure A2.12. As it is the UVB activation of the semiconductor which initiates the reduction reaction and $r_i \propto I_{abs}$ (see Figure A2.9)

which in turn depends upon [SnO_2], it was expected that an increase in [SnO_2] would in turn cause an increase in the rate of reduction.

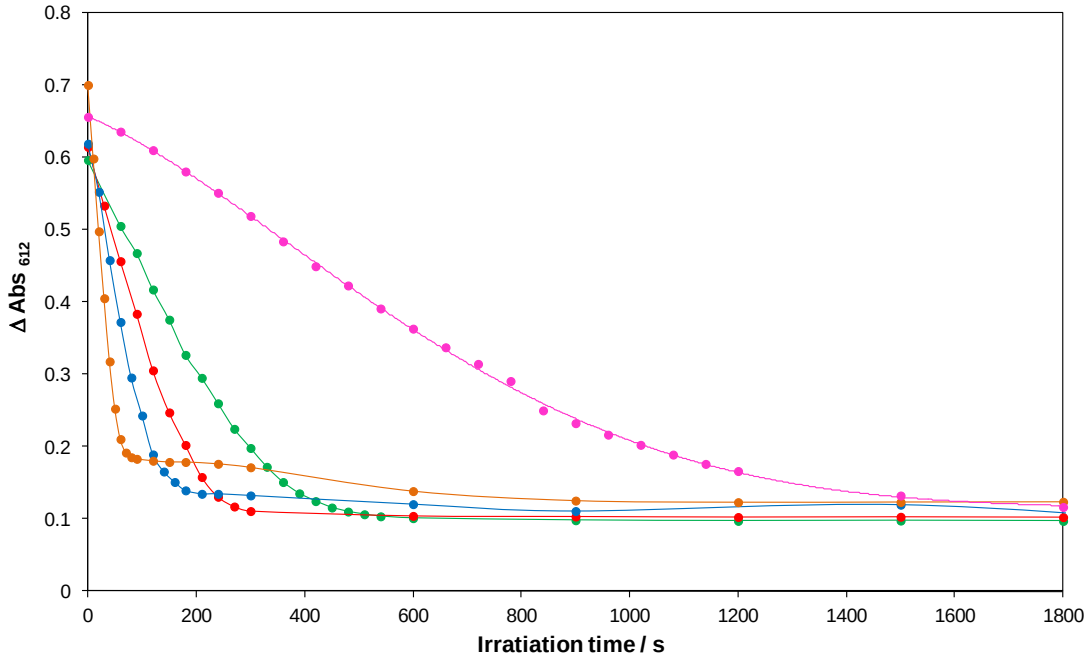

Figure A2.29 A plot of ΔAbs_{636} against irradiation time for HEC films containing 5 phr Rz, 100 phr glycerol and 10 phr, 30 phr, 50 phr, 100 phr and 200 phr SnO_2 after irradiation with 3 mW cm^{-2}.

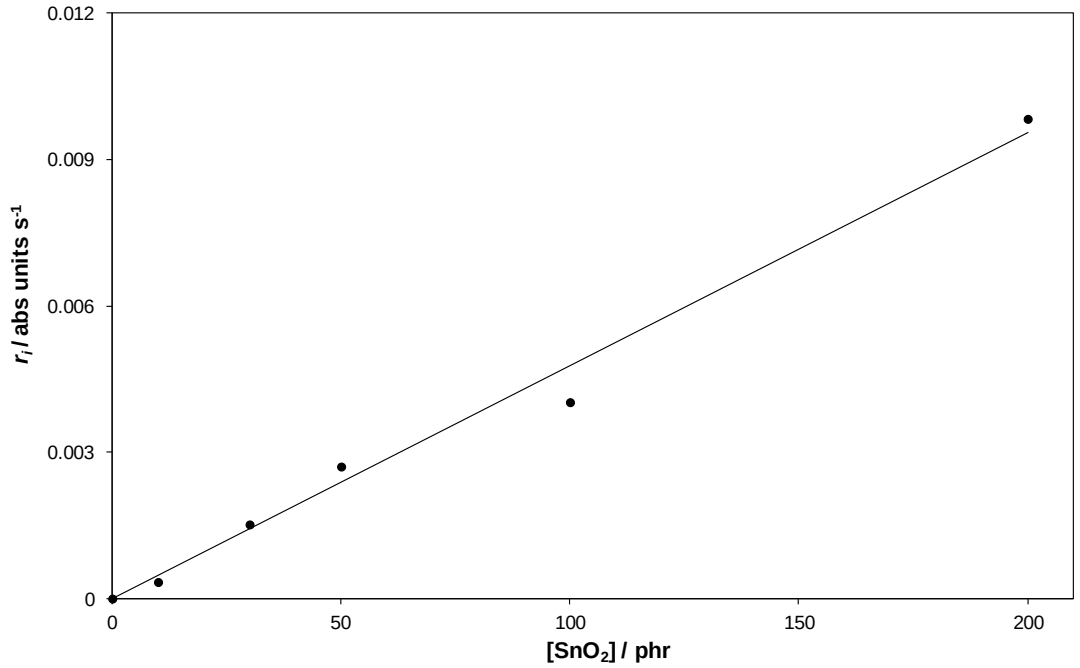

Figure A2.30 A plot of r_i against [SnO_2].

A2.3.3 Solar-simulator UV work using a Rz film

In a final set of experiments UV solar simulated light (UVI 5) was used to irradiate a standard RZ film. The observed variation of the absorbance of this film at 636 nm, *i.e.* ΔAbs_{636}, as a function of MED (for skin type II) is illustrated in Figure 3.18. These results show that a standard Rz ink is a little too UV sensitive for use as an indicator of impending sunburn for someone with skin type II since it is fully bleached by MED = 0.45.

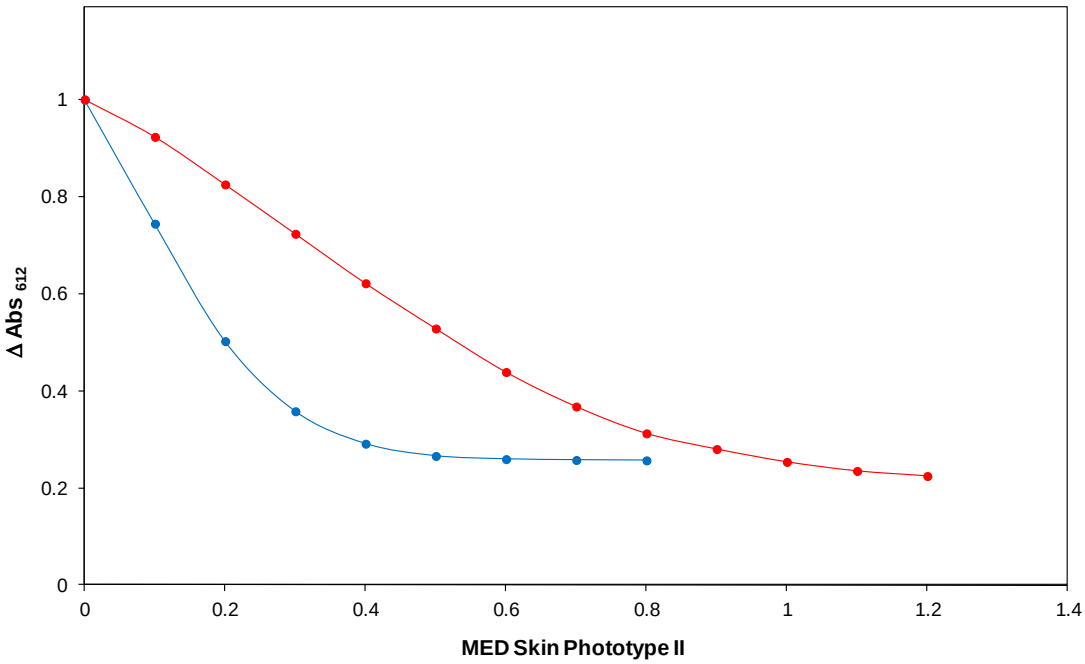

Figure A2.31 A plot of ΔAbs_{636} against MED for skin phototype II received for HEC films containing 5 phr Rz, 100 phr glycerol with 100 phr (standard formulation) and 50 phr SnO_2, on exposure to solar simulated light at UVI 5.

However, previous work had demonstrated that the UV sensitivity of a RZ/SnO_2/glycerol/HEC film can be moderated by using less SnO_2. (see Figure A2.12). Thus, in a separate experiment the level of SnO_2 in the RZ film formulation was dropped from 100 to 50 phr and its photobleaching monitored as a function of MED, the results of which are also illustrated in Figure A2.13.

These findings show that the latter film is bleached by an MED = 1.1 and so is an appropriate warning indicator of a solar UV dosage sufficient to cause sunburn in a person with skin type II. By varying the levels of SnO_2 it is possible to make UV dosimeters that would indicate when sunburn was imminent for most other skin types

A2.3.4 Longevity of Rz films

In order to be viable as a commercially available sun protection product the Rz dosimeter must have a reasonable shelf life, say 3 to 6 months but ideally >12 months. A set of standard Rz UV dosimeter films were therefore prepared and stored in a sealed container and monitored periodically. Unlike the DCIP UV dosimeter previously developed the Rz films still maintained their initial blue colour and responded to UVB light after storage in the dark under ambient conditions for 1 year.

A2.4 Conclusions

HEC films, containing the dye Rz, in the presence of SnO_2 and glycerol undergo a semiconductor-activated reduction when exposed to UVB radiation. The rate at which the dosimeter film photobleaches increases with increasing UV irradiance and the system has a quantum efficiency of *ca*. 3.4%. The kinetics of photobleaching are directly proportional to the level of SnO_2 and to a lesser extent the level of glycerol present but are independent of [Rz]. The Rz UVB dosimeter films respond well to solar simulated light and can be tailored to be fully photobleached at different MED levels (for different skin types) by varying the level of SnO_2 present, and as such have great potential in the role of warning of imminent sunburn for different skin types.

A2.4 References

1. A. Mills, S. Lee and M. Sheridan, *Analyst*, 2005, **130**, 1046-1051.
2. A. Mills and S. L. Hunt, *J. Photochem. Photobiol. A:Chem*, 1997, **108**, 1-35.
3. A. I. Martinez, D. R. Acosta and G. Cedillo, *Thin Solid Films*, 2005, **4090**, 118-123.
4. H. Ohsaka, N. Konai, Y. Funkunga, M. Suzukia, T. Watanabe and K. Hashimoto, *Thin Solid Films*, 2006, **502**.
5. A. Fujishima, T. E. Reilkoff, A. W. Lemon, M. M. Scherer and B. A. Balko, *Photochem.Photobiol. C:Photochemistry Reviews*, 2000, **1**, 1-21.
6. W. Liao, E. Yang, J. Chou, W. Chung, T. Sun and S. Hsiung, *IEEE Trans. Elect. Dev.*, 1999, **46**, 2278-2281.
7. J. M. Ottaway, in *Indicators*, ed. E. Bishop, Pergamon Press, Oxford, 1972.
8. A. Mills, J. Wang and M. McGrady, *J. Phys. Chem.*, 2006, **110**, 18324-18331.
9. A. Mills, G. Hill, M. Crow and S. Hodgen, *J. Appl. Electrochem.*, 2005, **35**, 641-653.

A3 Publications

- UV dosimeter based on dichlorindophenol and tin(IV)oxide A. Mills, P. Grosshans, Analyst, 135, 2009, 845-850.

- UV dosimeters based on neotetrazolium chloride, A. Mills, P. Grosshans and M. McFarlane, J. Photochem. Photobiol. A: Chemistry, 201, 2009, 136-141.

- Flagging up sunburn: a printable, multicomponent UV-Indicator that warns of the approach of erythema, Chem. Commun., A. Mills, K McDiarmid, M. McFarlane P. Grosshans 11, 2009, 1345-1346.

- A novel reversible relative-humidity indicator ink based on methylene blue and urea, A. Mills, P. Grosshans and D. Hazafy, Analyst, 2010, 135, 33–35

- Intelligent pigments and plastics for CO_2 detection, A. Mills, G. A. Skinner and P. Grosshans, J. Mater. Chem., 2010, 20, 5008-5010.

- Hydrogen peroxide vapour sensor, A. Mills, P. Grosshans and E. Sadden, Sens. Acuat. B: Chemical, 136, 2009, 458-463.

Analyst

Interdisciplinary detection science

www.rsc.org/analyst

Volume 134 | Number 5 | May 2009 | Pages 809–1012

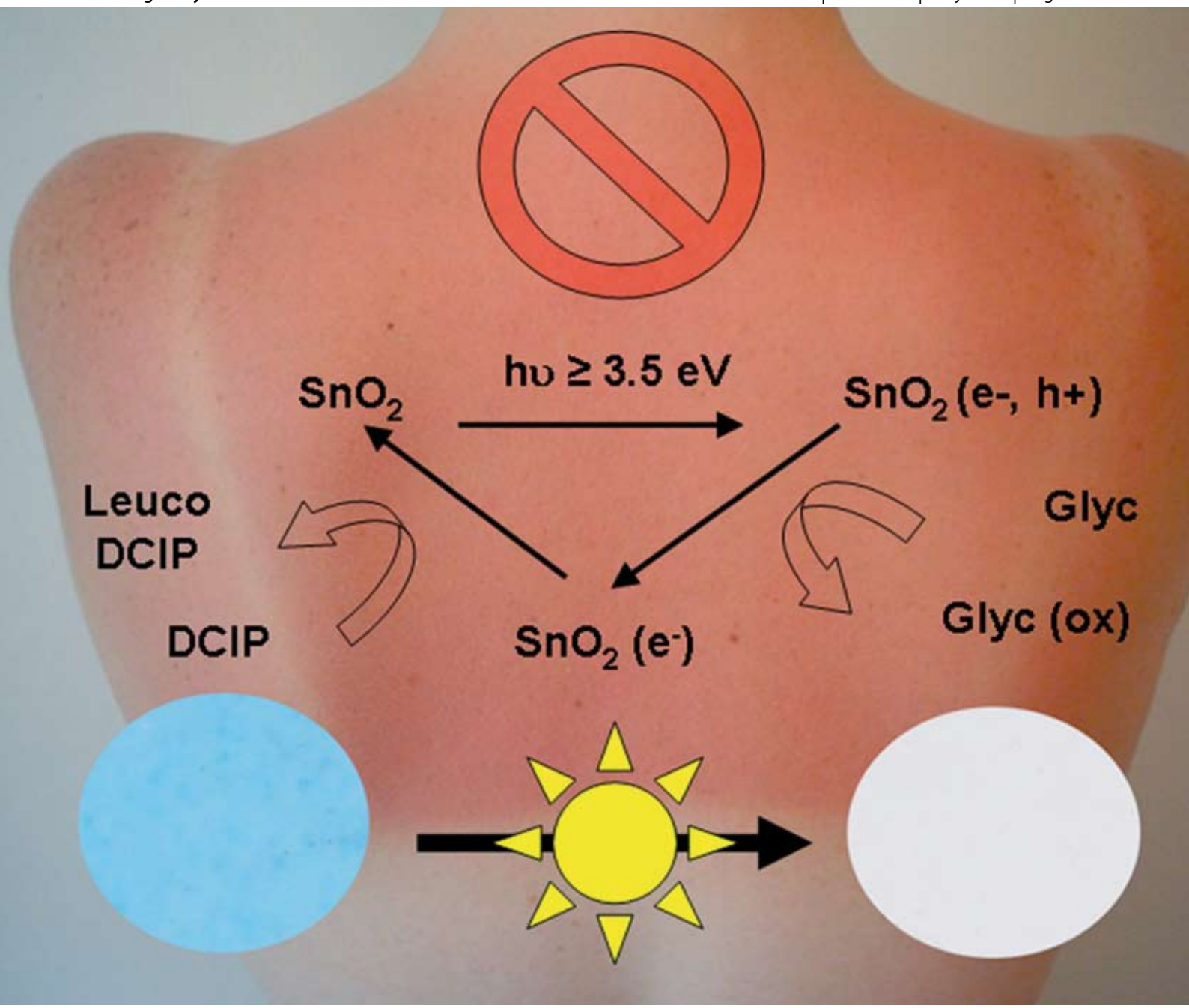

ISSN 0003-2654

RSC Publishing

UV dosimeter based on dichloroindophenol and tin(IV) oxide

Andrew Mills* and Pauline Grosshans

Received 12th November 2008, Accepted 6th February 2009
First published as an Advance Article on the web 27th February 2009
DOI: 10.1039/b820288e

A UVB specific dosimeter is described comprising: a redox dye (2,6-dichloroindophenol, DCIP), a semiconductor (tin(IV) oxide, SnO_2) and a sacrificial electron donor (glycerol) dispersed in a polymer (hydroxy ethyl cellulose, HEC) film. The dosimeter is blue in the absence of UVB light but rapidly loses colour on exposure to UVB light. The spectral characteristics of a typical UVB dosimeter film and the mechanism by which the colour change occurs are detailed. DCIP UVB dosimeter films exhibit a response that is related to the irradiance level and duration of UVB exposure, the level of SnO_2 present and to a lesser extent the level of glycerol present. The response of the dosimeter appears to be independent of dye concentration and film thickness. Furthermore, DCIP UVB dosimeter films respond to solar simulated light, exhibiting a colour loss that can be simply related to the Minimal Erythemal Dose (MED) exposure for skin type II. As a consequence, such indicators have potential for measuring solar radiation exposure and providing an early warning of erythema for most Caucasian skin (*i.e.* skin type II).

Introduction

Ultraviolet radiation (UVR) is the section of the electromagnetic spectrum which lies between X-rays and visible light. The greatest natural source of UV radiation is the sun, although many artificial sources also exist including: black-lights, halogen lights, fluorescent and incandescent lamps, welding arcs and certain types of lasers. UVA, *i.e.* electromagnetic radiation spanning the wavelength range 315–400 nm, is the most common, naturally-encountered form of UVR, as only a small portion of solar UVA is absorbed by atmospheric ozone while the reverse is true for solar UVB, *i.e.* 280–315 nm, a large portion of which is blocked by the ozone layer. On a typical summer's day approximately 6% of terrestrial light is UVB and this contributes 80% towards the harmful effects associated with the sun, while the remaining 94% UVA contributes to the remaining 20%.[1] The higher energy UVR, UVC light ($\lambda < 280$ nm), is not observed in nature at significant levels as it is absorbed by the earth's atmosphere.

Over-exposure to UVR can be hazardous to human health and the severity of the damage depends on many factors including: the source of UV, its wavelength and intensity, the duration of exposure and an individual's sensitivity towards UVR. Short-term exposure can cause acute effects such as erythema, *i.e.* the reddening of the skin or sunburn, and enhanced melanogenesis, the process that causes an individual to develop a suntan. While the latter still remains a largely socially-desired side effect, the former is not. UVR can also damage DNA under the skin resulting in local immune suppression.[2] Acute UV-induced ocular conditions include photokeratitis and photo-conjunctivitis, which are best described as the reversible sunburn of the cornea and conjunctiva respectively.[2] Although neither condition normally results in long-term damage, in severe cases of photokeratitis, blindness can occur resulting in the loss of vision for 2–3 days.

Chronic exposure to UVR has several other severe health consequences. For example, UVR causes damage to human DNA, and while DNA has the capability to mend itself, errors can arise during the repair and replication steps and as a result cumulative DNA damage can encourage the development of skin cancers.[3–8] Skin cancers are classified as either malignant melanoma (MM) or non-melanoma skin cancer (NMSC). NMSC is described as either basal cell carcinoma (BCC) or squamous cell carcinoma (SCC). According to Cancer Research UK,[9] around 75 000 cases of NMSC are diagnosed each year in the UK; however, since it is readily treatable and frequently cured, it is often omitted from national statistics. In contrast, MM is not easily treated and statistics show that each year in the UK, approximately 9000 malignant melanoma cases are diagnosed and around 1800 die from the condition.[9] Chronic ocular conditions associated with long-term UVR exposure include one of the most common causes of vision impairment worldwide, cataracts. This is a clouding of the lens, which blocks the passage of light entering the eye that, consequently, obscures vision. Cataracts are commonly encountered among the elderly and require surgery to correct.

Incident UV levels are often reported in terms of the Global Solar UV Index (UVI)[10] which characterises ultraviolet radiation levels on the earth with a value that provides an overall indication of the UV intensity of the incident sunlight and its ability to cause erythema. It can take on values ranging from zero upward, with higher values signifying a greater potential to cause harm in a given time period. Thus, on a typical summer's day in the UK the UVI is typically 5 (Glasgow) or 6 (London) (*i.e.* 125–150 mW m^{-2}) at around mid-day.[11]

The amount of solar UV radiation absorbed by the skin at any time is known as the erythemal dose. In quantifying an

University of Strathclyde, Department of Pure and Applied Chemistry, Thomas Graham Building, 295 Cathedral Street, Glasgow, UK G1 1XL. E-mail: a.mills@strath.ac.uk; Fax: +44 (0) 141 548 4822; Tel: +44 (0) 141 548 2458

individual's personal exposure to UVR, the term the '*minimum erythemal dose*' (MED) is useful, where the MED is defined as the minimum amount of radiation likely to cause erythema. The MED for an individual is largely dependent on their skin type, of which there are six (I–VI).[1] For example, for individuals with skin phototype II, which is typical for many Caucasians, the MED is equal to 250 J m^{-2}, *i.e.* 69.4 mW m^{-2} per hour. Since a UVI value of 1 $\equiv$ 25 mW m^{-2} it follows that even under mild UV solar conditions such as a UVI value of 3 (*i.e.* 75 mW m^{-2}) as may be observed in April or September in the UK[11] most Caucasians will sunburn within 1 hour if not properly protected.

As a consequence, there is an increasing need for an inexpensive, disposable, personal UV dosimeter, which would provide an individual with a continuous measure of their total UV exposure during the day. An excellent review on personal UV dosimeters is given by the International Commission on Illumination, CIE.[12]

There are many electronic UV dosimeters available; unfortunately, most are rather bulky and relatively expensive for personal use.[13] Since erythema is a consequence of DNA damage, it follows that very effective UV dosimeters can be constructed based on biological material, such as: spores, bacterial cells or bacteriophages.[14,15] The only downside to such biological dosimeters is the need to develop the films, which can take typically up to a day.

A number of promising UV-activated photochemical reactions have been identified as possible routes to generate an effective dosimeter, and some have been commercialised. Perhaps the most well-known of these use thin films of polysulfone,[16,17] a polymer which, upon exposure to UV, increases in its absorbance in the UV due to a photodegradation reaction. The polymer which is normally incorporated in a badge is particularly successful because polysulfone has an initial spectral profile not too dissimilar to that of the spectral responsivity of human skin with respect to erythemal sources. The main practical drawback to this dosimeter is the need for a UV absorbance spectrophotometer to measure the change in film absorbance, since it is not assessable by eye (*i.e.* no distinct colour change occurs).

One commercial product which does undergo a visible colour change is the solar wristband developed by Solar Safe®[18,19] for people with skin type II. It comprises a polymer matrix in which a structurally photochromic material is dispersed. The wristbands are personal dosimeters, which change colour upon exposure to UVR and are designed to indicate when to apply sunscreen and when it is time to get out of the sun. The wristband changes from light brown to purple upon initial exposure to UV as a result of a photochromic reaction and, over time, this species degrades, and the wristband turns dark brown, indicating the need to reapply sunscreen. Prolonged UV radiation of the wristband returns it to its original light brown colour, and signals that sunburn is imminent.[18] Interestingly, others have reported on the limited applicability of photochromics as inexpensive UV indicators due to the often marked temperature sensitivity of the colour change.[19]

SunHealth Solutions LCC has produced a dosimeter called a SunSignal UV Sensor.[21,22] These respond specifically to UVB radiation and are comprised of a radiation-sensitive material, including an organic halogen such as hexachloroethane, which is capable of producing at least one acidic product, such as HCl, upon UV exposure, and a pH indicator, such as methyl orange, capable of producing a colour change in response to the UV generation of the acidic product.[22] The dosimeter is originally yellow in colour and progresses though various shades of orange before finally turning red and indicating that it is time to get out of the sun.

In a recent paper we reported a colorimetric UV indicator and dosimeter that utilises a semiconductor photocatalyst.[23] The UVA indicator comprised an hydroxy ethyl cellulose film containing: the redox dye, methylene blue (MB), the sacrificial electron donor triethanolamine (TEOA) and titania (TiO_2) nanoparticles. The TiO_2 nanoparticles absorb the UV light and photo-oxidise the TEOA. The trapped photogenerated electrons are then able to reduce the redox dye from its highly coloured (blue) oxidised form, *i.e.* MB, to its colourless form, leuco methylene blue (LMB). Oxygen present in air reacts rapidly with the LMB, re-oxidising it to MB. As a result the degree of bleaching exhibited by a naked MB film is dependent directly upon the level of UVR, due to a dynamic equilibrium between the photoreduction process (MB $\rightarrow$ LMB) and the dark re-oxidation process (LMB + O_2 $\rightarrow$ MB). When covered with an O_2 impermeable barrier, such as glass or regenerated cellulose, the latter step is not possible and the covered MB film is able to act as a UV dosimeter.

In the above UV indicator/dosimeter the titania particles absorb light of wavelengths $\leq$380 nm (*i.e.* UVA and UVB light), and as a result the covered MB dosimeters reported previously[23] are very responsive to both UVA and UVB light. However, as noted earlier, it is mostly the UVB component of solar UV that is responsible for solar-induced biological damage, such as sunburn. Clearly what is required is a semiconductor photocatalyst that has a larger band-gap than titania (3.2 eV) and so is more effective in absorbing UVB light than UVA. In addition, a more attractive alternative to MB as a redox indicator would be a dye that is not only readily reduced by the photogenerated electrons generated on the semiconductor photocatalyst particles but, unlike MB, has a reduced form that is not readily re-oxidised by ambient O_2. Such a feature would avoid the need for an O_2 barrier and make fabrication of this UVB-sensitive dosimeter relatively simple. In this paper we describe the characteristics of such an improved UV dosimeter, using tin(IV) oxide (SnO_2) as the large band-gap, UVB-absorbing semiconductor (3.5 eV) and 2,6-dichlorindophenol (DCIP) as the O_2-insensitive redox indicating dye.

Experimental

Materials

All chemicals were purchased from Aldrich Chemicals and used as received unless otherwise specified. The water used to produce inks was double distilled and deionised, and the polymer used to produce the films was hydroxy ethyl cellulose (HEC) (medium viscosity) which was purchased from Fluka. 2,6-Dichlorindophenol sodium salt hydrate, 98% dry weight, was purchased from Alfa Aesar. The tin(VI) oxide used was a nanopowder (< 100 nm particle size (BET)).

Methods

UV/visible spectra for sample films were recorded using a Lambda 35 UV/visible spectrophotometer (Perkin Elmer, UK).

The DCIP UV dosimeter films were irradiated typically for 300 seconds with UVR and absorption spectra recorded at different intervals during this process.

UV irradiation of samples was carried out using UVA or UVB light provided by two 8 W fluorescence tubes (Vilber Lourmat), with the appropriate emission spectra maximum peak in these regions, *i.e.* at 365 and 315 nm respectively. For each of the UV light sources the sample–light source distance was set so that the irradiance (*i.e.* radiant power per unit area) was 3 mW cm^{-2}, as measured using a Multi-sense 100 UV light meter fitted with the appropriate UVA and UVB sensors.

The UV solar simulator used in this work comprised a 180 W xenon arc lamp (Speirs Robertson), with UG5 and WG320 filters placed in-line as described previously by Diffey.[1] The former filter allows transmission at UV wavelengths and absorbs in the visible region, while the latter absorbs in the short wavelength UVC region. The cumulative effect of both filters and the Xe arc lamp is an emission spectrum that provides a good match with the UV spectrum of the sun. The UVI of the UV solar simulated light was measured using a SafeSun™ solar meter[13] and typically found to have a UVI value of 5. The UV-induced colour change in any of the films under test was measured by monitoring the change in absorbance at λ_{max} (636 nm), *i.e.* ΔAbs_{636}, at regular intervals with the spectrophotometer.

UV ink and dosimeter preparation

A typical UV dosimeter casting ink was prepared by dissolving 5 g of HEC in 95 ml water at room temperature, followed by stirring for 24 hours. 5 mg of DCIP, 100 mg SnO_2 and 100 mg glycerol were then added to 2 g of the HEC polymer solution. The solution was well stirred to ensure dissolution of the dye and the dispersion of the SnO_2. The blue-coloured casting solution contained 5 phr of DCIP, *i.e.* 5 parts per hundred resin (or 5 g of DCIP for 100 g polymer). Films were cast on quartz discs, 25 mm in diameter and 1 mm thick, using a spin coater. Thus, a few drops of casting solution were deposited on the surface of the disc, which was then spun at 2400 rpm for 15 seconds. The final product was then dried for 2–3 minutes at 70 °C and cooled to room temperature (5 minutes) before use. The final UV dosimeter film product was a blue-coloured, *ca.* 3.9 μm thick (as measured using a scanning electron microscope) film on a quartz disc, referred to forthwith as a standard DCIP film.

Results and discussion

Optical characteristics of a DCIP film

A series of casting solutions were prepared comprising the standard DCIP UV-sensitive ink formulation with various components omitted, with the exception of the encapsulating polymer HEC and solvent, water. These solutions were used to cast the following films on quartz discs: HEC, glycerol/HEC, DCIP/HEC and the typical dosimeter itself DCIP/SnO_2/glycerol/HEC. The UV/Visible absorption spectra of these films were recorded and the results are illustrated in Fig. 1.

From Fig. 1 it is clear that the polymer (HEC), the electron donor (glycerol) and the redox dye (DCIP) do not absorb to any great extent in the UVA and UVB regions, whereas SnO_2 does absorb significantly, especially in the UVB region. SnO_2 is a wide band-gap semiconductor (E_g = 3.5 eV, *i.e.* absorption threshold 354 nm)[24] and is responsible for the broad, strong absorption band between 200 and 300 nm seen in the UV visible absorption spectrum of the standard ink film (see Fig. 1). The DCIP/HEC spectrum has a maximum absorption, λ_{max}, at 636 nm which gives the film its blue colour.

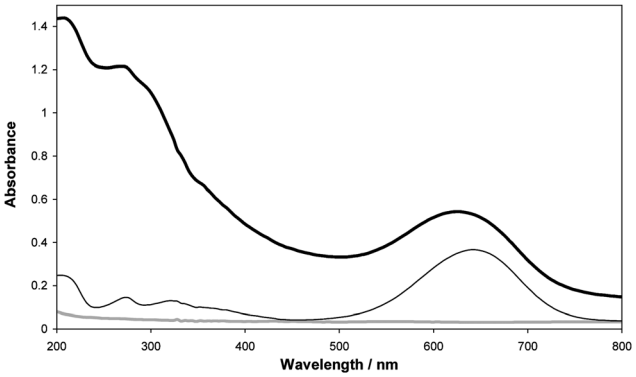

Fig. 1 Absorption spectrum of standard DCIP film prior to irradiation (thick black line). Also shown are the absorption spectra for a blank HEC film and HEC film with glycerol alone (both represented by the same grey line) and HEC with DCIP alone (thin black line).

When irradiated with UVB light (λ_{max} (emission) = 315 nm) a typical DCIP film changes colour from blue to white/colourless as seen in Fig. 2. This process was monitored spectrophotometrically *via* the disappearance of the absorption band due to the DCIP at 636 nm. The colour change observed arises as a result of photogenerated holes in the SnO_2 reacting with the glycerol present, a sacrificial electron donor, to yield glyceraldehyde which can then be oxidised further to glyceric acid. The photogenerated electrons are then able to reduce DCIP to its leuco-form, which is stable in air when encapsulated in HEC, since E° (DCIP/leuco-DCIP) = 0.688 V.[25] These major processes are illustrated in the reaction scheme in Fig. 3.

A typical set of UV/visible absorption spectra recorded for a DCIP film as a function of UVB irradiation time is illustrated in Fig. 4. Using these data, and those from the same experiment conducted using UVA light, it was possible to plot the variation in the change in absorbance at λ_{max}, *i.e.* ΔAbs_{636}, as a function of irradiation time that is illustrated in the inset diagram in Fig. 4. These results show that the photo-induced decolouration of the standard DCIP film was not observed when the film was irradiated with 3 mW cm^{-2} UVA light, rather than UVB, indicating

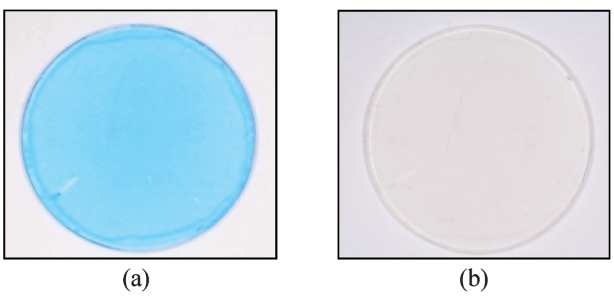

Fig. 2 Photographs of a typical DCIP film (a) before and (b) after exposure to UVB light.

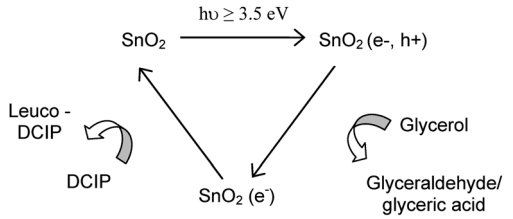

Fig. 3 Reaction scheme illustrating the main mechanistic features of a typical DCIP/SnO_2/glycerol/HEC UV indicator film, upon irradiation with UVB light.

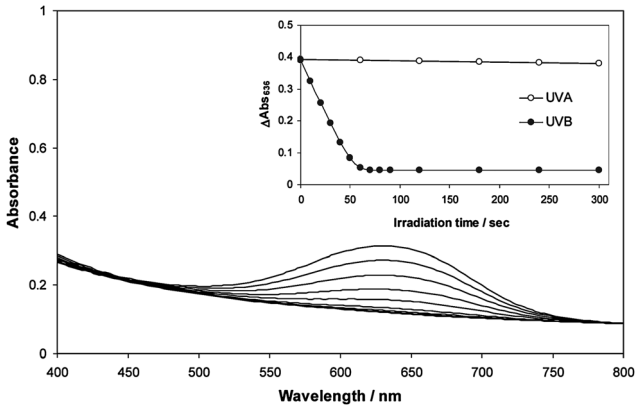

Fig. 4 Absorption spectra of a typical DCIP film during irradiation with 3 mW cm^{-2} UVB light. Inset shows a comparison of a typical DCIP film irradiated with 3 mW cm^{-2} UVA. The spectra were recorded every 10 seconds for the first 90 seconds, then every 30 seconds for a total of 300 seconds.

that the light emitted by the UVA lamp (a black-light lamp, λ_{max} (emission) = 365 nm) does not contain photons of sufficient (high) energy to create the necessary electron–hole pairs to effect the photoreaction of DCIP. Other work showed that even when UVB light was used, no decolouration occurred for a DCIP film in which the SnO_2 had been omitted, *i.e.* the SnO_2 semiconductor sensitiser particles are essential for the DCIP film to work as a dosimeter.

Recovery of DCIP films

In the reaction scheme reported earlier, it was assumed that the photocatalysed bleaching of DCIP by glycerol, sensitised by SnO_2, is irreversible, *i.e.* the reduced form of DCIP, colourless leuco DCIP, is not readily oxidised by ambient oxygen in the polymer/glycerol film environment. This feature is obviously necessary for the DCIP indicator to function as a dosimeter. In order to demonstrate this feature and determine the post-irradiation stability of a photobleached standard film, such a film was fully converted into its bleached form by irradiating for 10 minutes under 3 mW cm^{-2} UVB light and then monitoring the absorbance of the film at 636 nm over the following 12 hours. This work revealed that over this time period the film regained little (8%) of its original colour and, for the purposes of a UV dosimeter, the photobleaching of DCIP can be considered as irreversible.

Kinetics of photobleaching of a DCIP film

In one set of experiments, a number of standard DCIP films were exposed to different UVB irradiances ranging from 1 to 6 mW cm^{-2} from the UVB source with a total exposure time of 300 seconds. The absorbances (at λ = 636 nm) of the DCIP films under test were measured spectrophotometrically and the initial rate, r_i, of decolouration for each film was determined from the plot of the change in absorbance, ΔAbs_{636}, as a function of irradiation time. The results of this work are illustrated in Fig. 5 along with the associated plot of r_i as a function of UVB irradiance. The observed direct dependence of r_i upon irradiance at these irradiance levels is not unusual in semiconductor photocatalysis[26,27] and, in this case, is indicative of very effective trapping of the photogenerated holes by the glycerol present. The DCIP concentration in a standard DCIP film is 0.07 M (≡ 5 phr) and film thickness is 0.00039 cm, which allows the number of moles of DCIP per cm^{-2}, *i.e.* n_o, to be determined as 6.99×10^{-8} moles cm^{-2}. Using this information, the gradient of the line of best fit to the data in the inset in Fig. 5 (= 0.0018 Abs units s^{-1} mW^{-1} cm^2) and the initial ΔAbs_{636} of a DCIP film (0.4055), the initial number of DCIP molecules that are photobleached per cm^2 per second, R_i^* was determined as 7.19×10^{13} molecules cm^{-2} s^{-1}. Since the UVB lamp used in this work emitted ~1.59×10^{15} photons s^{-1} cm^{-2}, and the fraction of UVB light (*i.e.* light at 315 nm) absorbed by the DCIP film was determined to be 0.845, a value for the quantum efficiency of the photobleaching process of *ca.* 5.4% was calculated.

The effect of dye concentration on the kinetics of the system was investigated by preparing a series of films with varying levels of DCIP. A set of casting inks were prepared containing 1–20 phr DCIP, which were cast on to quartz discs and irradiated with 3 mW cm^{-2} UVB light. The r_i of decolouration for each film was determined from the plot of ΔAbs_{636} against irradiation time profiles illustrated in Fig. 6. A subsequent plot of r_i *vs.* [DCIP], shown in the inset diagram in Fig. 6, showed r_i to not change significantly with [DCIP] suggesting that the kinetics of DCIP photobleaching are zero order. Such zero order kinetics are not uncommon in semiconductor

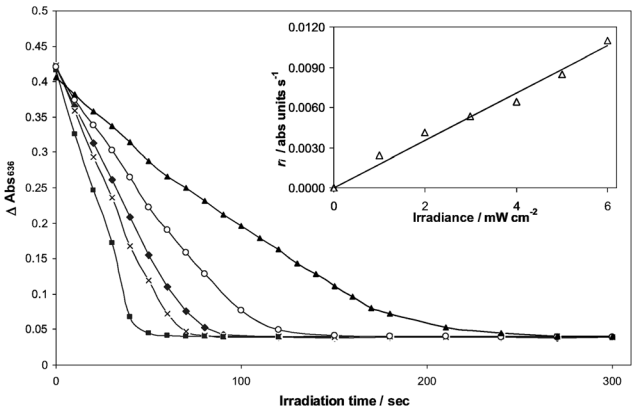

Fig. 5 Plot of ΔAbs_{636} against irradiation time for typical DCIP dosimeter films after irradiation with 1 mW cm^{-2} (▲), 2 mW cm^{-2} (○), 3 mW cm^{-2} (◆), 4 mW cm^{-2} (×) and 5 mW cm^{-2} (■) UVB light. Inset diagram shows variation of initial rate with irradiance, calculated using the data in the main diagram.

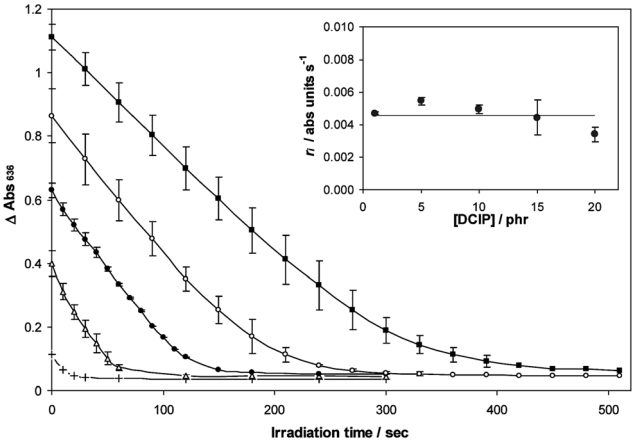

Fig. 6 Plot of ΔAbs_{636} against irradiation time for HEC films containing 20 phr (■), 15 phr (○), 10 phr (●), 5 phr (△) and 1 phr (+) DCIP, 100 phr glycerol and 100 phr SnO_2 upon irradiation with 3 mW cm^{-2} UVB. Inset diagram shows the variation of initial rate with [DCIP], calculated using the data in the main diagram.

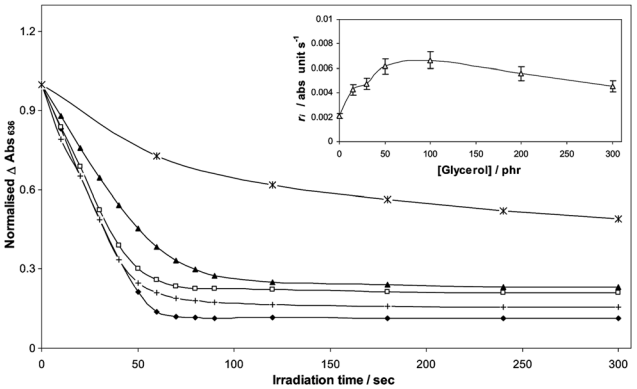

Fig. 8 Plot of ΔAbs_{636} against irradiation time for HEC films containing 5 phr DCIP, 100 phr SnO_2 and 0 phr (*), 15 phr (▲), 30 phr (□), 50 phr (+) and 100 phr (◆) glycerol after irradiation with 3 mW cm^{-2} UVB. Inset diagram shows the variation of initial rate with [glycerol], calculated using the data in the main diagram and from films containing 200 phr and 300 phr glycerol which were also tested.

photocatalysis, especially where coatings on photocatalytic films are involved[28] and indicate that DCIP molecules occupy all the available photocatalytic sites. This is hardly surprising as the standard film has an effective [DCIP] of approximately 0.07 M in the film.

The sensitivity of the standard DCIP UV dosimeter towards UVB light can be readily varied by changing the amount of UV-absorbing semiconductor (SnO_2) present. Thus, a series of SnO_2/DCIP/glycerol/HEC casting inks were prepared containing 10–200 phr SnO_2 and used to spin-cast films on quartz discs. Using these films a series of ΔAbs_{636} *versus* irradiation time profiles were generated with a 3 mW cm^{-2} UVB source and the results are illustrated in Fig. 7. The value of r_i for each film was determined from these profiles and found to be directly proportional to the level of SnO_2 present over the range studied, *i.e.* $r_i = 7.0 \times 10^{-5}[SnO_2]$ with a correlation coefficient value of 0.99. As it is the UVB activation of the semiconductor which initiates the reduction reaction and $r_i \propto I_{abs}$ (see Fig. 5) which in turn depends upon $[SnO_2]$, it was expected that an increase in $[SnO_2]$ would in turn cause an increase in the rate of reduction.

The effect of the level of glycerol present on the initial rate of DCIP film photobleaching was also investigated. As mentioned previously, glycerol acts as a sacrificial electron donor, SED, trapping the photogenerated holes and thus promoting the reduction of the DCIP molecules by the photogenerated electrons. A series of casting inks were prepared, containing different loadings of glycerol covering the range 0–300 phr; these inks were used to produce films which were then irradiated with 3 mW cm^{-2} UVB light whilst their absorbance at 636 nm was monitored. The series of ΔAbs_{612} *versus* irradiation time profiles arising from this work are shown in Fig. 8, along with the variation in r_i as a function of [glycerol] that can be derived from these data, see inset diagram in Fig. 8. These results show that above a glycerol loading of 100 phr the initial rate of photobleaching of DCIP is not improved, suggesting that hole-trapping is very efficient above this level. Also of note is the observation that photobleaching of the DCIP is effected in the absence of glycerol, although at a much slower rate, implying that SnO_2 is able to utilise the polymer, HEC, as an SED.

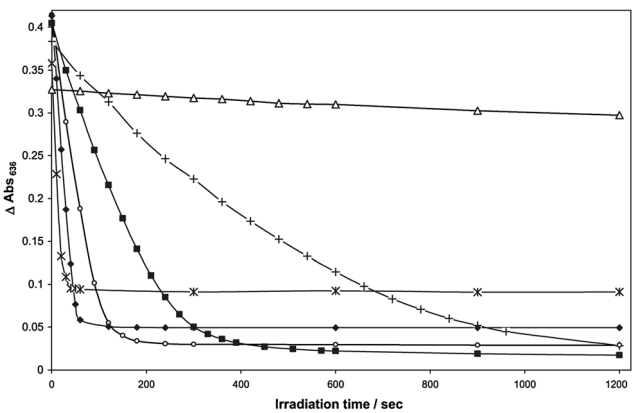

Fig. 7 Plot of ΔAbs_{636} against irradiation time for HEC films containing 5 phr DCIP, 100 phr glycerol and 0 phr (△), 10 phr (+), 30 phr (■), 50 phr (○), 100 phr (◆) and 200 phr (*) SnO_2 after irradiation with 3 mW cm^{-2} UVB.

Solar-simulator UV work using a DCIP film

In a final set of experiments UV solar simulated light (UVI 5) was used to irradiate a standard DCIP film. The observed variation of the absorbance of this film at 636 nm, *i.e.* ΔAbs_{636}, as a function of MED (for skin type II) is illustrated in Fig. 9 (–●–). These results show that a standard DCIP ink is a little too UV-sensitive for use as an indicator of impending sunburn to someone with skin type II since it is fully bleached by MED = 0.4. However, previous work had demonstrated that the UV sensitivity of a DCIP/SnO_2/glycerol/HEC film can be moderated by using less SnO_2 (see Fig. 7). Thus, in a separate experiment the level of SnO_2 in the DCIP film formulation was dropped from 100 to 45 phr and its photobleaching monitored as a function of MED, the results of which are also illustrated in Fig. 9 (–○–).

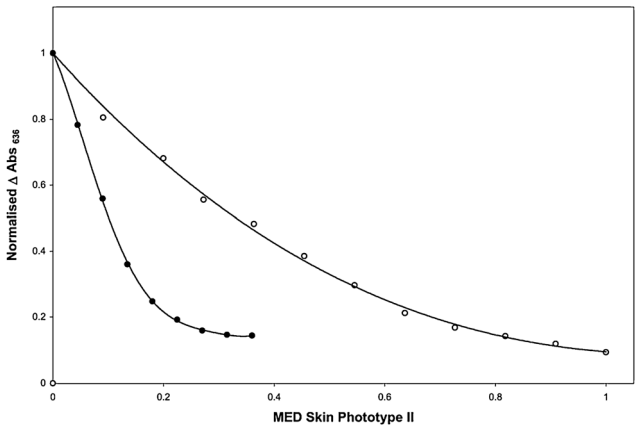

Fig. 9 Plot of ΔAbs_{636} against MED for skin phototype II received for HEC films containing 5 phr DCIP, 100 phr glycerol with 100 phr (●) (standard formulation) and 45 phr SnO_2 (○), spun out at 2400 rpm after irradiation with solar simulated light at UVI 5.

These findings show that the latter film is bleached by an MED = 1 and so is an appropriate warning indicator of a solar UV dosage sufficient to cause sunburn in a person with skin type II. By varying the levels of SnO_2 it is possible to make UV dosimeters that would indicate when sunburn was imminent for most other skin types.

Conclusions

HEC films containing the dye DCIP in the presence of SnO_2 and glycerol undergo a semiconductor-activated reduction in when exposed to UVB radiation. The rate at which the dosimeter film photobleaches increases with increasing UV irradiance and the system has a quantum efficiency of *ca.* 5.4%. The kinetics of the photobleaching film are directly proportional to the level of SnO_2 and to a lesser extent the level of glycerol present but are independent of [DCIP]. The DCIP UVB dosimeter films respond well to solar simulated light and can be tailored to be fully photobleached at different MED levels (for different skin types) by varying the level of SnO_2 present.

References

1 B. L. Diffey, *Methods*, 2002, **28**, 4–13.
2 M. Lebwohl and S. Ali, *J. Am. Acad. Dermatol.*, 2001, **45**, 487–499.
3 http://www.who.int/uv/publications/UVEHeffects.pdf (accessed on 05/11/2008).
4 Y. Matsumura and H. N. Anathaswamy, *Toxicol. Appl. Pharmacol.*, 2004, **195**, 298–308.
5 R. M. Mackie, *Prog. Biophys. Mol. Biol.*, 2006, **92**, 92–96.
6 F. Urbach, *Photochem. Photobiol. B: Biology*, 1997, **40**, 3–7.
7 G. I. Harrison and A. R. Young, *Methods*, 2000, **28**, 14–19.
8 D. W. Edsrtöme, A. Porwit and A. Ros, *Photodermatol. Photoimmunol. Photomed.*, 2001, **17**, 66–70.
9 http://info.cancerresearchuk.org/cancerstats/types/skin/ (accessed on 11/11/2008).
10 http://www.unep.org/PDF/Solar_Index_Guide.pdf (accessed on 11/06/2008).
11 http://www.metoffice.gov.uk/weather/europe/europe_uv.html (accessed on 05/11/2008).
12 CIE Publication No. 98: Personal Dosimetry of UV Radiation, Central Bureau of the CIE, Vienna, 1992.
13 http://www.cgmdirect.com.au/CGM_Main/Archive/SafeSun.htm (accessed on 11/11/2008).
14 L. E. Quintern, G. Horneck, U. Eschweiler and H. Bücker, *Photochem. Photobiol*, 1992, **55**, 389–395.
15 P. Rettberg and C. S. Cockell, *Photochem. Photobiol. Sci.*, 2004, **3**, 781–787.
16 A. Davis, G. H. W. Deane and B. L. Diffey, *Nature*, 1976, **261**, 169–170.
17 B. L. Diffey, Ultraviolet radiation dosimetry with polysulfone film, in *Radiation measurement in photobiology*, ed. B. L. Diffey, Academic Press, New York, 1989, ch. 7, pp. 135–159.
18 www.solarsafe.com/tradepack2007-english.pdf (accessed on 11/11/2008).
19 O. Faran, E. Natan and D. Lastochkin, US Pat. 6132681, 2000.
20 M. Weber, K. Schulmeister and H. Brusl, *Photochem. Photobiol. Sci.*, 2006, **5**, 707–713.
21 http://www.sunhealthsolutions.com/ (accessed on 11/11/2008).
22 S. A. Jackson, US Pat. 6504161, 2003.
23 A. Mills, S. Lee and M. Sheridan, *Analyst*, 2005, **130**, 1046–1051.
24 W. Liao, E. Yang, J. Chou, W. Chung, T. Sun and S. Hsiung, *IEEE Trans. Elect. Dev.*, 1999, **46**, 2278–2281.
25 J. M. Ottaway, in *Indicators*, ed. E. Bishop, Pergamon Press, Oxford, 1972, ch. 8.
26 A. Mills, J. Wang and M. McGrady, *J. Phys. Chem.*, 2006, **110**, 18324–18331.
27 A. Mills, M. McGrady, J. Wang and J. Hepburn, *Int. J. Photoenergy*, 2008, **2008**, 504945.
28 A. Mills, G. Hill, M. Crow and S. Hodgen, *J. Appl. Electrochem.*, 2005, **35**, 641–653.

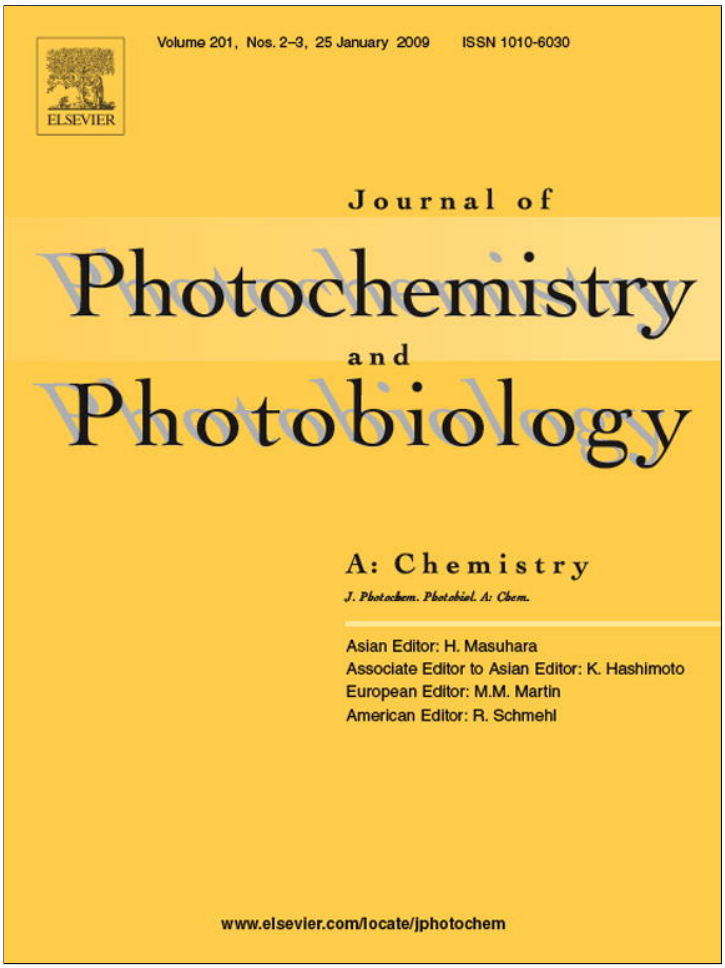

Journal of Photochemistry and Photobiology A: Chemistry 201 (2009) 136–141

Contents lists available at ScienceDirect

Journal of Photochemistry and Photobiology A: Chemistry

journal homepage: www.elsevier.com/locate/jphotochem

UV dosimeters based on neotetrazolium chloride

Andrew Mills*, Pauline Grosshans, Michael McFarlane

WestCHEM, University of Strathclyde, Department of Pure and Applied Chemistry, Thomas Graham Building, 295 Cathedral Street, Glasgow G1 1XL, UK

ARTICLE INFO

Article history:
Received 4 July 2008
Received in revised form 6 October 2008
Accepted 10 October 2008
Available online 21 October 2008

Keywords:
UV dosimeter
Tetrazolium
UV index
MED

ABSTRACT

A novel UV dosimeter is described comprising a tetrazolium dye, neotetrazolium chloride (NTC), dissolved in a film of polymer, polyvinyl alcohol (PVA). The dosimeter is pale yellow/colourless in the absence of UV light, and turns red upon exposure to UV light. The spectral characteristics of a typical UV dosimeter film and the mechanism through which the colour change occurs are detailed. The NTC UV dosimeter films exhibit a response to UV light that is related to the intensity and duration of UV exposure, the level of dye present in the films and the thickness of the films themselves. The response of the dosimeter is temperature independent over the range 20–40 °C and, like most UV dosimeters, exhibits a cosine-like response dependence upon irradiance angle. The introduction of a layer of a UV-screening compound which slows the rate at which the dosimeter responds to UVR enables the dosimeter response to be tailored to different UV doses. The possible use of these novel dosimeters to measure solar UV exposure dose is discussed.

1. Introduction

Tetrazolium salts are water soluble organic heterocycles that can be readily reduced to form partially soluble and insoluble formazans. Tetrazoliums are generally colourless or pale yellow in solution while formazans are highly coloured species typically red, blue and purple. A general tetrazolium reduction reaction is as follows:

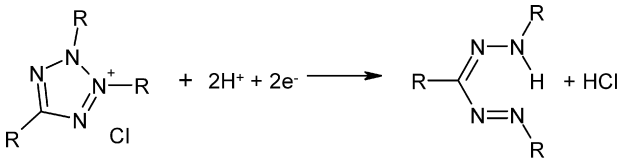

colourless **coloured** (1)

This colour changing reaction has made tetrazolium salts a popular choice of indicator for the evaluation of bacterial metabolic activity [1] as well as the detection of diseases such as tuberculosis [2]. The literature has numerous references to the "Tetrazolium Test" or the "Nitro Blue Test" [3–7] in which the tetrazolium dyes provide a quick visual indication of cell activity *via* its addition to a cell culture.

As well as occurring *via* electron transfer in biological environments, the reduction of tetrazoliums can also be induced by γ-radiation, which enables tetrazoliums to be used as dosimeters for measuring absorbed dose of γ-rays. Much work in this area has been carried out using triphenyl tetrazolium chloride (TTC) [8–11] the structure of which is illustrated in Fig. 1, along with some other cited compounds.

TTC based dosimeters for γ-radiation monitoring have been proposed in the form of aqueous [8,9] and alcoholic [10] solutions but also as agar gels [8]. Less well studied has been the use of tetrazolium dyes in films for UV dosimetry.

Ultraviolet radiation (UVR) plays an important role in maintaining the human body. The main benefit of UVR is generally ascribed to its role in the synthesis of vitamin D3 [12], which is required in many important functions within the human body, such as aiding the absorption of dietary calcium in the gut required to sustain healthy bones [12,13]. Individuals suffering from skin conditions such as psoriasis can also benefit from UV phototherapy [14]. Overexposure to UVR can, however, be hazardous to human health [15] with the severity of the damage caused depending on the type of UV, the intensity and length of the exposure and the sensitivity of the individual. Acute effects arising from short-term exposure to the skin and eyes include erythema i.e. the reddening of the skin more commonly known as sunburn, photokeratitis and photoconjunctivitus, the reversible sunburn of the cornea and conjunctiva, respectively [15,16]. Long-term exposure can lead to chronic conditions such as photoaging [12,17] and skin cancer [12–21] and cause clouding of the lens of the eye, i.e. cataracts [22]. There is also evidence that the human immune system is suppressed due to

* Corresponding author. Tel.: +44 141 548 2458; fax: +44 141 548 4822.
E-mail address: a.mills@strath.ac.uk (A. Mills).

1010-6030/$ – see front matter © 2008 Elsevier B.V. All rights reserved.
doi:10.1016/j.jphotochem.2008.10.010

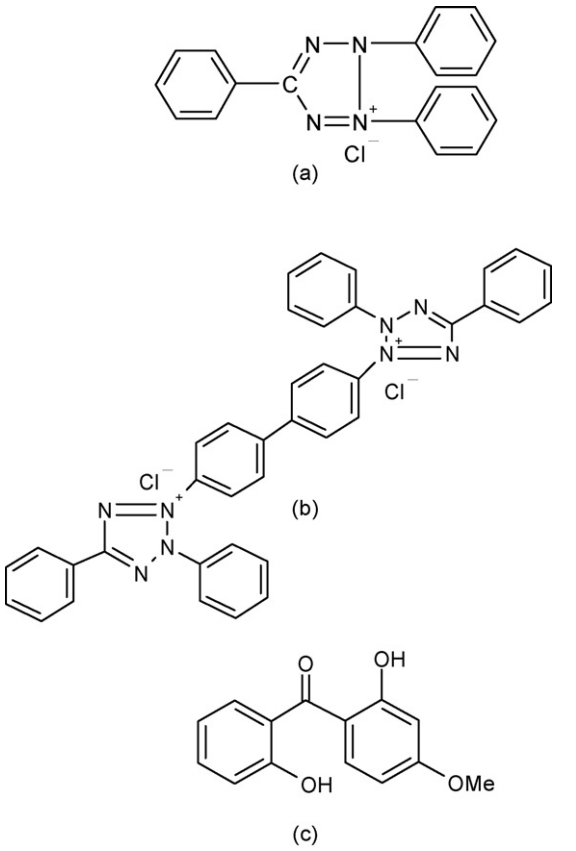

Fig. 1. The chemical structures for (a) triphenyl tetrazolium chloride (TTC), and (b) neotetrazolium chloride (NTC) and 2,2 dihydroxy-4-,metnoxy benzopohenone (DMB).

acute UVR exposure [16]. Incident UV levels are measured using a UV Index system, which on a typical summer's day in the UK will peak at 5 (Glasgow) or 6 (London) (≡125–150 mW m^{-2}) at around mid-day [23].

The amount of solar UV radiation absorbed by the skin at any time is known as the erythemal dose. In quantifying an individual's personal exposure to UVR, the term the '*minimum erythemal dose*' (MED) is useful, where the MED is defined as the minimum amount of radiation likely to cause erythema. The MED for an individual is largely dependent on skin type, of which there are six [24], I–VI. For example, for individuals with skin phototype II, which is typical for many Caucasians, the MED is equal to 250 J m^{-2} i.e. 69.4 mW m^{-2} per hour. Since a UV Index value of 1 is 25 mW m^{-2} it follows that even under mild UV solar conditions such as a UVI value of 3 (≡75 mW m^{-2}) as may be observed in the UK and much of Europe in April or September [23] most Caucasians will sunburn within 1 h if not properly protected.

The measurement of effective UV dosage experienced by an individual is essential if they are to avoid exceeding their MED, i.e. avoid sunburn. With the rise in number of people suffering from UVR-related health problems there is a growing need for a real-time, inexpensive, disposable, personal solar UV dosimeter to provide the user with a current measure of the cumulative dose of UV they have been exposed to during the day.

Since erythema is a consequence of DNA damage, it follows that the best UV dosimeters are ones that utilize biological material, such as, spores, bacterial cells or bacteriophages [25]. Work on spores, most noticeably *Bacillus subtilus*, has been particularly successful in generating an effective biofilm for use as a UV dosimeter, since, with an appropriate filter, the spectral responsivity of this system is very close to the responsivity curve attributed to human skin erythema [25,26]. The latter feature renders the UV dosimeter an effective indicator of erythema regardless of UV source and UV emission profile. The only downside to such biological dosimetry is the need to develop the films, which can take typically up to a day.

Of the many non-biological UV dosimeters, the most notable is that based on thin films of polysulphone [27,28]; a polymer which, upon exposure to UV, increases in its absorbance in the UV. This film is particularly successful because the polymer has an initial spectral profile not too dissimilar to that of the spectral responsivity of human skin with respect to erythema—although not as close at the *B. subtilus* UV dosimeter. The main practical drawback to this dosimeter is the need for a UV absorbance spectrophotometer to measure the change in film absorbance, since it is not assessable by eye.

In contrast to the above, effective, but non-real-time UV dosimeters, a number of colour-based, real-time dosimeters have been reported. The advantage of such devices is that they provide a real-time measure of the UV dosage an individual receives via a clearly perceivable colour change. However, their main disadvantage is that they utilize UV absorbing dyes that usually provide a poor match with the spectral sensitivity of human skin. As a result, such UV dosimeters are only appropriate when calibrated for use with a light source which has a fairly constant spectral profile. Thus, they are usually designed to work best on a clear day from mid-morning to mid-afternoon, using the sun as the source of UV, i.e. as sunburn warning indicators, since the shape of the solar spectrum changes, with the relative level of UVA with respect to UVB increasing, only in the early and late hours of the day when sunburn is 'practically impossible' [29].

Most of the latter systems to date are based on irreversible photochromic dyes [30] and photo-induced pH changing reactions [31]. Few are based on UV-induced electron transfer reactions, the focus of this work, which describes a simple colouration indicator based on the dye, neotetrazolium chloride (NTC) that can be used to indicate UV exposure dose and to warn of possible erythema. The structure of NTC is illustrated in Fig. 1.

2. Experimental

2.1. Materials

All chemicals were purchased from Aldrich Chemicals unless specified. The water used to produce inks was double distilled and deionised while the polymer used to produce the NTC films was 98–99% hydrolysed polyvinyl alcohol (PVA), with an average mol. wt. 124,000–186,000. The polymer used to produce the UV-screening ink was poly(vinyl butryal-*co*-vinyl-alcohol-*co*-vinyl acetate) (PVB), with an average mol. wt. 70,000–100,000.

2.2. Methods

UV/visible spectra for sample films were recorded using a Lambda 35 UV/visible spectrophotometer (PerkinElmer, UK). The NTC UV dosimeter films under test were typically irradiated for a total of 30 min, with spectra being recorded at 5 min intervals.

UV irradiation of samples was carried out using either UVA (λ_{max}(emission) = 365 nm) or UVB (λ_{max}(emission) = 315 nm) lights, both of which comprise two, 8 W fluorescence tubes (Vilber Lourmat). The irradiance (i.e. radiant power per unit area) for each of the UV sources was measured as 4 mW cm^{-2} using a Multi-Sense 100 UV light meter fitted with the appropriate UVA or UVB sensor.

The UV solar simulator used in this work comprised a 180 W xenon arc lamp (Speirs Robertson), with UG5 and the WG20 fil-

ters placed in the light path as described previously by Diffey [32]. The former allows transmission at UV wavelengths and absorbs in the visible region, while the latter absorbs in the short wavelength UVC region. The combination of these two filters with the emission spectrum of the Xe lamp provides a good match with the noonday UV spectrum of the sun [32]. Unless stated otherwise, the UV dosimeter films under test were placed square on to the UV light beam emitted by the Xe lamp placed 45 cm away. In this system the UVI of the UV solar simulated light was measure using a SafeSun^{TM} solar meter and was typically a UVI of 5 [33]. The UV induced change in the absorbance of the dosimeter film under test was measured at 532 nm, i.e. ΔAbs_{532}, at regular intervals with the UV/Vis spectrophotometer.

2.3. UV ink and dosimeter preparation

A typical NTC/PVA solution was prepared by dissolving 10 g PVA in 90 ml of water at 90 °C, which was then cooled to room temperature and stirred overnight. 20 mg of the NTC dye were then dissolved in 4 g of the PVA solution at room temperature with stirring. The casting ink was pale yellow in appearance and contained 5 phr of NTC i.e. 5 parts per hundred resin (or 5 g of dye to 100 g polymer). Films of the ink were cast on to 25 mm diameter, 1 mm thick, quartz discs using a spin coater. Thus, a few drops of polymer solution were deposited on the surface of the disc, which was then spun at 1200 rpm for 15 s. The final product was then dried for 2 min in oven at 70 °C, and allowed to cool to room temperature (5–10 min) and stored in the dark until used. The final product was a clear, colourless ca. 2.3 μm thick film on a quartz disc which will be referred to as a typical NTC film. Work carried out using the solar simulator used films produced from a standard formulation ink but cast at 300 rpm to make the films thicker (ca. 8 μm) and so ensure a more striking colour change, since the absorbance changes were as a consequence ca. four times larger, upon exposure to UV light. Such films will be referred to as typical solar NTC films.

3. Results and discussion

3.1. Optical characteristics of a NTC film

A typical NTC film was produced and the spectral fraction of light, f_A, it absorbs calculated from its absorption spectrum; the results are shown in Fig. 2, along with the known spectral sensitivity of human skin with respect to erythema, $S(\lambda)$ [34]. The film has an absorption maximum at 252 nm with a shoulder peak at 353 nm. From the data in Fig. 2 it is clear that the NTC dosimeter, like most dye-based chemical dosimeters, has a very poor overlap with $S(\lambda)$. This renders it only appropriate as a UV dosimeter for skin erythema when calibrated using the relevant UV light source, assuming the latter's profile does not change with time. Fortunately, as noted earlier, the solar spectrum does not change significantly in shape from mid-morning to mid-afternoon, the most likely time sunburn will take place.

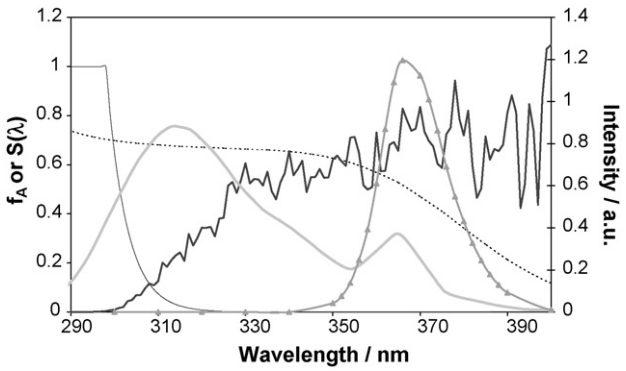

Fig. 2. A plot of the fraction of light (f_A) (- - - -) absorbed by the NTC film and human skin eythemal sensitivity, $S(\lambda)$ (—), vs. wavelength with overlays of the emission spectra of the: solar simulator (▬), UVA (–▲–) and UVB lamps (▬) used in this work.

The emission spectra of the UVA and UVB light sources and the UV solar simulator are also illustrated to highlight their overlap with the NTC film. Note from the data in Fig. 2 that the typical NTC film dosimeter absorbs a greater proportion of UVB than UVA. The latter is a useful feature in any UV dosimeter as it is UVB in particular that is responsible for sunburn. For example on a typical summer's day approximately 6% of terrestrial light is in the UVB wavelength range (i.e. 290–320 nm) and contributes 80% towards the harmful effects associated with the sun, while the remaining 94% UVA component in sunlight (320–400 nm) contributes to the remaining 20% [32].

3.2. UV irradiation of NTC film

When irradiated with either UVA or UVB light a typical NTC film develops a striking pink/red colour with time as seen in Fig. 3, which shows photographs of such a film before and after 30 min irradiation with UVB light (4 mW cm^{-2}). This feature is further illustrated in Fig. 4 which shows the UV/visible absorption spectral changes, exhibited by this film as a function of irradiation time. The insert diagram in Fig. 4 shows that the photocolouration process, as measured by the increase in absorbance at 532 nm i.e. ΔAbs_{532}, as a function of irradiation time, occurs at a greater rate under UVB radiation than UVA radiation of the same intensity. This difference in UV responsivity is expected given that the NTC dye absorbs a greater total fraction of UVB light (f_{UVB} ca. 0.60) than UVA light (f_{UVA} ca. 0.49), as is apparent from the spectral data in Figs. 2 and 4.

The colour change observed arises as a result of the partial reduction of NTC to give the stable monoformazan which proceeds by means of the step-wise addition of electrons and occurs *via* a transient state consisting of one tetrazolinyl radical centre and one tetrazolium centre as detailed in Fig. 5 [35]. Further reduction of the monoformazan, λ_{max} (532 nm) can yield the diformazan form of the dye, a purple species that absorbs at longer wavelength λ_{max} (550 nm) [36,37].

3.3. Kinetics of colouration of an NTC film

In one set of experiments a set of typical NTC films were exposed to different UVA and UVB irradiances for the same length of time. Specifically 1, 2 and 3 mW cm^{-2} from the UVA source and 0.5, 1, 2 and 3 mW cm^{-2} from the UVB source, with a total exposure time of 30 min for each film. The absorbances of the NTC films under test were measured spectrophotometrically and the initial rate, r_i, of colouration for each film was determined from a plot of ΔAbs_{532} vs. irradiation time. The plot of r_i as a function of UV irradiance arising from this work is illustrated in Fig. 6 and shows that r_i is directly related to irradiance, as might be expected for such a simple, direct photochemical process. From the gradient in Fig. 6 the UVB irradiation experiment, i.e. 1×10^{-4} (Abs unit s^{-1}/mW cm^{-2}), and given that the reduced NTC has a molar absorptivity of 22,000 M^{-1} cm^{-1} and a typical film is 2.3 μm thick, a formal quantum efficiency for the photoreduction of NTC in the PVA film was calculated as $(2.8 \pm 0.3) \times 10^{-3}$ molecules/photons of UVB. Similarly a value of $(1.7 \pm 0.2) \times 10^{-3}$ molecules/photons of UVA was calculated using the UVA irradiation data in Fig. 6.

The sensitivity of the NTC UV dosimeter towards UV light can be readily varied by changing the amount of dye in the film formula-

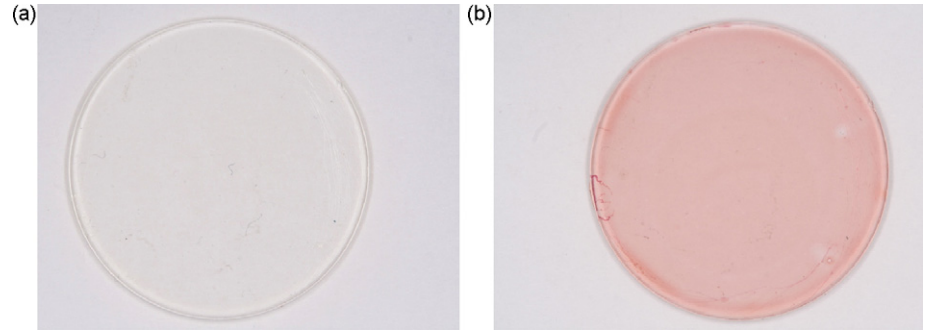

Fig. 3. Photographs of standard films taken before (a) and after (b) irradiation with UVB light.

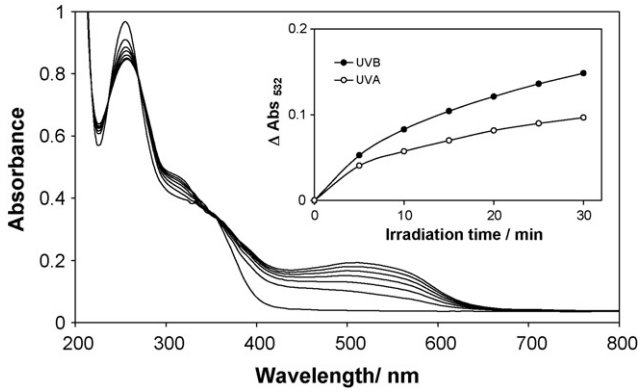

Fig. 4. Absorption spectra of a standard NTC films, after irradiation with 4 mW cm^{-2} UVB. Insert diagram is a comparison of the response of films to 4 mW cm^{-2} UVA.

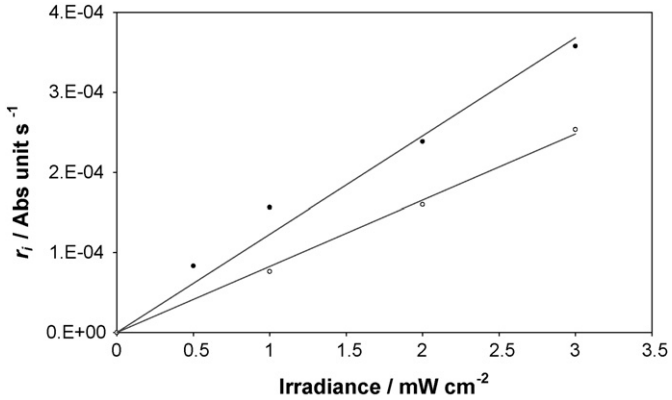

Fig. 6. A plot of initial rate of colouration, r_i as a function of UV irradiance for typical NTC films irradiated with different intensities of UVA (bottom) and UVB (top) light.

tions. Thus, a series of NTC casting inks were prepared containing 10–80 mg NTC, which were then cast on to quartz discs to produce films with NTC levels ranging from 2.5 to 20 phr, respectively. Using these films a series of ΔAbs_{532} vs. irradiation time profiles were generated with a 4 mW cm^{-2} UVB light source and the results are illustrated in Fig. 7. These show that the initial rate increases with increasing levels of NTC, i.e. [NTC]. The initial rate of colouration, r_i, was plotted against the fraction of UVB light absorbed f_{UVB}, by the NTC dye in each film and is shown in the inset diagram in Fig. 7, revealing r_i is directly proportional to f_{UVB}, as expected for a simple, direct photochemical process for which the rate of the photoreduction process is directly proportional to the absorbed irradiance.

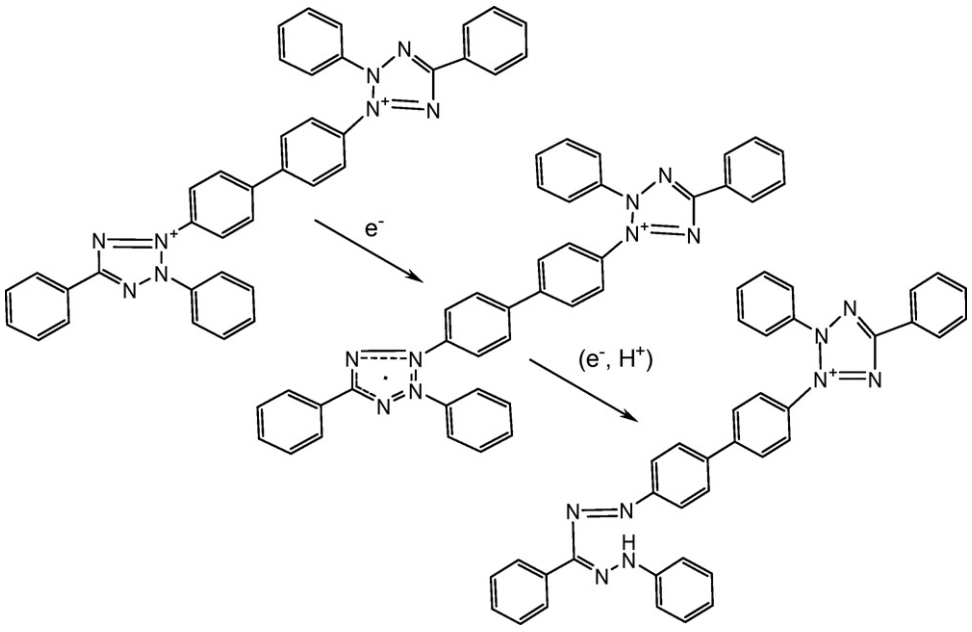

Fig. 5. Mechanism for the reduction of neotetrazolium dye (yellow) to its monoformazan (red).

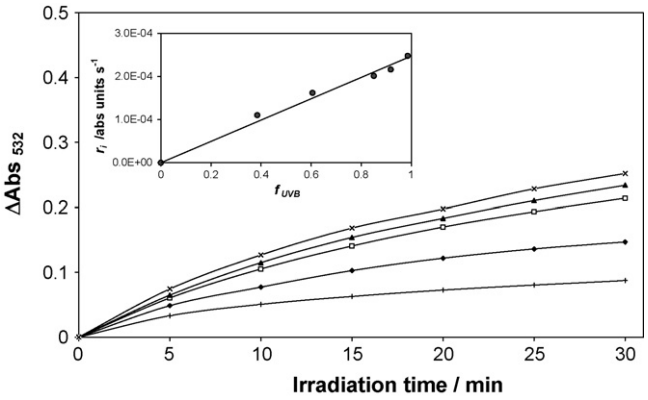

Fig. 7. A plot of ΔAbs_{532} against irradiation time for films containing different [NTC] after irradiation with 4 mW cm^{-2} UVB light. From top to bottom concentrations are 20, 15, 10, 5 and 2.5 phr. Insert diagram is a plot of the r_i against f_{UVB} for each film.

3.4. Enhancement of photocolouration of an NTC film

The NTC UV dosimeter reported here functions *via* a UV-induced photoreduction process, in which the dye converts to its formazan form (see Fig. 5). Since this process occurs in a polymer encapsulation medium (PVA in this case), it is presumed that the photoreduction of the NTC is accompanied by the oxidation of the polymer. It would appear likely, therefore, that the UV-induced photoreduction of NTC may be more easily effected if a more readily oxidised reagent, such as triethanolamine (TEOA) or glycerol, were present. In order to test this idea, casting solutions were prepared following the standard procedure, but with the addition of either 100 mg glycerol or triethanolamine. Films of these inks were cast on quartz discs in the usual way and irradiated with 4 mW cm^{-2} UVB light for 30 min. The variation in the parameter ΔAbs_{532} for these films was monitored spectrophotometrically as a function of irradiation time and the results are shown in Fig. 8. This plot compares the response of the typical film with those films containing glycerol or TEOA, and shows that the addition of an easily oxidisable electron donor, such as TEOA or glycerol increases the initial rate at which the NTC is photoreduced by UV light. Interestingly, the film containing the glycerol develops a purple colour when irradiated with UVB light, with an absorbance peak at 550 nm, rather than that of 532 nm found for the usual red coloured formazan generated using a typical NTC film. These results indicate that, in the presence of glycerol some of the monoformazan produced is further photoreduced to give the diformazan product, which is known to exist as an insoluble purple coloured solid [36,37].

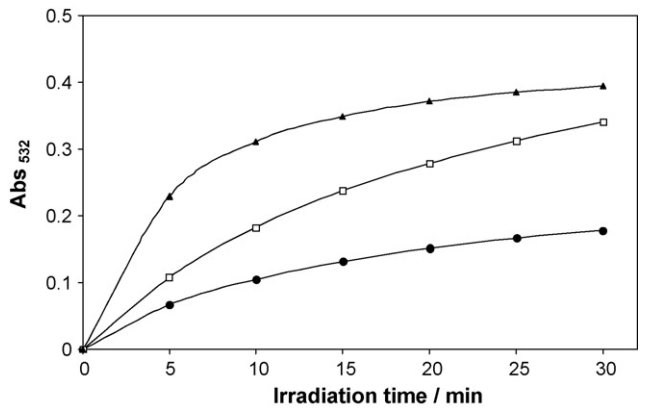

Fig. 8. A plot showing, from top to bottom, the responses of PVA films containing 5 phr NTC with the addition of glycerol or TEOA compared to the standard film after irradiation with 4 mW cm^{-2} UVB light.

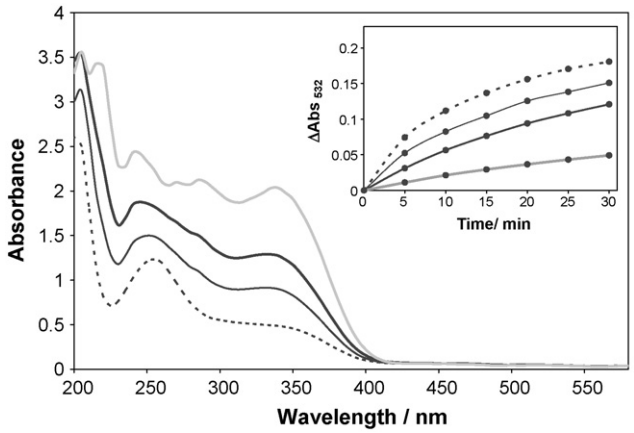

Fig. 9. A plot showing, from top to bottom, the absorption spectrum of a NTC film coated with 100 phr DMB/PVB layer, NTC film coated with 40 phr DMB/PVB layer, NTC films coated with 20 phr DMB/PVB layer and a standard NTC film with no blocker layer. The inset diagram is a plot of ΔAbs_{532} vs. irradiation time for the above-mentioned films generated under 4 mW cm^{-2} conditions.

3.5. Effect of UV blockers on the photocolouration of an NTC film

In order to effect the screening process a coating of a UV-screening solvent based ink (DMB in PVB) was cast on top of a typical NTC film. In this experiment a series of UV-screening solutions comprising of a 5% (w/w) PVB in *n*-butanol polymer solution were prepared containing different levels of DMB ranging from 40 to 100 phr. A set of standard NTC films were then each coated with a layer of one of the solvent based UV-screening inks, by spin coating them on top of the standard films at 1200 rpm, and drying the final product in the oven at 70 °C. The UV/visible spectra for these NTC/UV-screened films are shown in Fig. 9. The films were then irradiated with 4 mW cm^{-2} UVB light for 30 min and their UV/Vis absorption spectra recorded at regular intervals. From this data a series of ΔAbs_{532} vs. irradiation time profiles were generated and are illustrated in the inset diagram of Fig. 9. In order to show that the addition of the sun screen layer merely reduces the amount of UV light reaching the sample and thus reduces the rate of reaction, without interfering with the photochemistry of the tetrazolium two films, namely an NTC film and a 20 phr/UV screen/NTC film were irradiated with 4 mW cm^{-2} until their red colour was fully developed. The former took 120 min, where as the latter took 320 min to achieve the same maximum absorbance (0.28) at 532 nm. The use of a UV screen top layer to reduce the UV sensitivity of a typical NTC film dosimeter suggests that such an approach could be used to adapt the NTC film to provide an indication of impending erythema for any skin type.

3.6. Solar UV work using an NTC film

In a final set of experiments, UV solar simulated light at four different UVI levels spanning the range: UVI 1–8 were each used to irradiate a typical solar NTC film produced at 300 rpm. The data arising from this work allowed the UV dose for each film to be calculated in terms of MED for skin type II and plotted in the form of ΔAbs_{532} as a function of UV dose as illustrated in Fig. 10. The results reveal that all the data points for films exposed to UVI 1, 3, 5 and 8 lie on a common line indicating that a typical NTC film can be used as a quantitative method for assessing the solar UV dosage received.

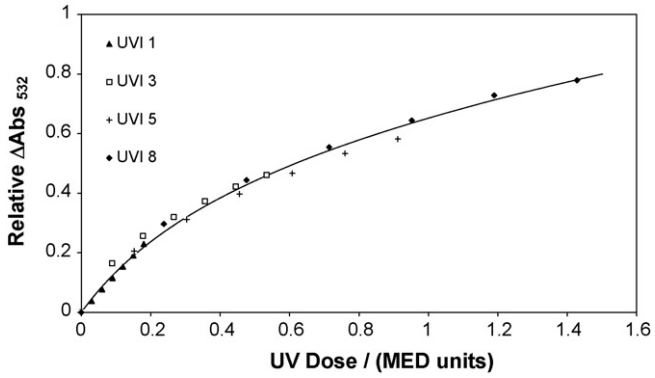

Fig. 10. A plot of ΔAbs_{532} vs. UV dose for skin phototype II received (where 1 = MED for skin type II i.e. 250 J m^{-2} h^{-1}) for standard formulation ink NTC films spun at 300 rpm. The solid line was calculated using Eq. (2).

For example, if upon exposure of a typical solar NTC film a ΔAbs_{532} value of approx. 0.67 is reached this will signify an MED value of 1 has been reached for skin type II and so erythema is likely to occur. In Fig. 10 the line of best fit to the data is given by the expression:

$$\text{UV dose (MED)} = (0.63 \pm 0.03)(\Delta Abs_{532} + \Delta Abs_{532}^2 + (1.85 \pm 0.29)\Delta Abs_{532}^3) \quad (2)$$

Which has the same form as that reported by Diffey [28] for the polysulphone UV dosimeter. Similar ΔAbs_{532} vs. MED curves were generated using solar UV. An error analysis of the data in Fig. 10 reveals that it is ca. 5% up to MED values of 0.3, but then increases with increasing MED, reaching 7% at MED = 1. As an alternative to reading off the measured value of ΔAbs_{532} as a method of determining the MED received, a colour match card could be used to enable the user to determine when they have been exposed to 1 MED, or more, for skin type II, although this is likely to increase significantly the likely error. If an additional polymer/sunscreen layer is introduced to the system, the indicator film could be used to show when erythema is likely to occur for other (higher) skin types. Further solar simulator work showed that the response of the dosimeter is temperature independent over the range 20–40 °C and, like most UV dosimeters, exhibits a cosine-like response dependence upon irradiance angle [25].

4. Conclusions

PVA films containing the dye NTC undergo reduction to the monoformazan form of NTC when exposed to UVA or UVB light. The rate at which the colouration of the films occurs is dependent on properties of the film, such as [NTC] and film thickness, and increases with increasing UV irradiance. The film response is temperature independent over the range 20–40 °C and exhibits a cosine-like response dependence upon irradiance angle. The rate of photocolouration can be reduced by the introduction of a UV-screening layer on top of the standard NTC dosimeter and the dosimeter films give a consistent response to solar simulated light of different irradiances. Using this light source the NTC film dosimeter can be used to identify the point when an MED = 1 has been reached and erythema is likely to occur upon further exposure to solar UV. Although a real-time UV dosimeter, like most dye-based UV dosimeters, the NTC film has a poor match with the erythemal spectral sensitivity of skin and so can only be used as an erythemal indicator when calibrated using the UV source of interest, which in most cases is the sun. The lack of overlap is in striking contrast to several biological UV dosimeters, such as that based on *B. subtilus*, and the polysulphone UV dosimeter, although the former requires extensive processing (taking about 1 day) and the latter requires access to a UV spectrophotometer. Clearly, dye-based UV dosimeters, such as the NTC films reported here, have a long way to go before they can challenge the more established biological and chemical UV dosimeters. However, they can play a useful role in warning of sunburn when used from the middle morning to middle afternoon.

References

[1] V. Créach, A. Baudoux, G. Bertru, B. Le Rouzic, J. Microbiol. Methods 52 (2003) 19–28.
[2] R.N. Mshana, G. Tadesse, G. Abate, H. Miörner, J. Clin. Microbiol. 36 (1998) 1214–1219.
[3] A.M. Gordon, R.M. Rowan, T. Brown, H.G. Carson, J. Clin. Pathol. 26 (1973) 52–56.
[4] A.M. Gordon, J.D. Briggs, P.R.F. Bell, J. Clin. Pathol. 27 (1974) 734–737.
[5] M.V. Beveridge, P.M. Herst, A.S. Tan, Biotechnol. Annu. Rev. 11 (2005) 127–152.
[6] L.J. Meerhof, D. Roos, J. Leukoc. Biol. 39 (1986) 669–711.
[7] R.L. Baehner, L.A. Boxer, J. Davis, Blood 48 (1976) 309–313.
[8] A.K. Pikaev, Z.K. Kriminskaya, Radiat. Phys. Chem. 52 (1998) 555–561.
[9] A. Kovacas, L. Wojnárovits, W.L. McLaughlin, S.E. Ebrahim Eid, A. Miller, Radiat. Phys. Chem. 47 (1996) 483–486.
[10] A. Kovacas, L. Wojnárovits, N.B. El-Assy, H.Y. Afeefy, M. Al-Sheikly, M.L. Walker, W.L. McLaughlin, Radiat. Phys. Chem. 46 (1995) 1217–1225.
[11] S. Ebraheem, A.A. Abdel-Fattah, F.I. Said, Z.I. Ali, Radiat. Phys. Chem. 57 (2000) 195–202.
[12] R.P. Gallagher, T.K. Lee, Prog. Biophys. Mol. Biol. 92 (2006) 119–131.
[13] W.B. Grant, F. De Gruijl, Photochem. Photobiol. Sci. 2 (2003) 1307–1310.
[14] M. Lebwohl, S. Ali, J. Am. Acad. Dermatol. 45 (2001) 487–499.
[15] WHO, Health and Environment Effects of Ultraviolet Radiation, a scientific summary of environmental health criteria, http://www.who.int/uv/publications/UVEHeffects.pdf (accessed on 03/07/2008).
[16] American Optometric Association, Statement on Ocular Ultraviolet Radiation Hazards in Sunlight, 1993, http://www.aoa.org/Documents/OcularUltraviolet.pdf (accessed on 03/07/2008).
[17] Y. Matsumura, H.N. Anathaswamy, Toxicol. Appl. Pharmacol. 195 (2004) 298–308.
[18] R.M. Mackie, Prog. Biophys. Mol. Biol. 92 (2006) 92–96.
[19] F. Urbach, J. Photochem. Photobiol. B: Biol. 40 (1997) 3–7.
[20] G.I. Harrison, A.R. Young, Methods 28 (2000) 14–19.
[21] D.W. Edsrtöme, A. Porwit, A. Ros, Photodermatol. Photoimmunol. Photomed. 17 (2001) 66–70.
[22] D. Allen, A. Vasavada, Br. Med. J. 333 (2006) 128–132.
[23] http://www.metoffice.gov.uk/weather/europe/europe_uv.html (accessed on 03/07/2008).
[24] T.B. Fitzpatrick, Arch. Dermatol. 124 (1988) 869–871.
[25] L.E. Quintern, G. Horneck, U. Eschweiler, H. Bŵcker, Photochem. Photobiol. 55 (1992) 389–395.
[26] L.E. Quintern, Y. Furusawa, K. Fukutsu, H. Holtschmidt, J. Photochem. Photobiol. B: Biol. 37 (1997) 158–166.
[27] A. Davis, G.H.W. Deane, B.L. Diffey, Nature 261 (1976) 169–170.
[28] B.D. Diffey, Radiation Measurements in Photobiology, Academic Press Ltd., 1989, ch 7, pp. 135–159.
[29] N. Kollias, A.H. Baqer, H. Ou-Yang, Photodermatol. Photoimmunol. Photomed. 19 (2003) 89–92.
[30] Faran et al., US Patent 6,132,681 (2000).
[31] A.A. Abdel-Fattah, El-sayed A. Hegazy, H. Ezz El-Din, J. Photochem. Photobiol. A: Chem. 137 (2000) 37–43.
[32] B.L. Diffey, Methods 28 (2002) 4–13.
[33] http://www.cgmdirect.com.au/CGM_Main/Archive/SafeSun.htm (accessed on 03/06/2008).
[34] B.L. Diffey, P.M. Farr, Clin. Phys. Physiol. Meas. 12 (1999) 311–325.
[35] A. Sadeghi, M. Chaychian, M. Al-Sheikhly, W.L. McLaughlin, Radiat. Phys. Chem. 64 (2002) 13–18.
[36] F.P. Altman, R.G. Butcher, Histochemie 37 (1973) 333–350.
[37] R.G. Butcher, F.P. Altman, Histochemie 37 (1973) 351–363.

Flagging up sunburn: a printable, multicomponent, UV-indicator that warns of the approach of erythema

Andrew Mills,* Kate McDiarmid, Michael McFarlane and Pauline Grosshans

Received (in Cambridge, UK) 12th January 2009, Accepted 2nd February 2009
First published as an Advance Article on the web 10th February 2009
DOI: 10.1039/b900569b

A printable, multicomponent, UV-sensitive indicator which provides different coloured, flag-like warnings of the approach to erythema is described.

Overexposure to ultraviolet radiation (UVR) is a recognised health hazard. Acute effects arising from short-term exposure include sunburn (erythema) and photo-conjunctivitis. Long-term exposure can lead to chronic conditions such as photo-aging, skin cancer and cataracts. Incident UVR levels are usually measured based on the UV index system, where a UVI value of 6 is typical of a summer's day in the UK and equivalent to an effective UV irradiance of 150 mW m^{-2}. The minimum erythemal dose, MED, is the minimum amount of UVR likely to cause erythema and MED = 1 is equivalent to 250 J m^{-2} for most Caucasians, *i.e.* skin type II. Thus, the latter would be likely to experience sunburn after only 28 min on a summer's day (UVI = 6) in the UK. All MED values referred to in this paper refer to skin type II unless stated otherwise.

Despite the much greater awareness of the general public of the potential dangers of UVR overexposure, the number of attributed cases of skin cancer continues to rise, such are the continued, perceived attractions in terms of health and wealth of a suntan. In the UK currently over 70 000 people develop skin cancer pa, 9000 of which are malignant leading to *ca.* 2000 deaths pa.[1]

The major problem with sunburn is that the usual signs of burning and damage are delayed, often taking 4–8 h to appear. Thus, it would be useful to have an easily read, real-time indicator which shows when an MED = 1 value has been reached for any particular skin type and thus when it is time to cover up from the sun. There are several notable UV dosimeters on the market, including SolarSafe, SunSignals and SunCheck.[2–4] Most utilise a single gradual colour change which makes it hard to identify useful stages in the development of sunburn, such as MED = 0.5 and 1. This paper describes a novel, printable, multicomponent indicator which could be used to provide a different, striking, flag of the approach to erythema.

The key feature of the overall indicator is the use of a UV-driven acid-release agent, ARAH, coupled to a pH-indicating dye, D^-. In this system, UV irradiation decomposes the acid-release agent:

$$ARAH \rightarrow ARA^- + H^+ \quad (1)$$

which promptly leads to the protonation of the dye and, therefore, a striking colour change:

$$D^- + H^+ \rightarrow DH \quad (2)$$

since D^- and DH are usually very different in colour. Examples of ARAHs include iodonium and sulfonium salts[5] and chloral hydrate (ClH).[6] Examples of pH indicators include thymol blue (TB) and malachite green (MG).

Prompt UV dosimeters based on this simple process are well known in the literature[7,8] and a commercial manifestation is the SunSignals dosimeter (yellow to orange colour change), which employs methyl orange as the pH indicating dye and an organic halogen, such as 1,2-dibromotetrachloroethane, as the UV-driven acid-release agent, ARAH.

In this work, a typical *prompt*, UV dosimeter that functions *via* reactions (1) and (2) was made by spin coating an ink comprising 20 mg MG, 100 mg chloral hydrate and 0.05 ml 0.1 M NaOH in 4 g of a 5% w/v polyvinyl butyral (PVB) solution in ethanol. The UV solar simulator used in this work comprised a 180 W xenon arc lamp (Speirs Robertson), with UG5 and the WG320 filters placed in the light path as described previously by Diffey.[9] The UV dosimeter films under test were placed square on to the UV light beam emitted by the UV solar simulator, set at a distance so that the UVI was 5, as measured using a SafeSun™ solar meter.

The above ink spin-coats (1200 rpm for 15 s) as an effectively colourless film on a 25 mm diameter glass disc. The typical spectral variations and colour change observed when this film is irradiated with UVI 5 solar simulated light are illustrated in Fig. 1.

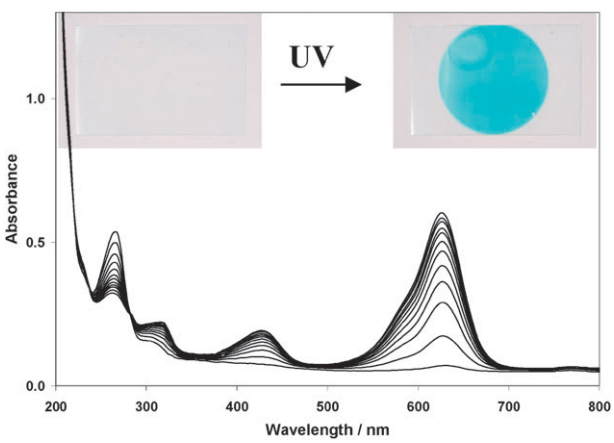

Fig. 1 Spectral changes (recorded every 3 min) and photos of a MG/ClH/PVB film before (LHS) and after (RHS) exposure to 33 min irradiation with UVI 5 solar simulated light (*i.e.* MED ~1).

Department of Pure & Applied Chemistry, University of Strathclyde, Glasgow, UK G1 1XL. E-mail: a.mills@strath.ac.uk; Fax: +44 0141 548 4822; Tel: +44 0141 548 2458

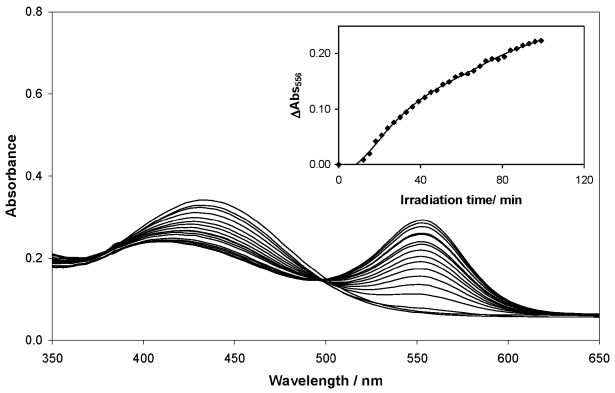

Fig. 2 Spectral changes (recorded every 6 min) upon exposure of a TB/DPIC/PVB film to UVI 5 solar simulated light. Insert: plot of change of absorbance at TB λ_{max} (556 nm) as a function of irradiation time, data from main figure.

The observed colour change (colourless to green in this case) for this type of indicator is *prompt* and drawn out and as such is of limited use as a dosimeter, which ideally should have a sharp colour change, especially around a UV dose corresponding to a MED = 1. Novelly, we find that this feature can be achieved by adding a base, like NaOH, to the ink formulation; the more base, the longer the delay. Thus, a typical *delayed* ARAH/pH indicator type UV dosimeter was made by mixing 0.5 ml ethanol solution, containing 0.8 mg TB and 60 μg NaOH, with 4 g of a 5% w/v PVB solution in ethanol, containing 3.2 mg of the ARAH diphenyliodonium chloride (DPIC). 0.33 g of this ink were spread over a 25 mm glass disc using a glass rod and allowed to dry overnight. The process was repeated three times to generate a strongly yellow-coloured initial film. The typical spectral variations and colour change observed (yellow to magenta) when this film was irradiated with UVI 5 solar simulated light are illustrated in Fig. 2. Note the delay in the colour response of the film—*i.e.* no change in colour even after 12 min irradiation (MED = 0.3).

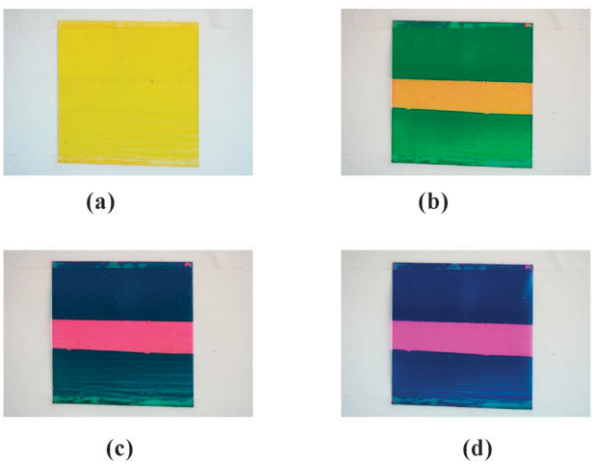

Fig. 3 Photographs of a combined MG/ClH/PVB and TB/DPIC/PVB film on a PP flag-type UV dosimeter: (a) before and after irradiation with UVI 5 solar simulated light so that: 0.5 (b), 1.0 (c) and 2.0 (d) MED doses were achieved, respectively.

It follows that the combination of these two differently responding UV dosimeters—one *prompt*, the other *delayed*—can be used to create a flag type UV dosimeter, as illustrated in Fig. 3. In this case a TB/DPIC/PVB film, containing 3.2 mg TB, 12.8 mg DPIC and 0.2 mg of NaOH, was coated on one side of a ~2.5 × 2.5 cm square of polypropylene (PP). A typical colourless MG/ClH/PVB film was then coated on the other side, with the exception of a 5 mm strip in the middle which was covered with a piece of Sellotape. After the ink film was allowed to dry the Sellotape strip was removed. The final film (illustrated in Fig. 3) was initially yellow but, upon irradiation with UVI 5 solar simulated light, the MG/ClH/PVB film coated areas rapidly develop a distinctive, dark green colouration at an MED = 0.5. Most importantly, at an MED = 1 (but not 0.5), the magenta colour is well developed and the MG/ClH/PVB coated areas have turned blue due to the combination of the green and red colourations of the two different dosimeter films. The rapid appearance of the magenta coloured central strip and blue background strips (from 0.5 to 1.0 MED) provides a striking indication of when an MED dose of 1 has been reached and skin type II should be covered up, as any further UV exposure is likely to lead to erythema. Note that after this point, the colour changes are less striking (see (d) in Fig. 3) which helps stress the key stage in the UV dose received, *i.e.* above this UV dosage erythema is increasingly likely. The response features of the overall indicator appeared unchanged over the temperature range 18–35 °C, nor does the film appear to change colour when exposed to visible light, rather than UV.

The notable features of this type of dosimeter are not only the creation of a delayed UV dosimeter, but also the combination of a *prompt* and *delayed* response UV dosimeter to make a flag-type response colorimetric UV dosimeter, with different colours appearing at different stages of the exposure process. The responsivities, and therefore colour change times, of these component films can be increased or decreased by altering the film composition, *e.g.* by using different ARAHs, pH dyes, bases and different concentrations thereof. UV block reagents can also be used to slow the response of one or both films. As a consequence, this type of indicator can be tuned to be effective for most if not all the different skin types. The components of the different inks are inexpensive and the inks themselves printable on many different surfaces including paper and plastics. As a consequence this type of indicator may prove a useful device for preventing sunburn and, by implication, skin cancer.

Notes and references

1 http://info.cancerresearchuk.org/cancerstats/, accessed December 2008.
2 http://www.solarsafe.com/, accessed December 2008.
3 http://www.sunhealthsolutions.com/, accessed December 2008.
4 http://www.suncheck.com/, accessed December 2008.
5 D. Crivello, *J. Polym. Sci., Part A: Polym. Chem.*, 1999, **37**, 4241–4254.
6 P. W. Danckworrt, *Arch. Pharm.*, 1942, **280**, 197–250.
7 A. A. Abdel-Fattah, M. El-Kelany and F. Abdel-Rehim, *Radiat. Phys. Chem.*, 1996, **48**, 497–503.
8 A. A. Abdel-Fattah, M. El-Kelany, F. Abdel-Rehim and A. A. El Miligy, *J. Photochem. Photobiol., A*, 1997, **110**, 291–297.
9 B. L. Diffey, *Methods*, 2002, **28**, 4–13.

A novel reversible relative-humidity indicator ink based on methylene blue and urea

Andrew Mills,* Pauline Grosshans and David Hazafy

Received 15th September 2009, Accepted 11th November 2009
First published as an Advance Article on the web 19th November 2009
DOI: 10.1039/b918985h

A new relative-humidity sensitive ink based on methylene blue and urea is described which can utilise the deliquescent nature of urea.

Humidity sensors are used extensively in industry as well as for environmental monitoring. Their widespread applications cover a broad range of domestic, medical and industrial applications. For example, in food packaging, excess moisture in meat packaging can accelerate food spoilage, and as a consequence desiccants are often included in packaging to extend the shelf life.[1] At low relative humidities (RHs) some dry grain products can undergo rapid free-radical oxidation and become rancid.[1] Most fruit and vegetables are composed largely of water, consequently their optimum storage conditions are typically 90–95% RH, $T = 0$ °C,[2] whereas products such as sugar and raisins lose their desirable texture if the RH is this high. Thus, most food stuffs require a degree of moisture management and humidity measurement to obtain optimum relative-humidity (RH) conditions.[1] Humidity control is also important for the preservation of artefacts such as books and paintings and to prevent bacterial and mould growth in certain manufactured products. Another application is in the packaging and transportation of sensitive electrical appliances/components which are adversely affected by high relative humidity and therefore require accurate monitoring to ensure efficient functionality.[3]

There are a wide range of commercial products currently available for monitoring relative humidity. These are, more often than not, electronic hygrometers based on capacitive or resistive systems which measure the change in conductivity of a polymer or ceramic film as a function of relative humidity.[4] Such devices have limitations in their operating conditions and can be expensive and bulky to use.[5,6]

There have been a number of proposed colorimetric relative-humidity indicators, the majority of which are based on the use of inorganic salts[7–17] such as cobalt(II) chloride, $CoCl_2$, which at a defined RH level (typically RH 40%) convert from their anhydrous form to their hydrated form, which is usually marked by a colour change, in the case of $CoCl_2$, blue (anhydrous) to pink (hydrated). The sensitivity of this type of indicator can be tailored to the desired application by one of three methods: changing the concentration of the inorganic salt,[18] adding a deliquescent synergic salt[19–21] or, for systems with a silica support, altering the drying and activation temperatures of the $CoCl_2$-doped silica.[7] Such relative-humidity indicators have been proposed for a variety of applications including: refrigerated systems,[12,13] clothes dryers,[14] shoe storage,[16] desiccant absorbent capacity indicators,[18,20,21] electronic device storage[17] and are often reversed by heating the hydrated salt to regenerate the anhydrous starting material. A typical commercial form, based on $CoCl_2$, is the Humitector® Humidity Indicator Card (Süd-Chemie Inc., USA).[22]

Recently, Matsushima *et al.* have proposed using thiazine and flavylium salts in gels as simple colorimetric humidity and temperature sensors.[23–25] These salts exhibit reversible colour changes from blue (dry) to purple (humid), as a result of a change in relative humidity. This has been attributed to the absorption of water vapour by the gel in humid conditions which encourages the dye to form dimers and so leads to a shift in λ_{max} absorbance (*ca.* 10–20 nm) to a lower wavelength.

Whilst looking at this system, we have found that when the thiazine dye, methylene blue (MB), is encapsulated within a polymer, such as hydroxy ethyl cellulose (HEC), with a notable excess of urea, (20 times w/w more than MB), the product ink is blue, but casts as a thin, opaque pink film, under ambient (RH = 60%, $T = 20$ °C) or dry conditions, and rapidly and reversibly is rendered blue coloured and clear when exposed to RH values >85%. Note that the observed colour changes for MB/urea/HEC films are the *opposite* of those observed by Matsushima *et al.*[23–25] for their MB/gel films so the explanation for the effect is very different. It is also unusual to find a relative-humidity indicator which gives such a sharp, reversible colour change at high relative humidities. Consequently, this novel and promising relative-humidity indicator is the subject of this communication.

In this work, all relative humidities were measured at 20 °C unless otherwise stated. A typical relative-humidity sensor was made by spin coating an ink comprising 5 mg MB, 100 mg urea in 2 g of a 5% w/v HEC aqueous solution, for 30 seconds at 3500 rpm on to a 25 mm glass disc. Following the drying of the film at 70 °C for a few minutes, the final product is an opaque pink film (*ca.* 1.7 μm thick) under ambient conditions (40–60% RH) with a λ_{max} at 570 nm, which upon exposure to high relative-humidity conditions (>85% RH) turns rapidly blue ($\lambda_{max} = 600$ nm) and clear as illustrated in Fig. 1 and Fig. 2.

This colour change process occurs rapidly (response and recovery times: 10 s and 60 s respectively) and is reversible as illustrated by the

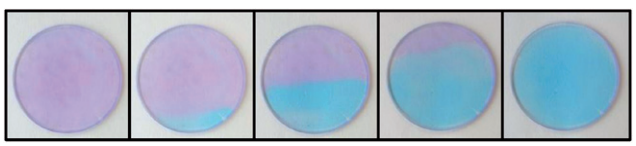

Fig. 1 Photographs of a typical MB/urea/HEC relative-humidity indicator changing colour from pink (left) to blue (right) upon exposure to 100% RH air, from the bottom right.

Department of Pure & Applied Chemistry, University of Strathclyde, Glasgow, UK G1 1XL. E-mail: a.mills@strath.ac.uk; Fax: +44 (0) 141 548 4822; Tel: +44 (0) 141 548 2458

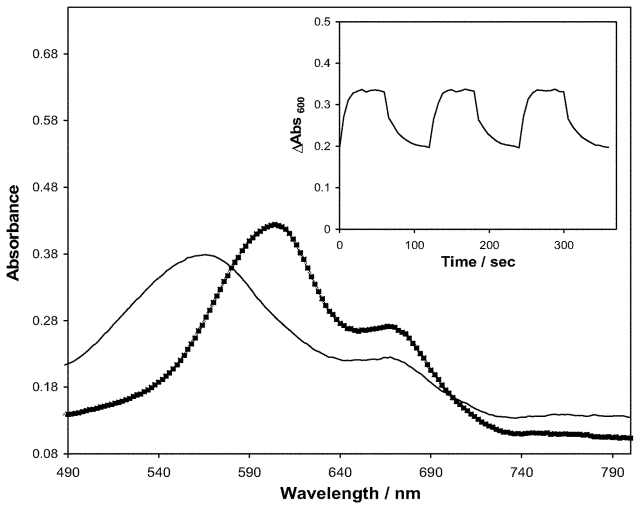

Fig. 2 Spectral changes of a typical MB/urea/HEC relative-humidity indicator film before (—) and after (■) exposure to 100% RH air. Inset diagram is a plot of the change in absorbance MB $\lambda_{max\ humid}$ (600 nm) for indicator film on exposure to 3 cycles of 1 min 100% RH air and 1 min dry air. Abs_{600} recorded every 6 s.

data in the inset of Fig. 2 which show the response and recovery of the absorbance (at λ_{max} for blue form, 600 nm) for a typical MB/urea/HEC relative-humidity indicator film upon exposure to repeated cycles of humid (100% RH) and dry air.

The initial spectrum of the dry film (see Fig. 2) is very different from that observed for the monomer and dimer, thus, it is not instantly apparent what the colour change is due to.[26–28] Under ambient conditions the film is pink and the absorption spectrum of the film ($\lambda_{max} = 570$ nm) is, if anything, like that of the MB trimer ($\lambda_{max} = 578$ nm).[26,28]

When exposed to high relative humidities the resulting blue film has a spectrum more characteristic of a mixture of the MB monomer and dimer.[26–28] The monomer is attributed to the smaller peak at 665 nm while the larger peak at 600 nm is attributed to the MB dimer. An inspection of films containing no dye reveals a concomitant change in the optical clarity of the urea/HEC film in the absence (opaque) and presence (clear) of a stream of air containing a high (100%) RH, as illustrated in Fig. 3.

Further work shows that urea forms highly crystalline, optically opaque films with a characteristic XRD peak at $2\theta = 22.25°$ at moderate and low RH. These crystallites rapidly dissolve when exposed to relative humidities above 85%, rendering a clear film. The urea XRD peak reappears when the opacity change is reversed by blowing dry air over the film or placing it in oven (70 °C for few minutes). Thus, it appears that the colour change associated with the MB in the urea film (pink (dry) ↔ humid (blue)) is linked to the change in crystallinity of the urea when exposed to high relative humidities. Indeed a dye-free relative-humidity indicator based on optical clarity can be simply created using just urea in a polymer, such as HEC, since Fig. 3 shows that such a film is opaque at medium and low (<85%) RH levels, but clear at RH values >85%; the process is entirely reversible. The polymer used, in this case HEC, does not appear to have any effect on the colour or opacity change, but merely acts as an encapsulation agent. This was confirmed by observing a similar effect in different polymers (such as polyvinyl alcohol, PVA and polyethylene oxide, PEO). Also in a polymer-free environment, achieved by grinding up a sample of urea with MB, the resulting pink powder exhibits a similar reversible colour change to blue when exposed to RH >85%.

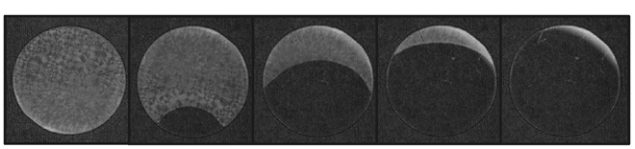

Fig. 3 Photographs of a urea/HEC with no dye changing from an opaque film (left) to a clear film (right) upon exposure to 100% RH air.

The simplest explanation is that under ambient conditions (RH < 85%) MB is encapsulated in urea crystals as the pink trimer and when exposed to high RHs the urea crystals dissolve, thereby releasing the MB into an environment in which its more stable form is the blue coloured MB dimer and monomer. In support of this, it is well known that urea is a hygroscopic compound which deliquesces under high RH conditions of >80% RH at 18 °C.[29–31]

The notable features of this type of relative-humidity indicator are not only that it can be used exclusively for monitoring high (>85%) relative humidities, but it is quick to respond, highly reversible and has a good long-term stability. As it stands, such a >85% RH indicator has a potential application ensuring the correct RH conditions for the storage and ripening of fruit,[32] for example. Further work is in progress developing this system using a series of hygroscopic, urea and non-urea-related, compounds which undergo deliquescence at different relative humidities (*e.g. N,N′*-dimethylurea deliquesces at RH >63% at 18 °C) to generate a set of relative-humidity indicators for providing a sharp register at different, defined relative-humidity levels that span the RH scale.

Notes and references

1 R. Esse and A. Saari, in *Smart Packaging Technologies*, ed. J. Kerry and P. Butler, John Wiley & Sons, West-Sussex, 2008, pp. 130–149.
2 J. E. Robinson, K. M. Browne and W. G. Burton, *Ann. Appl. Biol.*, 1975, **81**, 399–408.
3 R. H. Feinzig and D. Sullivan, Commissioning Humidity Control Systems in Critical Environments, in *National Conference on Building Commissioning*, held at Chicago, IL, 2–4 May 2007.
4 N. Yamazoe and Y. Shimizu, *Sens. Actuators*, 1986, **10**, 379–398.
5 http://www.hannainst.com/usa/prods2.cfm?id = 012001, last accessed November 2009.
6 http://www.michell.co.uk/products/classification/browse/portables, last accessed November 2009.
7 P. B. Davis, *US Pat.* 2460065–2460070, 1949.
8 P. B. Davis, *US Pat.* 2580737, 1949.
9 D. L. Fuller, *US Pat.* 4034609, 1977.
10 D. L. Fuller, *US Pat.* 4150570, 1979.
11 J. S. Haswell, *US Pat.* 5520041, 1996.
12 W. O. Krause, *US Pat.* 3533277, 1970.
13 W. O. Krause, *US Pat.* 3499616, 1970.
14 J. F. McBride, *US Pat.* 4909179, 1990.
15 S. D. Price, *US Pat.* 3121615, 1964.
16 E. Wroth and K. Sheraw, *US Pat.* 5950323, 1999.
17 Y. Yamakawa, *US Pat.* 7316198 B2, 2008.
18 M. Hamada, *US Pat. Appl.* 2007/0157702 A1, 2007.
19 P. B. Davis and J. N. Pryor, *US Pat.* 2526938, 1950.
20 M. Gattiglia, *US Pat.* 6655315 B1, 2003.
21 M. Gattiglia and E. Gandolfo, WO 02/44712 A1, 2002.
22 http://www.sud-chemie.com/scmcms/web/page_en_6254.htm, last accessed November 2009.
23 R. Matsushima, N. Nishimura, K. Goto and Y. Kohno, *Bull. Chem. Soc. Jpn.*, 2003, **76**, 1279–1283.

24 R. Matsushima, A. Ogiue and S. Fujimoto, *Chem. Lett.*, 2000, 590–591.
25 R. Matsushima, A. Ogiue and Y. Kohno, *Chem. Lett.*, 2002, 436–437.
26 E. Braswell, *J. Phys. Chem.*, 1968, **72**, 2477–2483.
27 A. Ghanadzadeh, A. Zeini, A. Kashef and M. Moghadam, *J. Mol. Liq.*, 2008, **138**, 100–106.
28 Z. Zhao and E. R. Malinawski, *Appl. Spectrosc.*, 1999, **53**, 1567–1574.
29 J. R. Adams and A. R. Merz, *Ind. Eng. Chem.*, 1929, **21**, 305–307.
30 A. Clow, *Nature*, 1940, **146**, 26.
31 E. A. Werner, *Nature*, 1937, **139**, 512.
32 C. Vazquez-Salinas and S. Lakshminarayana, *J. Food Sci.*, 1985, **50**, 1646–1648.

Intelligent pigments and plastics for CO_2 detection

Andrew Mills,* Graham A. Skinner and Pauline Grosshans

Received 2nd March 2010, Accepted 30th April 2010
First published as an Advance Article on the web 24th May 2010
DOI: 10.1039/c0jm00582g

A novel CO_2 intelligent pigment is incorporated into a thermoplastic polymer to create a long-lived CO_2-sensitive plastic film which is characterised and then compared to a traditional solvent-based CO_2 indicator film.

A number of optical indicators have been developed[1–7] in recent years to detect the presence of CO_2 at different levels, depending on the desired application. The majority of CO_2 indicators work *via* the change in pH which occurs when CO_2 dissolves in water. A pH-sensitive dye, D^-, changes colour when it reacts with the protons generated from the dissolution of CO_2 in water, *i.e.*,

$$D^- \text{ (colour A)} + H^+ \Leftrightarrow HD \text{ (colour B)} \quad (1)$$

where A is the colour of the dye (in its anionic, deprotonated form) before exposure to CO_2 and B is the colour of the dye (in its protonated form) after exposure to CO_2. Thus, upon exposure of such indicators to CO_2, the pH of the ambient environment decreases sufficiently to protonate the dye and so causes a measurable and observable change in absorbance of the indicator. The widespread detection of CO_2 by most thin-film, optical indicators has been hindered by their interaction with ambient acidic gas species (such as SO_2 and NO_2), which irreversibly acidify and markedly reduce the shelf-life of the indicator.[3] This paper identifies a route for producing CO_2 indicators with increased shelf-life stability, through the incorporation of a fast-acting, reversible, stable (>6 months) CO_2-indicating pigment into a flexible, extrudable, thermoplastic polymer.

To 2.0 g of hydrophobic silica (Degussa/Evonik Aerosil R812, specific surface area = 260 ± 30 $m^2\ g^{-1}$, average particle size = 7 nm), 0.08 g of *m*-cresol purple (MCP), 100 ml of ethyl acetate and 1.5 ml of 1 M tetrabutylammonium hydroxide in methanol were added. (The silica employed has been rendered hydrophobic, by the manufacturer, by reacting the surface hydrophilic silanol groups (Si–OH) with dimethyldichlorosilane to produce hydrophobic Si–Me groups.) This mixture was mixed thoroughly and the solvent (ethyl acetate) then removed under reduced pressure using a rotary evaporator. The resultant powder was ground up using a pestle and mortar to generate a fine blue powder. The anionic form of MCP, MCP^-, is rendered hydrophobic by ion-pairing with the quaternary ammonium cation, Q^+, to form $Q^+MCP^- \cdot xH_2O$; note: the presence of a few molecules of water is known[3] to associate with such ion-pairs.

As a result, rotary evaporation of this solvent-soluble ion-pair with the hydrophobic silica generates particles with a coating of $Q^+MCP^- \cdot xH_2O$, which are able to respond rapidly and reversibly to the presence of CO_2 *via* the following equilibrium reaction:

Department of Pure & Applied Chemistry, University of Strathclyde, Glasgow, UK G1 1XL. E-mail: a.mills@strath.ac.uk; Fax: +44 (0)141 548 4822; Tel: +44 (0)141 548 2458

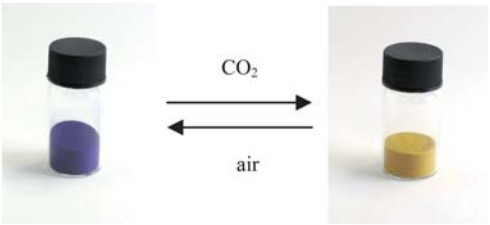

Fig. 1 Colour change of CO_2-sensing pigment exposed to 100% CO_2.

$$Q^+MCP^- \cdot xH_2O + CO_2 \Leftrightarrow \underset{\text{(blue)}}{Q^+HCO_3^-} \cdot (1-x)H_2O \cdot \underset{\text{(yellow)}}{MCPH} \quad (2)$$

This same key reaction features[3] in MCP, solvent-based CO_2-sensitive plastic films. Thus, as illustrated by the photographs in Fig. 1, in the absence of CO_2 the MCP is in its blue anionic (MCP^-) state, but in the presence of CO_2 it is converted, *via* the reversible reaction (2), to its yellow, protonated form (MCPH).

The resulting CO_2-sensitive pigment is fast-acting (<1 s), reversible and very stable (>6 months), when stored in a darkened bottle under air.

In order to make the corresponding intelligent *plastic* CO_2 indicator, 0.6 g of the hydrophobic *pigment* was added to 4.0 g of powdered polyethylene (Alfa Aesar, LDPE, 1000 μm) and the mixture ground up using a mortar and pestle until the colour was a uniform blue. A small sample (*ca.* 0.3–0.4 g) of the powder mixture was heat pressed using a Specac Atlas™ Series Heated Platens at 115 °C to create a blue polyethylene film (0.1 mm thick) which was used in subsequent indicator work. The composition of the final CO_2 intelligent plastic, in terms of parts per hundred resin (pphr), was PE/MCP/SiO_2/TBAH = 100/0.6/15/2.9.

For comparison purposes, a similar solvent-based ink was prepared by dissolving 0.08 g of *m*-cresol purple in 3 ml methanol and 1.5 ml 1 M tetrabutylammonium hydroxide (TBAH) in methanol. This solution was stirred for 15 minutes, placed in a sonicating bath for 10 minutes, then stirred further until fully dissolved. This solution was added to 20 g of 10% w/v ethyl cellulose in toluene/ethanol (80 : 20), along with 2 ml of tributyl phosphate. The final ink solution

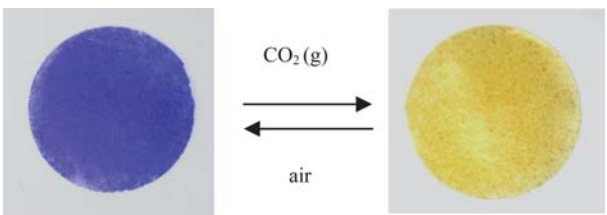

Fig. 2 Colour change of CO_2-sensing pigment incorporated into polyethylene plastic film, when exposed to 100% CO_2.

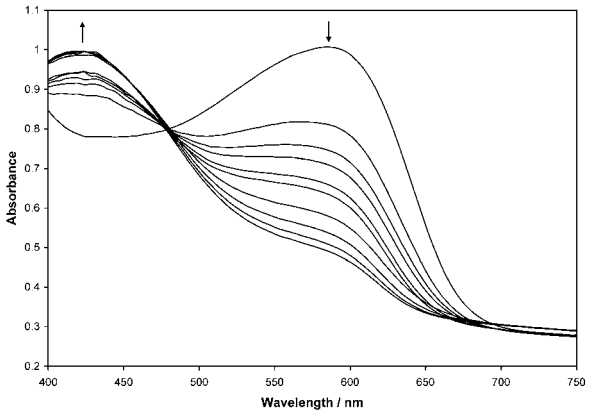

Fig. 3 UV/visible absorption spectra of the MCP/silica/PE plastic film as a function of $\%CO_2$, for $\%CO_2$ (from top to bottom) of 0, 1, 2, 3, 4, 5, 20, 30, 60, 100%, respectively. Abs_∞ is ~0.44.

was stirred for at least 30 minutes. The composition of the deposited dried ink film, 0.8 μm thick, in terms of pphr, was EC/MCP/TBAH/tributyl phosphate = 100/4/19.5/97.

The MCP/silica pigment in polyethylene plastic film is initially blue coloured but, as with the bare pigment (see Fig. 1), it changes to yellow upon exposure to carbon dioxide gas, as illustrated in Fig. 2. This characteristic, blue to yellow, colour change was also observed for the MCP solvent-based ink, which uses the same quaternary base.

Fig. 3 shows the recorded UV-visible spectra of the MCP/silica pigment plastic film as a function of $\%CO_2$. As with its solvent-based film counterpart, the change in colour, due to λ_{max} shifting from 592 to 424 nm, is a result of the MCP^- forming MCPH *via* reaction (2). The variation in the absorbance due to the MCP in the plastic film as a function of $\%CO_2$ is illustrated in Fig. 4.

It is useful to define the parameter, R, which is directly proportional to the ratio of concentrations [MCPH]/[MCP^-], *via* Beer's law, through the expression:

$$R = (Abs_0 - Abs)/(Abs - Abs_\infty) = [MCPH]/[MCP^-] \quad (3)$$

where Abs_0 is the value of absorbance of the dye at λ_{max} (MCP^-) when $\%CO_2 = 0$ (*i.e.* when the dye is fully in its deprotonated form)

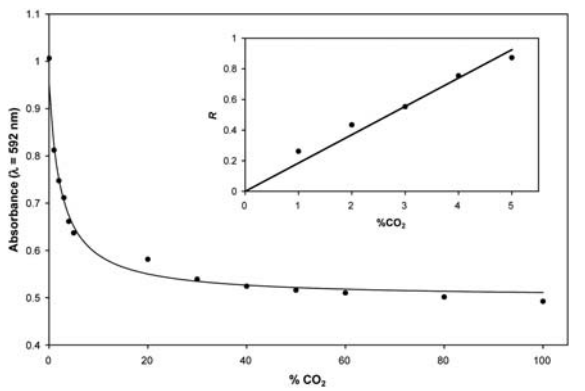

Fig. 4 Plots of absorbance of MCP/silica pigment plastic film at 592 nm *versus* $\%CO_2$. Data from Fig. 3. Solid lines were best fit to the data, revealing an α value of $0.185 \pm 0.02\%CO_2^{-1}$.

and Abs_∞ is the absorbance of the film when all the dye has been converted into its protonated form *i.e.* when $\%CO_2 = \infty$. Since MCPH does not absorb at λ_{max} (MCP^-), it is convenient to estimate Abs_∞ at 592 nm. For such indicators it can be shown[3] that:

$$R = [MCPH]/[MCP^-] = \alpha\%CO_2 \quad (4)$$

and the linear relationship between R and $\%CO_2$, as illustrated in the inset diagram in Fig. 4, reveals an α value of $0.185 \pm 0.02\%CO_2^{-1}$. A similar experiment carried out on the solvent-based CO_2-indicator reveals an α value of $0.80 \pm 0.08\%CO_2^{-1}$. Since α is a measure of indicator sensitivity, it appears that the solvent-based sensor shows a greater sensitivity (4 times) towards CO_2 compared to the MCP/silica pigment plastic indicator, possibly in part due to the greater permeability of CO_2 (by a factor of *ca.* 9) in ethyl cellulose compared to polyethylene.[8] Although the two indicator systems tested have markedly different dye levels ([dye] = *ca.* 7 times more—in terms of phr in the solvent based indicator), this is unlikely to be responsible for the difference in sensitivity for two reasons. Firstly, the sensitivity of such indicators is expected[9] to be independent of dye concentration, except at very high dye levels. Secondly, at high dye concentrations the dye will buffer the system and so the indicator would appear less sensitive (not more, as found for the higher dye-containing solvent-based indicator).

The MCP/silica pigment plastic indicator is fully reversible and responds quickly (within a few minutes) when exposed to 100% CO_2, but has a slow recovery time (*ca.* 2 hours to fully recover). In contrast the solvent-based CO_2-indicator has response and recovery times of both <1 and 3 s respectively. The above differences between the two indicators are due to the diffusion dependence of indicator film response and recovery times which, as a consequence, will depend upon film thickness and CO_2 permeability. Thus, the much slower recovery time of the polyethylene indicator will be due to its greater film thickness (100 compared to 0.8 μm) and lower CO_2 permeability (different by a factor of *ca.* 9). Both CO_2-indicators can be used repeatedly without any loss in performance.

As noted earlier, it is known[1,3,10] that most solvent-based CO_2-sensitive inks suffer irreversible acidification from interfering acidic gases, such as NO_2 and SO_2. Indeed, all optical CO_2 indicators that operate *via* a pH changing dye are non-selective with regard to other acidic gases and the indicators reported in this paper are no different. This is a particular problem when it comes to film storage since NO_2 and SO_2 are typically present in an urban environment at levels of 150 and 50 ppb, respectively.[10] And so it is an important feature of the MCP/silica pigment plastic CO_2-indicator films that they have a much greater longevity compared to that of a conventional solvent-based ink. For example, in our hands a solvent-based, indicator film will typically begin to acidify irreversibly, under ambient conditions within 1 week and be completely unusable within 5 weeks, when stored in a sealed container under ambient conditions. In contrast, the pigment/polymer composite film shows no visual sign of acidification after months of storage under the same sealed ambient, dark, conditions and works as if new. This is a significant advantage of the MCP/silica pigment plastic film indicators. Others[1] have shown the tolerance level of solvent based indicators for these acidic gases is only *ca.* 5 ppm. Interestingly, other work shows that the MCP/silica pigments have much higher tolerances (300 and 30 ppm for NO_2 and SO_2, respectively), which helps explain their greater longevity when stored under ambient air.

MCP/silica pigment plastic films over the range 20–40 °C show a decrease in sensitivity (*ca*. 0.06% per °C) with increasing temperature, similar to that of the solvent-based indicator[3] (*ca.* 7% per °C). This decrease is not unexpected given the nature of the key reaction (2).

It was also found that the MCP/silica pigment plastic indicator shows little or no sensitivity towards relative humidity, presumably due to the extremely hydrophobic nature of the indicator. In contrast, the MCP solvent-based indicator, whilst showing little or no sensitivity over a wide humidity range (typically 20–70%RH), does exhibit a slight decrease in sensitivity for %RH higher than 70%RH. Similar results have been found by others[6] studying other CO_2-sensitive, solvent-based indicators.

Fast-acting, reversible and stable, intelligent CO_2-sensitive pigments incorporated into thermoplastics, such as polyethylene, are easy and cheap to prepare. The resulting plastic films exhibit excellent reversibility, a striking colour change and a markedly longer shelf-life than similar, solvent-based CO_2-sensitive inks. As a consequence they have great potential for use in a wide range of applications—including food packaging.[11]

Notes and references

1 J. F. Fernandez-Sanchez, R. Cannas, S. Spichiger, R. Steiger and U. E. Spichiger-Keller, *Sens. Actuators, B*, 2007, **128**, 145–153.
2 M. J.-P. Leiner, J. Tusa and I. Klimant, *EP*, 1 965 198, 2008.
3 A. Mills, Q. Chang and N. McMurray, *Anal. Chem.*, 1992, **64**, 1383–1389.
4 A. Mills, A. Lepre and L. Wild, *Sens. Actuators, B*, 1997, **39**, 419–425.
5 G. C. Upreti, Y. Wang and A. S. H. Kueh, *Int. Pat.*, 079024, 2008.
6 C. R. Schroeder and I. Klimant, *Sens. Actuators, B*, 2005, **107**, 572–579.
7 R. Ostrowski and M. P. Debreczeny, *Int. Pat.*, 039424, 2008.
8 J. Brandrup, E. H. Immergut and E. A. Grulke, *Polymer Handbook*, Wiley-Interscience, 1999.
9 A. Mills and Q. Chang, *Anal. Chim. Acta*, 1994, **285**, 113–123.
10 H. N. McMurray, *J. Mater. Chem.*, 1992, **2**, 401–406.
11 A. Mills, *Chem. Soc. Rev.*, 2005, **34**, 1003–1011.

Sensors and Actuators B 136 (2009) 458–463

Contents lists available at ScienceDirect

Sensors and Actuators B: Chemical

journal homepage: www.elsevier.com/locate/snb

Hydrogen peroxide vapour indicator

Andrew Mills*, Pauline Grosshans, Eilidh Snadden

WestCHEM, University of Strathclyde, Department of Pure and Applied Chemistry, Thomas Graham Building, 295 Cathedral Street, Glasgow, G1 1XL, UK

ARTICLE INFO

Article history:
Received 2 August 2008
Received in revised form
29 November 2008
Accepted 12 December 2008
Available online 25 December 2008

Keywords:
Indicator
Hydrogen peroxide
Lissamine green
Triarylmethane
Vapour
TATP

ABSTRACT

A hydrogen peroxide vapour indicator is described comprising a triarylmethane dye, lissamine green (LG), dissolved in a polymer, polyvinyl alcohol (PVA). The indicator is green/blue in the absence of hydrogen peroxide vapour but is rapidly bleached in the presence of hydrogen peroxide vapour. The kinetics of LG bleaching appear approximately first order with respect [LG] and the concentration of H_2O_2, which, in turn, is proportional to the partial pressure of H_2O_2. However, the kinetics also appear to depend directly upon the reciprocal of the film thickness, implying some dependence upon the diffusion of the H_2O_2 vapour through the indicator film. Like most other H_2O_2 indicator films (such as starch-iodide paper), the LG/PVA indicator is not particularly selective and responds to most other volatile strong oxidising agents, such as ozone and chlorine. However, it is rapid in response (<5 min) and easy to use and has potential as a simple indicator of strong oxidising agents; in particular it may be used to screen the headspace above liquids for H_2O_2, which can be used for making *in situ* explosives, such as triacetone triperoxide (TATP).

1. Introduction

Hydrogen peroxide, H_2O_2, is a pale blue liquid, slightly more viscous than water. It is a weak acid with strong oxidising properties and is inexpensive and readily available for use as a common bleaching agent and disinfectant [1]. Its widespread use is in part due to its environmentally friendly nature, given that it decomposes to produce water and oxygen. Popular uses include as a disinfectant for medical equipment and surfaces [2] and for sterilising surgical instruments [3,4]. Hydrogen peroxide has been used in the standard method for cleaning and storing many types of soft contact lenses since 1990 [5]. Further applications include the chemical treatment of water systems to control diseases such as Legionnaires' disease in hospitals [6], a slurry disinfectant [7], and as a bleach for paper production in the wood pulp industry [8].

A more recent use of hydrogen peroxide is in the production of "kitchen sink" explosives by terrorists. As the name suggests these improvised explosive devices are usually made with common household ingredients. One such example is triacetone triperoxide (TATP), the structure of which is shown in Fig. 1. TATP has been used in several, well-publicised terrorist attacks in recent years, including the July 2005 London bombings and the attempted bombing by Richard Reid, the 'shoe bomber', of a trans-Atlantic flight in December 2001 [9]. TATP itself is a white crystalline material with a low chemical stability that is highly sensitive to mechanical stress and open flames [10]. It is very volatile, losing 68% of its weight within 14 days at room temperature [11], and has an explosive power comparable with that of TNT [10].

TATP can be easily synthesised by mixing acetone, hydrogen peroxide and a strong acid catalyst using ingredients that are readily available for purchase in the public domain. For example, H_2O_2 can be purchased from a chemist as a disinfectant at 6 wt% in water and concentrated down to *ca.* 30 wt% for TATP synthesis [9,10], acetone is available over the counter in nail polish remover, and many household drain cleaners contain sulphuric acid. Not only are the ingredients cheap and readily accessible but TATP is sufficiently easy to make that there are concerns it could be prepared *in situ* at the target site from otherwise apparently innocuous materials.

Of all the key ingredients, hydrogen peroxide is the most difficult to detect. It is very soluble in water and has a high boiling point (150 °C), thus there is very little present, *ca.* 360 ppm, above the headspace of even a highly concentrated (50 wt%) aqueous solution [12]. Such solutions are effectively odourless and cannot be easily sensed, even by sniffer dogs.

With the increased threat of terrorist attacks at airports and on aircraft, there is a real need for a simple and easy-to-use hydrogen peroxide vapour indicator that will alert security officials to its presence in any liquids that are carried on board. Ideally the indicator should be cheap to produce, straightforward to use and understand, non-invasive (i.e. responds rapidly when held over suspect liquid), and undergoes a clear response, such as a striking colour change, when exposed to hydrogen peroxide vapour. Obviously, other possible applications of such an indicator include the detection of H_2O_2

* Corresponding author. Tel.: +44 141 548 24 58; fax: +44 141 548 48 22.
E-mail address: a.mills@strath.ac.uk (A. Mills).

0925-4005/$ – see front matter © 2009 Elsevier B.V. All rights reserved.
doi:10.1016/j.snb.2008.12.032

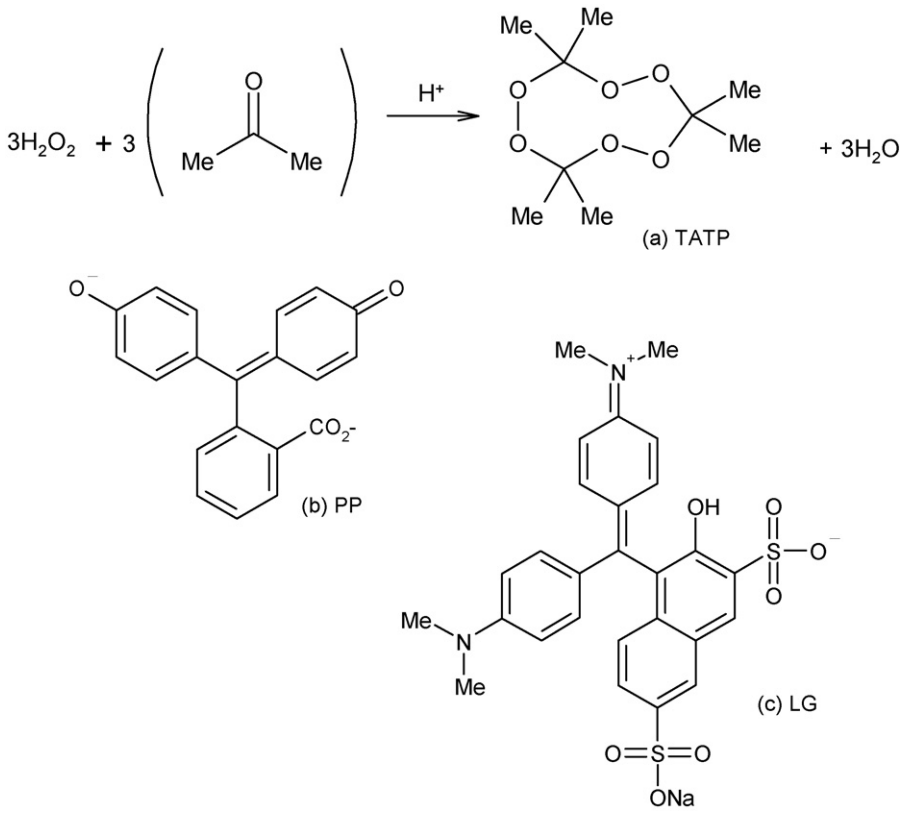

Fig. 1. The chemical structure of the cited compounds (a) triacetone triperoxide (TATP), (b) phenolphthalein (PP) and (c) lissamine green (LG).

vapour in sterilisers and water disinfectant units in hospitals, or, indeed, wherever H_2O_2 is produced or used.

Hydrogen peroxide is a common oxidising agent capable of generating highly reactive hydroxyl radicals, which are able to oxidise many complex organic compounds, including dyes [13–17]. Previous studies have shown that alkaline, aqueous solutions of triarylmethane dyes such as phenolphthalein (PP) and lissamine green (LG) (see Fig. 1) undergo rapid oxidative degradation, accompanied by bleaching, upon the addition of H_2O_2; although under neutral or acidic conditions this reaction is usually very slow [18–22].

Intriguingly, initial work showed that the triarylmethane dye, lissamine green (see Fig. 1), is particularly vulnerable to oxidative bleaching by H_2O_2 vapour when encapsulated in a largely neutral, polymeric environment. Thus, this paper details the characterisation of a simple colorimetric H_2O_2 vapour indicator, comprising the triarylmethane dye, LG, in the polymer, polyvinyl alcohol (PVA).

2. Experimental

2.1. Materials

All chemicals were purchased from Aldrich Chemicals and used as received unless specified. The water used to produce the casting inks was double distilled and deionised, and the polymer used to produce the films was average Mol. Wt 124 000–186 000, 98–99% hydrolysed polyvinyl alcohol. The hydrogen peroxide solutions were prepared from a 50 wt% aqueous hydrogen peroxide stock solution.

2.2. Preparation of LG ink and films

A typical LG/PVA ink solution was prepared as follows: 10 g of PVA were dissolved in 90 ml of water at 90 °C, cooled to room temperature and stirred overnight. 40 mg of LG dye were then dissolved in 4 g of the PVA solution at room temperature with stirring to generate an ink with LG present at 10 parts per hundred resin (phr) (≡0.21 M). The ink (pH 5.7) was dark green/blue in appearance. Films of the ink were then cast onto 25 mm diameter borosilicate glass discs, using a spin coater. Thus, a few drops of casting ink were deposited on to the surface of the disc and then spun at 2400 rpm for 25 s. The product was dried for 2 min in an oven at 70 °C and allowed to cool to room temperature before use. The final product was a green/blue film, typically *ca.* 1.1 μm thick (as measured by SEM) on a glass disc and is referred to henceforth as a typical LG film. The LG/PVA films when stored in a cool dark place, under otherwise ambient conditions, appear unchanged and active for over 1 year.

2.3. UV–visible spectrometry

In a H_2O_2-containing solution well equilibrated with its headspace, the vapour pressure due to the H_2O_2, $p_{H_2O_2}$, is directly proportional to the concentration of H_2O_2 in the solution, i.e. $[H_2O_2]$ [12]. Thus, gas streams containing different levels of hydrogen peroxide vapour were generated by passing air (flow rate = 2 l min^{-1}) through 150 ml of aqueous solutions of H_2O_2 of different concentrations contained in a Drechsel bottle, fitted with a glass sintered tip to ensure the effective dispersion of the carrier gas as bubbles and their saturation with H_2O_2 vapour.

UV–visible spectra for sample films were recorded using a Cary Model 50 UV-Visible Spectrophotometer. Typically, upon exposure of a LG film to H_2O_2 vapour, the absorbance spectrum of the film was recorded every 30 s until the film was fully bleached. In order to carry out this work, any film under test was housed in a gas cell through which was flowed the gas stream containing the H_2O_2 vapour under test; typically derived from a 1 wt% H_2O_2 solution ($p_{H_2O_2}$ = *ca.* 7 ppm) for most work.

3. Results and discussion

3.1. Bleaching of LG in aqueous solution

Solutions of 1.7×10^{-5} M LG were prepared in water (pH 6.3 blue/green, λ_{max} 636 nm) and a pH 9.2 borate buffer (blue, λ_{max} 614 nm). Each of these LG solutions were then mixed with 50 wt% aqueous H_2O_2 in a glass cuvette in a ratio of 30:3 (v:v) to produce an approx. 5 wt% H_2O_2 aqueous solution, and the bleaching followed spectrophotometrically via the decay in the absorbance of LG at 636 nm. The results of this work, plotted in the form of the relative change in absorbance with time, are illustrated in Fig. 2 and reveal that LG is bleached slowly ($t_{1/2}$ = 96 min) at pH 6.3, but much more rapidly (>340 times; $t_{1/2}$ = 17 s) at pH 9.2. These results are consistent with the work of Thompson et al. [18] in their study of the oxidation of aqueous phenolphthalein by H_2O_2, who also noted that oxidative bleaching of such triarylmethane dyes in solution is comparatively very slow at neutral or acidic pHs. These results lend support to the proposal by these workers that bleaching in aqueous solution occurs via nucleophilic attack by the peroxy anion, HOO^-, at the central carbon of the triarylmethane unit. Thus, at pHs significantly below the pK_a of H_2O_2 (11.75), the rate of trialkylmethane dye oxidation (LG or PP) is very low.

3.2. Visual bleaching of standard LG films

The above results in aqueous solution indicate it is very unlikely a typical LG/PVA film (where the pH of the casting ink = 5.7) will be bleached rapidly by the H_2O_2 vapour above even a strong (50 wt%) H_2O_2 solution, not only because the amount of H_2O_2 in the vapour phase is so low (*ca.* 360 ppm), but also because the reaction rate is so slow in a neutral or acidic medium, such as aqueous solution at pH 6.3 ($t_{1/2}$ = 96 min). However, in practice, and for reasons that as yet remain unclear, the bleaching kinetics of LG in polymer films by H_2O_2 vapour are rapid. For example, when a typical LG film was placed on top of a sample vial containing 5 ml of 50 wt% H_2O_2 in water, film side down, the H_2O_2 vapour above the solution (*ca.* 360 ppm) caused the LG film to bleach within minutes, as illustrated by the photographs in Fig. 3.

3.3. Spectral and response characteristics of a LG film

An aqueous solution of LG has a peak in its absorption spectrum at 636 nm, whereas in a PVA film not only is the peak slightly broader, with a shoulder emerging at ~605 nm, but it is red-shifted to 650 nm, most probably due to the formation of dimers, which is not surprising given [LG] in films = 0.21 M. Indeed, a 0.1 M LG aqueous solution has a λ_{max} at 640 nm and a shoulder peak at 601 nm,

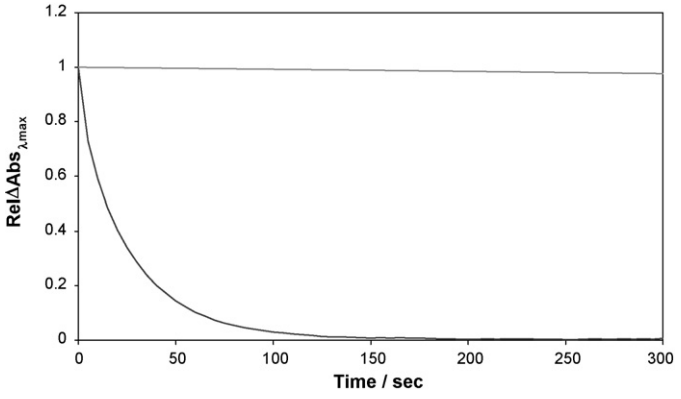

Fig. 2. A comparison of the bleaching of 1.7×10^{-5} M LG (aq) at pH 6.3 (grey line) where $t_{1/2}$ = 96 min, and at pH 9.2 (black line) where $t_{1/2}$ = 17 s.

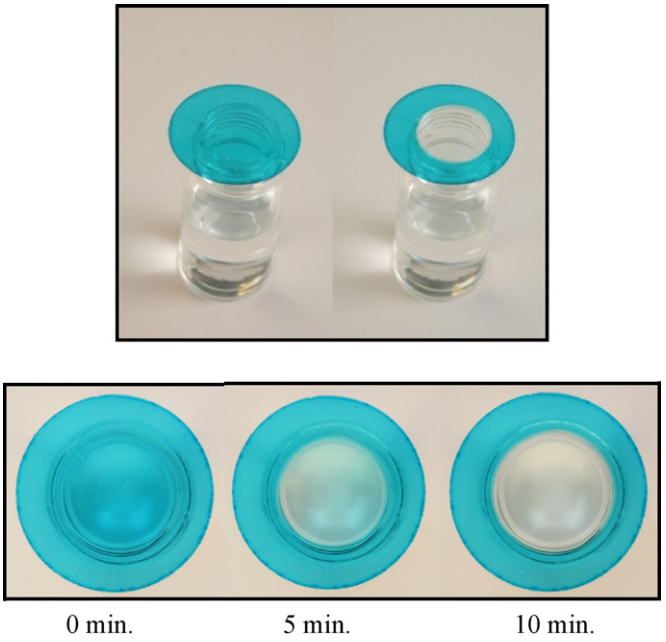

Fig. 3. Photographs illustrating the chemical bleaching of a typical LG film when placed above a 50 wt% aqueous H_2O_2 solution.

also implying dimer formation at high dye concentrations. It is possible that such dimers are more vulnerable to oxidative attack by hydrogen peroxide. It is also possible that a change in microenvironment polarity is responsible for the significant increase in reactivity of LG with H_2O_2 vapour when the dye is encapsulated in a PVA film. Indeed, using as alternative encapsulation polymers to PVA, polyethylene oxide (PEO) and hydroxyethyl cellulose (HEC), the relative rates of bleaching by H_2O_2 vapour were found to be 1.6:1:0.6 for HEC, PVA and PEO, respectively, indicating the more polar the polymer environment the faster the rate.

Although the underlying cause for the marked increase in the rate of LG with H_2O_2 is not fully understood, the effect is clearly demonstrable (see Fig. 3), and was studied in more detail. For example, a typical LG film was mounted in gas cell and exposed to H_2O_2 vapour from a 1 wt% aqueous H_2O_2 solution. The loss of colour of the LG film was followed spectrophotometrically, and the results are displayed in Fig. 4. Using this data, a plot of the change in absorbance at λ_{max}, i.e. ΔAbs_{650}, against time was generated and revealed that, after an slight initial delay, possibly due to an experimental artefact associated with gas switching, the kinetics of LG bleaching by H_2O_2 vapour above a 1 wt% aqueous H_2O_2 solution give a reasonable fit (r^2 = 0.996) to a first order bleaching process ($t_{1/2}$ = 3.5 min).

Extending this study, the kinetics of LG bleaching in a typical LG/PVA film were studied as a function of the H_2O_2 vapour pressures above different aqueous [H_2O_2] solutions over the range of 0–20 wt%, and the results are illustrated in Fig. 5. First order kinetics analysis of these results generated the plots of k_1 versus wt%H_2O_2, illustrated in Fig. 6, where k_1 is the first order rate constant.

As noted earlier, previous work has established that the kinetics of the bleaching of PP in aqueous alkaline solution by H_2O_2 are first order kinetics with respect to [H_2O_2] and [PP] and we find similar kinetics apply to LG in aqueous solution (see Fig. 2) [18]. The results illustrated in Fig. 5 indicate that the kinetics of LG bleaching in a LG/PVA film are first order with respect to [LG], and those in Fig. 6 indicate they are also first order with respect to [H_2O_2] and, therefore $p_{H_2O_2}$, below 1 wt% [H_2O_2]. However, above *ca.* 1 wt% H_2O_2 the value of the apparent first order rate constant, k_1, appears to level off with increasing [H_2O_2] (see Fig. 6), possibly due to the heterogeneous nature of the polymer environment, which often results in a

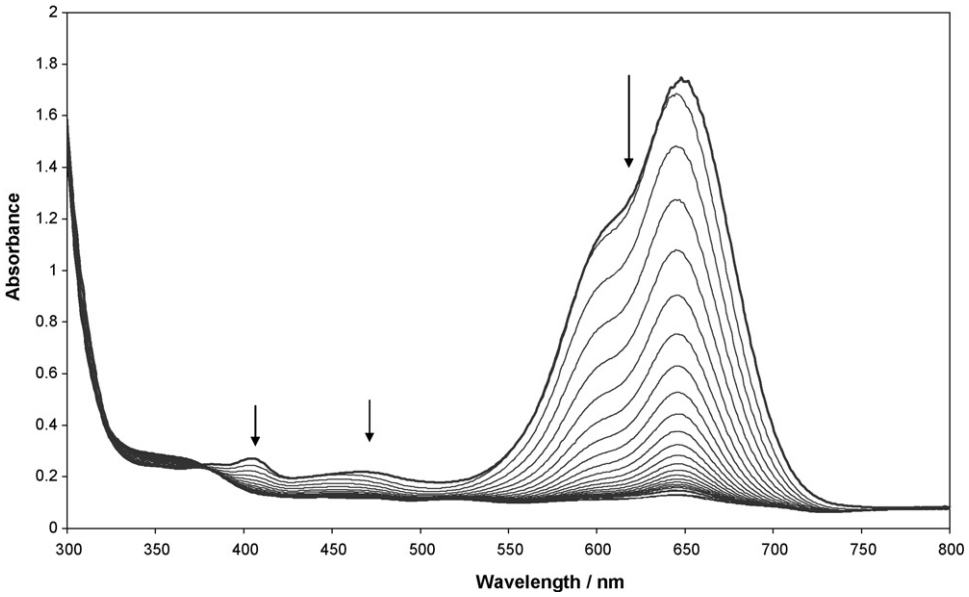

Fig. 4. The absorption spectra of a standard LG film on exposure to hydrogen peroxide vapour from a 1 wt% H_2O_2 solution at a flow rate of 2 l min^{-1}. Spectra recorded at 1 min intervals.

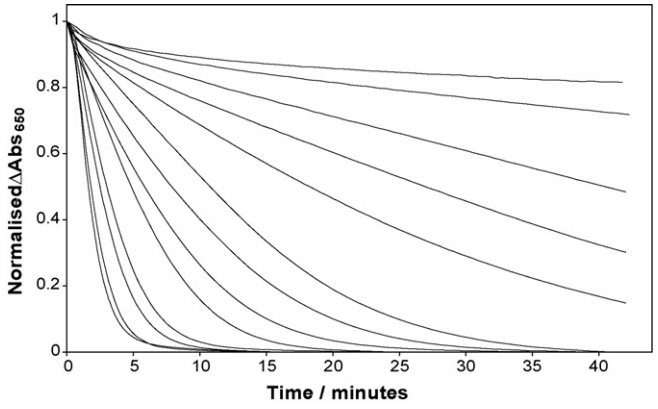

Fig. 5. A normalised plot of ΔAbs_{650} against time for typical LG films exposed to H_2O_2 vapours from solutions of different [H_2O_2] at a flow rate of 2 l min^{-1}. The concentrations of aqueous H_2O_2 solutions used to produce the different vapours are, from top to bottom: 0, 0.01, 0.03, 0.05, 0.1, 0.2, 0.3, 0.5, 1, 3, 5, 10 and 20 wt%.

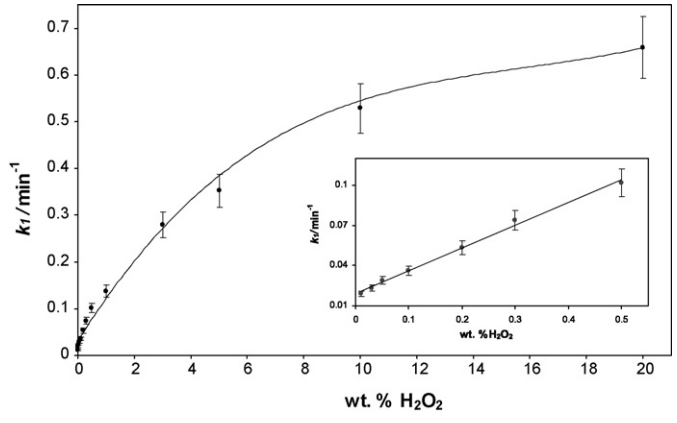

Fig. 6. A plot of k_1 vs. wt% H_2O_2. Insert diagram shows an expanded view of the region from 0 to 1 wt% H_2O_2.

distribution of reaction rate constants. For example, this feature is typical of luminescent quenching by O_2 of oxygen-sensitive luminescent dyes encapsulated in polymer films including PVA [23]. Further work revealed that the kinetics of dye bleaching in the LG/PVA films are independent of the gas flow rate at or above the gas flow rate used in this work (typically 2 l min^{-1}), indicating that the kinetics are independent of the mass transfer of the H_2O_2 in the vapour to the LG/PVA film.

3.4. Film thickness

In the study of kinetics of LG bleaching as a function of film thickness, *d*, a slightly modified LG/PVA ink casting solution, containing 2.5 phr (rather than 10 phr) LG, was prepared by dissolving 5 mg (instead of 20 mg) of LG in 2 g of 10 wt% PVA in water. This lower [LG] was used in order to allow much thicker films, with higher absorbances, to be prepared using slower spin speeds. From this slightly less coloured LG/PVA ink, a series of films of different thicknesses were produced using a spin coater by varying the spin speed from 600 to 2500 rpm. These films were then exposed to H_2O_2 vapour from a 1 wt% aqueous H_2O_2 solution. As before, bleaching of the samples was monitored spectrophotometrically at 650 nm and a plot of the ΔAbs_{650} against time was generated for each film spin speed and the collected decay profiles are shown in Fig. 7. A plot of $\ln(\Delta Abs_{650})$ against time yielded a set of k_1 values.

If the kinetics of LG bleaching were dependent solely upon diffusion of H_2O_2 through the film it would be expected that $k_1 \propto 1/d^2$, whereas in practice it appears that they are approximately proportional to $1/d$ as seen from the inset in Fig. 7. Thus, the kinetics of LG bleaching in LG/PVA films appear to be only partially controlled by the diffusion of the H_2O_2 through the PVA film.

3.5. Comparison of LG films with starch-iodide paper

A commonly employed indicator of the presence of strong oxidising agents, such as H_2O_2, is of course, starch-iodide paper. However, this very effective indicator needs to be damp in order to allow the dark blue starch–iodine complex to be formed [24]. If water is not present the less colourful straw-yellow colour of iodine is generated. Fig. 8a and b illustrate the typical colour responses of

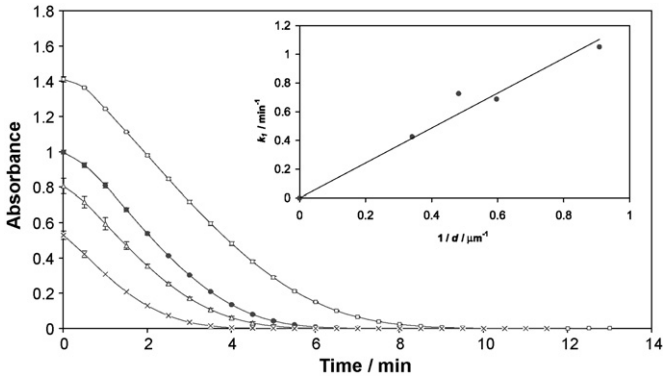

Fig. 7. A plot of ΔAbs_{650} against time for 5 phr LG films, generated at different spin speeds (from top to bottom 600, 1200, 1800 and 2500 rpm) upon exposure to H_2O_2 vapour from a 1 wt% H_2O_2 aqueous solution. The flow rate used was 2 l min^{-1}. Inset diagram shows a plot of k_1 vs. $1/d$, with $m = 1.22$ and a correlation coefficient of 0.961.

both dry and damp commercial starch-iodide paper when placed above a 50 wt% aqueous H_2O_2 solution. The response times of dry and damp starch-iodide paper are similar to that of a LG film, but only the damp starch-iodide paper produces a striking colour response. Although an attractive method for detecting the presence of a strong oxidising agent, such as H_2O_2, in many cases the need to wet the indicator makes the starch-iodide paper test less convenient that the LG film-based indicators.

3.6. Selectivity

An ideal H_2O_2 vapour indicator is one which responds specifically to H_2O_2 vapours; however, both the conventional starch-iodide paper and the LG film-based indicators respond not only to H_2O_2 vapours but also to other volatile strong oxidising agents, such as ozone, chlorine or nitrogen dioxide. This lack of selectivity is obviously undesirable, although the detection of such vapours would be indicative of a liquid containing a strong oxidising agent and so the ability to detect such agents is still useful.

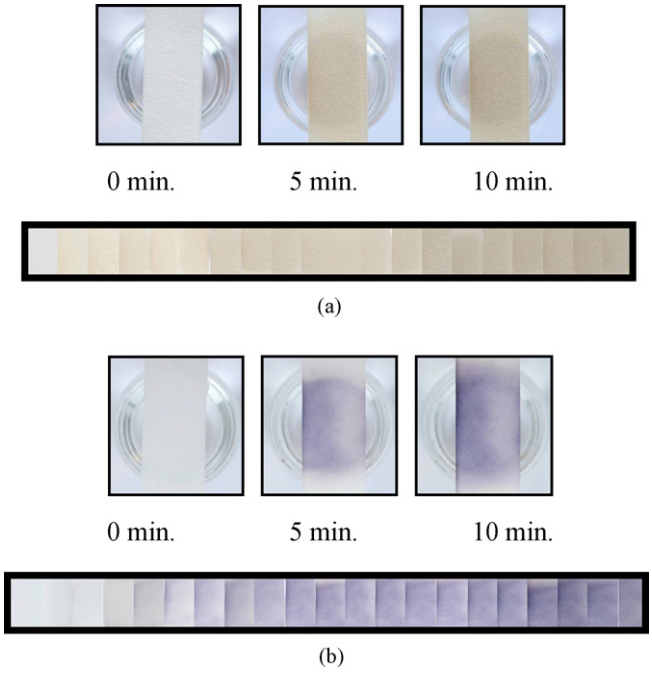

Fig. 8. Photographs illustrating the colouration of (a) dry and (b) wet starch-iodide paper when placed above a 50 wt% aqueous H_2O_2 solution.

4. Conclusions

LG/PVA films are stable over many months and, in contrast to starch-iodide paper, need no wetting to respond rapidly to the vapour associated with aqueous H_2O_2 solutions that could be used to make so-called 'kitchen sink' explosives *in situ*, i.e. 30 wt% in water. In a flowing gas stream the kinetics of the bleaching process are first order with respect to [LG] and $[H_2O_2]$ at low concentrations $[H_2O_2]$ (<1 wt%); but tend to zero-order with respect to $[H_2O_2]$ as the latter is increased above this level. The kinetics of LG bleaching are also dependent upon the film thickness ($\propto 1/d$), indicating some degree of diffusion control. Overall, these LG/polymer indicators appear promising for the detection of H_2O_2 vapour and other volatile, strong oxidising agents, and so, amongst other things, may find application in the detection of peroxide-based terrorist bombs.

References

[1] G. McDonnell, A.D. Russell, Antiseptics and disinfectants: activity, action, and resistance, Clin. Microbiol. Rev. 12 (1999) 147–179.
[2] B.M. Andersen, M. Rasch, K. Hochlin, F.-H. Jensen, P. Wismar, J.-E. Fredriksen, Decontamination of rooms, medical equipment and ambulances using an aerosol of hydrogen peroxide, J. Hosp. Infect. 62 (2006) 149–155.
[3] G. Fichet, K. Antloga, E. Comoy, J.P. Deslys, G. McDonnell, Prion inactivation using a new gaseous hydrogen peroxide sterilisation process, J. Hosp. Infect. 67 (2007) 278–286.
[4] D.M. Reid, Hydrogen peroxide indicator and method, US Pat. 6,790,411 (2004).
[5] J. Gavin, N.F. Button, I.A. Watson-Craik, N.A. Logan, Efficacy of standard disinfectant test methods for contact lens-care solutions, Int. Biodeterior. Biodegrad. 36 (1995) 431–440.
[6] B.R. Kim, J.E. Anderson, S.A. Mueller, W.A. Gaine, A.M. Kendall, Literature review—efficacy of various disinfectants against *Legionella* in water systems, Water Res. 36 (2002) 4433–4444.
[7] A. Tofant, M. Vucemilo, Z. Panic, D. Mimic, The hydrogen peroxide, as a potentially useful slurry disinfectant, Livestock Sic. 102 (2006) 243–247.
[8] R.J. Michalowski et al., Bleaching of cellolosic pulps using hydrogen peroxide, US Pat. 4,732,650 (1988).
[9] D.F. Laine, C.W. Roske, I.F. Cheng, Electrochemical detection of triacetone triperoxide employing the electrocatalytic reaction of iron(II/III)-ethylenediaminetetraacetate and hydrogen peroxide, Anal. Chim. Acta 608 (2008).
[10] F. Dubnikova, R. Kosloff, J. Mlmog, Y. Zeiri, R. Boese, H. Itzkaky, A. Alt, E. Keinan, Decomposition or triacetone triperoxide is an entropic explosion, J. Am. Chem. Soc. 127 (2007) 1146–1159.
[11] J. Yinon, Forensic and Environmental Detection of Explosives, John Wiley & Sons Ltd., 1999.
[12] http://ww.h2o2.com/intro/properties/physical.html#13 (accessed August 2008).
[13] S. Das, P.V. Kamat, S. Padmaja, V. Au, S.A. Madison, Free radical induced oxidation of the azo dye acid yellow, J. Chem. Soc., Faraday Trans. (1992) 1219–1223.
[14] M.E. Abdelsalam, P.R. Birken, A study investigating the sonoelectrochemical degradation of an organic compound employing fenton's reagent, Phys. Chem. Chem. Phys. 4 (2002) 5340–5345.
[15] J.R. Darwent, A. Lepre, Photo-oxidation of methyl orange sensitized by zinc oxide. Part 1—mechanism, J. Chem. Soc., Faraday Trans. 282 (1986) 1457–1468.
[16] K. Dutta, S. Bhattacharjee, B. Chaudhuri, S. Mukhopadhyay, Chemical oxidation of C. I. Reactive red 2 using fenton-like reactions, J. Environ. Monit. 4 (2002) 754–760.
[17] V. Nadtochenko, J. Kiwi, Photoinduced adduct formation between orange II and $[Fe^{3+}(aq)]$ or $Fe(ox)_3^{3-}$–H_2O_2. Photocatalytic degradation and laser spectroscopy, J. Chem. Soc., Faraday Trans. 93 (1997) 2373–2378.
[18] K.M. Thompson, W.P. Griffith, M. Spiro, Mechanisms of bleaching by peroxides. Part 1. Kinetics of bleaching of phenolphthalein by hydrogen peroxide as high pH, J. Chem. Soc., Faraday Trans. 89 (1993) 1203–1209.
[19] K.M. Thompson, W.P. Griffith, M. Spiro, Mechanisms of bleaching by peroxides. Part 3. Kinetics of bleaching of phenolphthalein by transition-metal salts in high pH peroxide solutions, J. Chem. Soc., Faraday Trans. 90 (1994) 1105–1114.
[20] D.M. Davies, A.U. Moozyckine, Kinetics and mechanism of bleaching of a triarylmethane dye by hydrogen peroxide and water: evidence for intramolecular base catalysis, J. Chem. Soc., Perkin Trans. 2 (2000) 1495–1503.
[21] A.U. Moozyckine, D.M. Davies, Green S as a prototype for an environmentally-degradable dye: the conception of a "green dye" in future green chemistry, Green Chem. 4 (2002) 4452–4458.
[22] P.H. d'Hausen, C.N. Tait, D.M. Davies, Effect of beta-cyclodextrin on the bleaching of a triarylmethane dye by hydrogen peroxide and alkali, J. Chem. Soc., Perkin Trans. 2 (2002) 398–403.
[23] A. Mills, Optical oxygen sensors: utilising the luminescence of platinum metals complexes, Platinum Met. Rev. 41 (1997) 115–127.
[24] R. Beavon, A. Jarvis, Structure, Bonding and Main Group Chemistry, revised edition, Nelson Advance Science, Nelson Thornes, 2003.

Biographies

Professor Andrew Mills gained his PhD in 1983 from University of London working on water-splitting photosystems. He currently holds the James Young Chair in Physical and Applied Chemistry at University of Strathclyde. His research interests include: semiconductor photochemistry and optical sensors.

Pauline Grosshans gained her degree in chemistry from University of Strathclyde in 2006 and is currently engaged in a PhD on novel optical sensors.

Eilidh Snadden is in her 3rd year of applied chemistry and chemical engineering degree at University of Strathclyde.